A study of electrode-tissue impedances encountered in cardiac pacing

Volume One

Sub title: The Small signal inter-electrode impedance

ERIC THOMAS McADAMS BSc

Submitted in accordance with the requirements for the degree of Doctor of Philosophy

The University of Leeds,
Department of Medical Physics.

June 1987

Acknowledgements

I should like to acknowledge with gratitude, the assistance given to me by various people, both during the execution of my research work and in the production of this thesis.

Firstly, I wish to indicate my gratitude to the late Professors Ellis and Parker for their interest and support and for the opportunity afforded me to work in their department over the period October 1980 to October 1983.

Next, to Dr F. Hepburn and Dr. T. Evans , I wish to express my thanks for their encouragement and assistance in this work and for their supervision and constructive criticism.

Also, I am indebted to Dr G. Davies of the Physics Department, Leeds University for the use of the Solartron 1250 frequency response analyser and for his encouragement at all times - many thanks!

I wish to express my appreciation to Mrs Christine Irvine for her patience in deciphering my 'hieroglyphics' and the excellent type which she has produced.

Appreciation is also due to my colleagues at the Bio engineering Research Centre, The University of Ulster, and to the Director of Research, Dr. J. Anderson, for their assistance in producing this manuscript.

Lastly, I would like to express my gratitude to my wife and family for their encouragement and forebearance throughout this work and I dedicate this thesis to them.

ABSTRACT

Any study of the electrical properties of electrode-electrolyte systems is rendered difficult by their dependance on, amongst other things, electrode history, electrode surface finish, electrode geometry, electrode area, electrolyte composition and the frequency and amplitude of the applied signal.

Distinguished scientists in this field have recently concluded that "there appears to be, so far, no model available which would account for both the linear and non-linear behaviour of the electrodes in the frequency and time domain" (Fischler and Schwan, 1981).

Such a model has, however, been developed in this thesis, which, it is believed, successfully interprets and models the wealth of empirical observations reported in the literature.

The source of the observed frequency dependence of the inter-electrode impedance is traced to the electrode-electrolyte interface impedance and is approximated by a "constant phase angle impedance", Z_{CPA}. It is established that the form of this impedance is largely due to electrode surface effects and to a lesser degree by those of specific adsorption.

It is demonstrated that the observed non-linearities of the electrode system are largely due to a charge transfer "resistance", R_{CT}, which shunts Z_{CPA}. Empirical expressions of the system's non-linearity found in the literature are physically interpreted and similar expressions are derived based on the model.

The changes in inter-electrode impedance due to electrode failures are investigated, modelled and interpreted. Such alterations in loading are found to give rise to changes in pacemaker output and current response waveform. For certain pacers these externally observable parameters can enable the detection and classification of electrode failure, sometimes in a latent stage before failure to pace.

NOMENCLATURE

Subscripts

a	anodic
A	adsorption
ac	alternating current
ac+dc	small amplitude ac signal superimposed on variable dc bias
b	bulk
CPA	constant phase angle
CT	charge transfer
dc	direct current
dl	double layer
e	a) electrolyte
	b) electrical
f	faradaic
F	forward
HF	high frequency
i	interface
L	limiting
LF	low frequency
m	metal
M.T.	mass transfer
n.f.	non faradaic
O	oxidised
P	parallel
R	reduced
s	a) surface
	b) series
rev.	reversible
W	Warburg

Roman Symbols

A	area (cm^2)
a_i^{α}	activity of substance i in a phase α (M)
B	adsorption coefficient, potential independent
$\overline{B}$	adsorption coefficient, potential dependent
C	a) concentration (M, mol/cm^3)
	b) capacitance (μF)
C*	complex capacitance
C_A	adsorption pseudo capacitance (μF)
C_A^L	Langmuir's adsorption capacitance (μF)
C_D	capacitance of the diffuse layer (μF)
C_{dl}	double layer capacitance (μF)
C_i	a) integral capacitance (μF)
	b) series interfacial capacitance
C^j	concentration of species j (M, mol/cm^3)
C_b^j	bulk concentration of species j (M, mol/cm^3)
C_s^j	surface concentration of species j(M,mol/cm^3)
C_{HF}	limiting value of the capacitance at high frequencies (μF)
C_{LF}	limiting value of the capacitance at low frequencies (μF)
ΔC	an adsorption capacitance, where $\Delta C = C_{LF} - C_{HF}$ (μF)
C_{OHP}	Outer Helmholtz Plane capacitance (μF)
C_p	parallel capacitance (μF)
C_s	series capacitance (μF)
D_j	diffusion coefficient of species j (cm^2/sec)
d	distance (cm)

E	potential of an electrode versus a reference (V)
E^o	standard potential of an electrode (V)
E_{rev}	reversible potential of an electrode (V)
e	quantity of charge on the electron (C)
erf(x)	error function of x
erfc(x)	error function complement of x
F	the Faraday; charge on one mole of electrons (C)
f	a) F/RT (V^{-1})
	b) frequency (sec^{-1})
f_h	highest frequency component, $f_h = 1/t_s$
G	Gibbs free energy (kJ)
ΔG	Gibbs free energy change in a chemical process (kJ)
ΔG^o	standard Gibbs free energy of activation (kJ/mol)
$\bar{G}$	electrochemical free energy (kJ)
g	conductivity (Ω^{-1} cm^{-1})
I_{ac}	amplitude of ac current (A, mA)
I_o	Bessel function of order zero
i	current (A, mA)
i_a	anodic component current (A, μA)
i_{ac}	ac current (A, mA)
i_c	cathodic component current (A, μA)
i_{dc}	dc current (A, mA)
i_{dL}	diffusion limited current (A, mA)
i_f	faradaic current (A, mA)
i_L	limiting current of linearity (A, mA)
inf	nonfaradaic current (A, mA)

i_o	exchange current (A, μA)
i_{TOTAL}	total current = $i_{nf} + i_f$ (A, mA)
J_j	flux of species j (mol cm^{-2} sec^{-1})
j	a) current density (A/cm^2, A/cm^2)
	b) $\sqrt{-1}$
K	a) faradaic charge required to form a monolayer of adsorbed ions (C, μC)
	b) magnitude of Z_{CPA} impedance ($\Omega sec^{-\beta}$)
	c) potential dependent rate constant
K^o	standard, potential independent, rate constant (cm/sec)
K_F	potential dependent rate constant for the forward reaction
K_R	potential dependent rate constant for the reverse reaction
l	depth of surface pores (cm)
M	metal electrode in the reaction $M \rightleftharpoons M+e$
m	fractional power constant
n	electrons per molecule oxidised or reduced
O	oxidised form of the standard system $O+ne \rightleftharpoons R$
P	reciprocal of penetration depth (cm^{-1})
Q	charge (C, μC)
q^-	excess charge of anions (C, μC)
q^+	excess charge on phase cations (C, μC)
q_j	excess charge on phase j (C, μC)
$q_s^{(CA)}$	charge of ions coulombically adsorbed onto the surface (C, μC)
$q_s^{(SA)}$	charge of ions specifically adsorbed onto the surface (C, μC)

R	a) reduced form of the standard system, $O + ne \rightleftharpoons R$
	b) gas constant (J mol^{-1} K^{-1})
	c) resistance (Ω)
R_A	adsorption resistance (Ω)
R_{CT}	charge transfer resistance (Ω)
$R_{CT(ac)}$	charge transfer resistance measured under ac large signal conditions (Ω)
$R_{CT(dc)}$	charge transfer resistance measured under dc large signal conditions (Ω)
$R_{CT(ac+dc)}$	charge transfer resistance measured under 'ac + dc' large signal conditions (Ω)
$R_{ELECTROLYTE}$	resistance of electrolyte (Ω)
R_e	resistance of electrolyte per unit length of surface pore ($\Omega\,cm^{-1}$)
R_i	series interfacial resistance (Ω)
R_{LEAD}	resistance of leads (Ω)
R_p	parallel resistance (Ω)
R_s	series resistance (Ω)
R_{SALINE}	resistance of saline (Ω)
R_{TOTAL}	total series resistance (Ω)
R_o	resistance when $\omega = o$ (Ω)
R_∞	resistance when $\omega = \infty$ (Ω)
r_o	radial distance from the centre of a spherical electrode (cm)
s	Laplacian operator, s = a+j
T	a) absolute temperature (°k)
	b) time period (sec)
T_p	total sampling period (sec)
t	time (sec.)

t_p	pulse duration (sec)
t_s	sample length (sec)
t	normalised time = t/T
v	a) volume (cm^3)
	b) Voltage (V)
V_{ac}	ac voltage amplitude (V)
V_{ecm}	electro capillary maximum voltage (V)
V_{dc}	dc voltage (V)
V_L	limit voltage of linearity (V)
$\hat{V_j}$	flux of species j (mol cm^{-3} sec^{-1})
X	reactance (Ω)
X_i	series reactance of interfacial impedance (Ω)
X_s	series reactance (Ω)
Y	admittance (Ω^{-1})
Z	impedance (Ω)
Z_{CPA}	constant phase angle impedance (Ω)
Z_{CT}	charge transfer impedance (Ω)
Z_f	faradaic impedance (Ω)
Z_i	interface impedance (Ω)
Z_{MT}	mass transfer impedance (Ω)
$Z_{n.f.}$	nonfaradaic impedance (Ω)
Z_o	impedance of surface pore (Ω)
Z_W	Warbug impedance (Ω)
Z_{WA}	Adsorption pseudo Warburg impedance (Ω)

Greek symbols

α	transfer coefficient
β	fractional power dependence on fequency of z_{CPA}
Γ	gamma function
Γ_j	surface excess of species j at equilibrium (mol/cm)
Γ_s	saturation coverage
	a/ surface tension (dyne/cm)
	b/ activity coeffecient
δ	Nernst diffusion layer thickness (cm)
δ_o	maximum thickness of the Nernst diffusion layer (cm)
ε	dielectric constant
ε_{HF}	limiting value of permittivity at high frequencies
ε_{LF}	limiting value of permittivity at low frequencies
ε_o	dielectric constant of free space $(C^2N^{-1}m^{-2})$
ε_r	dielectric constant of medium
ε_r^*	complex dielectric constant of medium
η	overpotential, $E - E_{rev}$ (V, mV)
η_{CT}	charge transfer overpotential (V, mV)
η_{MT}	mass transfer over-potential (V, mV)
θ_j	fractional coverage of an interface by species j
μ_j^{α}	chemical potential of species j in phase α (kJ/mol)

$\mu_j^{o,\alpha}$	standard chemical potential of species j in phase α (kJ/mol)
$\bar{\mu}_j^{\alpha}$	electrochemical potential of species j in phase α (kJ/mol)
ρ	resistivity (Ω cm)
σ	diffusion coeffecient (Ω - $sec^{1/2}$)
$\tilde{\tau}$	time constant (sec)
$\tilde{\tau}_o$	coverage time constant (sec)
ϕ_f	a) electrostatic potential (V)
	b) phase angle (degrees, radians)
ϕ	phase angle of faradaic impedance (degrees,radians)
ψ	loss angle, where $\psi = 90 - \phi^o = m\pi/2 = (1-\beta)/2$ rads
ω	angular frequency (sec^{-1})
ω_o	value of ω at which X_s has its maximum
$\omega_{10\%}$	angular frequency at which the impedance changes by 10% due to nonlinearities

Abbreviations

DDRT	Distribution of Dielectric Relaxation Times
DR	Decay Ratio
DRT	Distribution of Relation Times
ECM	ElectroCapillary Maximum
FFT	Fast Fourier Transform
IHP	Inner Helmholtz Plane
OHP	Outer Helmholtz Plane
PZC	Potential of Zero Charge
RHE	with Reference to the Hydrogen Electrode

Table of Contents

LIST OF DIAGRAMS

DIAGRAMS CONTINUED

DIAGRAMS CONTINUED

DIAGRAMS CONTINUED Page No

DIAGRAMS CONTINUED Page No

Chapter 4

DIAGRAMS CONTINUED Page No

DIAGRAMS CONTINUED — Page No

Chapter 5

DIAGRAMS CONTINUED — Page No

DIAGRAMS CONTINUED Page No

Chapter 7

LIST OF TABLES

TABLES CONTINUED Page No

TABLES CONTINUED

Chapter 6

TABLES CONTINUED Page No

Chapter 7

INTRODUCTION TO THESIS

- Why have pacemakers?

The ventricular muscle mass of the heart is responsible for pumping blood around the body. The source of the heart's pumping action is an electrical impulse which is generated by a group of specialised myocardial cells termed collectively the S.A. node, and which spreads to the rest of the heart to give rise to a co-ordinated contraction.

Pacemakers were created when it was discovered that an artificial impulse from an electrical impulse generator can cause the heart to contract in a similar way to the actual impulse generated by the S.A. node. A pacemaker is a specially developed design of such an impulse generator for implantation in patients whose normal heart control or conduction processes are deficient. It is used to supply the artificial stimulation necessary to activate the heart muscle when either the S.A. node does not provide an adequate natural one or when there is interference with the conduction of the electrical impulse to any part of the heart i.e. " heart block ".

- Implanted System

The pacemaker is normally implanted in the chest wall and a transvenous lead connects the generator to the apex of the right ventricle, (see figure 0.1). The pacemaker battery circuit generates an impulse which

passes through the insulated transvenous lead, is delivered to the heart wall by the electrode tip and returns via chest tissue to the anode attached to the pacemaker. The lead is connected to the negative end of the pacemaker battery as it has been found that cathodal stimulation depolarises cells more easily than anodal stimulation.

Hence the implanted system consists of the pulse generator (a power source and its required electronic circuitry) and the conducting lead with its exposed electrode tip.

- Ideal Pacemaker

The ideal pacemaker battery should have the following features:

1) It should be able to generate up to 5 volts (more than is generally necessary to stimulate the heart).

2) It should be hermetically sealed,ie airtight.

3) It should have a long "shelf life".

4) It should have a long working life.

5) It should fail gradually and in a predictable manner.

In the past Mallory (ie. mercury-zinc) batteries were

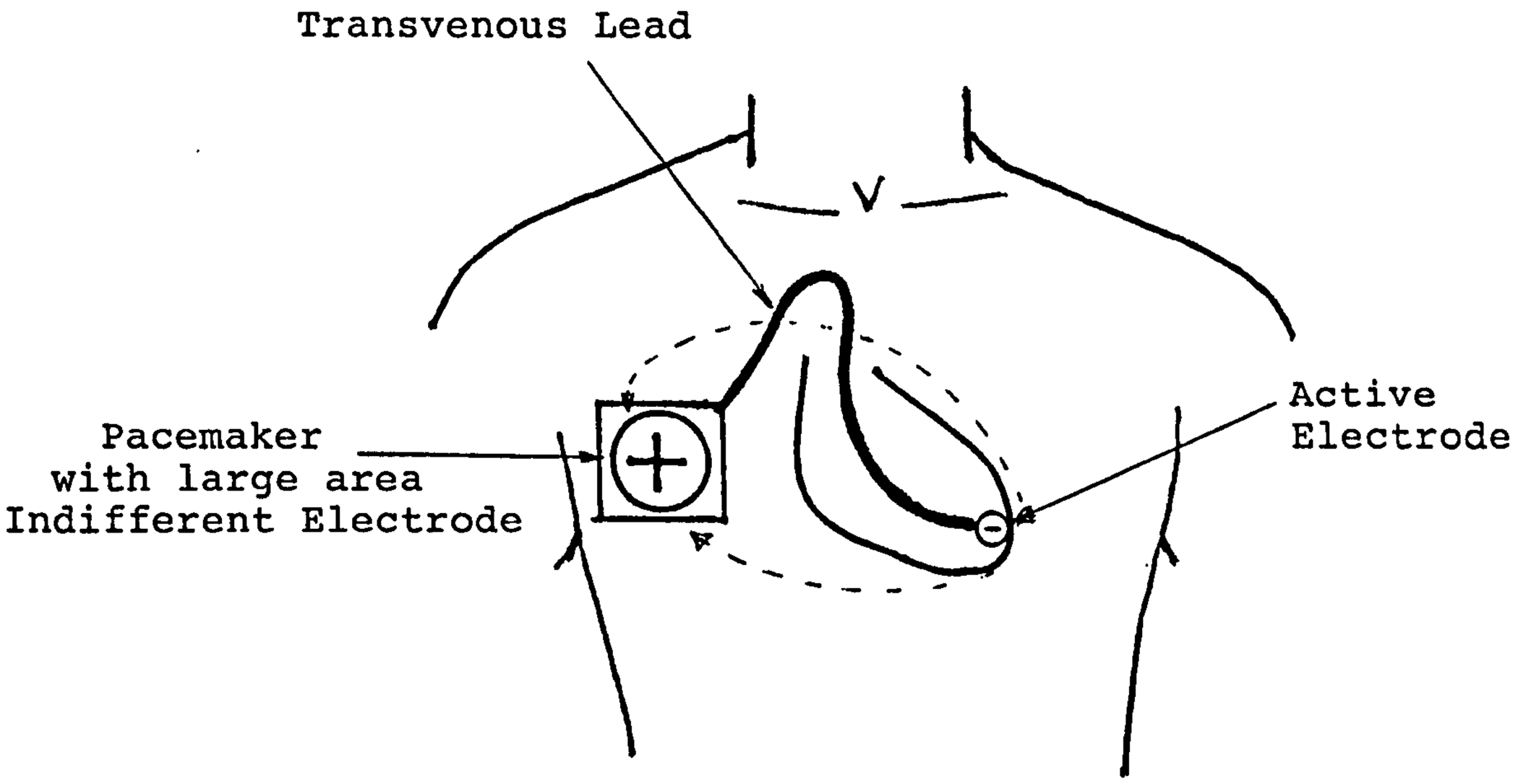

IMPLANTED PACING SYSTEM

Figure 0.1

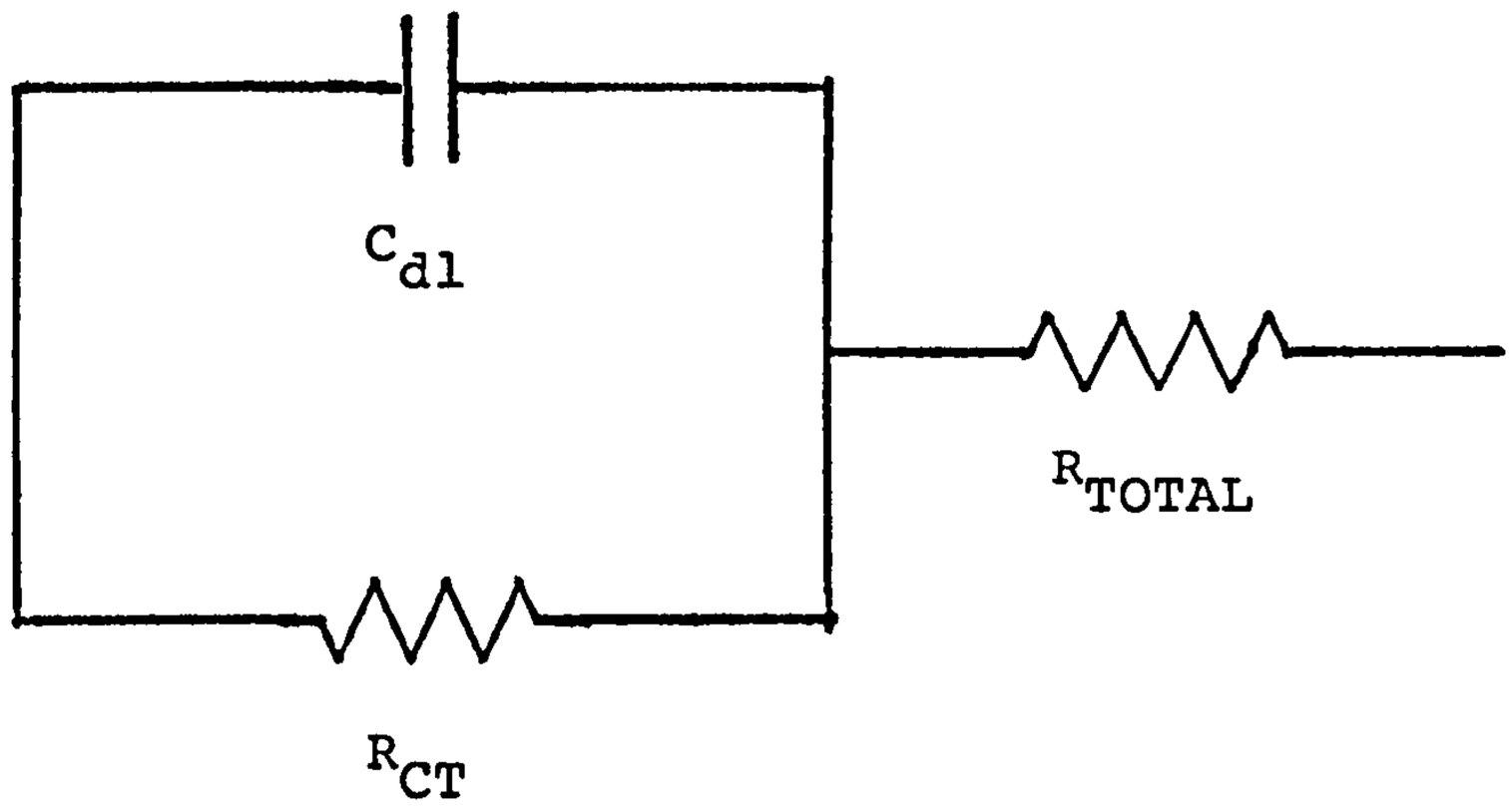

"3 COMPONENT" MODEL

Figure 0.2

most commonly used. These however had several shortcomings. They could not be hermetically sealed as they generated gases, they had a relatively short clinical life (1-5 years) and were susceptible to sudden failure.

The more recent Lithium iodine battery has many advantages over the mercury-zinc battery. It does not generate any gases and hence can be hermetically sealed, and it has a relatively long clinical life (over 5 years).

- Ideal Lead Wire

Lead wires are made of a range of alloys such as stainless steel, Elgiloy and platinum-Iridium. They should be highly conductive and fatigue resistant. They are generally coiled to increase flexibility and multifilar to provide redundancy. The lead wires are generally insulated with Silastic or polyurethane.

- Ideal Electrode Tip

The exposed lead tip forms the electrode and is generally made from a different metal to the lead wire. A good electrode should, among other things, -

1) be electrochemically inert, ie it should not go into solution (dissolve) upon the passage of current as this could possibly generate toxic by-products

2) have a low electrical resistance

3) give rise to a small electrode-electrolyte interface impedance.

After some years of unsatisfactory trials with stainless steel (it suffers from electrochemical electrolysis) the most common electrode tip materials are now Platinum, Platinum-Iridium , Elgiloy (a cobalt nickel alloy) and vitreous carbon.

- Monitoring Technique - "Photo-analysis"

Two major problems arise in the long term management of patients with implanted pacemakers. The first is the uncertainty of when a pacemaker will fail and secondly determining the cause of the failure. A technique which enables the physician to analyse and monitor the implanted unit could provide the answers to the above questions. Such a technique, to be clinically acceptable, would have to have the following characteristics:

a) It should be external, thus enabling the monitoring of the unit to be made easily, frequently and without trauma to the patient.

b) It should be reproducible so that changes in the implanted system are not masked by those of the measurement system.

c) It should enable timely diagnosis of impending defects so that the required remedial action can be planned and prepared for.

In 1965 Knuckey et al proposed a technique, termed photo analysis, which, it is believed, met the above criteria.

When the implanted pacemaker delivers an impulse to the heart a wave of electric current flows through the body. This wave, proportional to the current impulse of the pacemaker, can be monitored externally in a manner similar to a routine ECG.

The stimulating current ($\simeq$10mA) from the inaccessible pacer causes small artefact voltage changes ($\simeq$ 0.1V) across the thorax between the shoulders and to the abdomen. These can be conveniently sensed through the limbs using electrodes placed on the accessible wrists and ankle. The stimulus rate, duration and waveform can be recorded, whilst the vector derived from the relative magnitudes of the artefacts sensed between each two of the three limb connections (in the standard or Einthoven Electrocardiographic lead connections to right and left arms and a foot), gives a useful approximation to the orientation of the two electrodes between which the stimulating current passes through the body tissue.

"Photo-analysis" consists of the interpretation of the

rate, duration, amplitude and shape of the wave displayed on the oscilloscope screen.

The form of the wave depends on the output characteristics of the individual pacemaker and on the impedance of the load on the pacemaker. Hence any change in the form of the wave will indicate a change in the pacemaker's performance and/or the impedance of the electrical load. Such changes could possibly be used to monitor the implanted unit and its electrodes and perhaps even help predict and determine cause of impending failure to pace.

- Sources of Pacing Failure

Failure to pace may be caused by one of the four following problems:

1) Depletion of the self-contained energy source.

2) Damage of the lead conveying the stimulus the heart muscle.

3) Defects in the pacemaker circuit.

4) Increase of the stimulation threshold caused by either the growth of connective tissue or by electrode displacement. This increase in threshold is often referred to as "exit block".

In the past battery exhaustion took place in a relatively short period of time and hence was the major cause of failure to pace. However with the

prolonged life and greater reliability of modern Lithium-iodine cells, problems caused by lead damage have become more significant and it is with this source of pacing failure that this thesis will be concerned.

- Electrode failures

Lead damage can occur in two ways - 1) the insulation around the wire can rupture; or 2) the lead wire can fracture.

Rupture of the insulation on the lead to the cardiac electrode provides a third electrode, hopefully of only gradually increasing area, which provides an alternative route for the pacer current into the tissue and thus increases the loading of the pacer output. With a 'constant voltage' source pacer, the leakage current is in addition to the cardiac electrode current and will cause the battery to be drained more rapidly. For a 'current- linked' source any leakage reduces the current through the heart muscle with the risk of pacing failure.

Wire fracture, with the lead insulation remaining intact , may be of only one strand in a multifilar, may be total but making intermittent connection, may be total and dry or may be bridged by tissue fluid, as from a nearby rupture. Obviously a wire fracture which is total and dry will cause a failure to pace. For the less extreme cases the load impedance will

increase. With a constant current generator there will not be a pacing failure but energy will be wasted in the additional fracture impedance thus decreasing the life of the implanted unit. With a constant voltage pacer there will be a decrease in the current flowing through the heart muscle and hence a risk of pacing failure. Insulation rupture can also lead to corrosion of the lead wire by the body fluids and hence to its eventual fracture.

It is of course possible that both the lead wire and the insulation are completely fractured. In this case the remaining exposed wire would form the new electrode tip some distance away from the original site. It is very probable that there would be failure to pace for both types of generator output.

The two main modes of lead failure will effect differently the load on the pacer output. Ruptured insulation will decrease the load impedance whereas wire fracture will increase the load impedance. Several questions then arise. Do these changes in load impedance change the observable characteristics of a pacer's output? If so, can this change be used to detect impending failure to pace and indicate the cause of the eventual failure?

- Effect of Electrode Failure on Pacer's Output

Changes in impulse amplitude and shape have certainly been observed and used to diagnose wire fracture and insulation faults (Green et al, 1969; Sowton and Gray,

1971). These signs are not however universally present since the constant current operation of some current limited pacemakers can almost completely mask the appreciable increase in load impedance at a wet wire fracture or can make the alternative current path from an insulation rupture near its electrode termination ineffective for eliciting any changes in artefacts (Hepburn, 1979).

Hepburn (1978) showed that further useful indications could be derived from the observed waveform if the stimulus rate and duration are load dependent. Hepburn (1977, 1978, 1979) connected a resistive load to a range of pacemaker outputs and found that stimulus rate and duration are indeed load dependent. He observed that, for most of the pacers tested, as the resistive load was decreased (insulation ruptures) pacing rate and pulse duration both decreased. Conversely, as the resistive load was increased (wire fracture) he observed generally that the pacing rate and pulse duration increased.

Although Hepburn's observations have received wide clinical confirmation (eg. Hepburn , 1978) Hepburn's use of a simple resistance to represent the pacer's invivo load was questioned.

- Problem of Electrode System's Impedance

It is well known that at a pacing electrode, a square wave voltage stimulus, for example, results in a

current flow decreasing with time in a roughly exponential manner. This would indicate that the load impedance is not purely resistive as implied by Hepburn's work (1977). Generally it has been assumed that the response is truly exponential and hence the three component equivalent circuit model shown in figure 0.2 has been proposed (Weinmann and Mahler, 1964; Ohm, 1979). The model comprises the parallel combination of a capacitor , C_{dl}, and a resistance, R_{CT}, both of which are in series with another resistance ,R_{TOTAL}. R_{TOTAL} is the sum of all the series resistances in the system, including those due to the leads and that of the electrolyte. C_{dl} and R_{CT} are considered to represent the impedance of the electrode-electrolyte interface. C_{dl} represents the double layer capacitance and R_{CT} the charge transfer resistance. Unfortunately the response of a electrode system is not truly exponential. For example, plots of log i(t) against time, t, for an applied voltage step are not straight lines as would be expected (Turney, 1967; Briller et al, 1966), and hence even the above three component model is inadequate in modelling a system whose time constant appears to vary with time and hence frequency.

A further complication is that the electrode load impedance has been found to be very nonlinear, ie it depends on the amplitude of the applied impulse (Fischler and Schwan, 1981). The magnitude of the impedance has been observed to decrease with signal

amplitude.

- Goal of Thesis

This thesis will therefore be largely concerned with the modelling, both with physical and equivalent circuit models, of the load impedance due to the electrode system. If successful this would prove to be a breakthrough as Fischler and Schwan (1981) pointed out "there appears to be, so far, no model available which would account for both the linear and nonlinear behaviour of the electrodes in the frequency and time domain."

- Format of Thesis

The project has three distinct aspects:

1) The measurement and equivalent circuit modelling of the electrode-tissue/electrolyte load impedance. Measurement will involve the use of a.c bridge and transient techniques.

2) Observation of the dependence of the parameters of the equivalent circuit model on different kinds and degrees of damage to the electrode system.

3) The assessment of different pacemakers' sensitivities to the impedance changes have been observed for the two main types of electrode damage.

The chapters of the thesis are divided in the following manner:

VOLUME 1 : The Small Signal inter-electrode impedance

a) In Chapter 1, the form and origin of the observed electrode impedance is investigated for small amplitude, high frequency (above 100Hz) a.c. excitation i.e. under linear a.c. conditions. This chapter includes a detailed review of past experimental results and theoretical interpretations as well as the experimental results from this study.

b) In Chapter 2 the electrode impedance is investigated down to ultra low frequencies (milli hertz), as there is reason to believe (Geddes et al, 1971) that the low frequency impedance differs from that measured at higher frequencies. A mathematical and equivalent circuit model is proposed which represents the electrode's impedance over both the high and low frequency regions. A physical explanation of the observed low frequency behaviour is also proposed.

c) In Chapter 3 results obtained using pulse techniques are analysed. It is shown that for small amplitude pulses (ie in the linear region) the same comprehensive model as derived using the a.c impedance technique is valid.

VOLUME 2 : Nonlinearity of the inter-electrode impedance and the study of electrode failures

d) In Chapter 4 the electrode system's nonlinearity is investigated using the a.c impedance technique. Changes in the equivalent circuit's component values with applied signal amplitude are studied and explained using the physical model.

e) In Chapter 5 the electrode system's nonlinearity is investigated using the transient technique and again changes in equivalent circuit component values are studied and explained.

f) In Chapter 6 the effects of various types of electrode failure on the system's impedance in both the linear and nonlinear regions are investigated and correlated using a.c and transient techniques.

g) In Chapter 7 the sensitivities of several different pacemakers to the above impedance changes are assessed in an effort to determine the feasibility of "photo-analysis" in predicting and distinguishing various types of electrode failure.

h) In chapter 8 the main points of the thesis are reviewed and areas for further research suggested.

CHAPTER ONE

The physical and equivalent circuit modelling of the interfacial impedance under high frequency (>100HZ), small signal a.c. conditions.

1.1 THEORETICAL SECTION

1.1.1 Introduction to the problem

-Electrode impedance as a function of frequency.

When stimulating or recording from biological systems, the inadequately understood characteristics of the electrode-tissue interface are an obstacle to detailed interpretation of observed phenomena. In order to record or stimulate some current must flow through the circuit. In the electrodes and the leads of the external circuit, charge is carried by electrons, whereas, in the solution or tissue between the electrodes, the current is carried by ions. Obviously there must be transitions at the interfaces between the electrodes and the solution/tissue. At the electrode-electrolyte interface, there is therefore an impedance to the transfer of charge from one kind of carrier to the other. Unfortunately this interfacial impedance, Z_i, is not trivial and the mechanism will therefore require detailed investigation.

If an alternating current is passed between two electrodes in an electrode- electrolyte system, an alternating voltage drop appears across the electrodes. The phase of this voltage drop lags behind the phase of the current, ie the impedance is capacitive. The ratio of the a.c. voltage to the a.c. current gives the inter-electrode impedance at the ap-

plied frequency. Information on the electrode system's impedance is frequently sought from, and expressed as, series real and imaginary components, R_S and X_S ($X_S=\frac{1}{\omega C_S}$), measured at successive frequencies over the range of interest. Measurements have shown (Wein, 1896; Warburg, 1899) that R_S and C_S decrease in magnitude as the frequency is increased. Generally the indifferent electrode has a much larger area than that of the active electrode, and, as impedance is inversely proportional to area, the contribution of the large area electrode can be ignored. After subtraction of the contribution of the frequency independent resistance, R_{TOTAL}, (due to the sum of the lead and saline resistances, R_{LEAD} and R_{SALINE}), the resultant values of the series reactance, X_i, and resistance, R_i, due to the interfacial impedance of the active, small area electrode have been observed to vary with the same fractional power, β , of the frequency, f, (Fricke, 1932; note that Fricke used different notation to that used here).

$$\text{ie} \quad -X_i = -X_S = A\omega^{-\beta} \qquad \text{eqn} \quad 1.1$$

$$R_i = R_S - R_{TOTAL} = B\omega^{-\beta}$$

where A and B are constants with units of $\Omega \text{sec}^{-\beta}$, $0 < \beta < 1$ and $\omega = 2\pi f$.

It has been observed that the phase angle, ϕ ,of the interfacial impedance ,Z_i,is almost constant over the measurement frequency range (Wein, 1896; Fricke, 1932)

as would be expected from the equation :-

$$\phi = \tan^{-1}(X_i/R_i) = \tan^{-1}(A/B) = \text{constant}$$

More interesting was Fricke's observation that the phase angle ϕ was related to the fractional power, β, such that

$$\phi = \beta\pi/2 \text{ radians} \qquad 1.2$$

[The relationship between phase angle and the exponent β is a necessary condition for a linear, stable system as shown by the Kramers-Kronig relation].

Hence it was found that the frequency dependent components of an electrode-system's impedance had its origin at the small area electrode-electrolyte interface and that these were in series with the resistances of the leads and the electrolyte as shown in figure 1.1

DeBoer and Van Oosterom (1978) suggested the combining of R_i and X_i to give the following expression for the interfacial impedance, Z_i.

$$Z_i = R_i - jX_i = B\omega^{-\beta} + jA\omega^{-\beta}$$

$$= K(j\omega)^{-\beta} \qquad 1.3$$

Where $K = B/(\cos\phi)$ has units of $\Omega\ \text{sec}^{-\beta}$

R_i and X_i can be expressed in terms of K and β as

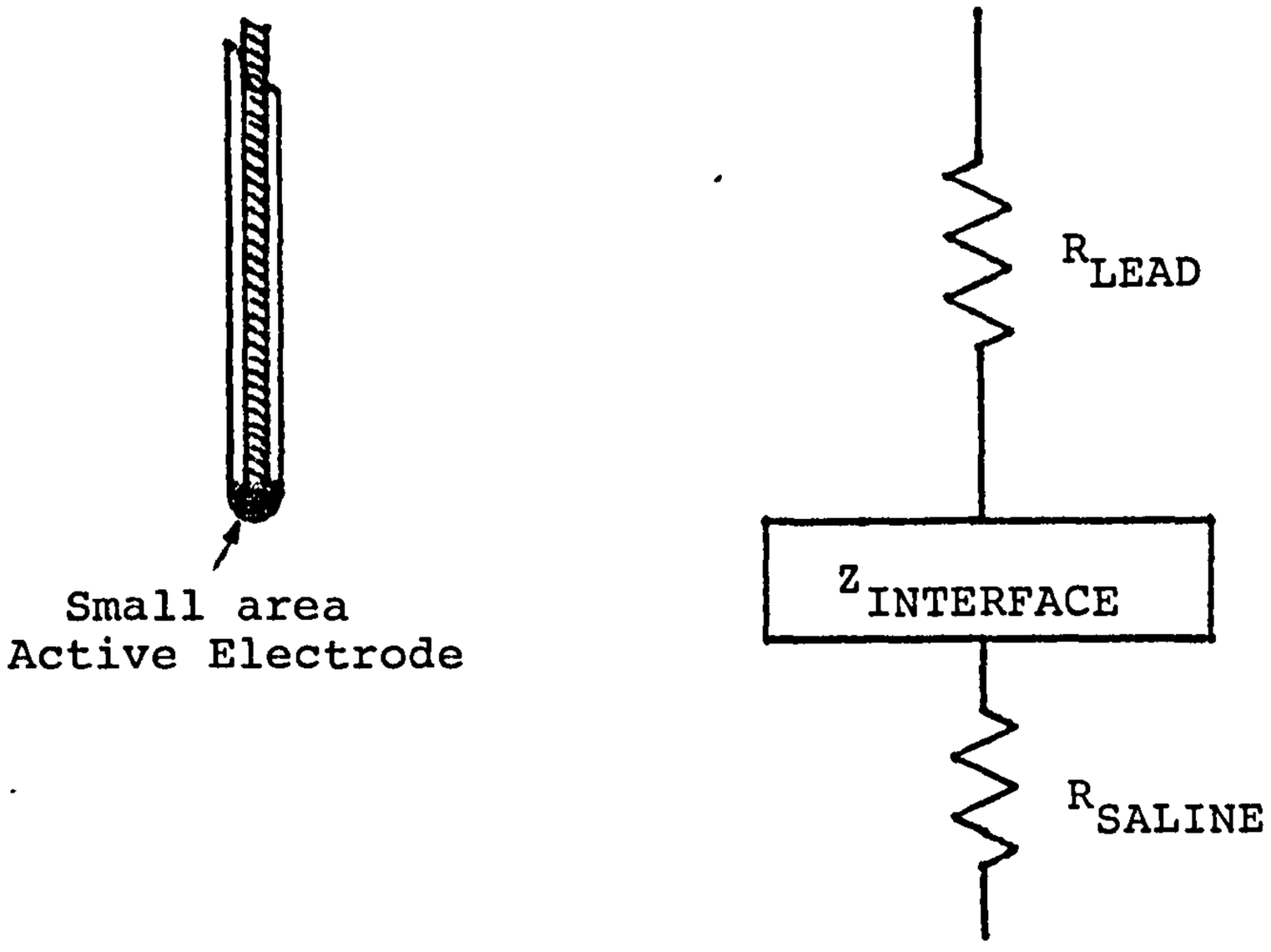

INTERELECTRODE IMPEDANCE

Figure 1.1

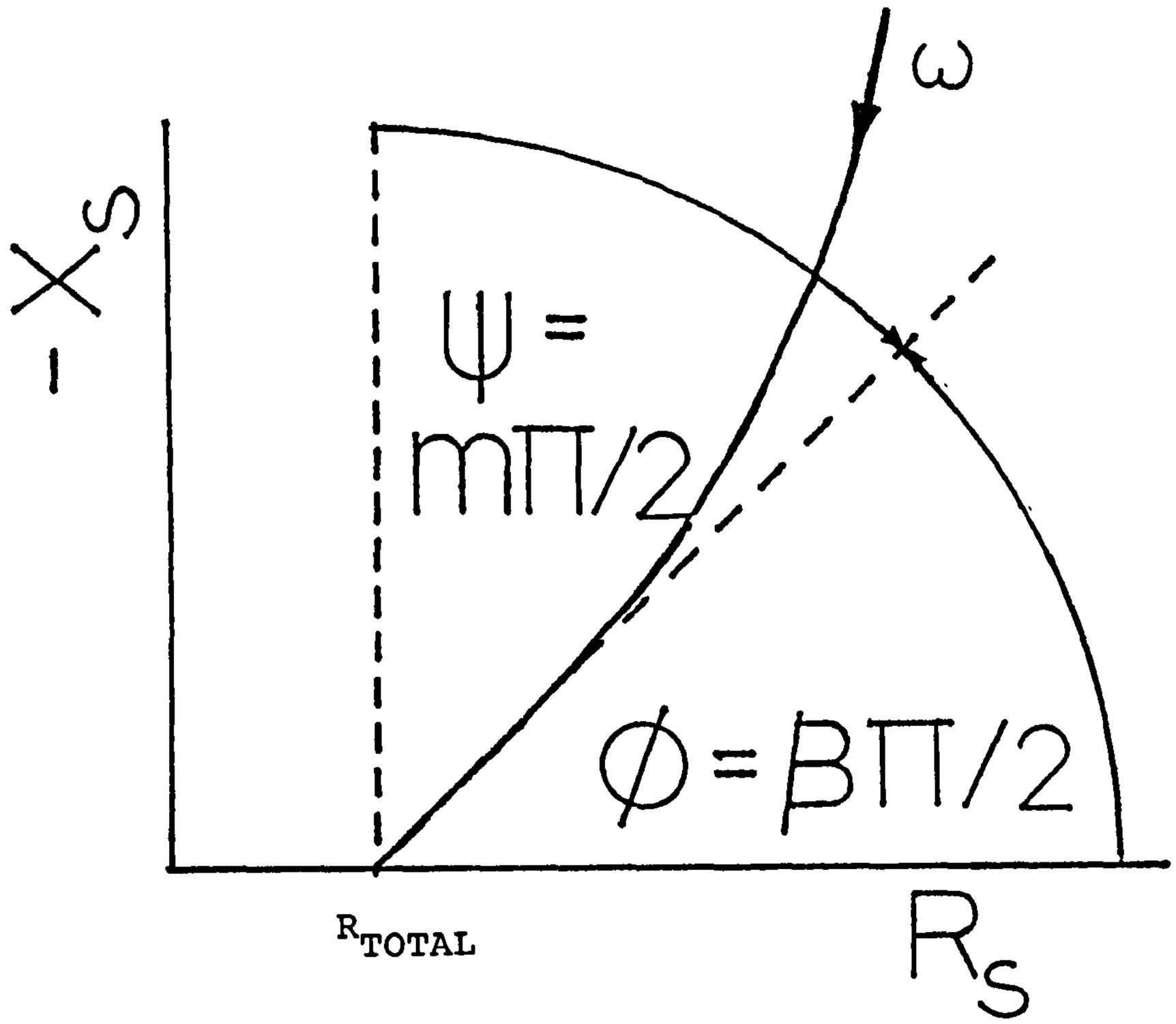

INTERELECTRODE IMPEDANCE LOCUS

Figure 1.2

follows:

$$R_i = K\,\omega^{-\beta}\,\mathrm{Cos}(\beta\pi/2)$$

$$-X_i = K\,\omega^{-\beta}\,\mathrm{Sin}(\beta\pi/2)$$

$$C_i = \frac{1}{K\,\omega}\;\mathrm{Cosec}(\beta\pi/2)$$

From the above it is noted that if one can measure $R_s(f)$ one can automatically account for the corrosponding $C_s(f)$ law or vice-versa. The magnitude of the interface impedance is given by:

$$Z_i = (R_i^2 + X_i^2)^{1/2} = K\omega^{-\beta}$$

and the phase angle by:

$$\phi = \arctan(X_i/R_i) = -\beta\cdot\pi/2 \text{ radians} \qquad \text{(eqn 1.2)}$$

The observation that the measured phase angle is constant and frequency independent over the applied range of frequencies has lead to the impedance being termed a "Constant Phase Angle" impedance, or Z_{CPA} for short. It must however be noted that a 'constant phase angle' impedance ,Z_{CPA}, cannot be represented by a finite number of capacitors and resistors (unless of course β =0 or 1), and that the use of the complex impedance, Z_{CPA}, is merely one way of expressing experimental results as it has no physical meaning in itself.

As the exponent β is generally not equal to zero,i.e. the electrode interface is not purely resistive, this infers that there is conservation of energy as well as dissipation of energy at the interface. As the phase angle is constant and independent of frequency the ratio of the average energy stored to the energy dissipated per cycle must also be a constant and independent of the applied frequency (Cole-Cole,1941).

It has been reported (Fricke, 1932; Schwan, 1963; Jaron et al, 1968), that when the interfacial impedance is measured over a wide frequency range, the value of is observed to gradually change with frequency. The low frequency value of β is larger than at high frequencies. Thus a plot of $-X_S$ versus R_S for an electrode system has the form shown in figure 1.2 over a wide frequency range (eg Delevie, 1965 and DeRosa and Beard, 1977).

Hence the phenomenological, constant phase angle impedance, Z_{CPA}, is only a good model of an electrode's impedance over a limited frequency range. For more extended ranges of frequencies this mathematical model must also contain terms which reproduce the observed increase in phase angle at low frequencies.

- Need of a Physical Model

Not only is a more adequate mathematical or equivalent circuit model necessary, but a physical explanation of the form of the observed electrode impedance is also

required.

Many researchers (eg Schwan, 1968; Simpson et al, 1980) attribute the peculiar frequency dependence of the interface impedance to "polarisation" effects. This terminology is very probably due to the work of Fricke (1932).

Fricke assumed arbitrarily that at a time t_o an impulse of current, idt_o, passed across the interface which produced a counter emf at a later time, T, given by:

$$V(T-t_o) = V(\Delta t) = V_o(\Delta t)^{-m}$$

here $1>m>0$

Hence the potential difference across the interface caused by the transfer of charge is assumed to decay with elapsed time, Δt, according to $V(\Delta t)=V_o(\Delta t)^{-m}$

He then used a Duhamel superposition integral to derive the following expressions:

$$R_i = V_o \omega^{-1+m} \Gamma(1-m)\sin(m\pi/2)$$

$$X_i = V_o \omega^{-1+m} \Gamma(1-m)\cos(m\pi/2)$$

$$C_i = \omega^{-m}/V_o \Gamma(1-m)\cos(m\pi/2)$$

$$\tan\psi = C_i\omega R_i = \tan(m\pi/2)$$

$$\psi = m\pi/2 \text{ radians}$$

Fricke's relationships are identical to equations 1.4 with

$$K = V_o\Gamma(1-m) \qquad \psi = \pi/2 - \phi$$

and

$$\beta = 1-m$$

Fricke attributed the frequency dependence to "spontaneous depolarisation" of the electrode, but the detailed mechanism of such a phenomenon was not explained. Fricke also termed R_i and C_i as "polarisation" elements and most researchers have since adopted this term. However Cole and Curtis (1938) pointed out that "the use of the term polarisation for describing the unexplained effects occurring at the metal electrolyte interface, is only an admission of our ignorance". In fact the term "polarisation" is incorrect in this instance and will be explained in section 1.1.2.2. [Note: Although Fricke is generally credited with first 'discovering' the above 'classical' equations, his derivations were not only wrong (D.C. Salter, 1979), but almost identical equations had been published many years earlier (Hopkinson and Wilson 1897)].

Hence one is still left with the problems of mathematically and physically modelling the observed electrode impedance.

1.1.2 Review of proposed physical and equivalent circuit models of the Interface Impedance under linear a.c. conditions

-Introduction

A review of the state of the art will involve the study of theories and experimental results from a wide range of disciplines, e.g. pacing, biomedical engineering, electrochemistry and solid state physics amongst others. In the past the majority of research carried out in this field by biomedical engineers has been empirical by nature with relatively little attention being paid to underlying physical processes. From time to time, what appear to be intuitive suggestions have been made without being rigorously investigated. As a consequence there exists in the published literature a range of possible physical explanations of the observed interfacial behaviour. These will be reviewed in this chapter (hence its size), some will be discarded as improbable while a few will be identified as probable candidates. It is hoped that this review, and the thesis as a whole, will lay the foundation for, and point the direction of, future, more concerted research into this interesting field of study.

.

According to Bockris and Drazic (1972),"Electrochemistry is the study of the effects occurring at the interface between an electronically conducting phase (usually a metal) and an ionically conducting phase (usually a solution in water)". It is therefore logi-

cal to first look to electrochemistry for an explanation of the observed impedance results.

In this field two main physical processes have been put forward to explain the observed frequency dispersion, namely diffusion and specific adsorption. However electrochemical theory is based on the assumption that the electrode surface is smooth, which is not the case with solid electrodes, and hence surface roughness effects will also have to be considered. Some electrochemists (eg De Levie, 1965; 1967) and many solid state physicists (eg Bottelberghs, 1976) have even attributed the observed frequency dispersion to the roughness of the electrode. Hence the following three main phenomena (along with several minor ones) will be considered - diffusion, specific adsorption and surface roughness.

In order to comprehend the electrochemist's view of an electrode-electrolyte system it must be understood that in the past the interface problem has been approached in two different ways by electrochemists, and it is important to discuss these before considering any of the above three phenomena.

(i) The "double layer" model arises from the assumption that little or no current is passing in either direction across the interface. When electrons are removed from or supplied to the metal side of the interface an excess charge will

exist. This charge on the metal side will attract ions of opposite charge to the solution side of the interface. There will now exist a "double layer" of charges at the interface which closely resembles a capacitance.

(ii) As pointed out, however, the above model does not consider any charge transfer across the double layer. This is a serious omission as any interface which is charged will have some current passing - even if the net current flow is zero. The study of the electrode processes involved in this flow of current is called "Electrode Kinetics", and this is the basis of the second electrochemical model.

Hence there are two types of processes occurring at electrodes.

1) Charges (eg electrons) are transferred across the electrode-electrolyte interface due to an electrochemical reaction. This electron transfer causes oxidation and reduction to occur and since these reactions are governed by Faraday's law, they are termed "faradaic processes". Faraday's law states that the amount of substance transformed by electrolysis is proportional to the amount of charge passed. A simpler definition is that any process which allows d.c. current to flow can be regarded as faradaic, whereas one

which does not can be regarded as nonfaradaic. Charge transfer and diffusion are considered as faradaic (Grahame, 1952).

2) In contrast to the above is the nonfaradaic process of charging the double layer. This has generally been represented by a simple capacitance, termed the "double layer" capacitance, C_{dl}. Although in this case charge does not cross the interface, external currents do however flow, albeit transiently.

The faradaic and nonfaradaic currents have generally been considered independent and to flow in parallel, as shown on figure 1.3.

In the past it has also generally been assumed that one could study faradaic and nonfaradaic components of the total current (and hence their impedances) separately as they were considered to be independent. It is now however well established that there is coupling between the nonfaradaic, double-layer charging process and the faradaic process, ie the double layer impedance depends on the concentrations of the electroactive species taking part in the faradaic process (Sluyters-Rehbach and Sluyters, 1970). Even when allowing for this dependence researchers have continued to represent the double layer charging process as a pure capacitance in parallel with the faradaic impedance. However recent evidence shows that even this assumption is incorrect (Reinmuth, 1968). The history of such approximations is

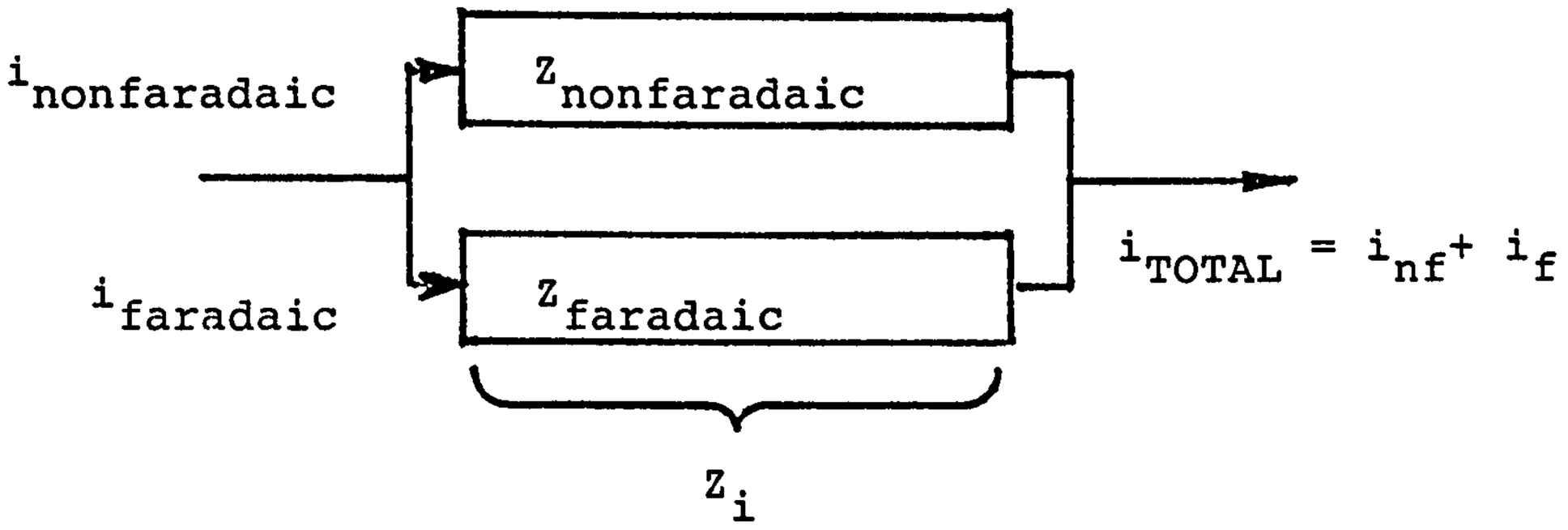

PARALLEL MODEL OF THE INTERFACE IMPEDANCE

Figure 1.3

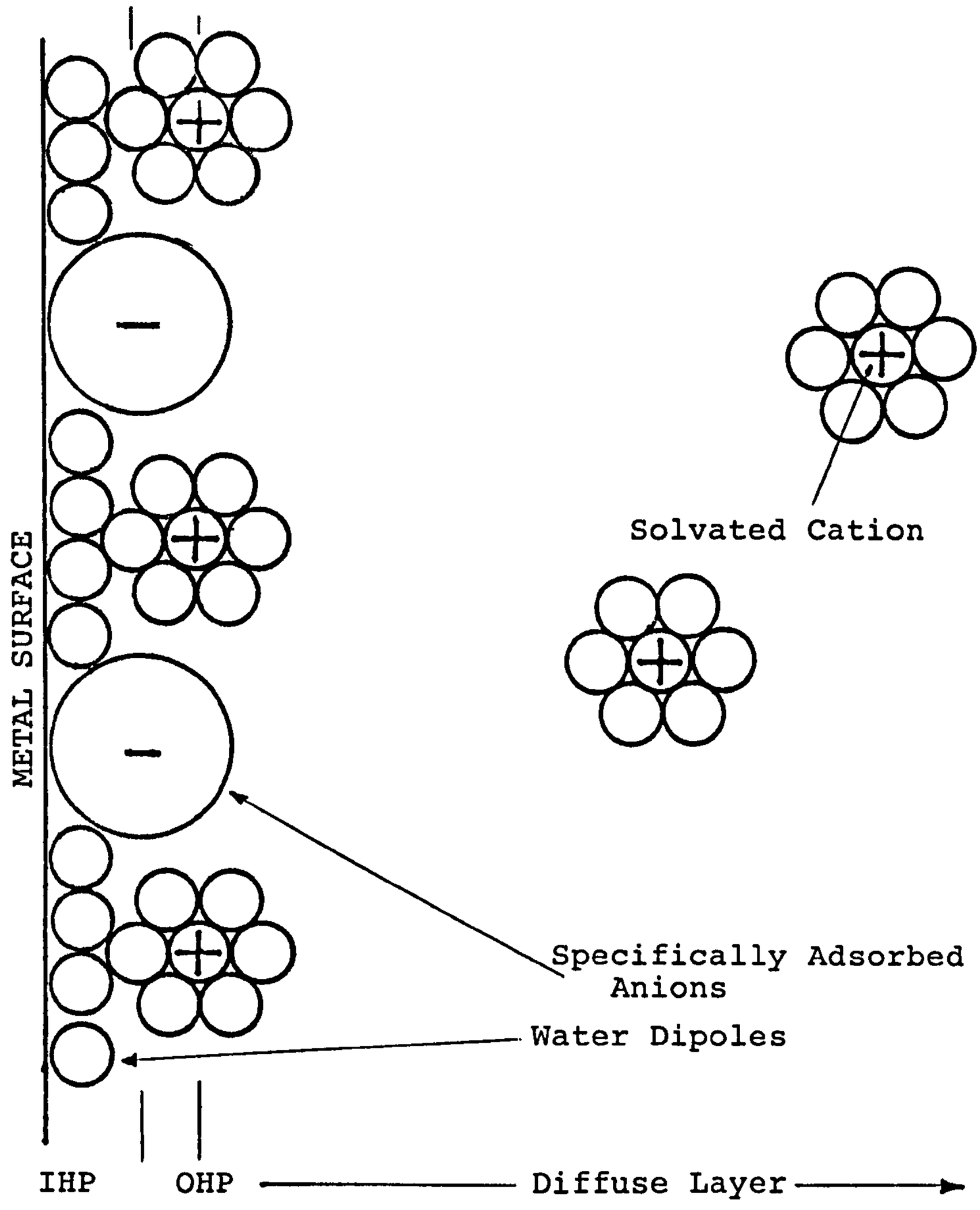

ELECTRODE-ELECTROLYTE INTERFACE

Figure 1.4

reviewed in more detail in later sections.

In the next few sections aspects of electrochemistry which have a bearing on the study of the impedance of the electrode-electrolyte interface are reviewed in some detail. These will include the nonfaradaic double layer capacitance and the faradaic processes of charge transfer and diffusion. Specific absorption can not be classified satisfactorily in either group as it has properties of both.

1.1.2.1 Double Layer Capacitance

Although the simple double layer capacitance has not generally been suggested by electrochemists to explain the observed frequency dispersion, it is necessary to introduce this process as it becomes important when considering surface roughness and adsorption effects.

The electrode-electrolyte interface has been found to behave somewhat as a capacitor. At a given potential there exists a charge on the metal electrode, q_m, and an equal but opposite charge in the solution, q_s, where $q_m = -q_s$.

The charge on the metal, q_m, represents an excess or deficiency of electrons and resides in a very thin layer on the metal surface. The charge in the solu-

tion, q_s is made up of an excess of either cations or anions near the electrode surface.

The simple "double layer" capacitor model was first suggested by Helmoltz, when it was imagined that the excess charges on the solution side formed a thin layer of charge similar to those on the metal surface. Thus he considered that there were two sheets of charge, having opposite polarity, separated by a very small distance (see figure 1.4). It is due to this simple model that the term "double layer" was first coined.

The electrode surface is largely covered by a layer of water dipoles and the excess charge on the metal produces a preferential orientation of these water dipoles. This water layer is termed the hydration sheath of the electrode. The solvated ions can only approach the electrode to a distance determined by the width of the electrode's hydration sheath and their own solvation sheath. The locus of centres of the closest solvated ions has been termed the Outer Helmholtz plane, O.H.P.

In the simple Helmholtz model the excess charge at the O.H.P. due to these solvated ions is equal and opposite to that on the metal, ie $q_m = q_s(OHP)$. Such a model is equivalent to a parallel plate capacitor and hence the stored charge density, q/A, is given by:

$$q/A=(\varepsilon_r \varepsilon_o V)/d \qquad 1.5$$

Where ε_r is the dielectric constant of the medium, ε_o is the permittivity of free space, d is the interplate spacing and V is the voltage across the electrode-electrolyte interface.

The differential "double layer" capacitance is therefore given by:

$$C_{dl} = \partial(q/A)/\partial V = \varepsilon_r \varepsilon_o / d \qquad 1.6$$

According to this equation C_{dl} is constant and independent of voltage and concentration. Unfortunately, however, it is well known that the double layer capacitance does vary with the above parameters (Bard and Faulkner, 1980) and hence this simple model is inadequate.

Gouy and Chapman (1910 and 1913) proposed that the charge in the solution side was diffuse and not concentrated in a thin film at the Outer Helmholtz Plane, ie the excess charge on the O.H.P. is not equal to, but is less than that on the metal. As an electrolyte has a relatively low density of charge carriers it will take a significant thickness of solution to accumulate the excess charge needed to counter balance the stored charge density on the metal side. The greatest concentration of excess charge will of course be near to the metal electrode, where electrostatic forces are most able to overcome the thermal motion

processes. The concentration will progressively lessen with distance from the interface as the weaker electrostatic forces are unable to hold the ions which are continually dispersed away from the interface by thermal motion. The average distance of charge separation should replace "d" in the above equation (1.6). One would expect that the average distance would depend on the potential and on the electrolyte concentration as is observed experimentally (Bard and Faulkner,1980).

Gouy and Chapman calculated that the differential capacitance of the diffuse layer, C_D, would have a hyperbolic dependence on voltage, ie C_D would be proportional to Cosh(V), where V is the voltage.

The plot of C_D against voltage should hence be 'U' shaped and C_D would have a minimum when $q = q_s = q_m = 0$. The potential at which this occurs has been termed the "Potential of Zero Charge", P.Z.C..

Gouy and Chapman considered the ions as point charges which could approach the surface arbitrarily closely - which is improbable. This assumption would result in the diffuse layer capacitance increasing indefinitely. However actual electrode systems show a flattening in capacitance at more extreme potentials (Bard and Faulkner,1980).

Stern (1924) finally suggested that the solution side

of the "double layer" was made up of at least two layers - his model in effect was a combination of the previous two:

1) In the simple case of electrostatic attraction the solvated ions in the electrolyte can only approach the interface as far as the Outer Helmholtz Plane.

2) The electrostatic forces are unable to hold all the ions present at the minimum distance (the Outer Helmholtz Plane) as thermal motion continually disperses them away from the electrode. This region beyond the Outer Helmholtz Plane forms the diffuse part of the double layer.

The interaction of these solvated ions with the charged metal only involves "long-range" electrostatic forces and their interaction is essentially independent of the chemical properties of the ions. These ions are therefore said to be "nonspecifically adsorbed".

A species is considered adsorbed when its concentration in the interface region differs from that in the bulk. As has been seen with reactive species, ions of opposite charge are attracted to metal surfaces and ions of similar charge are repelled. This type of adsorption is termed 'non-specific' or Coulombic adsorption and can be explained by coulombic forces. However in many real cases there is a specific (ie ion dependent) force at the interface which renders void the

simplicity of the electrostatics approach. This "specific" adsorption will be studied in a later section.

The measured capacitance of an electrode (in the absence of specific adsorption) has been represented by an equivalent electrical circuit consisting of a series combination of the capacitances due to the outer Helmholtz layer and that due to the diffuse layer.

The overall "double layer" capacitance in terms of the contributions of these two regions is given by:

$$\frac{1}{C_{dl}} = \frac{1}{C_{OHP}} + \frac{1}{C_D}$$

The value of C_{OHP} is independent of potential whereas C_D varies with potential. The composite capacitance, C_{dl}, will show a complex behaviour and will be governed by the smaller of the components.

At large polarisations C_D becomes so large that it no longer contributes to C_{dl} and one is left with a constant capacitance equal to C_{OHP}.

Gouy and Chapman's model has been reviewed in this chapter as a possible source of the electrode's observed voltage dependence. Unfortunately, however, except in very dilute solutions, the diffuse charge

region is so thin that the so called "diffuse charge" is in fact located on a plane - the O.H.P. This would give rise to a constant, voltage independent capacitance as before. The observed voltage dependence in moderately concentrated solutions must therefore be due to some other factor. It will be shown later that this factor is "specific adsorption" and that "specific adsorption" effects give rise to frequency dependence of the interface impedance. It is therefore an important area of study.

1.1.2.2 Faradaic Processes

- Charge Transfer and Diffusion

-Faradaic reactions

Current which flows across the electrode-electrolyte interface by virtue of reactions such as reduction and oxidation (ie "redox" reactions) is termed faradaic current, as the reactions involved obey Faraday's law.

The simplest situation to consider is that of a metal electrode placed in a solution of its own ions. In such a case the metal electrode takes part in the chemical reaction. However, noble metals, which are generally used for biomedical applications, are said to act only as catalytic surfaces on which reactions occur and do not enter into the reaction themselves as does the above "metal-ion" electrode.

An example of the catalytic role of noble metals is the

immersion of platinum electrodes in a solution containing chloride ions with chlorine gas bubbling around the cathode. The oxidation-reduction reaction is:

$$2Cl \rightleftharpoons Cl_2 + 2e^-$$

In this case electrons are supplied to or from the platinum electrode without it actually taking direct part in the reaction. Unfortunately the noble metal-electrolyte interface is much more complicated than shown above. Many different reactions are possible, several may take place simultaneously and the noble metal may even take part in some of the reactions (Brummer and Turner,1977).

The simple metal-ion electrode reaction system will, therefore, be discussed first to illustrate the basic principles involved.

- Equilibrium Conditions

When a metal electrode is immersed in a solution of its own ions a potential is established between the metal and the solution. The magnitude of this potential difference is determined by the electrode material and the composition of the solution.

Some electrode atoms lose electrons and pass into the solution as metal ions causing the electrode to become negatively charged with respect to the solution:

$$M \rightarrow M^+ + e$$

The above reaction is termed oxidation.

The above reaction is termed oxidation.

Similarly, some of the metal ions in solution will take electrons from the metal and deposit as metal ions, leaving the electrode charged positively with respect to the solution:

$$M^{+} + e \rightarrow M$$

This reaction is termed reduction.

The final potential set up at the interface depends upon the position of this equilibrium which, in turn, depends upon the relative activities of the oxidised and reduced species involved. As the system is in thermodynamic equilibrium the potential is called the "reversible" electrode potential, E_{rev}.

[Note:Activity expresses the availability of a given ion species to participate in a chemical reaction. It is the concentration of ions that, when interionic effects are absent, would produce the same effects as the real solution. The activity, a, is expressed as:

$$a = \gamma C$$

where C is the concentration

and γ is the activity coefficient.

γ is the factor by which the activity differs from the concentration and is therefore a measure of the interaction between the ions. When the

solution is infinitely dilute, $\gamma = 1$ and the activity is equal to the concentration.]

The relationship between the electrode potential and the activities of the oxidised and reduced forms is given by the Nernst equation:

$$E_{rev} = E^{o} + \frac{RT}{nF} \ln \frac{\text{activity of oxidised form}}{\text{activity of reduced form}} \qquad 1.7$$

where

E_{rev} is the reversible electrode potential

E^{o} is the standard electrode potential

(ie the electrode's potential relative to the standard hydrogen electrode)

R is the Gas constant

n is the number of electrons involved in the electrode reaction $m^{+n} + ne \rightleftharpoons m$

T is the temperature (^{o}K)

F is the Faraday constant

At the equilibrium or reversible potential the currents due to the oxidation reaction and the reduction reaction are equal and opposite, ie there is no net current flow. Such 'reversible' charge transfer will therefore always involve both an oxidation reaction and the corresponding reduction reaction. The common value of the currents is termed the "exchange" current, i_o, and is an important parameter as shall be seen later.

-Non-Equilibrium Conditions

Polarization , Over-potential and Faradaic impedance

If the electrode system is now connected to an external source which applies a potential of magnitude E, a faradaic current, i_f, will be forced to flow through the system and the electrode potential shifts to the new value. A voltage of magnitude $i_f Z_f$ will be dropped across the faradaic impedance, Z_f, such that:

$$i_f Z_f + E_{rev} = E$$

(neglecting the contribution of R_{TOTAL}, see figure 1.5)

The departure of the electrode potential from its reversible value, E_{rev}, is termed 'polarisation' and the electrode system is now said to be operating irreversibly.

The term 'polarisation' is often misused and sometimes applied to aspects of an electrode's electrical behaviour which are not understood. Polarisation can be defined as "the departure of the electrode potential from the reversible value upon passage of faradaic current" (Bard and Faulkner, 1980). The larger the departure, the larger the extent of polarisation is said to be. The extent of polarisation is measured by the over-potential, η , where:

$$\eta = E - E_{rev} = i_f Z_f \qquad 1.8$$

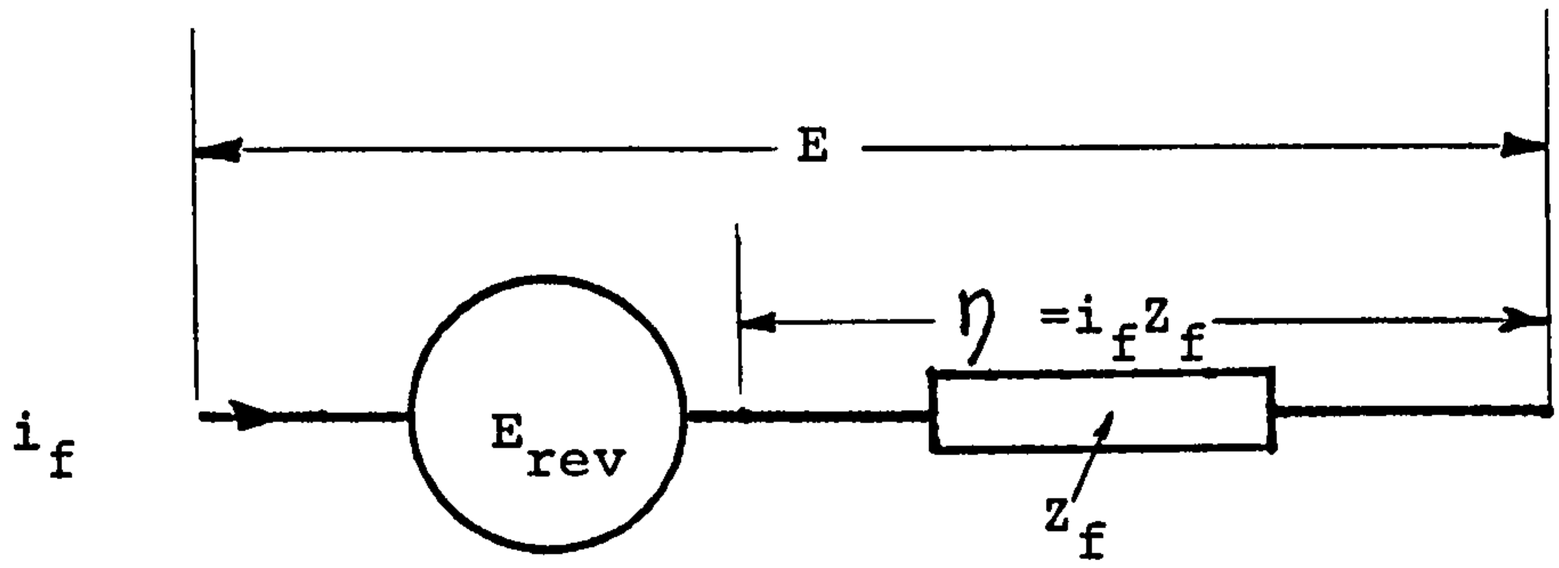

OVERPOTENTIAL

Figure 1.5

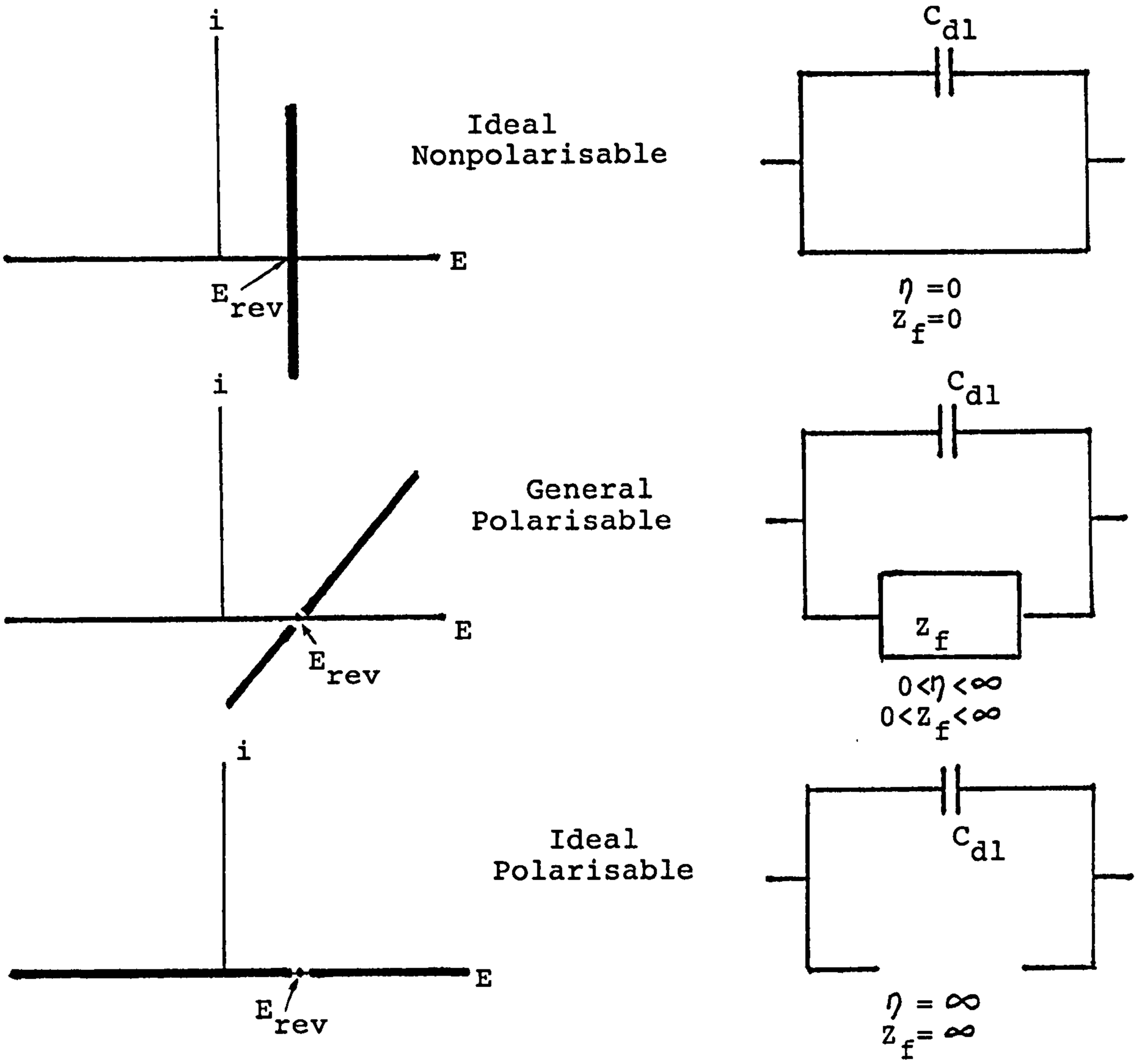

POLARISATION

Figure 1.6

Hence if η is non-zero, the electrode is polarised and operating irreversibly.

For an ideal " nonpolarisable" electrode there is no impedance to faradaic current, ie $Z_f = 0$. Thus in this case the electrode potential does not change upon the passage of current, that is, it remains at the reversible potential, E_{rev}.

For an ideal "polarisable" electrode no faradaic current flows across the interface, ie Z_f is infinitely large. For such an electrode system there would be an extremely large over- potential, η , upon the passage of even an infinitesimal current if that were possible.

In real situations an electrode is neither ideally polarised nor ideally nonpolarised. The current flow across the electrode-solution interface will experience a finite, non zero faradaic impedance, across which an over-potential is developed (see figure 1.6).

- Subdivision of the Faradaic impedance

The faradaic electrode reaction, $O + n \rightarrow R$, is composed of a series of steps that cause the conversion of the dissolved oxidised species, O, to a reduced form R also in solution. The simplest reactions involve only mass transfer of a reactant to the electrode, electron transfer (involving non-specifically adsorbed species) and mass transfer of the product back to the

bulk solution (see figure 1.7)

As we have seen, for a given current, i_f, there will be an over-potential, $\eta = i_f Z_f$, dropped across the faradaic impedance, Z_f. This over-potential can however be considered as the sum of a series of smaller over- potentials due to the different reaction steps, eg

ηM.T.(O) (the mass transfer over-potential for the oxidised species)

ηC.T. (the charge transfer over-potential) and

ηM.T.(R) (the mass transfer over-potential for the reduced species)

The impedance, Z_f, which represents the total electrode reaction, can therefore also be subdivided into a series of smaller impedances representing the various steps in the overall reaction: $Z_{M.T.(O)}$, $Z_{C.T.}$, $Z_{M.T.(R)}$ etc. (see figure 1.8).

$$\eta = i_f Z_f - i_f Z_{MT(O)} + i_f Z_{CT} + i Z_{MT(R)}$$

$$= \eta_{CT} + \eta_{MT(O)} + \eta_{MT(R)}$$

The impedances for the mass transfer of the oxidised and reduced species are generally lumped together

$$\eta_{MT(O)} + \eta_{MT(R)} = \eta_{MT}$$

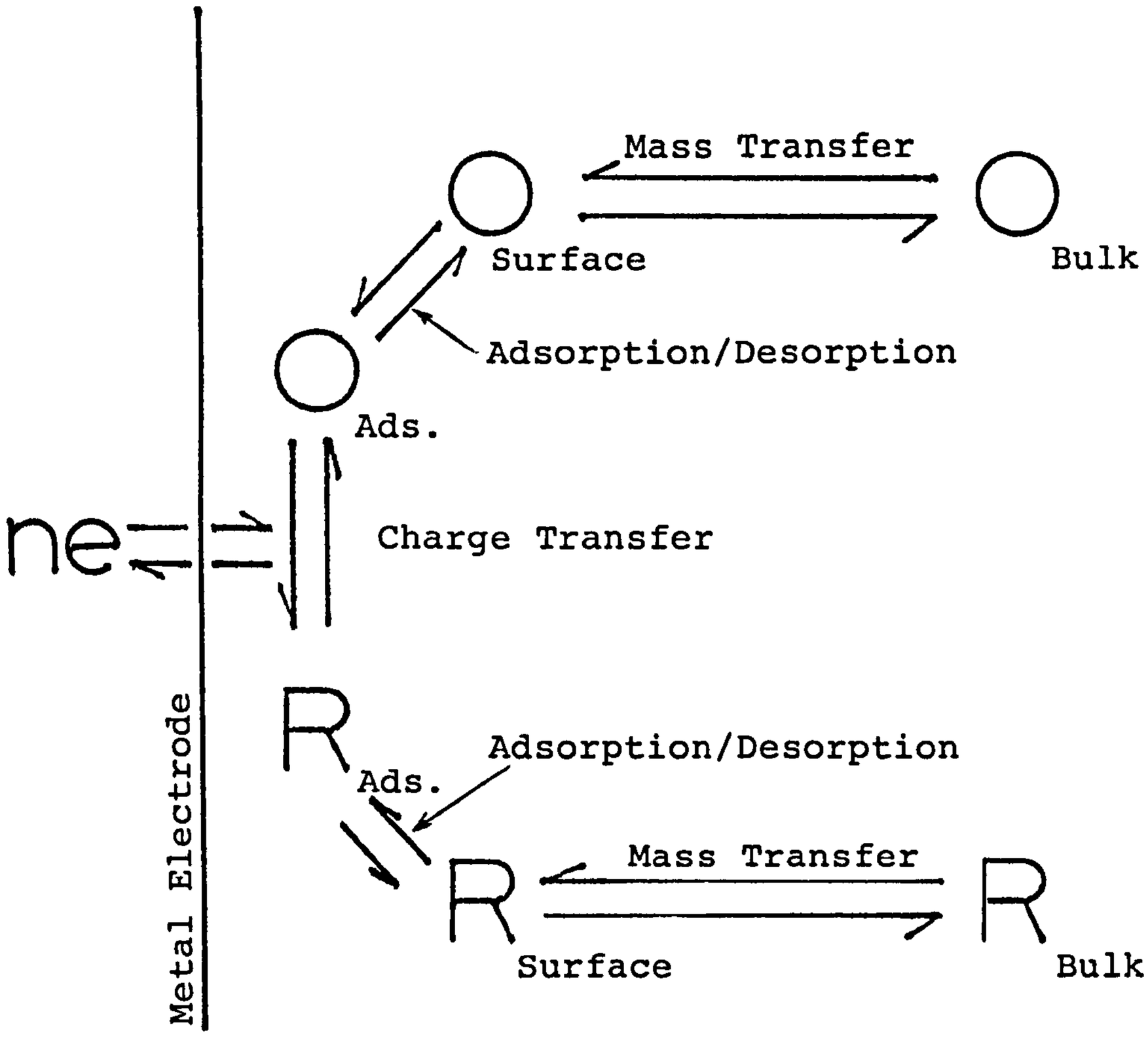

REACTION STEPS

Figure 1.7

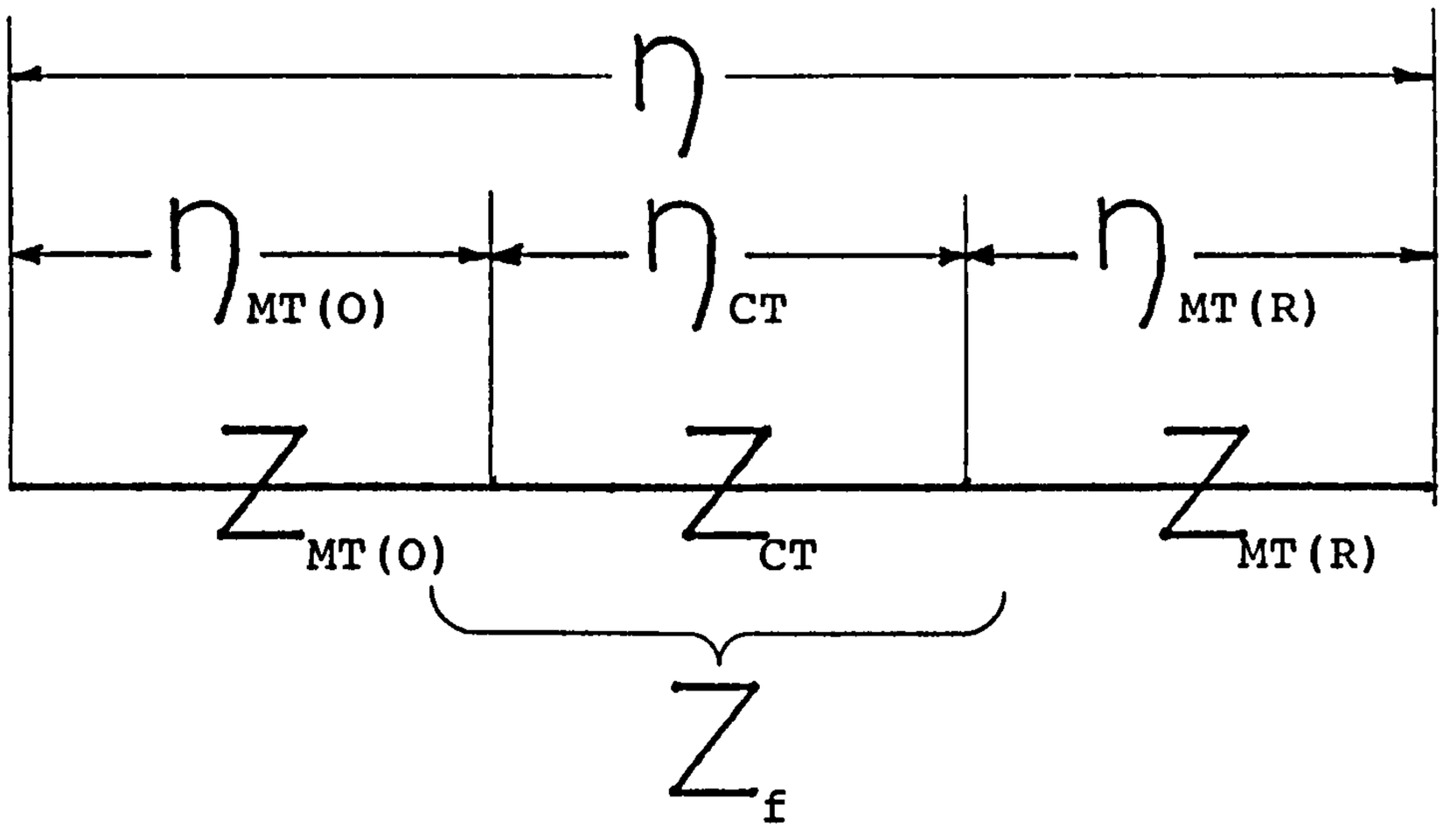

SUBDIVISION OF Z_f

Figure 1.8

A fast reaction step has a small impedance to current flow, whereas a slow step has a large impedance. The slowest step in a reaction, ie the one which gives rise to the largest impedance to current, dominates the overall faradaic impedance. Such a slow step is called the "rate-determining step" as the rates of all the other reaction steps are limited by that of the slow step.

- Charge Transfer

Transfer of charge across the interface consists essentially of the exchange of electrons between the electrode and ions on the solution side, ie in IHP or OHP. Such an exchange of course implies that current flows across the interface.

If, for example, the electrode system is connected to an external source of potential more positive than the reversible potential of the electrode, electrons will leave the electrode at a greater rate than in the reversible operation. This loss of electrons will disturb the equilibrium.

In an attempt to meet the need of electrons and hence restore equilibrium the metal electrode dissolves to give up electrons to replace those removed. The resultant metal cations flowing into the solution:

$$M \rightarrow M^{+} + e$$

As we have seen, the exchange current, i_o, is equal to

the dissolution current under equilibrium conditions. If the dissolution of the metal is relatively slow, ie if the new current i is larger than i_o, the rate of loss of electrons will be greater than the rate of production by dissolution of the metal. There will therefore be a build up of positive charge on the electrode causing it to become more positive than the reversible potential i.e. the electrode becomes polarised and there is an over potential, η_{CT}.The slower the dissolution the more easily will polarisation develop. As the exchange current density is a measure of the speed of the dissolution reaction it will provide an indication of the liability of the system to polarise. It is evident that the larger the value of i_o, the easier the electrode can cope with a given current, i, and the smaller will be the charge transfer over potential, η_{CT}.

As the charge transfer impedance, Z_{CT}, is equal to η_{CT}/i, it will be inversely proportional to the exchange current, i_o.

- Diffusion or Mass Transfer

For an electrode reaction to continue, the electron donors/acceptors have to move to the interface. If the faradaic removal of these electroactive ions (ie their reduction or oxidation at the electrodes) proceeds faster than their transport from the bulk electrolyte can replenish their supply, the transport process be-

comes important and will control the rate of charge transfer across the interface. The slow transport process will give rise to a over-potential, $\eta_{M.T.}$

For small currents the transport process will be able to keep up with the demand for ions at the electrode surface. However as the applied potential is increased, thus demanding more and more ions from the solution, a current is reached where the supply of ions from the bulk of the solution is not able to keep up with the increasing demand. This will result in a finite difference in concentration between the solution at the electrode surface and that in the bulk. This in turn results in a voltage drop between liquid close to the electrode surface and the bulk of the solution. This voltage is equal to the difference between the operating potential and the reversible potential of the electrode (ignoring η_{CT}) and is termed the 'concentration' or 'mass transfer' over- potential.

For the example where the external potential is greater than the reversible potential, at the cathode cations are removed from the solution and at the anode the supply of cations will be increased. The concentrations of the cations in the immediate vicinity of the electrode surfaces, C_s, will differ from that of the bulk of the solution, C_b. The same is true, of course, for anions except that their concentration will be higher at the cathode. (see figure 1.9)

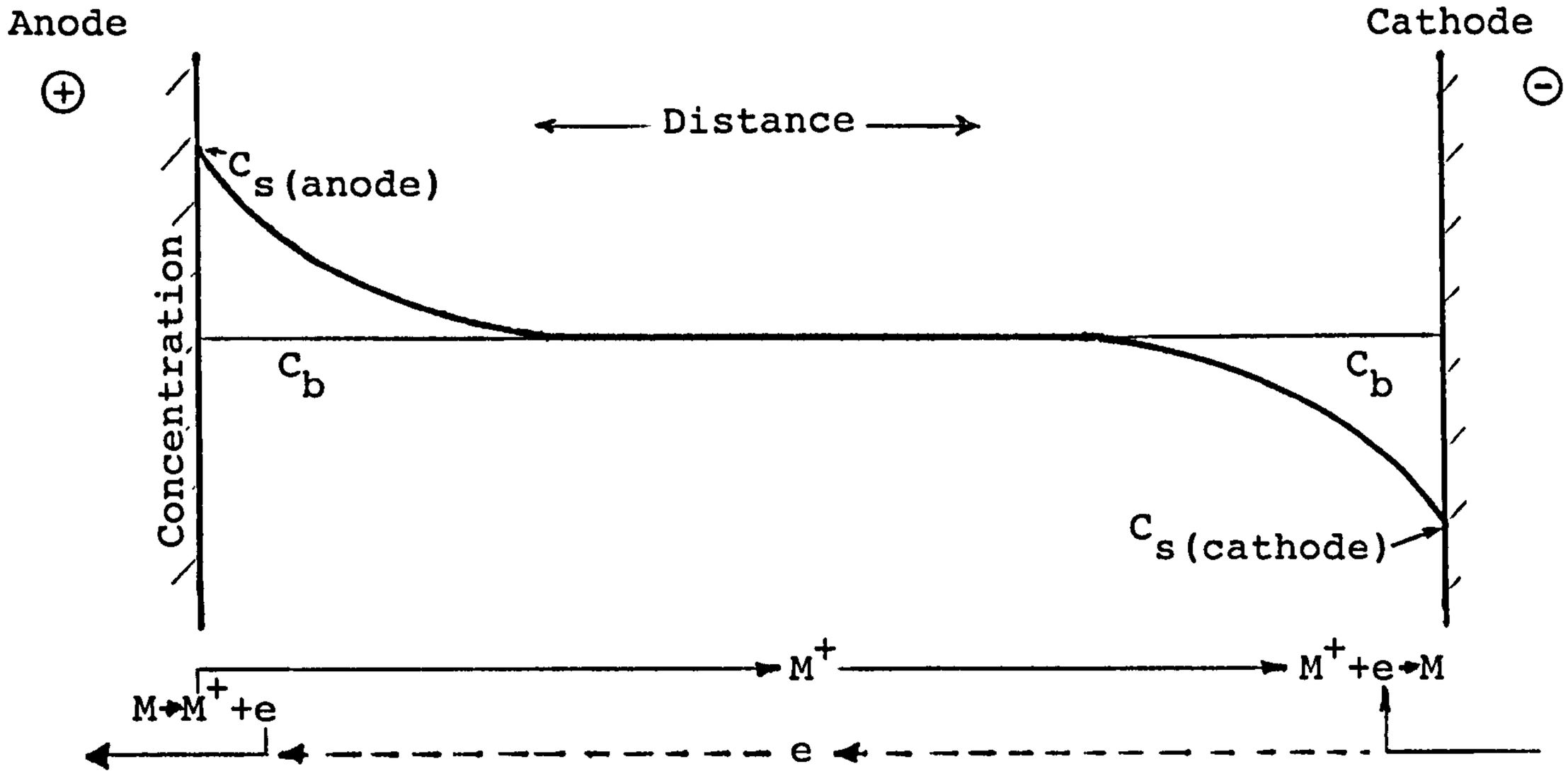

CONCENTRATION PROFILE

Figure 1.9

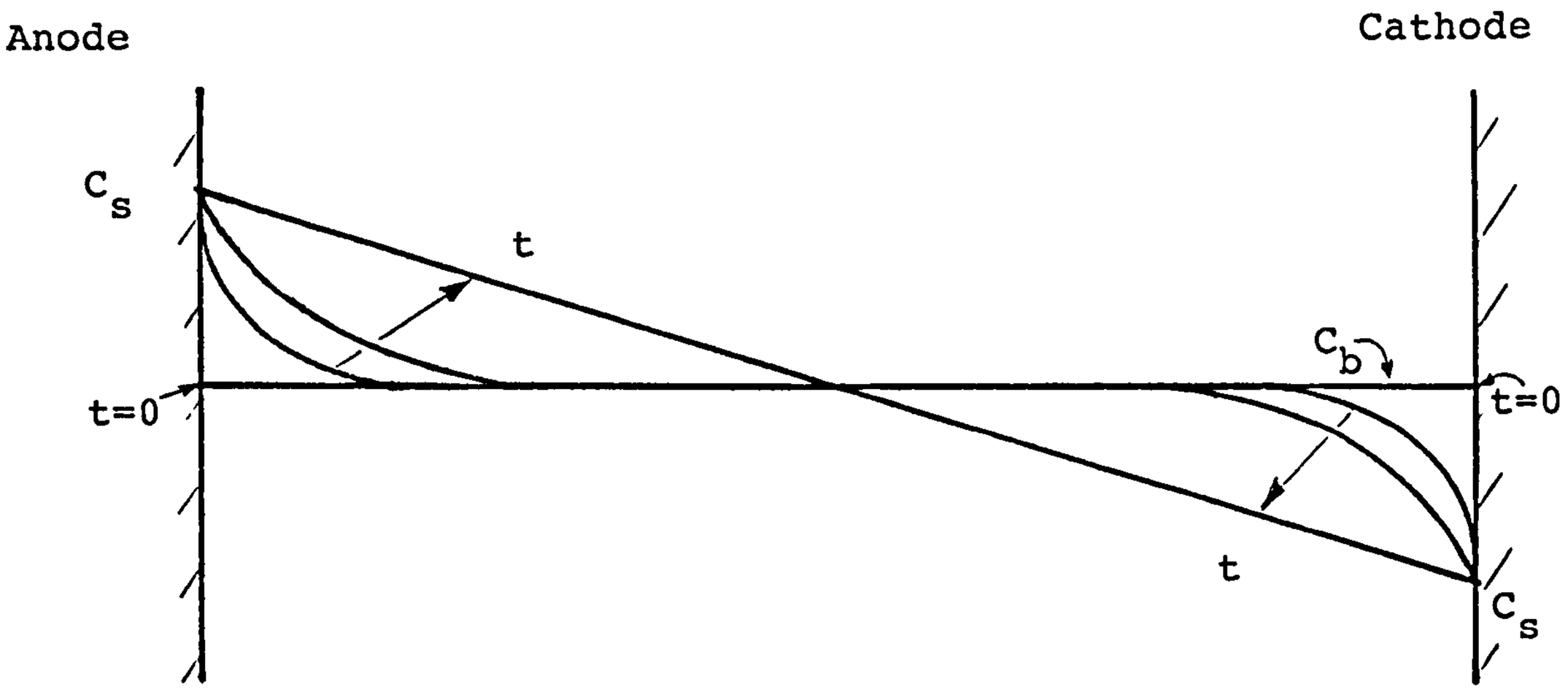

EFFECT OF TIME ON CONCENTRATION PROFILE

Figure 1.10

These differences in concentration of cations (and anions) will, at least partially, be reduced by diffusion and migration.

> Note:Diffusion is the movement of a species under the influence of a gradient of chemical potential (ie a concentration gradient).
>
> Migration is the movement of a charged body under the influence of an electric field (a gradient of electrical potential) (Bard and Faulkner, 1980).

It is generally considered that migration contributes little to the mass transfer compared with diffusion. If diffusion is relatively slow a finite difference in concentration of cations and anions will continue to exist. In an unstirred solution this concentration will be a function of distance, d, from the electrode and time, t. For example, when a potential is applied to the electrodes the concentration of the cations at the anode is rapidly raised to C_s and the solution in the neighbourhood of the electrode becomes progressively more replete with cations (see figure 1.10).

In an unstirred solution the concentration gradient near the electrodes will decrease with time. The flux of O and R at the electrode surfaces depend upon the concentration gradients at the interface in accordance with Fick's first law:

$$J_O = nFA = -D_O\left(\frac{\partial C^O}{\partial d}\right)_{d=o} \qquad \frac{-i}{} = \frac{dQ}{dt}$$

$$J_R = nFA = -D_R\left(\frac{\partial C^R}{\partial d}\right)_{d=o} \qquad \frac{i}{} = \frac{dQ}{dt}$$

where

i is the current

J is the flux in moles per unit time per unit area (mol sec^{-1} m^{-2}) normal to the surface

D is the diffusion coefficient (m^2 sec^{-1})

Q is the charge

C^O is the concentration of the oxidised species

C^R is the concentration of the reduced species

d is distance

Hence the current,i, which is proportional to the concentration gradient will also decrease with time, or, put another way, the mass transfer impedance will increase with time.

Initially, at t = 0, before any external potential is applied to the electrodes, the concentration is uniform throughout the solution and has a value, C_b. Using concentration, C, ($C = a/\gamma$) instead of activity, a, in the Nernst equation (1.7), the reversible potential is given by:

$$E_{rev} = E^O + \frac{RT}{nF} \quad nF \quad \ln C_b \qquad 1.9$$

If one now applies the new potential, E, ($\neq E_{rev}$) to the system, the new concentration of ions at the electrode surface, C_s, will be given by:

$$E = E^{O} + \frac{RT}{nF} \quad nF \quad \ln C_s \qquad 1.10$$

The difference between these potentials is the concentration or mass transfer over-potential which is given by:

$$\eta_{M.T.} = E - E_{rev} = \frac{RT}{nF} \quad nF \quad \ln \quad \frac{C_s}{C_b} \qquad 1.11$$

Taking into consideration both the oxidised and reduced species:

$$\eta_{M.T.} = \frac{RT}{nF} \ln \frac{(C_s^{O}/C_s^{R})}{C_b^{O}/C_b^{R}} \qquad 1.12$$

Nernst approximated the concentration-distance curve, at any time, by a straight line (as shown on figure 1.11) and the above voltage and concentration drop were assumed to be across a layer of thickness, δ, which increases with time. δ is defined as the thickness of the "Nernst diffusion layer".

When the voltage is first switched on, the distance over which the concentration changes, δ , is small. At this point in time the current, $i = nFA\ D/\delta\ (|C_b - C_s|)$, is very large. As time passes, the region over which this change extends increases and hence the current decreases. As the over-potential, η_{MT}, is time independent the mass transport impedance must increase with time. The mass transport impedance will therefore depend on the frequency of an applied ac signal - its impedance increasing as the frequency decreases. In order to derive expressions for the charge transfer and mass transfer impedances it will first be necessary to derive the faradaic current-potential relationship,$i-\eta$.

- Derivation of the faradaic current-potential relationship

For the following reaction at an electrode-electrolyte interface

$$M^{+n} + ne \underset{K_R}{\overset{K_F}{\rightleftharpoons}} M$$

the observed current flowing through an external circuit is equal to the difference between the currents for the forward (cathodic) and reverse (anodic) processes i.e.

$$i = i_c - i_a \qquad 1.13$$

Where

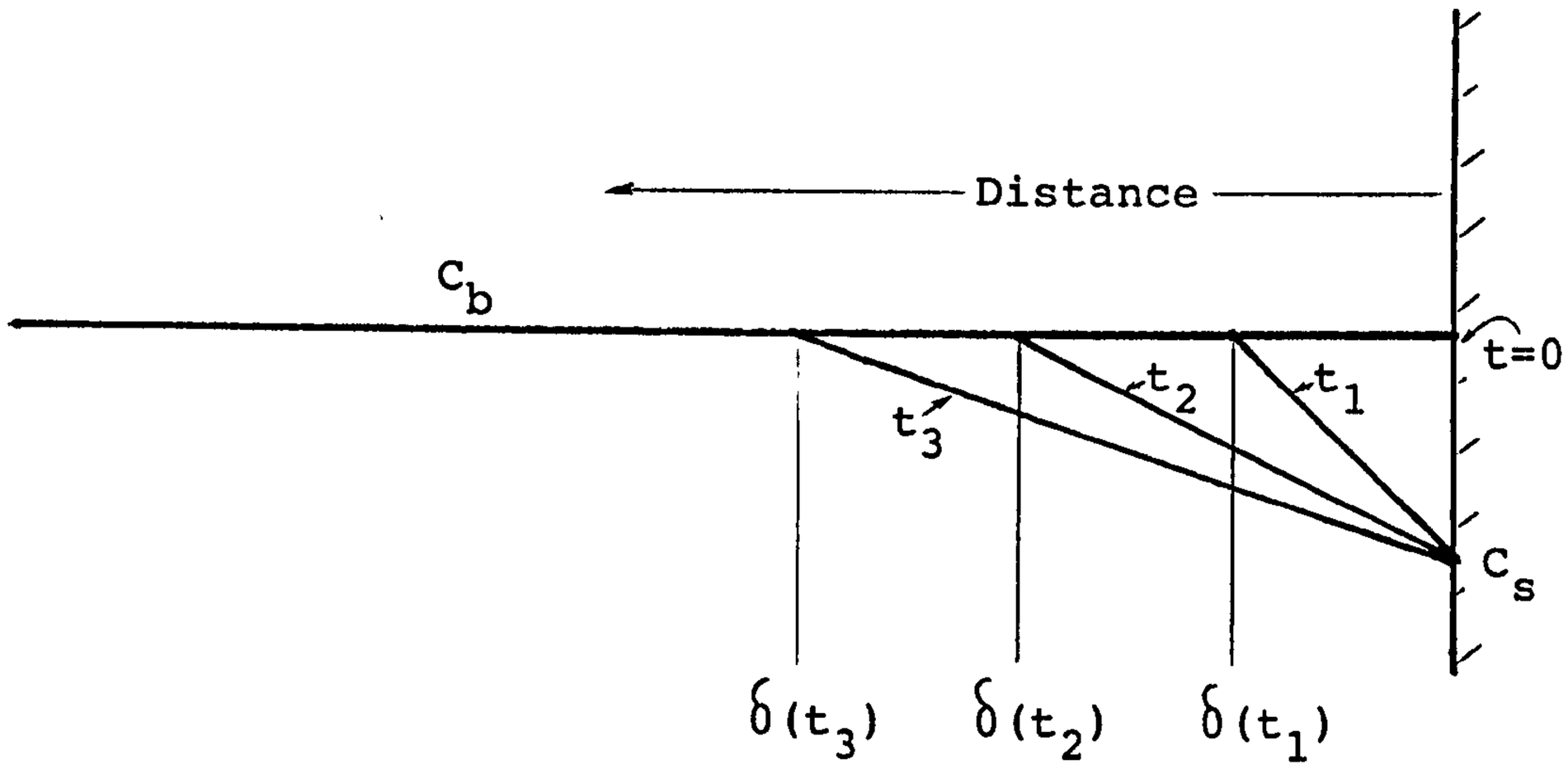

NERNST'S APPROXIMATION TO THE CONCENTRATION PROFILE

Figure 1.11

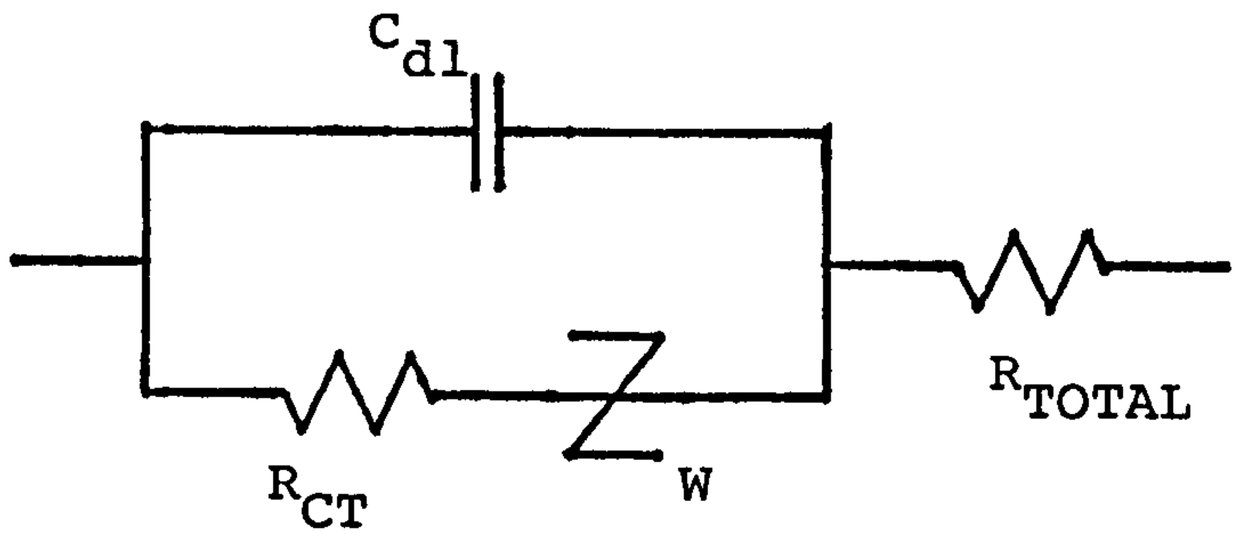

THE 'RANDLES AND ERSHLER' CIRCUIT MODEL

Figure 1.12

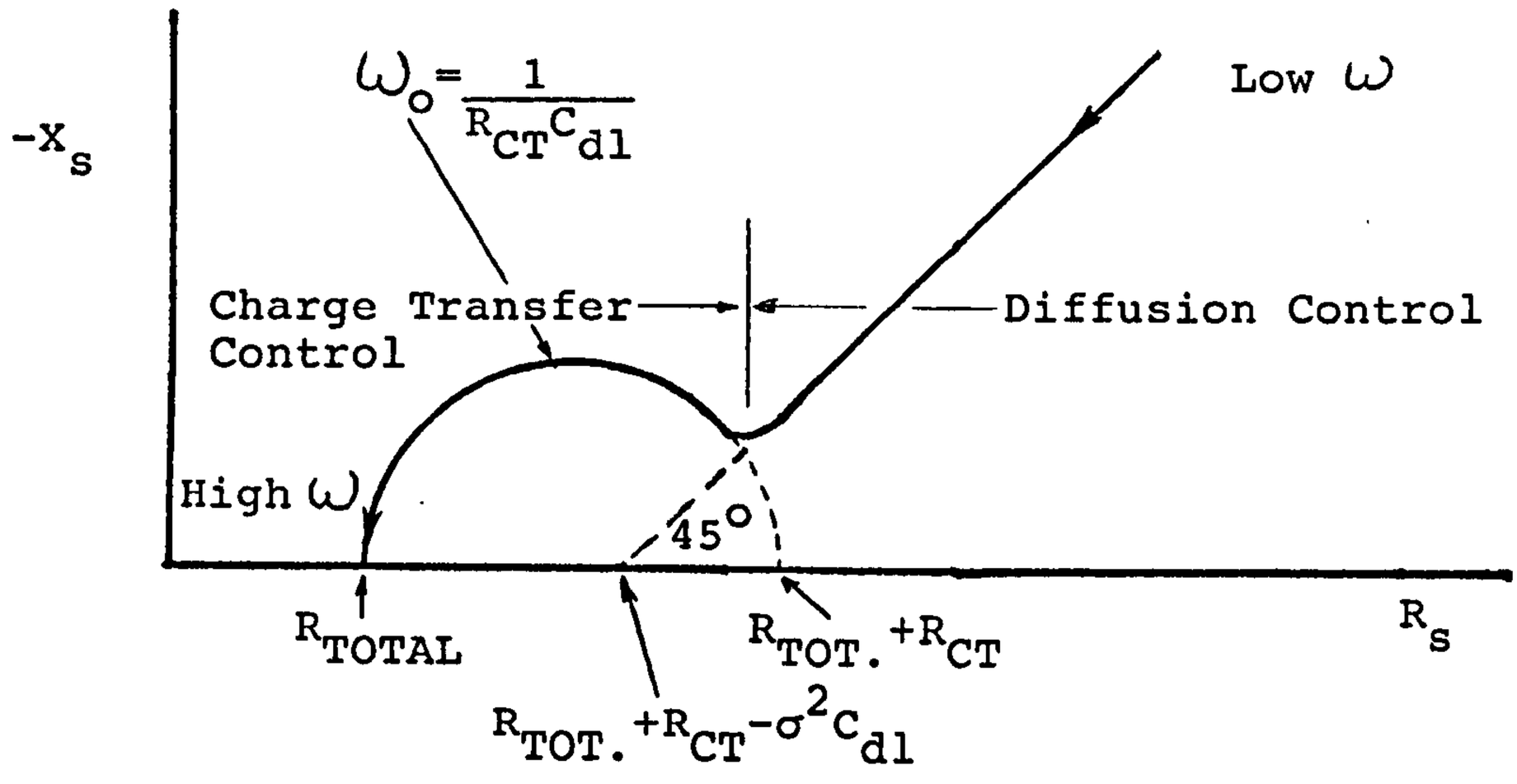

IMPEDANCE LOCUS OF 'RANDLES AND ERSHLER' CIRCUIT MODEL

Figure 1.13

$$\frac{i_c}{nFA} = K_F\ C_s^{O}, \qquad \frac{i_a}{nFA} = K_R\ C_S^{R} \qquad 1.14$$

K_F and K_R are the potential dependent rate constants for the above reaction.

Hence eqn 1.13 becomes

$$i = nFA\ [K_F C_s^{O} - K_R\ C_s^{R}] \qquad 1.15$$

According to activated complex theory the forward and reverse rate constants, K_F and K_R, can be expressed in terms of potential as follows (Bard and Faulkner, 1980)

$$K_F = K_F^{O} \exp\ (-\ \alpha nFE/RT) \qquad 1.16$$

and $K_R = K_R^{O} \exp\ ((1-\alpha)nFE/RT)$

Where K_F^{O} and K_R^{O} are potential independent constants termed standard rate constants, and α is the transfer coefficient.

Substituting the above expressions for K_F and K_R into the expression for the current (eqn 1.15) one has

$$i = nFA(C^{O}_S\ K^{O}_F \exp(-\ \alpha nFE/RT) - C^{R}_S K^{0}_R \exp((1-\alpha\ )nFE/RT)) \qquad 1.17$$

At equilibrium, when $E = E_{rev}$, the total current is zero and no concentration gradients exist, i.e.

$$C^{O}_s = C^{O}_b \text{ and } C^{R}_s = C^{R}_b$$

Therefore

$$i = nFA[C^{O}_{b}K^{O}_{F}\exp(-\frac{\alpha nFE_{rev}}{RT}) - C^{R}_{b}K^{O}_{R}\exp(\frac{(1-\alpha)nFE_{rev}}{RT})]$$

$$= 0$$

Remembering that at equilibrium

$$i_o = i_a = i_c$$

one can write

$$i_o = nFAC^{O}_{b}K^{O}_{F}\exp(\frac{-\alpha nFE_{rev}}{RT}) = nFC^{R}_{b}K^{O}_{R}\exp(\frac{(1-\alpha)nFE_{r_{ev}}}{RT})$$

1.18

If one substitutes this expression for i_o into equation 1.17 one obtains the simpler expression

$$\frac{i}{i_o} = \frac{C^{O}_{s}}{C^{O}_{b}}\exp[\frac{-\alpha nF\eta}{RT}] - \frac{C^{R}_{s}}{C^{R}_{b}}\exp[\frac{(1-\alpha)nF\eta}{RT}]$$

1.19

Equation 1.19 is known as the Butler-Volmer equation.

- Derivation of the faradaic impedance

The faradaic impedance is derived from the linearised Butler-Volmer equation by first deriving expressions for C^{O}_{s} and C^{R}_{s} from the Frick equations of diffusion with appropriate boundary and initial conditions (For a

detailed derivation see Delahay, 1961).

For small values of η the linearised Butler-Volmer equation becomes (Bard and Faulkner, 1980)

$$i_{(\eta \to o)} = i_o\left[\frac{C^o{}_s}{C^o{}_b} - \frac{C^R{}_s}{C^R{}_b} - \frac{nF\eta}{RT}\right]$$

If η is a small amplitude, ac signal equal to $-V \sin \omega t$, the complete solution is obtainable using Laplace transform (Delahay, 1961)

$$\eta = -i\frac{RT}{nF}\left[\left(\frac{1}{i_o} + \frac{1}{\sqrt{2}nF\sqrt{\omega}}\left(\frac{1}{C^o{}_b\, D_o^{1/2}} + \frac{1}{C^R{}_b\, D_R^{1/2}}\right)\right)\sin \omega t + \left(\frac{1}{\sqrt{2}nF\sqrt{\omega}}\left(\frac{1}{C^o{}_b\, D_o^{1/2}} + \frac{1}{C^R{}_b\, D_R^{1/2}}\right)\right)\cos \omega t\right] \qquad 1.20$$

Where D_O and D_R are the diffusion coefficients (cm^2/sec) for the oxidised and reduced species respectively.

If the faradaic impedance at any single frequency is represented by a resistance, R_s, and a capacitance, C_s, in series, the corresponding current-voltage characteristic for such a combination is

$$V = -I\left(R_s \sin \omega t + \frac{1}{j\omega C_S}\cos \omega t\right)$$

One can see on comparison that this has the same form as equation 1.20. and one can put

$$R_s = \left(\frac{RT}{nF}\right)\left[\frac{1}{i_o} + \frac{1}{\sqrt{2}nF\sqrt{\omega}}\left[\frac{1}{C^o_b D_o^{1/2}} + \frac{1}{C^R_b D_R^{1/2}}\right]\right]$$

and $$X_S = \frac{1}{\omega C_s} = \left(\frac{RT}{nF}\right)\left[\frac{1}{\sqrt{2}nF\sqrt{\omega}}\left[\frac{1}{C^o_b D_o^{1/2}} + \frac{1}{C^R_b D_R^{1/2}}\right]\right] \qquad 1.21$$

The series resistance, R_s, is composed of a frequency independent term, RT/nFi_o , which is equated with the charge transfer resistance (as it involves the exchange current, i_o) and a frequency dependent mass transfer impedance. Upon inspection it becomes apparent that X_s is the imaginary component of this mass transfer impedance. This therefore leads to the division of the faradaic impedance into a charge transfer resistance, R_{CT}, and a "Warburg" impedance, Z_W, (named after Warburg (1899) who first derived the expression for this impedance) which corresponds to pure diffusion or mass transfer control i.e.

$$Z_f = R_{CT} + Z_W$$

where

$$R_{CT} = RT/nFi_o, \qquad 1.22$$

$$Z_W = \sigma\omega^{-0.5} \mp j\sigma\omega^{-0.5}$$

$$= (1-j)\sigma\omega^{-0.5} \qquad 1.23a$$

and $$\sigma = \frac{RT}{\sqrt{2}n^2F^2}\left[\frac{1}{C^o_b D_o^{1/2}} + \frac{1}{C^R_b D_R^{1/2}}\right] \qquad 1.23b$$

Note that R_{CT} is inversely proportional to the exchange current density, i_o. Earlier it was shown that i_o is a measure of the anodic and cathodic reactions occurring at the electrode at the reversible potential. i_o also provides an indication of the liability to polarisation of a particular electrode-electrolyte system. From equation 1.22 one can see that an electrode system with a low exchange current, i_o, will have a high charge transfer resistance. With such a system only a small current (slightly larger than i_o) is necessary to flow through the interface to cause a large voltage drop across the large charge transfer resistance present. Such an electrode system will therefore be very easily polarised. It can be concluded that a good electrode will be one with a very large value of i_o resulting in low values of R_{CT} and η_{CT}

Typical values of i_o fall in the range

10^{-2} to 10^{-16} A cm^{-2} (Denaro, 1971) which result in values of R_{CT} in the range

$$R_{CT} = 0.026/ni_o = 2.6/n \text{ to } 2.6 \times 10^{14}/n \ \Omega cm^2$$

The magnitude of the Warburg impedance, Z_W, is given by

$$|Z_W| = \sqrt{2}\,\sigma\omega^{-\frac{1}{2}} \qquad 1.24$$

i.e. it is inversely proportional to the square root of the frequency. At high frequencies its impedance be-

comes negligible whereas at low frequencies it tends towards infinity.

The phase angle of the Warburg impedance is given by

$$\phi = \tan^{-1}\left(\frac{1}{\omega R_s C_s}\right) = \tan^{-1}\left(\frac{\sigma\omega^{-\frac{1}{2}}}{\sigma\omega^{-\frac{1}{2}}}\right) = 45^{o} \quad 1.25$$

Hence the current through, and the voltage across, the Warburg impedance always differ in phase by 45^{o}, irrespective of the frequency.

- Total equivalent circuit model and its impedance characteristic

Randles (1947) and Ershler (1947) assumed that the non-faradaic branch could be modelled by a simple double layer capacitance, C_{dl}, and that it could be connected in parallel across the faradaic branch. Their assumptions give rise to the circuit shown in Figure 1.12.

It must be stressed that this circuit represents the system impedance under the most simplified conditions. One such simplification is in ignoring the effects of specific adsorption (see Section 1.1.2.3).

Sluyters (1960) suggested plotting the impedance on an Argand diagram where $-X_s$ is plotted against R_s over a range of frequencies.

As the total impedance of "Randles and Ershler's" circuit is given by

$$Z = R_{TOTAL} + \frac{1}{j\omega C_{dl} + \frac{1}{R_{CT} + (1-j)\sigma\omega^{-\frac{1}{2}}}} \qquad 1.26$$

then R_s and X_s can be written in terms of ω (where $\omega = 2\pi f$) as below

$$R_s = R_{TOTAL} + \frac{R_{CT} + \sigma\omega^{-\frac{1}{2}}}{(C_{dl}\sigma\omega^{\frac{1}{2}} + 1)^2 + \omega^2 C_{dl}^2 (R_{CT} + \sigma\omega^{-\frac{1}{2}})^2}$$

$$X_s = \frac{\omega C_{dl}(R_{CT} + \sigma\omega^{-\frac{1}{2}})^2 + \sigma\omega^{-\frac{1}{2}}(\omega^{\frac{1}{2}} C_{dl}\sigma + 1)}{(C_{dl}\sigma\omega^{\frac{1}{2}} + 1)^2 + \omega^2 C_{dl}^2 (R_{CT} + \sigma\omega^{-\frac{1}{2}})^2}$$

Plotting $-X_S$ against R_S for a range of frequencies one obtains the locus shown in figure 1.13.

At low frequencies the impedance reduces to

$$Z = R_{TOT} + R_{CT} + (1-j)\sigma\omega^{-\frac{1}{2}} - j2\sigma^2 C_{dl}$$

At these low frequencies the magnitude of the Warburg impedance is very large and dominates that of R_{CT}. The impedance locus is therefore a straight line at 45° to the real axis i.e. the phase angle characteristic of a diffusion controlled process (see figure 1.14).

As the frequency increases, Z_W decreases and the contributions of R_{CT} and C_{dl} become more important. There is a departure from the low frequency straight line to a semicircular arc. The impedance is now approximated by

$$Z = R_{TOT} + \frac{R_{CT}}{1 + \omega^2 C_{dl}^2 R_{CT}^2} - j\frac{\omega C_{dl} R_{CT}^2}{1 + \omega^2 C_{dl}^2 R_{CT}^2}$$

or, by eliminating ω between R_s and $-X_s$, one can write

$$(R_S - R_{TOT} - \frac{R_{CT}}{2})^2 + (X_S)^2 = (\frac{R_{CT}}{2})^2$$

This is the equation of a semicircle centred at $R_s = R_{TOT} + R_{CT/2}$, $X_s = 0$, and of radius $R_{CT/2}$.

The phase angle of the faradaic impedance, Z_f, (where $Z_f = Z_W + R_{CT}$) at any frequency is given by

$$\text{Cot } \phi_f = \frac{R_S}{X_S} = \frac{R_{CT} + \sigma\omega^{-\frac{1}{2}}}{\sigma\omega^{-\frac{1}{2}}} = \frac{R_{CT}\omega^{\frac{1}{2}}}{\sigma} + 1$$

$$\text{or} \quad \text{Cot } \phi_f = 1 + U\omega^{\frac{1}{2}} \qquad 1.27$$

Where U is a constant.

For example, when there is little or no impedance to charge transfer, $R_{CT} \rightarrow 0$ and $\phi_f = 45^o$.

If however R_{CT} has a finite value but there is no diffusional impedance, i.e. $Z_W = 0$, the phase angle, ϕ_f, will be zero. Hence the faradaic phase angle will lie between 0^o and 45^o when there is only charge transfer and/or diffusion control.

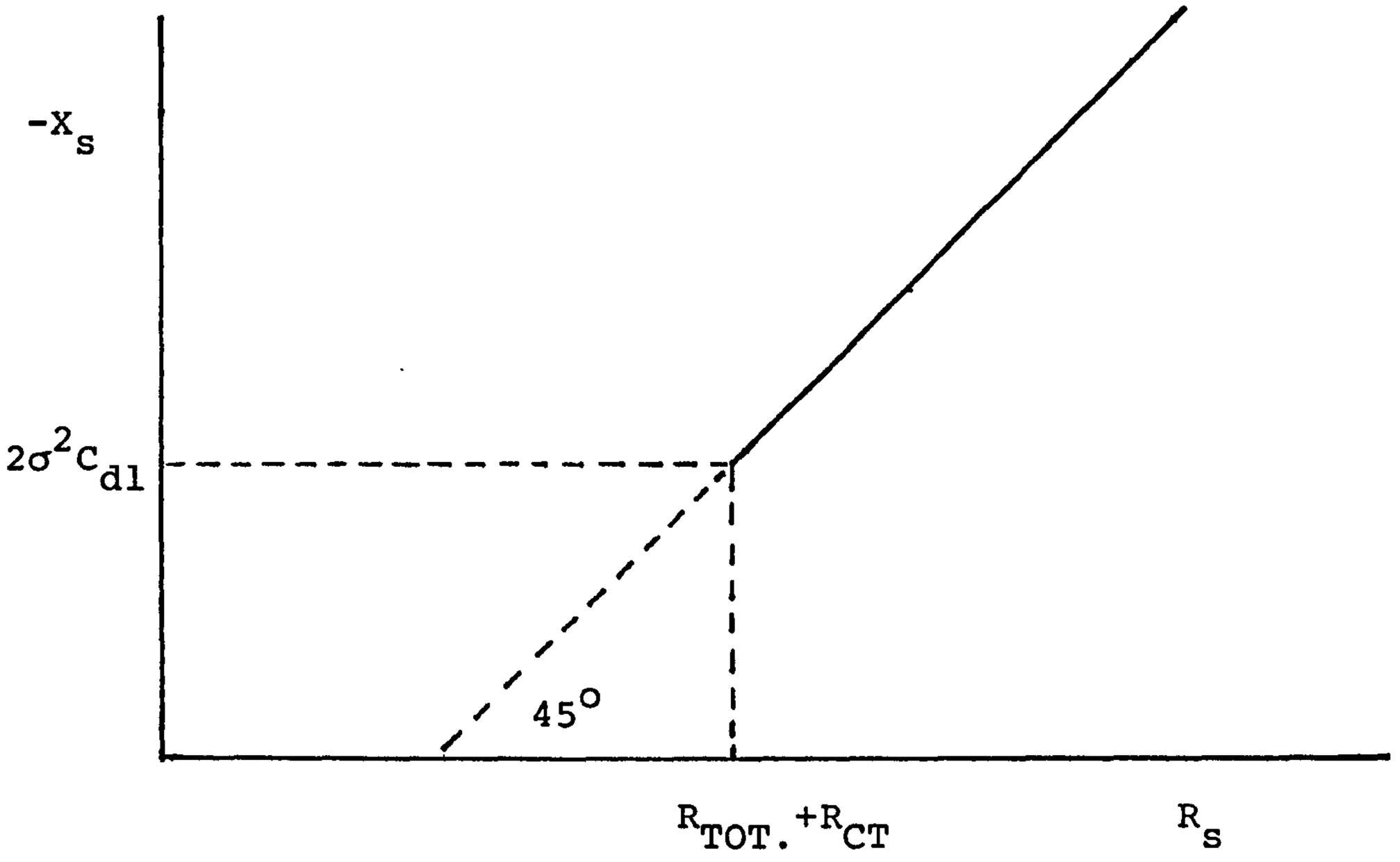

LOW FREQUENCY IMPEDANCE LOCUS OF THE
'RANDLES AND ERSHLER' CIRCUIT MODEL

Figure 1.14

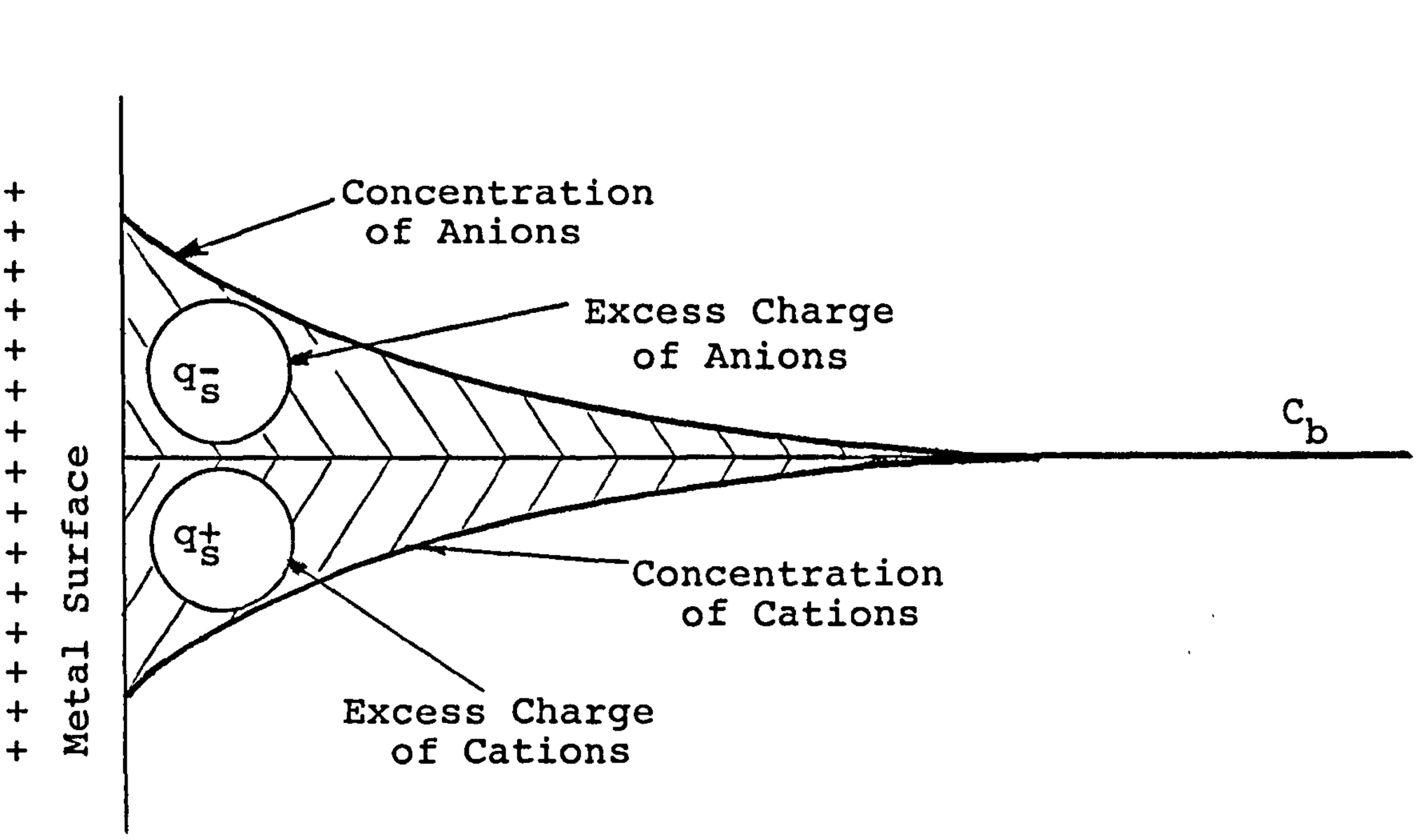

COULOMBIC ADSORPTION

Figure 1.15

- Diffusion effects at Biomedical electrodes

Attention in the past has been focused on the diffusional impedance, Z_W, as it is frequency dependent (Dymond, 1976). Several bio-engineers have considered that the observed frequency dependence of the interfacial impedance is due to diffusional effects (e.g. Greatbatch and Chardack, 1968; Geddes et al, 1971; Pollak 1974).

Pollak (1974), for example, used the equivalent circuit proposed by electrochemists Bockris and Reddey (1970). Their equivalent circuit is similar to that of Randles and Ershler (1947) except that they connected the double layer capacitance, C_{dl}, only across R_{CT}, with Z_W in series with this parallel combination. Such a circuit will however have an impedance locus very similar to that of Randles and Ershler, with a low frequency phase angle of 45^{o} ($\beta = 0.5$) due to Z_W.

Pollak's model assumes that the electrode surface is "ideally flat" and disregards the possibility of adsorption of ions at the metal surface. In order to rectify the first assumption Pollak introduced a correction coefficient to account for the difference between effective area and "geometric" area due to "surface texture". This unfortunately assumes that surface roughness only increases the effective surface area, thus decreasing the magnitude of the interfacial impedance, and does not effect the form of the im-

pedance. This is not, however, the case as shall be shown in section 1.1.2.5.

Pollak's results, far from confirming his equivalent circuit model, show that for most of the electrode systems tested the interfacial impedance has values of β larger than 0.5 and would appear to be better modelled by a Constant Phase Angle impedance, Z_{CPA}. Pollak's results further demonstrated that surface roughness (caused by etching) not only decreased the magnitude of his electrodes' impedances but also affected their form. Surface roughness effects are therefore important and may even be the cause of the frequency dispersion at his "smooth" polished electrodes.

A further complication arises in that Pollak's electrolytic etching process, i.e. the application of large ac voltages to electrodes dipped in physiological saline until gas bubbles appeared at their surfaces, not only roughened the surfaces but most probably coated them with layers of adsorbed ions and/or oxides. Pollak admitted that "structural changes at the electrode surface may ... also play a part".

Geddes et al's results (1971) can also at least partly be accounted for by surface roughness effects (they "polished" their electrodes with 6-0 emery paper) and not by the diffusion of ions. Although they recognised the dependence of the interfacial impedance of the sur-

face finish of the electrode, they too imply that it only affects the magnitude of the impedance (by increasing the effective surface area) and not its form.

In summary, the reported experimental results indicate that the diffusional impedance is an inadequate model and that the probable cause of the observed form of the impedance characteristic was the surface roughness of the electrodes used.

1.1.2.3 Specific Adsorption

- Introduction

It was expected from the above theory that after the subtraction of the contributions of R_{TOTAL} and C_{dl}, the faradaic impedance of an electrode process without adsorption of the components of the reaction would be characterised by a phase angle, $\phi_f \leqslant 45^o$.

In 1952 Randles and Somerton obtained phase angles for the faradaic impedance larger than the expected maximum of 45^o. They considered it very probable, on the basis of additional experiments and intuitive arguments that "specific adsorption" of one or both members of the redox couple played a role. Since then a faradaic phase angle, ϕ_f, larger than 45^o has been taken as an indication of specific adsorption. "Specific adsorption" is therefore of great interest as it appears to be a physical process which is characterised by an impedance which is frequency dependent and has a phase angle larger than 45^o - similar to biomedical electrode - electrolyte interfaces.

- Definition of 'Specific Adsorption'

As pointed out in Section 1.1.2.1 there are two kinds of adsorption - coulombic and specific.

(1) Coulombic adsorption

With simple coulombic (or electrostatic) adsorption, as the charge on the metal is increased (e.g. making it more positive), anions are attracted and cations repelled in a simple symmetrical manner. Such a problem can be simply dealt with in terms of electrostatics (Bockris and Drazic, 1972).

On the metal there is an excess of positive charge, q_m. On the solution side there is an excess of negative charge due to the increased concentration of anions, q_s^-, and a deficiency of positive charge due to the decrease in concentration of cations, q_s^+. (See Figure 1.15).

The charges on the metal must be equal to the charges in the solution, i.e. to the total of the charges due to the cations and anions. Hence

$$-q_m = q_s = q_s^+ + q_s^- \qquad 1.28$$
$$= F\ (\Gamma_+ + \Gamma_-)$$

Where Γ_+ and Γ_- are the individual surface excesses of cations and anions and F is the Faraday constant.

In the case of simple electrostatic adsorption

$$q_s^+ = q_s^-$$

(ii) Specific adsorption

It was shown (see figure 1.4) that with coulombic adsorption the solvated ions can only approach the electrode surface as far as the Outer Helmholtz Plane, OHP. Their interaction with the electrode only involves "long range" electrostatic forces and hence is essentially independent of their chemical properties.

In most electrolyte solutions, however, there are some ions which manage to adsorb directly onto the metal surface. To do this such ions have to shed their solvent sheaths, displace the adsorbed water molecules and come in direct contact with the bare electrode surface. The plane through the centres of these ions 'stuck' to the electrode surface is known as the Inner Helmholtz Plane, IHP.

If an ion is strongly hydrated, much energy would be required to divest the ion of its hydration sheath, making the transition to the IHP energetically not worthwhile. Ions which are strongly hydrated do not therefore readily specifically adsorb.

As hydration is very dependent on the radius of the ion there is a correlation between 'contact' adsorption and an ion's radius. Large ions such as Cl^-, Br^- and I^- adsorb easily whereas small ions such as Na^+ and K^+ do not easily contact adsorb. Anions in general are found to be prone to contact adsorption, they are even found to adsorb onto a negatively charged electrode! It is obvious that some force other than electrostatics is involved. This force seems to depend on the chemical

nature of the ion and hence is "specific" i.e. ion dependent. Ions adsorbed in this way are said to be "specifically adsorbed". The exact nature of specific adsorption forces are still however a matter of some controversy.

When such specific or contact adsorption is present, anions will be attracted to the electrode in greater amounts than are necessary to simply counter the positive charge, q_m, on the metal electrode. The concentration of the cations will therefore be higher than under simple coulombic conditions in order to cancel the additional negative charge of the specifically adsorbed anions and make the charge on the solution side equal in magnitude to that on the electrode (see figure 1.16).

The charges on the metal must be equal to the charges in the solution i.e. to the total of the charges due to the coulombically adsorbed cations, the coulombically adsorbed anions and the specifically adsorbed anions. i.e.

$$-q_m = q_s = F\Gamma_- + F\Gamma_+ = q_s^{-(S.A.)} + q_s^{-(C.A.)} + q_s^{+(C.A.)}$$
$$= q_s^{-(S.A.)} + q_s^{(C.A.)}$$

where S.A. and C.A. refer to specific and coulombic adsorption respectfully

(Note $F\Gamma_+ = q_s^{+(C.A.)}$

as no cations are specifcally adsorbed)

Hence $$|q_m| - |q_s^{C.A.}| = |q^{-(S.A.)}| \qquad 1.29$$

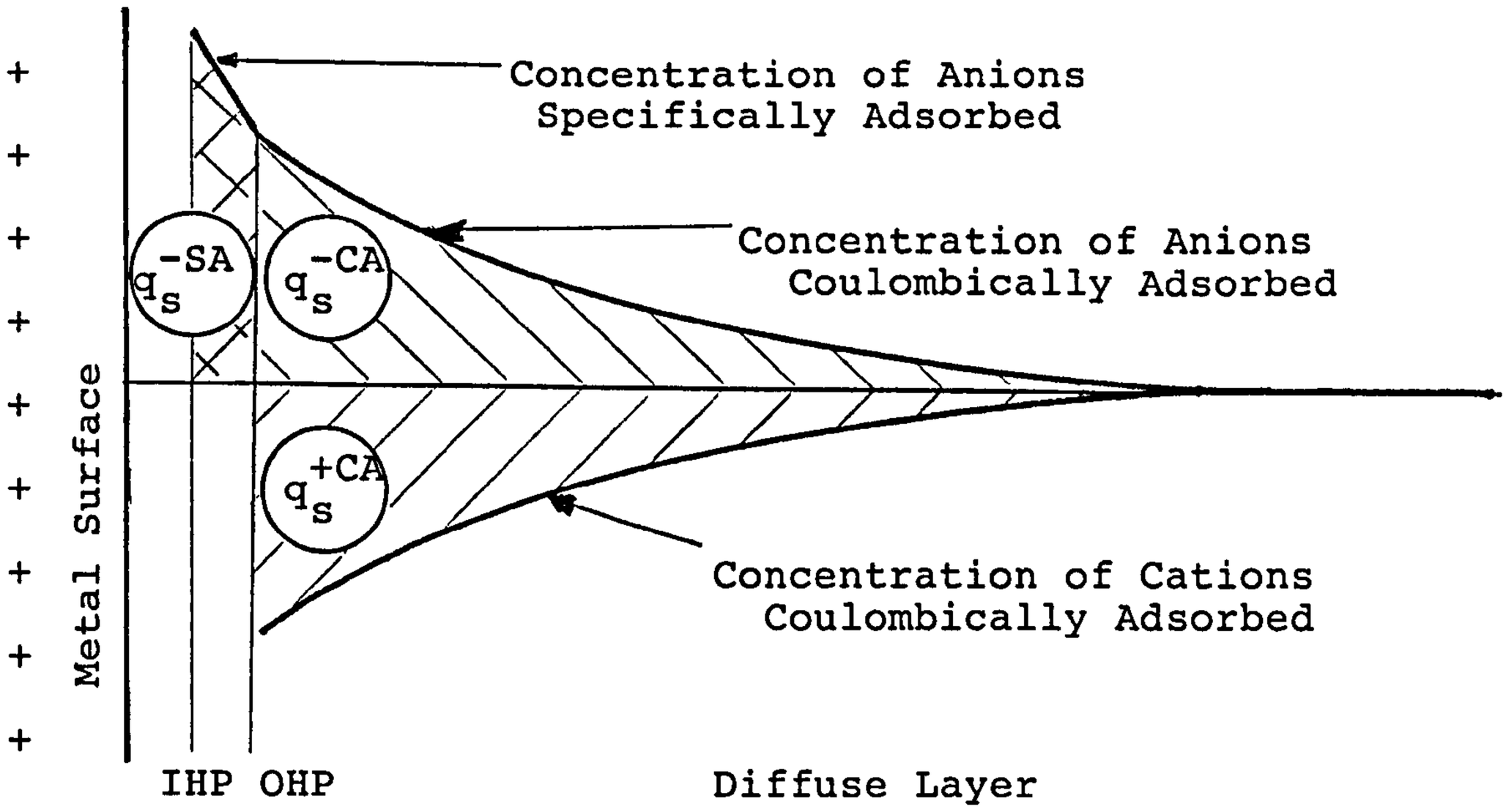

SPECIFIC ADSORPTION

Figure 1.16

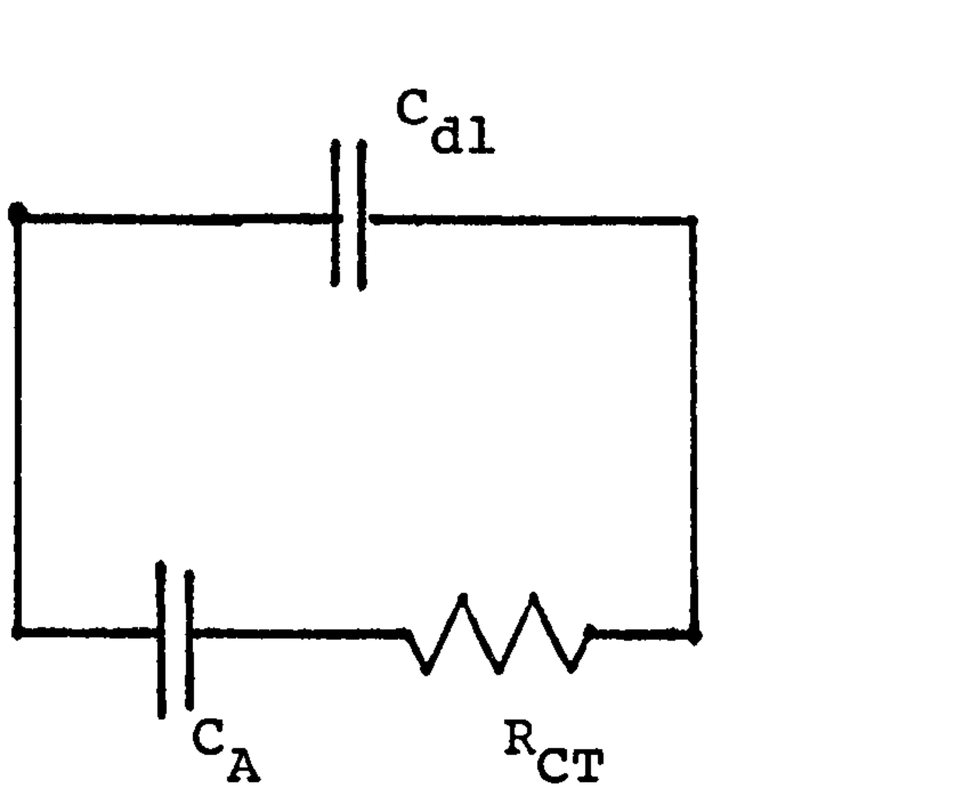

DOLIN AND ERSHLER
Figure 1.17

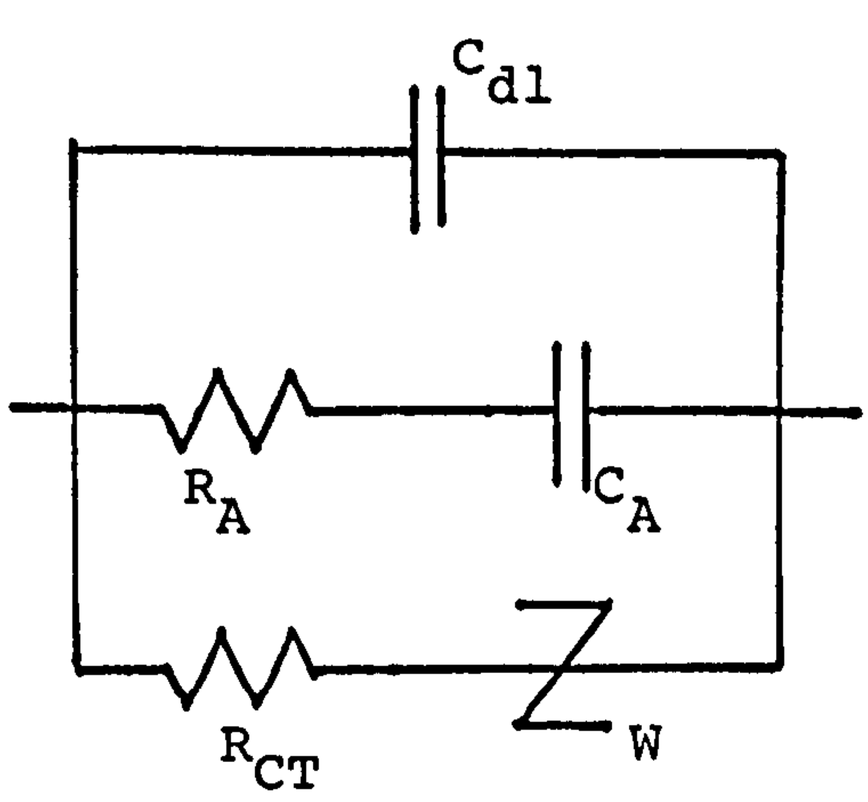

LAITINEN AND RANDLES
Figure 1.18

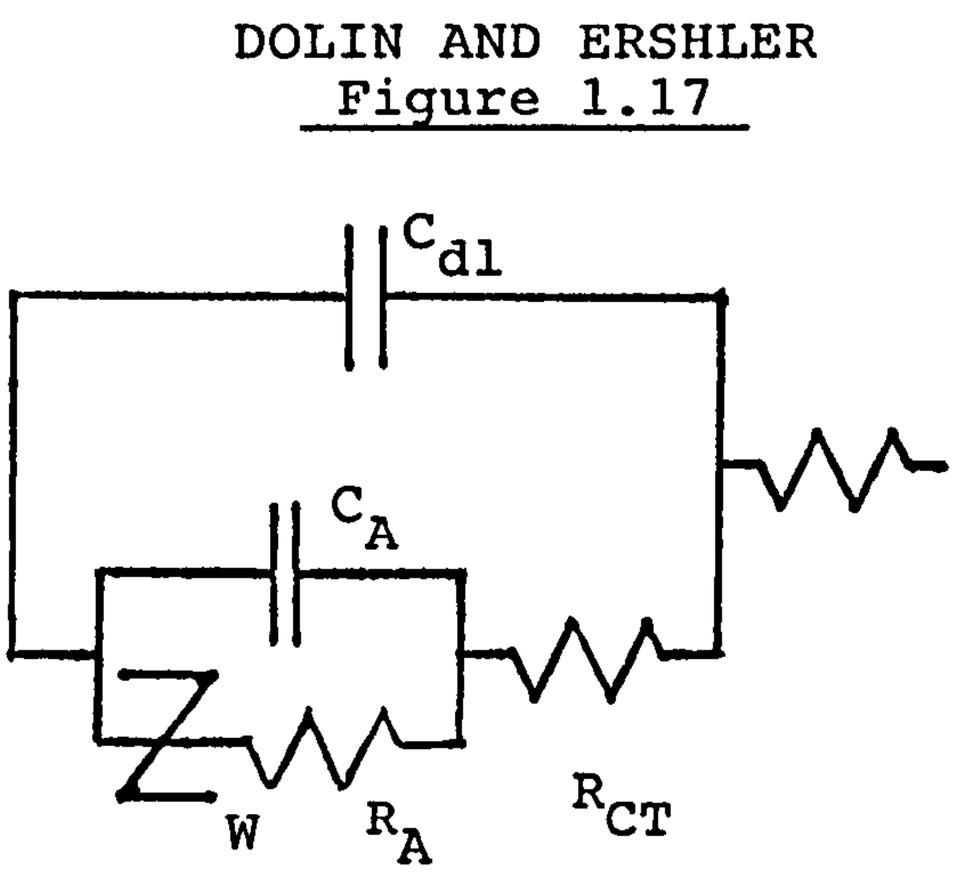

LLOPIS ET AL.
Figure 1.19

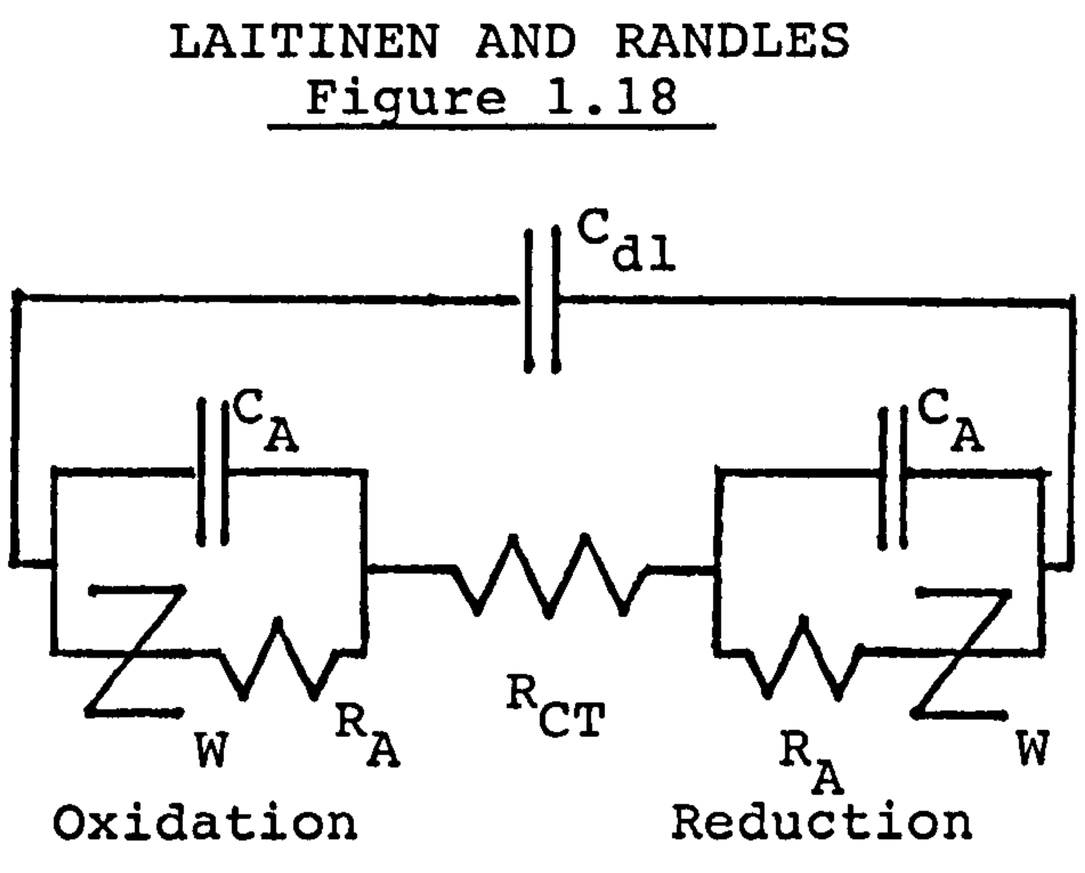

SENDA AND DELAHAY
Figure 1.20

Specific adsorption at the interface can be defined as the adsorption which is in excess or deficit of the amount which would be expected to be present at the interface under simple coulombic considerations.

- Adsorption Pseudo Capacitance

Ions specifically adsorbed on the electrode surface have the ability to store charge and hence act somewhat as a capacitance. This 'capacitance' is found to be dependent on the applied potential and hence the differential adsorption capacitance, C_A, is used, where

$$C_A = \left(\frac{\partial q^{SA}}{\partial V}\right) \qquad 1.30$$

and q^{SA} is the charge specifically adsorbed at the IHP.

The degree of coverage of the electrode surface, θ, will be proportional to the faradaic charge passed i.e. (Dymond, 1976)

$$q^{SA} = K\theta \qquad 1.31$$

Where K is the faradaic charge required to cross the interface to complete a monolayer of adsorbed ions

[note: the degree of coverage is related to the surface excesses, Γ , by the equation

$$\theta = \frac{\Gamma}{\Gamma_S} \qquad 1.32$$

where Γ is the amount of species adsorbed and Γ_s is its saturation coverage.

Hence when $\theta = 1$, IHP is saturated with adsorbed ions]

$$\text{As} \qquad q = nF\Gamma$$

$$K = q^{SA}/\theta = nF\Gamma_S$$

The capacitance due to the variation of q^{SA} with potential can therefore be expressed as

$$C_A = \frac{dq^{SA}}{dV} = K\frac{d\theta}{dV} = nF\frac{d\Gamma}{dV} \qquad 1.33$$

and is known as a pseudo capacitance as opposed to the true double layer capacitance which is independent of voltage. This pseudo capacitance arises in a different way to the double layer capacitance. The coverage, θ, can only be changed upon the passage of faradaic current across the interface of a non-ideally polarised electrode ($0 < R_{CT} < \infty$), whereas C_{dl} represents an ideally polarisable electrode ($R_{CT} = \infty$). Although C_A behaves electrically as a capacitance it has been found to vary with potential and applied signal frequency (Gileadi and Conway, 1964) and hence is the possible source of similar behaviour noted at biomedical electrode interfaces.

The adsorption pseudo capacitance is in parallel with

the voltage and frequency independent double layer capacitance. At voltages where there is little or no specific adsorption, C_A is negligible and only the double layer capacitance, C_{dl}, will be observable. However for potentials to either side of this "double layer" region specific adsorption takes place and C_A increases in magnitude until it dominates C_{dl} [for a more detailed treatment see Chapter Four]. Potential and frequency dependence of the impedance will therefore be noted in these regions.

To derive an expression for the pseudo capacitance one needs to know how q^{SA}, θ or Γ vary with the electrical state of the system as C_A is proportional to $\frac{dq^{SA}}{dv}$, $\frac{d\theta}{dV}$ or $\frac{d\Gamma}{dV}$. Adsorption isotherms are just such theoretical relationships, relating the degree of coverage, the activity or concentration of the species in the bulk of the solution and the potential. The use of different isotherms and other assumptions made give rise to different expressions of the adsorption pseudo capacitance.

The derivation of the adsorption pseudo capacitance using adsorption isotherms is considered in more detail in Chapter 4. At present equivalent circuits derived by various researchers for electrode systems where adsorption effects are known or suspected to exist will be reviewed and their impedances compared with that experimentally found for biomedical electrodes systems (figure 1.2).

- Equivalent Circuit Models of Adsorption Effects

It has often been assumed that the faradaic and non-faradaic components of the impedance are independent and can be connected in parallel. Hence it was also considered that the nonfaradaic branch could be studied in the absence of the reacting species which give rise to the faradaic branch.

This assumption led Grahame (1946), after demonstrating the frequency invariance of the Mercury electrode's capacitance (Mercury being an "ideal" polarisable electrode with a very large faradaic impedance), to conclude that any frequency dispersion observed in an electrode's total impedance is located in the faradaic component. This belief was widespread for many years and led many researchers to consider the frequency dependent adsorption effects as faradaic or at least not "non-faradaic".

However the faradaic and nonfaradaic currents and impedances are not independent (Delahay, 1968), adsorption is not a purely faradaic process, and frequency dispersion has been observed even in the absence of a faradaic process (Sluyters-Rehbach and Sluyters, 1970).

In the next sections we will review

(i) the effects of adsorption on the faradaic branch;

(ii) adsorption effects on the nonfaradaic branch and finally

(iii) adsorption effects on the total interface impedance.

- Adsorption Effects on the Faradaic Impedance

Over the years several groups of researchers have considered the problem of specific adsorption and its effect on the electrode's faradaic impedance. Choice of isotherm, and other assumptions made, have resulted in more or less different new expressions for the faradaic impedance. The derived equivalent circuit models contain additional "adsorption" resistive and capacitive elements in various combinations and positions. Some examples are those of Dolin and Ershler, 1940 (figure 1.17) Laitinen and Randles, 1955 (figure 1.18), Llopis et al, 1959 (figure 1.19) and Senda and Delahay, 1961 (figure 1.20).

It is interesting to note that the majority of the above equivalent circuits have similar impedance loci - of the form shown in figure 1.21. Such loci comprise two high frequency semicircular arcs, one due to the charge transfer resistance and the double layer capacitance and the other due to adsorption effects, as well as a low frequency, straight line portion at 45^{o} to the real axis due to diffusion effects.

It has been noted (Randles and Somerton, 1952) that adsorption is characterised by a faradaic phase angle

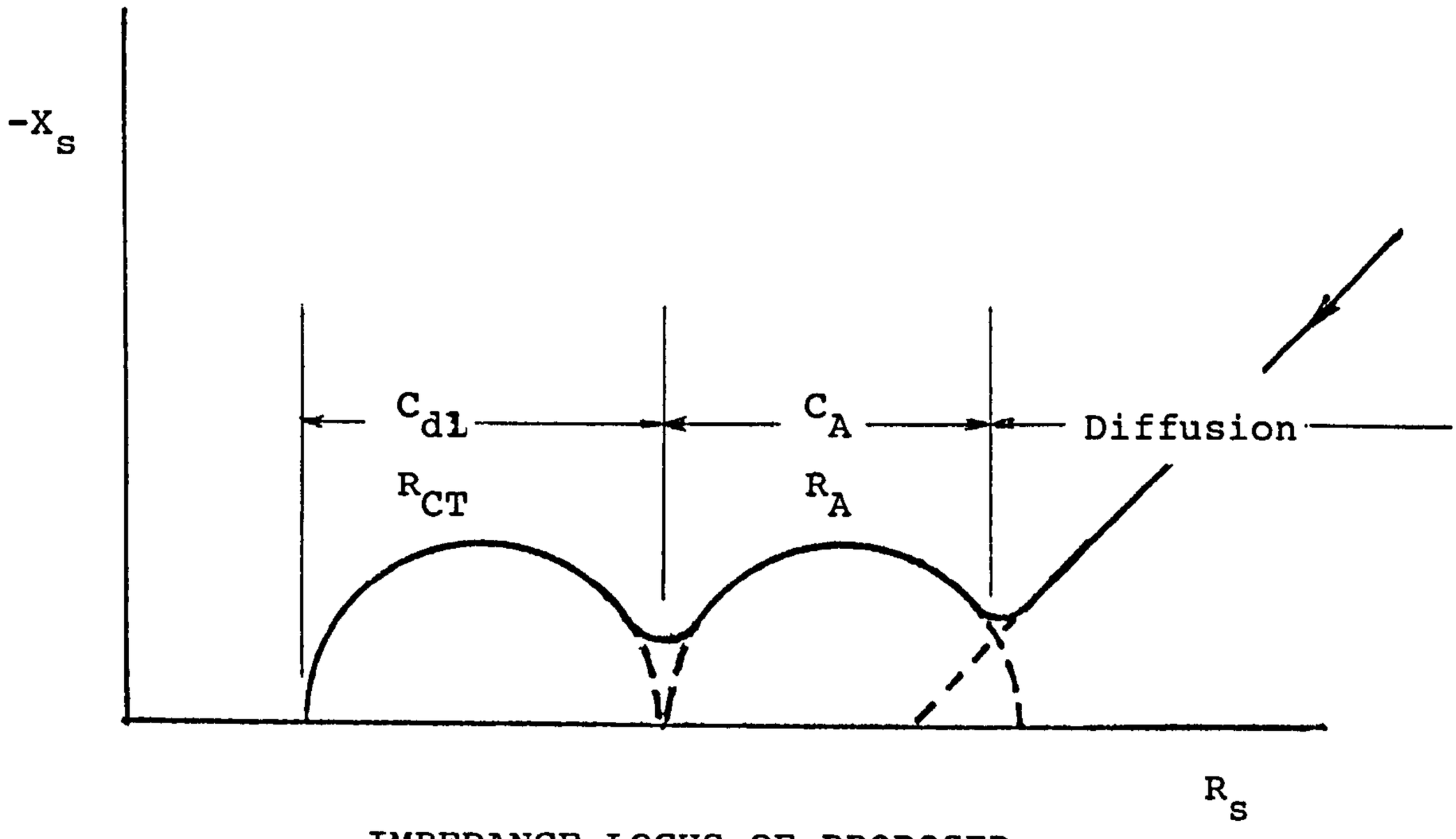

IMPEDANCE LOCUS OF PROPOSED
EQUIVALENT CIRCUITS

Figure 1.21

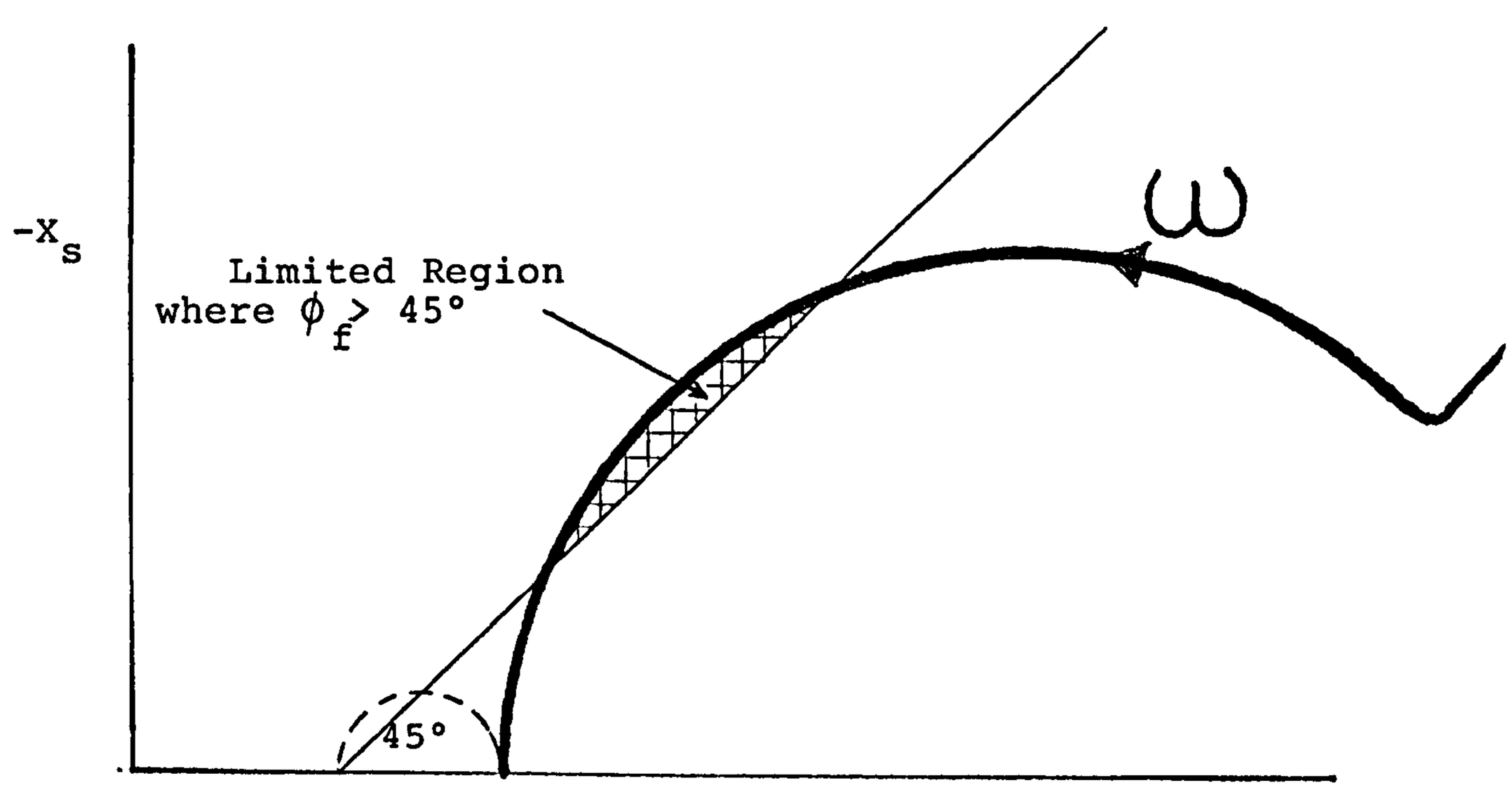

FARADAIC IMPEDANCE LOCUS

Figure 1.22

larger than 45°. For the above equivalent circuits, however, after the subtraction of C_{dl} and R_{TOTAL} from the total impedance, the faradaic phase angle will, however, only be above 45° if the adsorption semi circle is relatively large and only over a limited frequency range (figure 1.22).

The above equivalent circuits are therefore unacceptable in representing the electrical properties of electrode-electrolyte interfaces.

From a phenomenological viewpoint one could ensure a concave locus whose phase angle is larger than 45° over a wide frequency range using conventional electrochemical equivalent circuit elements by connecting in series a Warburg impedance and a capacitance. This would be a reasonable approximation to the observed impedance of the electrode-solution interface in the presence of adsorption effects (see fig 1.2). It is therefore interesting to note that several researchers have used such a combination to model the electrode system when adsorption effects are dominant. Their work will be briefly reviewed in the next two sections.

- Adsorption effects on the nonfaradaic impedance

Studies of electrode impedances in the absence of a faradaic process often reveal frequency dispersion of the double layer "capacitance" contrary to Grahame's (1946) statement that frequency dispersion is solely a

faradaic phenomena (Sluyters - Rehbach and Sluyters, 1970)

Disturbing the double layer from its equilibrium state involves the flow of current due to the change in the surface charge, q_m. As q_m ($-q_m = q_s = \Sigma_i F \Gamma_i$) is a function of electrode potential and surface excesses of the adsorbed materials this may result in noncapacitive behaviour if the adsorption process is too slow to follow the potential changes at the applied frequency (Sluyters-Rehbach and Sluyters, 1970). We will review briefly the work of two research groups on this problem.

(1) Frumkin and Melik-Gaikazyan

Frumkin and Melik-Gaikazyan (1951) considered the case of purely diffusion controlled adsorption of neutral molecules to explain the dispersion of the double layer capacitance when organic molecules are adsorbed. They derived the circuit shown on figure 1.23.

The 'nonfaradaic' branch comprised a high frequency capacitance, C_{HF}, in parallel with the series combination of Z_{WA} (a pseudo Warburg impedance due to adsorption) and an adsorption capacitance $\Delta C = C_{LF} - C_{HF}$

(2) Lorenz and Mockel

Lorenz and Mockel (1956) and later Lorenz (1958) also

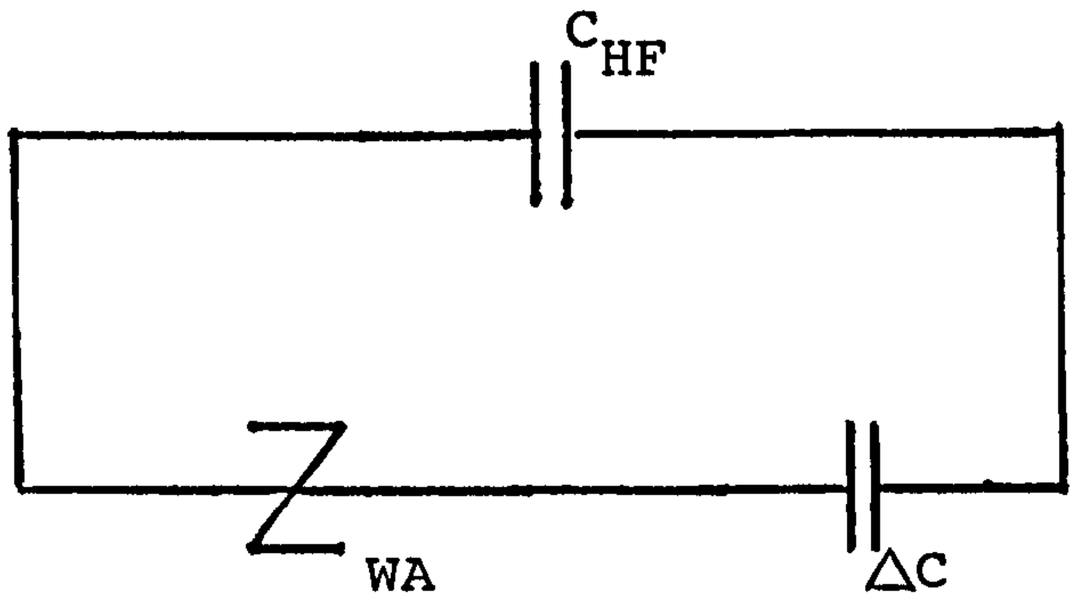

FRUMKIN AND MELIK-GAIKAZYAN

Figure 1.23

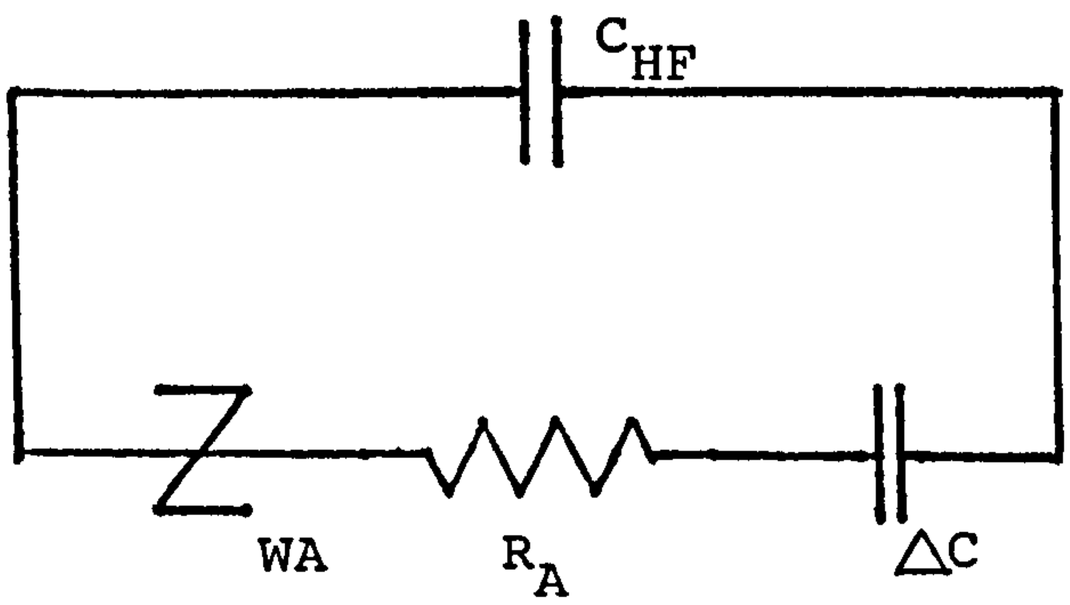

LORENZ AND MOCKEL

Figure 1.24

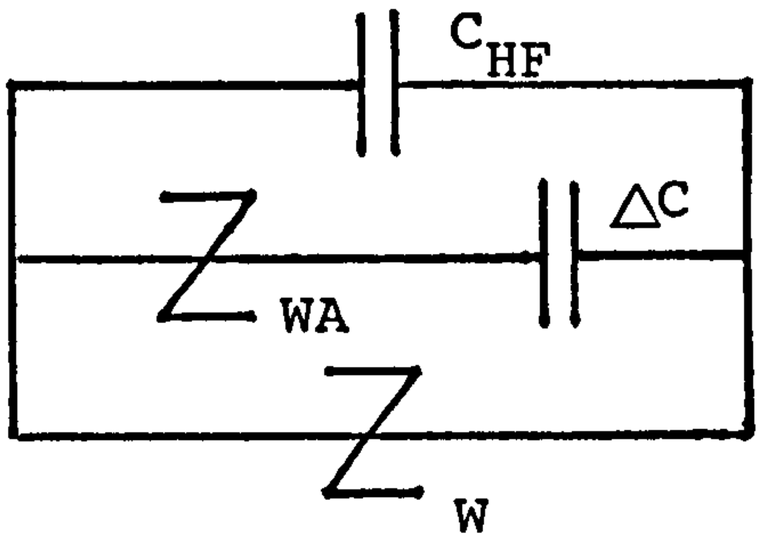

TIMMER ET AL.

Figure 1.25

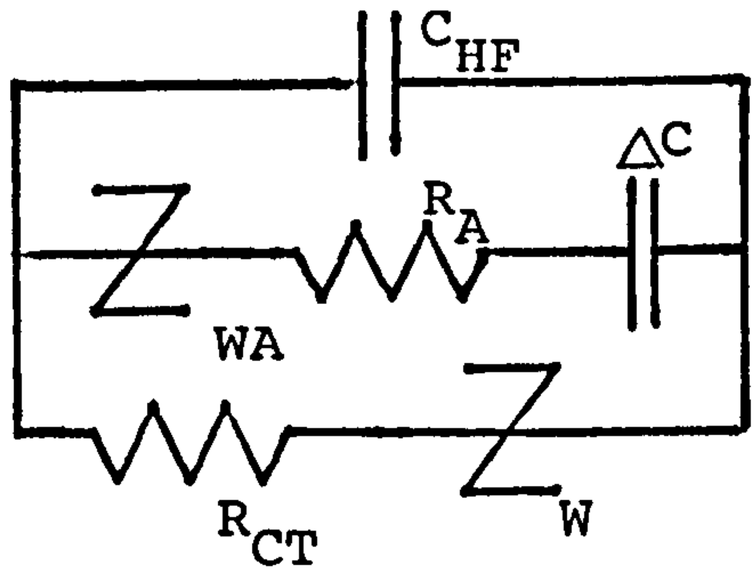

'COMPLETE' EQUIVALENT CIRCUIT MODEL

Figure 1.26

studied the effect of adsorption of electro inactive species on the "non faradaic" impedance. They derived an equivalent circuit model (shown on figure 1.24).

Both the above circuits should represent reasonably well the observed electrical properties of electrode interfaces.

- Adsorption Effects on the total interfacial impedance

Delahay and Susbielles (1966) were the first to really take the coupling between the faradaic and non faradaic processes into account. They argued that there is no theoretical justification for the commonly accepted 'a priori' separation of the faradaic and double layer charging currents and expressed this coupling concept in three equations

(a) The rate of an electrode reaction, $\frac{i_f}{nF}$, is generally equated to the flux of, say, the oxidised species, away from the electrode surface, V_o. In Delahay's more comprehensive case, the term, $d\Gamma_o/dt$, describing the changes in surface concentration of the oxidised species due to the imposed perturbation is included, i.e.

$$i_f/nF = V_o + d\Gamma_o/dt \qquad 1.34a$$

$$\text{where } V_o = D_o \left(\partial C^o/\partial d\right)_{d=o}$$

(b) Normally the mass balance equation is given by

$$v_R = v_O$$

However a term must be included relating the fluxes of the electroactive components to their surface excesses, i.e.

$$v_R = v_O + d(\Gamma_o + \Gamma_R)/dt \qquad 1.34b$$

(c) The total current is obtained by summing the flux of the reacting ions, v_O, together with those of the nonreacting ions in solution, i.e.

$$i_{TOTAL} = nFv_o + d(q_m + nF\Gamma_o)/dt \qquad 1.34c$$

This equation is the most important of the three proposed by Delahay. Others had used the first two equations (1.34a and b) but had always assumed that the nonfaradaic current was given by

$$i_{nF} = dq_m/dt$$

and that this was independent of the faradaic current. Delahay, on the other hand, argued that only i_{TOTAL} (which includes a function of $q_m + nF\Gamma_o$) can be observed and that its division into two components, q_m and $nF\Gamma_o$, is only an assumption.

Delahay's first two equations are the boundary conditions for which the mass transfer problem must be

solved. The resulting value of V_o is then used in the third equation to give the total current. Knowing the total current and the applied voltage, the electrode system's impedance can be derived. Indeed Holub (1967) using Delahay's equations derived a very complicated expression for the electrode impedance. Reinmuth (1968) simplified Delahay's analysis by assuming an infinite exchange current, i_o (i.e. $R_{CT} = 0$) and an infinite rate of adsorption, i.e. $R_A = 0$.
Timmer et al (1967) used the simplified Reinmuth analysis to derive the equivalent circuit shown on figure 1.25.

As a consequence of the coupling concept the usual double layer capacitance has been replaced by a high frequency capacitance, C_{HF}, which includes a term due to reactant adsorption at the electrode (see equation 4.35).

The adsorption impedance, Z_{WA}, has the form of a Warburg impedance (i.e. its impedance is proportional to $\omega^{-0.5}$) and is in series with an adsorption capacitance, $\Delta C = C_{LF} - C_{HF}$ (see equations 4.37 and 4.38).

If there is no reactant adsorption ΔC is zero and the electrode can be represented by the classical Randles circuit (minus R_{CT}), i.e. by a Warburg impedance in parallel with the double layer capacity, $C_{dl} = C_{LF} = C_{HF}$. When adsorption is weak, Z_{WA} and C_{HF} are negligible and the circuit is simply a Warburg impedance in parallel with the low frequency capacitance, C_{LF}. As

C_{LF} is equal to C_{HF} in the former case, both the weak and no adsorption cases can be considered the same and modelled by a Randles circuit - minus R_{CT}.

If reactant adsorption is strong, Z_{WA} and Δ C dominate the electrode's total impedance and the impedance locus has a form similar to that shown in figure 1.2.

At high frequencies the total impedance has a phase angle of 45^{o} due to Z_{WA}. At low frequencies the phase angle increases towards 90^{o} due to the series capacitance.

The above theoretical equivalent circuit for strong reactant adsorption and its impedance locus are very similar to those derived empirically from experimental results obtained for biomedical electrode interfaces (e.g. DeRosa and Beard, 1977).

It must be remembered that the following assumptions were made in deriving the above model

(i) an infinite rate of adsorption - i.e. no R_A and

(ii) an infinite rate of charge transfer - i.e. no R_{CT}

If these omissions are corrected for a more general equivalent circuit would be as shown in figure 1.26.

- Adsorption effects at Biomedical electrodes

Greatbatch and co-workers (1969) have pointed out the important role of adsorbed oxygen in charge transfer on noble metals. Shigemitsu and Matsumoto (1979) suggested that their observed interfacial impedance, with a phase angle of 60^{o}, could perhaps be explained by the

adsorption of oxygen on the electrode surface, remembering that adsorption with its series combination of a Warburg-like impedance, Z_{WA}, and a capacitance is characterised by a phase angle larger than 45^{o}.

It was however DeRosa and Beard (1977) who used the equivalent circuit of Timmer et al (1967) to model "smooth" surfaced biomedical electrode systems. To simplify the calculations and hence the equivalent circuit, DeRosa and Beard assumed that Z_{W}, due to diffusion, could be neglected - leaving the circuit model of Frumkin and Melik-Gaikazyan (1951) [see figure 1.23].

The above equivalent circuit model appeared to produce good agreement with experimental data over a limited frequency range (400-1,500 Hz). However, at higher frequencies the calculated phase angle of Z_{WA} was found to be larger than 45^{o} and hence the model is not completely satisfactory. Carim, Beard and Miller (1977) also found the same limitations for De Rosa et al's equivalent circuit. Further, it would appear from their results that the determination of C_{LF} and C_{HF} (used in the calculation of Z_{WA}) was very inaccurate and would suggest that their model could in fact be in even less agreement with the results than appeared.

From their figure 13, which is very similar to figure 1.2 in this thesis, it is probable that a better fit with experimental data would be obtained using the series combination of a $Z_{CPA}(\beta \simeq \cdot 8)$ and a capacitance. Although their model did not give very good quantitative agreement with experimental results, it was however able to explain qualitative changes in the

electrode impedance due to variations in concentration and composition of electrolyte.

It would appear that such ions as chloride, bromide and iodide, when present in the electrolyte, displace adsorbed oxygen on electrode's surface. Sites thus occupied by these adsorbed anions are therefore no longer available for the adsorption of oxygen. This inhibits the reduction of molecular oxygen on the electrode surface and greatly effects the electrode's impedance. Increasing the concentration of halide ions in the electrolyte was observed to increase the measured value of Z_{WA} and decrease those of C_{LF} and C_{HF} i.e. the total impedance increases. DeRosa and Beard concluded that the form of the electrode system's impedance was primarily due to the adsorption of oxygen at the electrode surface.

Undoubtedly absorption effects do contribute to the form and magnitude of electrode's observed impedance. However solid electrode surfaces are very rough in microscopic detail and it is known that this also gives rise to frequency dispersion (Delevie, 1964, see section 1.1.2.5). Separating effects due to the electroactive system from those due to the electrode surface is very difficult. Even "smooth" electrode surfaces (e.g. those that have been meticulously polished) will still have a residual frequency dependence caused by remaining surface imperfections. Hence the frequency dispersion observed with pacemaker electrodes will probably be due to both adsorption and surface roughness effects with surface roughness being

the dominant factor as pacing electrode surfaces are generally rough on a microscopic scale. Hence, although adsorption theory will be able to provide qualitative interpretation of experimental results, one cannot expect quantitative agreement as the theory assumes perfectly smooth surfaced electrodes which is not the case with biomedical electrodes.

In Chapter 4 it will be seen that adsorption effects also contribute to the nonlinearity of the interfacial impedance.

1.1.2.4. Distribution of Dielectric Relaxation Times, D.D.R.T.

- Introduction

Armstrong et al (1968) and Takahashi (1968) noted that the equations for the impedances of the circuits of Dolin and Ershler (1940) and Lorenz (1958) were analogous to those for a dielectric relaxation phenomenon proposed by Cole and Cole (1941).

Bockris et al (1966) however went one step further and suggested that relaxation in the reorientation of solvent dipoles adjacent to the electrode surface actually accounts for the observed frequency dispersion if there is a distribution of relaxation times present. They used Cole-Cole's (1941) empirical treatment as a starting point for their model.

- Equivalent Circuit Model

Cole and Cole had recognised that the classical Debye theory describing the dielectric behaviour of a dilute suspension of free dipoles did not correctly reproduce the frequency dispersion of complex dielectric function, ε_r^*, (where admittance $Y = 1/Z = j\omega\varepsilon_o\varepsilon_r^*$ and ε_o is the permittivity of free space) in most real situations. Note that it was assumed that the system was nonconducting [i.e. $g = 0$, where g is the conductivity].

If the electric field applied to a dielectric changes

rapidly, viscous damping hinders the dielectric polarisation from following such changes instantaneously. In the simplest case, this lag can be characterised by a first order differential equation with a single time constant. This approximation is known as the classical Debye theory and the mathematical equation is

$$\varepsilon_r^* = \varepsilon_{HF} + \frac{\varepsilon_{LF} - \varepsilon_{HF}}{1 + (j\omega T)} \qquad 1.35$$

The equivalent circuit model is shown in figure 1.27a. ε_{HF} represents the permittivity at high frequency, the dipoles relax with a time constant, T , and ε_{LF} is the low frequency permittivity value. The complex permittivity, or Cole-Cole, plot for such a system is a semicircle as shown in figure 1.27b.

However Cole and Cole (1941) noted that a purely dissipative Debye resistor was not adequate as in general experimental results revealed "depressed arcs" and not semicircles on the complex permittivity plot (see figure 1.28b).

They found that such arcs could be modelled mathematically by the empirical expression

$$\varepsilon_r^* = \varepsilon_{HF} + \frac{\varepsilon_{LF} - \varepsilon_{HF}}{1 + (j\omega T)^{1-\beta}} \qquad 1.36$$

They derived this now famous equation by the simple mathematical operation of the tilting of a semicircle through an angle of $\frac{\beta\pi}{2}$ radians.

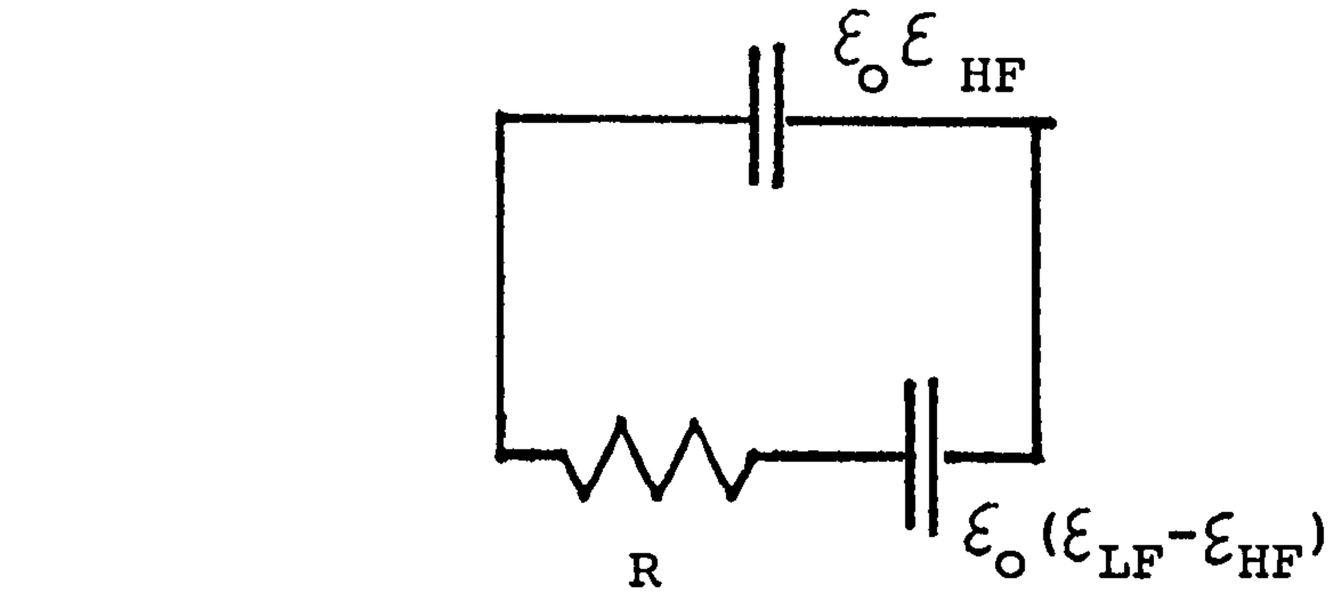

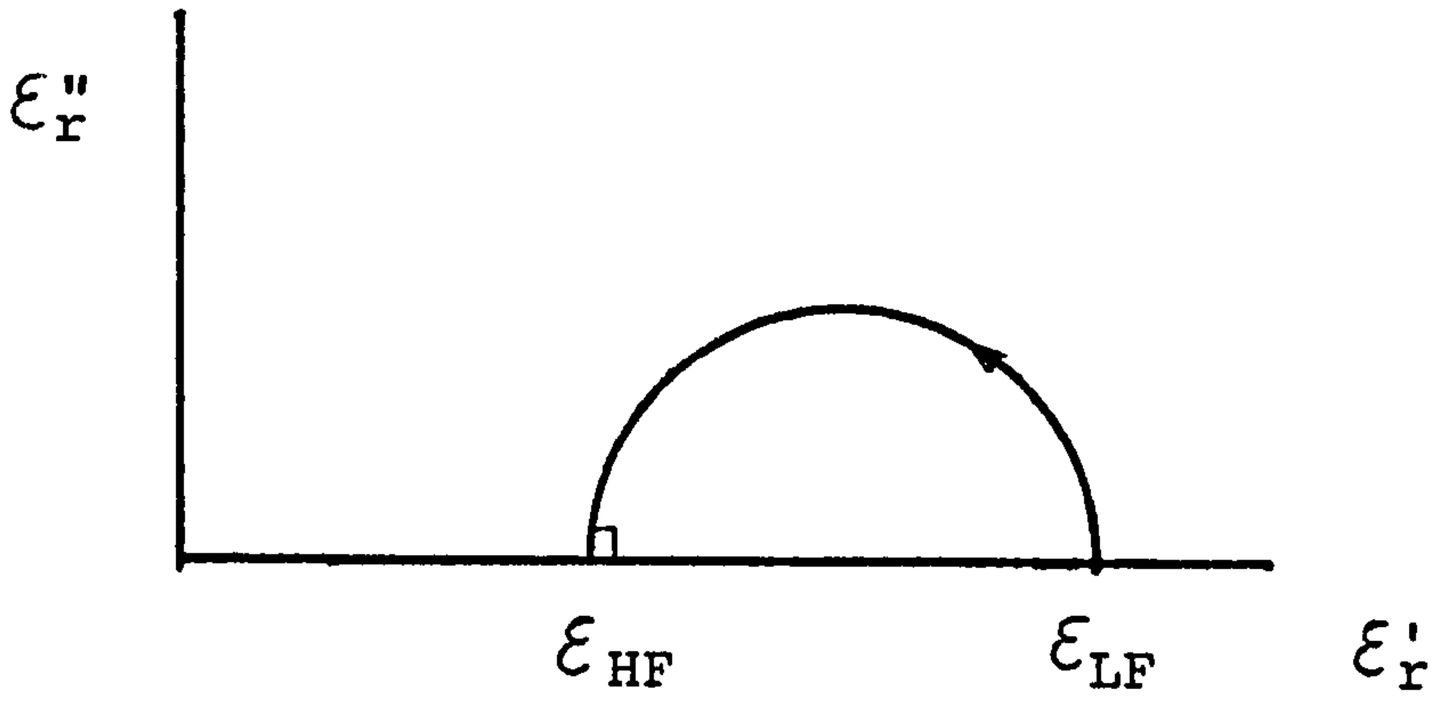

DEBYE COMPLEX PERMITIVITY PLOT

Figure 1.27

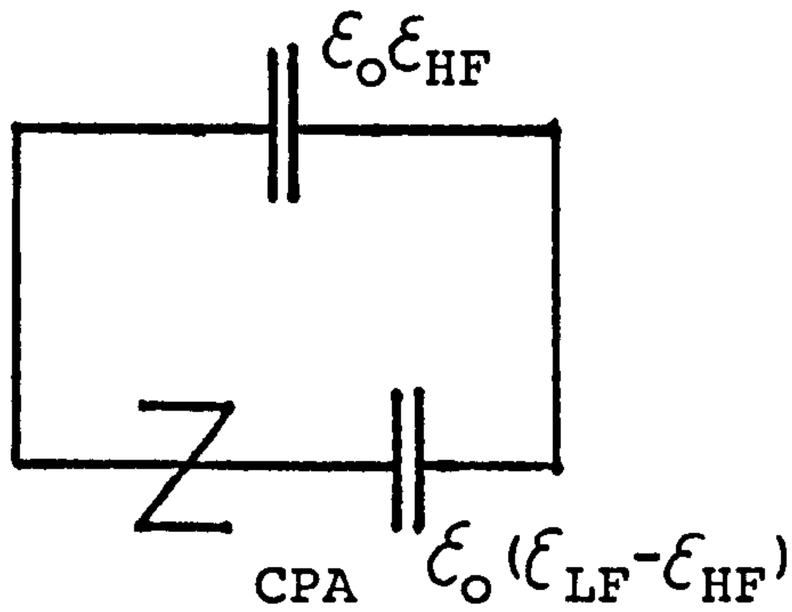

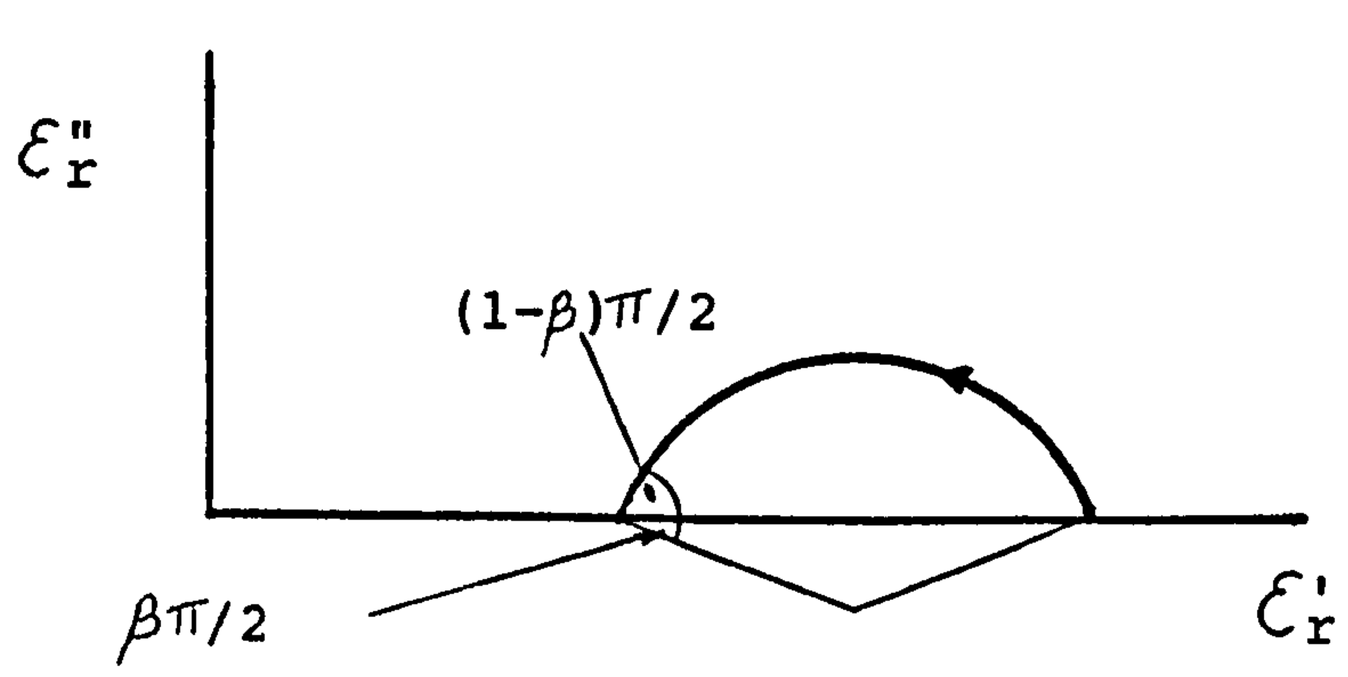

COLE-COLE COMPLEX PERMITIVITY PLOT

Figure 1.28

They also pointed out that this equation could be applicable to a particular system with a "distribution of relaxation times" (D.R.T.), where τ would stand for the average relaxation time and β would be a distribution parameter related to the width of the particular distribution.

Although Cole himself stated that the concept of a distribution of relaxation times was "an alternative expression of our ignorance of the mechanism" it has since become very popular in both the study of dielectrics and electrode interfaces (e.g. Stibitz and McCann, 1974).

From Cole-Cole's equation an equivalent circuit can be derived (Cole-Cole, 1941) and is shown on figure 1.28a.

The circuit is similar to that derived for the simple Debye case, except that the "Debye" resistance has been replaced by a constant phase angle impedance, Z_{CPA}, where

$$Z_{CPA} = \frac{T(j\omega T)^{-\beta}}{\varepsilon_o(\varepsilon_{LF}-\varepsilon_{HF})} = K(j\omega)^{-\beta}$$

$$\text{and} \quad K = \frac{T^{(1-\beta)}}{\varepsilon_o(\varepsilon_{LF}-\varepsilon_{HF})} \qquad 1.37$$

The "non-Debye" Z_{CPA} has the striking property that its phase angle $(\frac{\beta\pi}{2})$ is independent of frequency, hence its title "Constant Phase Angle" impedance, Z_{CPA}

The combination of a Z_{CPA} in series with a capacitance is, as we have seen, a very good equivalent circuit model of the observed electrode-electrolyte interface impedance - hence the interest shown in Cole-Cole's work over the years.

It can be seen by comparing equivalent circuits that Debye's type of dielectric dispersion ($\beta = 0$) is analogous to the case where adsorption kinetics are entirely controlled by the rate of the adsorption process (see circuit proposed by Dolin and Ershler, 1940, figure 1.17).

In the situation where the kinetics of adsorption are diffusion controlled, the equivalent circuit is the same as that of Cole-Cole (1941) with $\beta = 0.5$, i.e. Z_{CPA} equals Z_{WA} (see fig. 1.23, the circuit proposed by Frumkin and Melik-Gaikazyan, 1951). In other words, a diffusion controlled adsorption process is analogous to a dielectric relaxation phenomenon with a particular spread of relaxation times (Armstrong et al, 1968; Takahashi, 1968).

Several electro-chemists (e.g. Armstrong et al 1968; Takahashi, 1968) have shown an interest in Cole-Cole's work on dielectrics because of the above similarities and have applied the Cole-Cole plot method of analysis to the study of the frequency dispersion of the interface impedance due to adsorption effects. It is interesting to note that if the analogy between dielectric

relaxation and adsorption phenomena is continued, a more general model of adsorption effects would include a constant phase angle impedance, Z_{CPA}, and not a 'Warburg' impedance, Z_{WA}. The experimental results of Takahashi (1968) for example confirms this observation as he obtained a wide range of values for β .

Bockris and co-workers (1966) went farther than the above researchers and suggested that it was in fact the relaxation of water dipoles at the interface which gave rise to the observed frequency dispersion of the interface impedance. Their theory, however, is not generally accepted by researchers in the electrochemical field (Armstrong et al, 1968; Sluyters-Rehbach and Sluyters, 1970) as even if the effect is present it will be relatively insignificant. The theory must therefore be set aside even though the derived equivalent circuit was very promising.

- Distribution of Dielectric Relaxation times applied to biomedical electrodes

Jaron et al (1968) adapted the mathematical relaxation model of Cole and Cole (1941) and applied it to the biomedical electrode system. To simplify the mathematics they set C_{HF} to zero and hence the equivalent circuit becomes simply the series combination of Z_{CPA} and C_{LF}.

The complex capacitance, C^* (= $A\varepsilon_o\varepsilon_r^*/d$) simplifies to (see equation 1.36)

$$C^* = \frac{C_{LF}}{1 + (j\omega T)^{1-\beta}}$$

The impedance, Z, is therefore

$$Z = \frac{1}{j\omega C^*} = \frac{1}{j\omega C_{LF}} + (j\omega)^{-\beta} \frac{T^{1-\beta}}{C_{LF}}$$

$$Z = \frac{1}{j\omega C_{LF}} + K(j\omega)^{-\beta}$$

$$\text{where } K = \frac{T}{C_{LF}}^{1-\beta}$$

On the impedance plot the phase angle will approach $\beta\pi/2$ radians (or βx 90 degrees) at high frequencies, and will tend towards 90^o at very low frequencies.

It will be noted that this model is very similar to that of DeRosa et al (1977). In the present case however the more general Z_{CPA} is used instead of the 'Warburg' impedance due to adsorption, Z_{WA}.

Jaron et al found very good agreement between their equivalent circuit model and experimental results. They did however note that there was less agreement at high frequencies (possibly due to the absence of C_{HF}). Although Jaron et al (1968) did not postulate any theory for the observed frequency dispersion it seems very probably, due to the coiled electrodes used, that surface roughness effects were the major cause with ad-

sorption effects playing a relatively minor role.

1.1.2.5 Surface Roughness

- Introduction

In most discussions of biomedical electrodes, and in electrochemistry in general, it has been assumed that there is a smooth planar interface between the metal electrode and the electrolyte. Surface charge is thought of as being uniformly distributed, equipotential loci are represented as parallel to the interface and current flow is considered as a one dimensional problem.

Unfortunately, real solid electrode surfaces are usually very rough and sometimes even porous. Hence both sides of the interface are interpenetrating and not planar. Apparently smooth electrode surfaces will, on a microscopic level, be found to be most irregular with cliffing, cratering and channelling (Scheider, 1975).

Even if the electrode surface were flat, it would be covered in places by films, oxides, precipitants and organic contaminants etc., resulting in microregions with different physical properties (Dymond, 1976). Charge will therefore not be uniformly distributed even over a smooth, planar electrode surface. The roughness of electrode surfaces has been found to cause frequency

dispersion of the interface impedance (Delevie, 1965, 1967 and Scheider, 1975). Grahame (1952) after demonstrating the almost frequency invariant "polarisation capacitance" for a self replenishing moving electrode surface suggested that the dispersion observed with solid electrodes was primarily a geometric effect attributable to lack of smoothness. This has been further reinforced by reports that dispersion is diminished on solid surfaces of intrinsic smoothness such as those formed from the melt (Borisova and Ershler, 1950; Thomas, 1964) and those of single crystals (Leikis and Kabanov, 1957). Also, polishing an electrode's surface has been found to diminish the observed frequency dispersion (Armstrong and Burnham, 1976).

Unfortunately surface roughness, due to its variability and the difficulty in quantifying its degree, is a very difficult problem to model and hence to solve. Few researchers have made serious efforts to define and tackle the problem. What work has been done will be reviewed in the next sections.

- Frumkin's Distribution of relaxation times

Frumkin (1960) and Ramaley and Enke (1965) suggested surface cracks and roughness to account for the observed frequency dispersion produced by solid electrode interfaces. Instead of modelling the total electrode-electrolyte interface impedance with a series resistor

and capacitor, they proposed that each region of the surface may have a different effective resistance and capacitance resulting in many parallel RC pathways. Each pathway would have a different relaxation time and hence the total impedance would show frequency dispersion.

Frumkin (1960) thought that it was the resistance to the different areas of the electrode surface that caused the range in time constants, whereas Ramaley and Enke (1965) thought it was the series capacitance which varied from point to point.

Cole and Cole (1941), who were one of the first groups to use the concept of a "distribution of relaxation times", showed that the particular distribution required to produce the observed Z_{CPA} behaviour (with $\beta \cong 0.8$) was physically most improbable. For example, if $\beta = 0.75$, only 72% of the relaxation times will be within the large range $0.001 < \frac{T}{T_o} < 1000$ (where T_o is the average time constant). It would therefore require an extremely broad distribution of relaxation times, (well over 1×10^6:1) to generate the observed impedance characteristic and there would be great difficulty in accounting for such a broad distribution. An even greater problem, according to Cole and Cole, is in accounting for the essentially logarithmic symmetry of the distribution required. Cole and Cole concluded that "in the absence of any satisfactory explanation of these features, the distribution function is nothing

more than a means of expressing the experimental results".

- Delevie's surface pores

Delevie (1964, 1967) has made some outstanding research into the effects of surface roughness. He accounted for the observed frequency dispersion in terms of changing current density distributions which are functions of the frequency. At high frequencies the impedance of the interface is small and the distribution of current follows closely the microstructure of the surface. At lower frequencies the current distribution is more evenly distributed over the geometrical average rather than the true surface and the impedance is found to be larger.

Delevie represented each pore on the surface by a transmission line as shown in figure 1.29

where $1/Z_i$ = admittance of the interface per unit of length of pore

R_e = resistance of the electrolyte in the pore per unit length

p^{-1} =penetration depth (as per Delevie's notation)

l = pore depth

Delevie calculated the impedance of the pore, Z_o, as

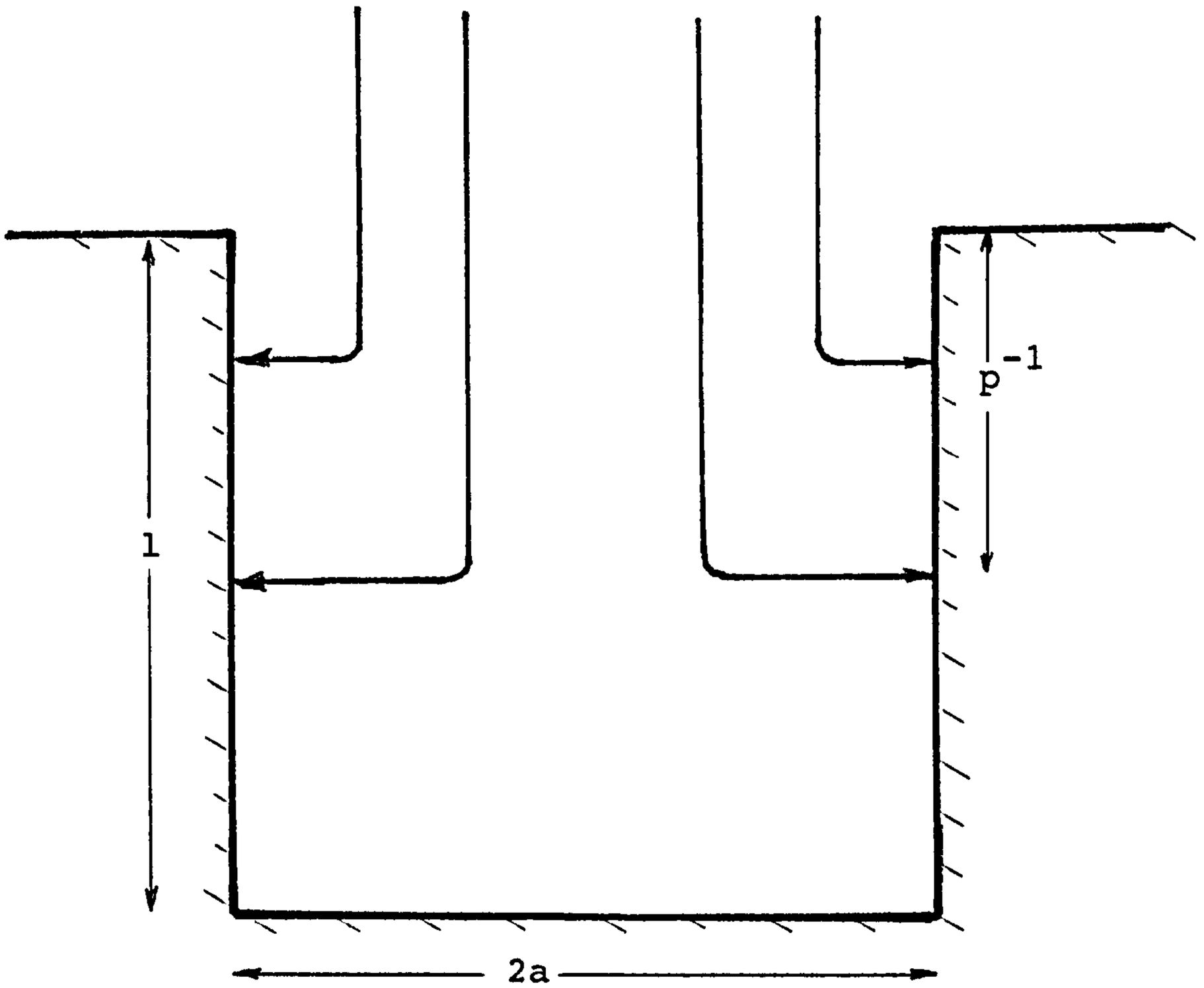

SURFACE PORE

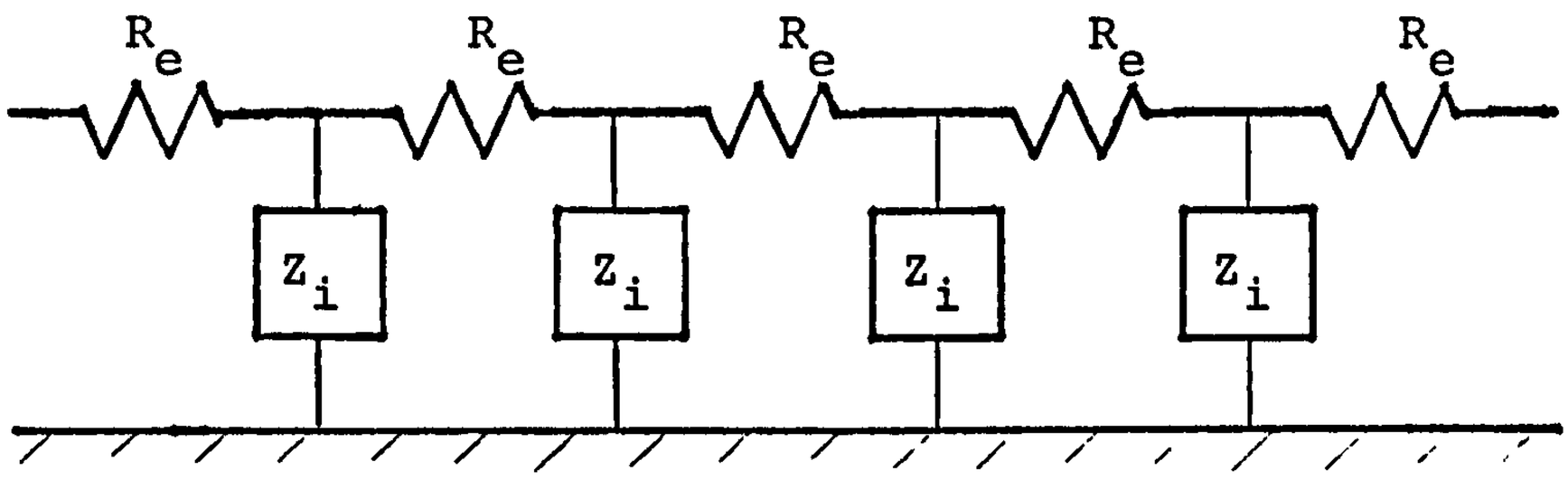

TRANSMISSION LINE MODEL

DELEVIE'S SURFACE PORE-TRANSMISSION LINE MODEL

Figure 1.29

$$Z_o = \sqrt{Z_i R_e}\ \text{Cotanh (pl)} \qquad 1.38$$

In the above equation one can rewrite the Cotanh term as

$$\text{Cotanh (x)} = \frac{e^x + e^{-x}}{e^x - e^{-x}} = 1 + \frac{2}{e^{2x}-1}$$

where $x = pl = (R_e/Z_i)^{1/2} l$ (Delevie 1964)

Expanding the exponentials one has

$$\text{Cotanh (x)} = 1 + \frac{2}{2x + \frac{(2x)^2}{2!} + \frac{(2x)^3}{3!} \ldots}$$

At low frequencies x is less than 1 and the higher terms in the Cotanh (x) expansion can be neglected, leaving

$$\text{Cotanh (x)} \simeq 1 + 1/x$$

At low frequencies, such that $(Z_i/R_e)^{1/2} > 1$, equation 1.38 therefore approximates to

$$Z_o = \sqrt{R_e\ Z_i} + Z_i/l \qquad 1.39$$

At high frequencies, $\text{Cotanh}(x) \simeq 1$ and $Z_o \simeq \sqrt{Z_i R_e}$ - the first term on the right hand side of equation 1.39.

If one assumes that Z_i is due to the double layer

capacitance (i.e. $Z_i = -j/\omega\Delta C_{dl}$) one can then model the electrode system by the series combination of a Warburg like impedance, Z_W, and a low frequency capacitance, C_{LF},

where $C_{LF} = \Delta C_{dl}\ l = C_{dl}$

(ΔC_{dl} is the double layer capacitance per unit length of the pore)

and

$$Z_W = (1-j)\ \left(\frac{R_e}{2\omega\Delta C_{dl}}\right)^{\frac{1}{2}}$$

At high frequencies 'p' is very large and the penetration depth, p^{-1}, is very small. Even a shallow pore will tend to behave as a semi-infinitely deep one. Hence the influence of porosity and surface roughness will be most evident at high frequencies. As p is very large, Cotanh (pl) tends to unity and can be ignored. The electrode's impedance is then

$$Z_o = \sqrt{Z_i\ R_e} = (1-j)\ \left(\frac{R_e}{2\omega\Delta C_{dl}}\right)^{\frac{1}{2}} = Z_W$$

This has the same form as a 'Warburg' diffusional impedance with a phase angle of 45°. Note that its magnitude is proportional to the square root of that of a smooth surfaced electrode, Z_i.

At low frequencies p reaches the critical value such that $p^{-1} = l$ (where l is the pore depth). At this point the a.c. signal reaches the bottom of the pores and the frequency distribution due to the pores no

longer contributes significantly to the overall electrode impedance. For very low frequencies the overall impedance will therefore be dominated by that due to the double layer capacitance.

Delevie's mathematical model's impedance locus and its equivalent circuit are similar to those derived from adsorption kinetics (section 1.1.2.3.). Both have a phase angle of 45^{o} at high frequency and one of 90^{o} at low frequency. This has caused some researchers to confuse surface roughness effects with those due to specific adsorption (Delevie, 1965).

As with adsorption the theoretical high frequency phase angle of 45^{o} is rarely seen in practice. Generally one deals with electrodes whose surfaces, though rough, are not so extreme as to be classified as porous. In these cases the high frequency phase angles have been observed to be generally larger than 45^{o} and hence better modelled by the more general Z_{CPA} in series with the low frequency capacitance.

- Scheider's "tangential charge spreading"

Scheider (1975) also investigated the effect of surface roughness on the impedance of the interface. Scheider considered that the observed constant phase angle impedance, Z_{CPA}, was the characteristic of a hitherto unconsidered process. According to Scheider the dispersion occurs in the diffuse double layer entirely within

the electrolyte phase. He associated it with tangential charge spreading along the irregular surface.

As already mentioned, lines of electric force do not converge evenly onto an uneven surface. It follows that the surface will therefore be charged unevenly as shown on figure 1.30.

Electric field lines, E, converge towards the peaks on the electrode surface and the valleys are, in effect, partially shielded. Ionic flow follows the lines of electric force and hence there is an accumulation of charge on the peaks. A concentration gradient is established and there is a lateral, time dependent, spreading of the charge to the valleys. Scheider believed that it is this phenomenon which gives rise to the frequency dependent impedance of constant phase angle.

The idea that tangential components of surface impedance could be related to the observed frequency dispersion was not new, in fact it was suggested nearly forty years previously by Fricke (1936, 1937).

Scheider noted that branched ladder networks with distributed properties also have input impedances with fractional power frequency dependence. He believed that the topological arrangement of these networks could bear a relation to the topology of the electrical processes present at the interface. With such networks

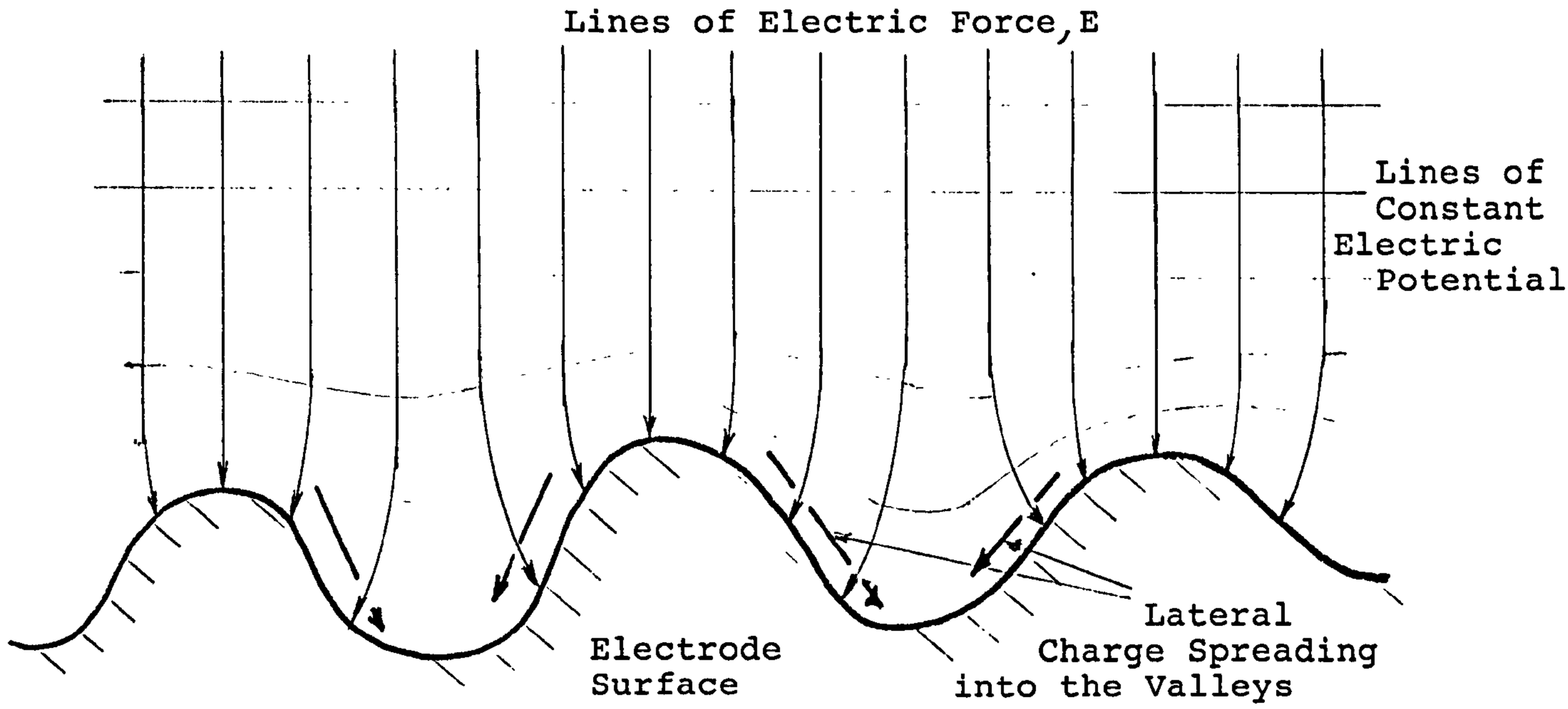

SCHEIDER'S "TANGENTIAL CHARGE SPREADING"

Figure 1.30

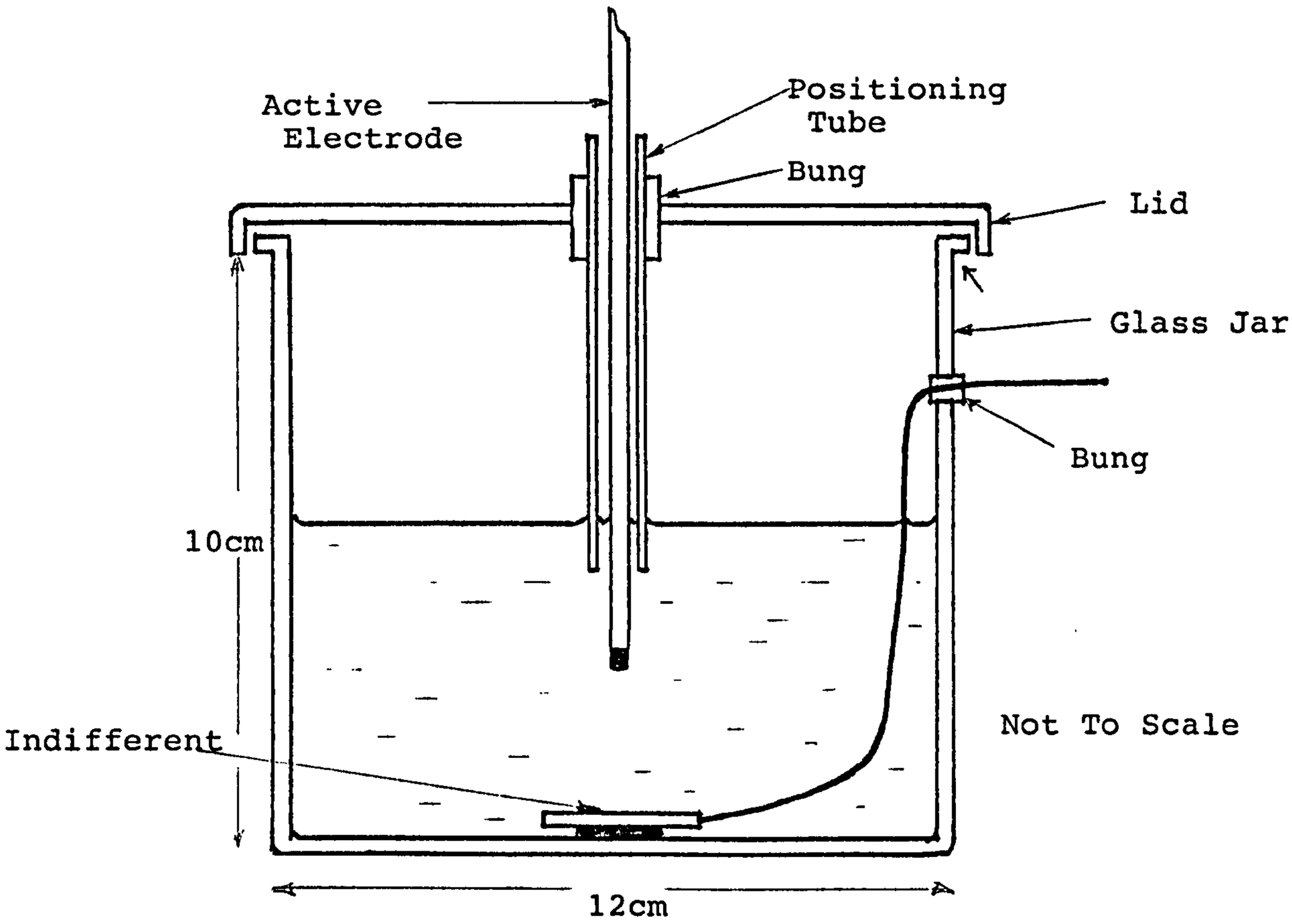

SALINE BATH

Figure 1.31

only discreet values of β can however be explained, limited by the extent of branching.

- Surface Roughness effects on Biomedical electrodes

As Dymond in his excellent review (1976) concluded "... evidence suggests the role of the electrode surface microstructure is highly relevant to the investigation of the behaviour of biomedical electrodes".

From Delevie's published results (1965) for rough surfaced platinum electrodes their impedance characteristic is very similar to that shown on figure 1.2. At high frequencies the impedance is best represented by a Z_{CPA} (Scheider, 1975) whose magnitude and phase angle decrease with the degree of surface roughness. At low frequencies the impedance approaches that of a smooth surface, with a phase angle approaching 90^{o} (Delevie 1965).

Pollak's (1974) experimental results indicate that K decreases with surface roughness. Kingma et al (1977) noted a decrease in the magnitude and phase angle of the interfacial impedance as they roughened the surface of Ag/AgCl electrodes. Wolf, as far back as 1926, noted that the phase angle ($\phi = \beta\pi/2$) increased after polishing the electrode's surface. Geddes et al (1971) found that for a highly polished surface the series capacitance, C_s (inversely proportional to K), is very small. They noted that even a slight roughening of the

surface increased C_s considerably (i.e. decreased K). The above, rather limited review, is sufficient to show that Delevie's model is at least qualitatively correct and that surface roughness effects are of major importance to the study of solid, unpolished biomedical electrode systems.

Ramaley and Enke (1965) made an interesting point when they stated that any model which attempts to explain the observed "dispersion effect" at electrodes must be able to explain why the "dispersion" increases (i.e. β decreases) as the solution conductivity decreases - as has been generally observed (e.g. Delevie 1965).

In Delevie's model there is a 'knee' in the impedance characteristic where Z_W behaviour gradually changes to $1/\omega C_{LF}$ behaviour. The frequency range of the "change over" region depends on the ratio of penetration depth, p^{-1}, to pore depth l,

$$\text{where } p^{-1} = (Z_i/R_e)^{1/2}$$

A given frequency range will be characterised by Z_W behaviour for small values of p^{-1} (or large values of R_e) and by $1/\omega C_{LF}$ behaviour for large values of p^{-1} (or small values of R_e). Hence frequency dispersion will be greater (i.e. the impedance will have a value of β closer to 0.5) over a given frequency range, for solutions of high resistivity or low conductivity. Delevie (1965) noted that the frequency dependence of the in-

terfacial "capacitance" was more pronounced for dilute solutions - and of course for rougher surfaces and at higher frequencies. Hence Delevie's model meets the criteria put forward by Ramaley and Enke (1965).

Another related point noted by Scheider (1975) is that the "polarisation capacitance", Cp, is dependent on the electrolyte conductivity, g, such that

$$[Cp]_{const\ \omega} = X[g]^{m}$$

where $m = 1 - \beta$ and X is a constant.

This relationship can be re-written as

$$Z = \frac{1}{\omega C_p} \propto \frac{1}{\omega g^{1-\beta}} \propto g^{-(1-\beta)}$$

i.e. the interfacial impedance is inversely proportional to the electrolyte conductivity. Why should this be so ?

At high frequencies, the interfacial impedance is given, according to Delevie, by

$$Z_o = \sqrt{Z_i R_e}$$

i.e. the observed interface impedance is proportional to $R_e^{1/2}$ or $g^{-1/2}$.

Delevie's model agrees with Scheider's observations only if $\beta = 0.5$.

1.1.2.6 - Summary on the high frequency, small signal electrode-electrolyte interface impedance

From the review it is evident that many researchers have noted and endeavoured to model physically and/or with equivalent circuits, similar impedance characteristics to that shown in figure 1.2.

According to Sluyters-Rehbach and Sluyters (1970) the two most probable theroories to account for observed frequency dispersion at solid electrode interfaces are adsorption and surface roughness. It would appear from the above review that this statement is true for biomedical electrodes. Surface roughness effects are definitely an important factor with pacing electrodes as many are made with deliberately roughened or porous surfaces in order to decrease their interfacial impedance. As has been shown, these affect the form of the impedance characteristic and are probably the dominant factor. The presence and effect of specific

adsorption have been underlined by the work of Greatbatch et al (1969) and De Rosa et al (1977). For very smooth electrode surfaces adsorption effects will make a significant contribution to the observed frequency dispersion. Even with 'rough' surfaced pacing electrodes adsorption will make some contribution. It will be shown in chapter 4 that adsorption effects give rise to part of the observed nonlinearity of the electrode-electrolyte interface impedance as the adsorption pseudo 'capacitance' is by definition nonlinear.

Although the physical models of Delevie (1964, 65, 67) and Timmer et al (1967) succeed in explaining qualitatively much of the observed experimental data, their mathematical or equivalent circuit models fail to accurately represent the same. Both models fail to reproduce the high frequency phase angle larger than 45^{o} observed at electrode interfaces.

It is the opinion of the author that, to date, the best equivalent circuit model over a wide frequency range of an electrode system's impedance which is dominated by surface roughness and/or adsorption effects is that originally proposed by Cole and Cole (1941) and used by Jaron et al (1968), namely a Z_{CPA} in series with a capacitance, both of which are shunted by another capacitance which may or may not contribute significantly.

In Section 1.2 results will be presented of experiments on the form of the interfacial impedance of several different electrodes. It will be verified that they are well represented by the above equivalent circuit and the effect of surface finish on the form of the impedance will be investigated.

1.2 EXPERIMENTAL SECTION

Introduction

In this, the experimental section of Chapter One, measurements will be taken of the linear (small signal), high frequency impedance of several different pacing electrode types. The results will then be fitted to the proposed model of a Z_{CPA} (with or without the low frequency capacitance, C_{LF}, as found necessary) and calculated parameter values compared.

Surface roughness effects on the interface impedance will be studied and compared with the theoretical predictions made in the first half of this chapter.

1.2.1 Equipment and Experimental Method

Electrode System

For the invitro experiments the electrode system shown on figure 1.31 was used.

The indifferent electrode (90%Pt - 10%Ir, area approx. 10 cm^2) was one removed from a Devices pacer and Araldited centrally to the bottom of the glass jar. The lead was placed along the bottom of the jar, up the side and out through a water tight hole in the glass approximately 3cm from the top and 2 cm above the level of the saline.

The active electrodes tested were either new or used clinical electrode leads of various manufacture which are described in full in Section 1.2.2. An active electrode was introduced through a central vertical sleeve which was supported vertically by external clamps. The active electrode was lowered to a separation of 1cm from the indifferent. Physiological saline (0.9%) was used which, according to Greatbatch and Chardack (1968), offers the same load impedance to a pacemaker as that seen when the same electrodes are in tissue, except that a small resistor,(185 Ω), must

be added in series with the saline bath to compensate for the body's lower electrical conductivity. (This, however, is incorrect as will be shown in chapter 7).

Measurement Systems

- Wien Kerr Impedance Bridge (C.T.530)

Initially a Wien Kerr Impedance Bridge was used with a separate Oscillator to measure the high frequency (0.5kHz to 5kHz) ac impedance of pacing electrode systems.

Apart from the rather limited frequency range the experimental set up suffered the drawback of being manually operated. One experiment, involving the measurement of impedance at a dozen or so frequencies, could take up to half an hour. As an electrode system can change with time, this was judged not very satisfactory.

- Solartron 1170

Professor Hampson of Loughborough University of Technology kindly carried out impedance measurements on some of our electrodes using their advanced equipment while we were on a one day visit to his department.

The electrode system impedances were determined using a frequency response analyser (Solartron Type 1170) and a potential controller (Kemitron PC-03). The im-

pedance data were retrieved from the analyser as in phase (R_S) and out of phase (X_S) components recorded on punch tape. The frequency response analyser automatically measured the impedance components at a series of frequencies in the range of kilohertz to tens of millihertz. Acquired data were read into the computer (Prinz 400) from the punch tape output and filed there. Argand plots and Randles plots (R_S and X_S versus $\omega^{-0.5}$) were constructed for each electrode.

- Solartron 1250

Several months before the end of my research the use of a frequency response analyser (Solartron 1250) was kindly offered by the Department of Physics, Leeds University.

The Solartron 1250's generator can provide sinusoidal waves in the frequency range 10μHz to 65.5 kHz with a frequency accuracy better than 1 part in 10^4. For this study of the linear, high frequency impedance of electrodes the frequency range 100 Hz to 10 kHz was chosen.

The generator's sinusoidal output can be set between 10mV and 10V(rms) and may be superimposed of a d.c. bias which can be in the range +10V to -10V. The smallest possible ac signal amplitude (10mV rms) was decided upon with no d.c. bias in order to minimise nonlinearity effects (see Chapter 4). Although a

manual frequency sweep is possible, the Solartron 1250 is capable of automatic sweeps. The user can define the minimum and maximum frequencies, whilst the intermediate steps are chosen from logarithmic or linear steps. In the experiments logarithmic steps, 5 per decade were used.

An electrode system may need time to settle between the application of a stimulus and a measurement commencing, or following a change of frequency during a sequence of measurements. A 10 cycle delay before measurement commenced at the next frequency point was arbitrarity chosen in an effort to avoid or at least minimise any settling problem.

The measurement of one frequency point is taken over at least one complete cycle of the applied frequency. When a signal contains noise or other spurious components it may be difficult to decide how long an integration is required in order to give a result with an acceptably small error. With the 1250 there is a choice of two levels of statistical error -

long integration: 1% error with 90% confidence

short integration: 10% error with 90% confidence

For most of the experiments long integration, ie with a 1% error, was used.

Analysis of the electrode system's response requires comparison of its response with the input in both amplitude and phase. The resultant current through the electrode system was sensed as a voltage across a small resistance, R, in series with the electrodes and fed into one input of the analyser, while the electrode voltage drive (from the Solartron's generator) was fed into the second channel for comparison. The voltage across the electrode system is $V_2 - V_1$ and the current flowing through it is V_1/R. Therefore (see Figure 1.32)

$$Z = \frac{(V_2-V_1)R}{V_1} = (\frac{V_2}{V_1} -1)R$$

The Solartron 1250 calculates the ratio V_2/V_1 and hence one must subtract 1 from the calculated value and then multiply by R, the small series resistance (10 Ω). The ratio V_2/V_1 can be displayed of each frequency in either cartesian, polar or log-polar format. Cartesian notation was chosen as it lends itself to the plotting of argand diagrams.

- Settling Time

Professor Hampson and his colleagues, whose Solartron 1170 was used, generally carry out impedance measurements on cells used to produce electric current by their chemical action. In these cases the electrodes have been in contact with the electrolyte for a long period of time and equilibrium conditions have long

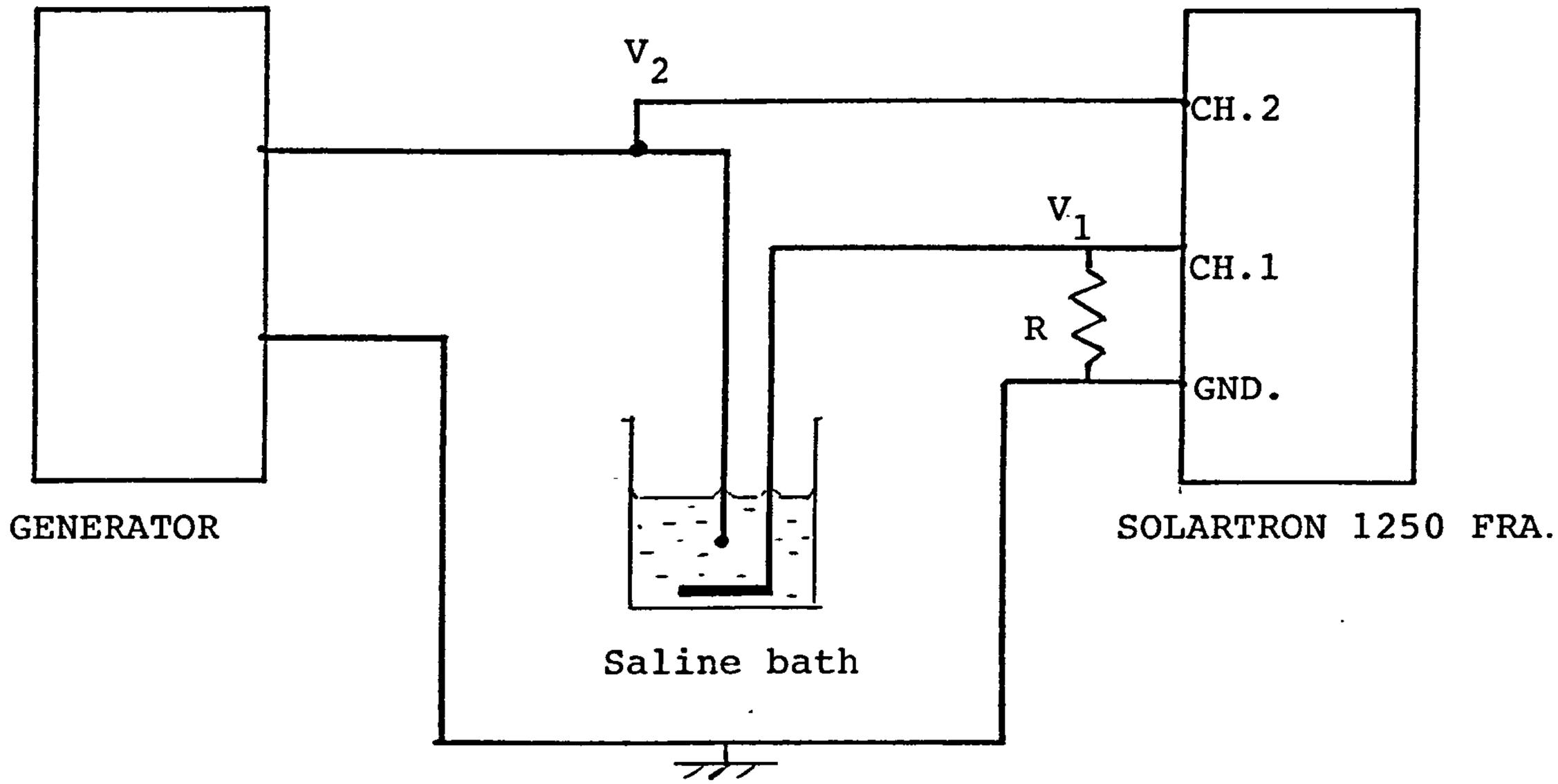

IMPEDANCE MEASUREMENT SYSTEM

Figure 1.32

been reached. When using his Solartron 1170 the electrodes were immersed in the saline solution just prior to the experiments. Equilibrium conditions had not been reached and the impedance of the system changed dramatically during the measurement time. This resulted in distorted impedance plots similar to that shown in Figure 1.33 for a Pt-Ir Devices L.C. electrode. It is evident that as time passes and the measuring frequency decreases, the magnitude of the phase angle rapidly increases from its initial (high frequency) value of less than 45°.

Similar plots, with bending over towards the imaginary axis and scatter of points, were also obtained using the Wien Kerr Bridge when insufficient time was allocated for the "soaking" of the electrodes.

It was found experimentally, both with the Wien Kerr and the Solartron 1250, that electrodes should be left in the electrolyte for at least 1.5 hours before readings are taken. After 1.5 hours the electrode system reaches a pseudo equilibrium and the impedance does not change significantly during the experimental measurement period. Due to this oversight most of the experiments carried out at Loughborough University of Technology were of no use with the notable exception of those carried out on the vitreous carbon electrode - see Section 1.2.3.2.3.

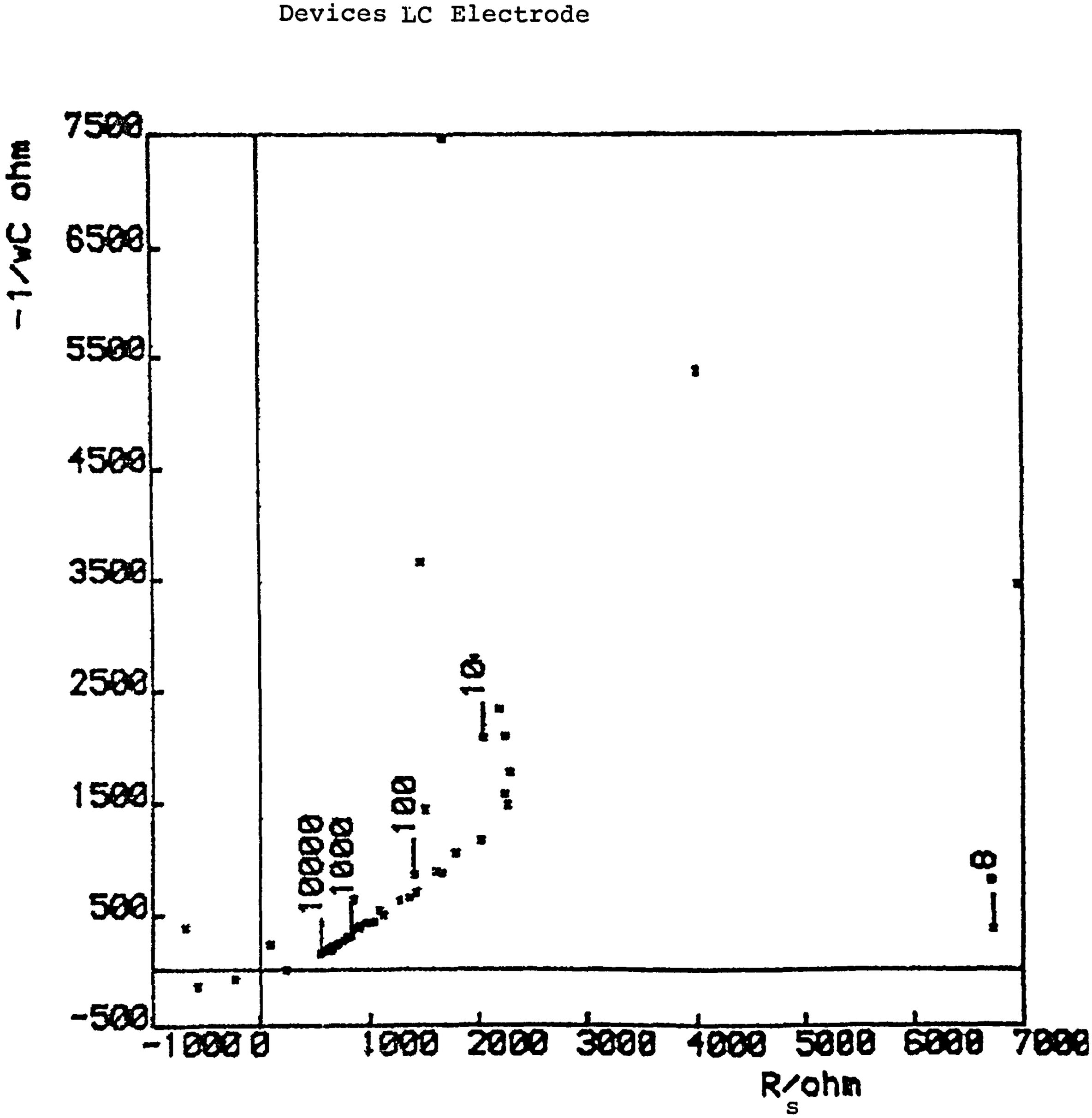

EFFECT OF INSUFFICIENT SETTLING PERIOD

Figure 1.33

Due to a change in R_{CT}- Fig.4.9

1.2.2 Electrodes tested

Electrode	Surface area mm^2	Tip material	Conductor material
Devices L.C.	12	PT-Ir	Stainless steel
Devices S.C.	21	Pt-Ir	Stainless steel
Vitatron Helifix	23	Pt-Ir	MP35N nickel alloy
Telectronic 224	10	Pt	Stainless steel 316L
Medtronic 6917A	6.6	Pt-Ir	Pt-Ir
Sorin S.80	8	Sintered Pt-Ir	Elgiloy
Siemens-Elema 411S	12	Activated Vitreous Carbon	Nickel alloy MP35N

TABLE 1.1

The electrodes can be divided into 3 broad categories:-

a) "smooth" surfaced Platinum and Platinum-Iridium electrodes

b) rough surfaced electrodes, ie the Sorin S80

c) very rough surfaced, activated vitreous carbon electrodes.

a) "Smooth" Platinum and Platinum-Iridium Electrodes

Metals which are not corroded by electrolysis are generally used as biomedical electrodes. Platinum is one such metal, but by itself it can be too weak mechanically to be of use as an electrode. Platinum is therefore generally combined with iridium to form a mechanically strong alloy, Platinum 90% - Iridium 10%, being 'proof' against electrolysis.

b) Rough Surfaced Electrodes

A rough or porous electrode surface in tissue fills up with cellular elements and subsequent organisation of these cells forms mature fibrous connective tissue. The manufacturers of sintered electrodes wish to encourage such tissue ingrowth as a more stable fixation may be expected due to the tissue bond to the endocardium.

The success of this approach will depend on the presence of only a minimal growth of fibrous tissue between the porous electrode surface and the endocardium. Too much fibrous tissue will be counter productive as it will separate the electrode from the active tissue and hence raise the current threshold. However the porous surface may well contribute in the minimising of this fibrous tissue response by reducing the micromovement which usually occurs between electrode and endocardium. This movement tends to produce mechanical injury and thus elicits more fibrosis (Wilson et al, 1983). For example, Gadaleta et al (1983) found that smooth Platinum-Iridium electrodes do not fix to the endocardium and continuously rub on the endocardial surface causing acute inflammation and fibrin deposition.

The advantages of porous electrodes can be summarised as follows (Amundson et al, 1979).

1) Fibrotic tissue grows into the electrode for early stabilisation and fixes the electrode to the endocardium.

2) the fixed electrode results in less mechanical injury and a smaller fibrous capsule and therefore lower chronic pacing thresholds, and

3) the porous surfaces dramatically reduces the interfaced impedance as shown in Section 1.1.2.5

The Sorin S80 electrode tip is made from platinum-iridium (90-10%) alloy with a sintered surface which is produced by covering the originally polished tip with two layers of granules (20-40 microns) of the same material.

c) Very Rough Surfaced Activated Vitreous Carbon Electrodes

At initial implant an electrode normally exhibits very low thresholds because of intimate contact with active myocardium. Chronic thresholds are much higher since fibrotic growth or other tissue damage displaces the electrode from direct myocardial contact. An implanted electrode will be surrounded by connective tissue layer within a few days. The thickness of the layer will depend on the electrode material used. Since the connective tissue is not excitable its growth is held to be responsible for the threshold rise. Connective tissue layers up to a thickness of 3mm have been observed for different electrodes. There are at least two reasons for the growth of fibrotic tissue - mechanical irritation and chemical reaction (Elmqvist et al, 1983). The

chemical interaction or biocompatibility is a rather complex problem. It would appear that the traditional platinum electrode can actually induce fibrotic growth at the tip because of the catalytic properties of platinum. The most promising material has been found to be carbon with the thinnest layer of induced connective tissue (Elmqvist et al, 1983; Mund et al, 1979; Kingma, 1977). Carbon electrodes are well known for their biocompatibility and they evoke only weak tissue reactions (Richter et al, 1979). Vitreous carbon is a strong, inert and conductive material apparently perfect for pacing electrodes.

Unfortunately the smooth vitreous carbon electrode has a very large interfacial impedance. Mund et al, (1976), for example , found a value of K = $10,400\Omega cm^2 s^{-\beta}$ for vitreous carbon whereas their platinum-iridium electrode only had a value of K = $1,167\Omega cm^2 s^{-\beta}$. Similar findings were reported by Mund et al (1979). As shown earlier, the impedance of an electrode can be greatly decreased by roughening its surface. A particularly desirable electrode would therefore be made by proceeding with a raw (untreated) carbon electrode and finally causing a roughening of its surface by activation. The process of activation involves heating the vitreous carbon in an oxidising atmosphere. The net result is a sur-

face with numerous minute pores (Edeling et al, 1983). The interface impedance of an activated carbon electrode is very low throughout the required frequency range for pacing (above 1kHz) (Elmqvist et al, 1983). In fact at high frequencies it is dominated by the series resistance R_{TOT}. According to Mund et al (1979) the value of K for the activated vitreous carbon electrode is 1.9 Ω $cm^2 s^{-\beta}$. Compared with the untreated electrode, a 'roughness factor' of approximately 2600 is obtained.

Not only does roughening the electrode surface decrease the electrical impedance, but it also minimises the growth of fibrotic tissue due to mechanical irritation as explained in Section b.

The activated vitreous carbon electrode therefore has a very low impedance and low fibrotic growth (whether due to chemical reaction or mechanical irritation), both of these properties being very desirable.

1.2.3 Experimental Results

1.2.3.1 Experimental results obtained using the Wien Kerr Bridge

Using the Wien Kerr Bridge (CT 530) to measure the a.c.

impedance several experiments were carried out for each of the following electrodes. The results were fitted to a Z_{CPA} - R_{TOTAL} combination - the frequency range was too limited to witness the presence of C_{LF}. Typical values for the Z_{CPA} impedance and the series resistance, R_{TOT} are listed below.

As the impedances of these electrodes have been measured more accurately in a later section and their impedance loci plotted over a wider frequency range, the plots obtained using the Wien Kerr have not been reproduced.

Electrode	$R_T(\Omega)$	ϕ	$K(k\Omega s^{-\beta})$	β	$R_L(\Omega)$	$R_S(\Omega)$
Dev LC(No 1)	105	74	270	.79	39	66
Dev SC(No 2)	182	79	73	.9	139	41
S.80 (No 1)	139	61	20	.61	52	88
AVC (No 1)	207	57	12	.61	135	72

$R_T = R_{TOT}$ $R_L = R_{LEAD}$ $R_S = R_{SALINE} = /4\ r_o$
r_o is the radius of the electrode tip

TABLE 1.2

The loci of the Argand diagram and the log |Z|-log f plots gave straight lines as expected. For each of the electrodes the value of the phase angle, ϕ, calculated from the Argand diagram was close to that calculated from the log - log plot ($\phi = \beta \times 90^o$). This would in-

dicate that the total impedance of the above electrodes is well modelled by the resistance, R_{TOT}, in series with a constant phase angle impedance, Z_{CPA}. However a much wider range of frequencies would need to be investigated with more accurate equipment.

- Effect of electrode surface area

It was observed that, the larger the electrode area, the smaller the value of K. For example it was observed that

$K = 270\ k\Omega s^{-\beta}$ for Devices L.C., ($12mm^2$) and

$K = 73\ k\Omega s^{-\beta}$ for Devices S.C., ($21mm^2$)

The value of R_{SALINE} is observed to decrease as the area of the electrode increases. For example

$R_{SALINE} = 66\Omega$ for Devices L.C., ($12mm^2$) and

$R_{SALINE} = 41\Omega$ for Devices S.C., ($21mm^2$)

- Effect of electrode surface finish.

The phase angle for the 'smooth' Pt-Ir electrodes varies between 74^{o} and 81^{o} whereas rough surfaced electrodes have smaller phase angles - 61^{o} for the Sorin S80 (sintered Pt-Ir) and 57^{o} for the S E 411S (A.V. Carbon). The impedances of the 'smooth' Pt-Ir electrodes are also much larger than the rough surfaced electrodes - $270\ k\Omega s^{-\beta}$ for the Devices L.C. compared to $12\ k\Omega s^{-\beta}$ for the Sorin S80. The activated vitreous carbon electrode appears to be the "best" of the four electrodes tested as it has the smallest impedance, K, and the smallest phase angle, ϕ, though it has the largest value of R_{TOT}.

1.2.3.2 Experimental results using the Solartron 1250

1.2.3.2.1 Smooth Pt-Ir electrodes

- Devices L.C. ($12mm^2$)

Using the Solartron 1250 the impedance of electrode No.1 (Exp. 52) was measured in 0.9% saline and the results are plotted on Figure 1.34. The impedance locus is a straight line and the calculated values of the elements of the equivalent circuit model (R_{TOT} and Z_{CPA}) are as listed on table 1.3.

TABLE 1.3

From X_S-R_S plot		From log Z -log f plot			
R_{TOT} (Ω)	ϕ	K ($\Omega S^{-\beta}$)	β	R_{LEAD} (Ω)	R_{SALINE} (Ω)
108	74°	102	0.8	39	69

It will be remembered that the impedance of this electrode (No.1) measured using the Wien Kerr Bridge (see 1.2.3.1) was found to be modelled by a Z_{CPA} with parameter values:-

$$K = 270\ k\Omega\ s^{-\beta} \quad \text{and} \quad \beta = .79$$

The dramatic decrease in K and the small decrease in β are very probably due to the intervening nonlinear experiments (Chapters 4 and 5) carried out on this electrode.

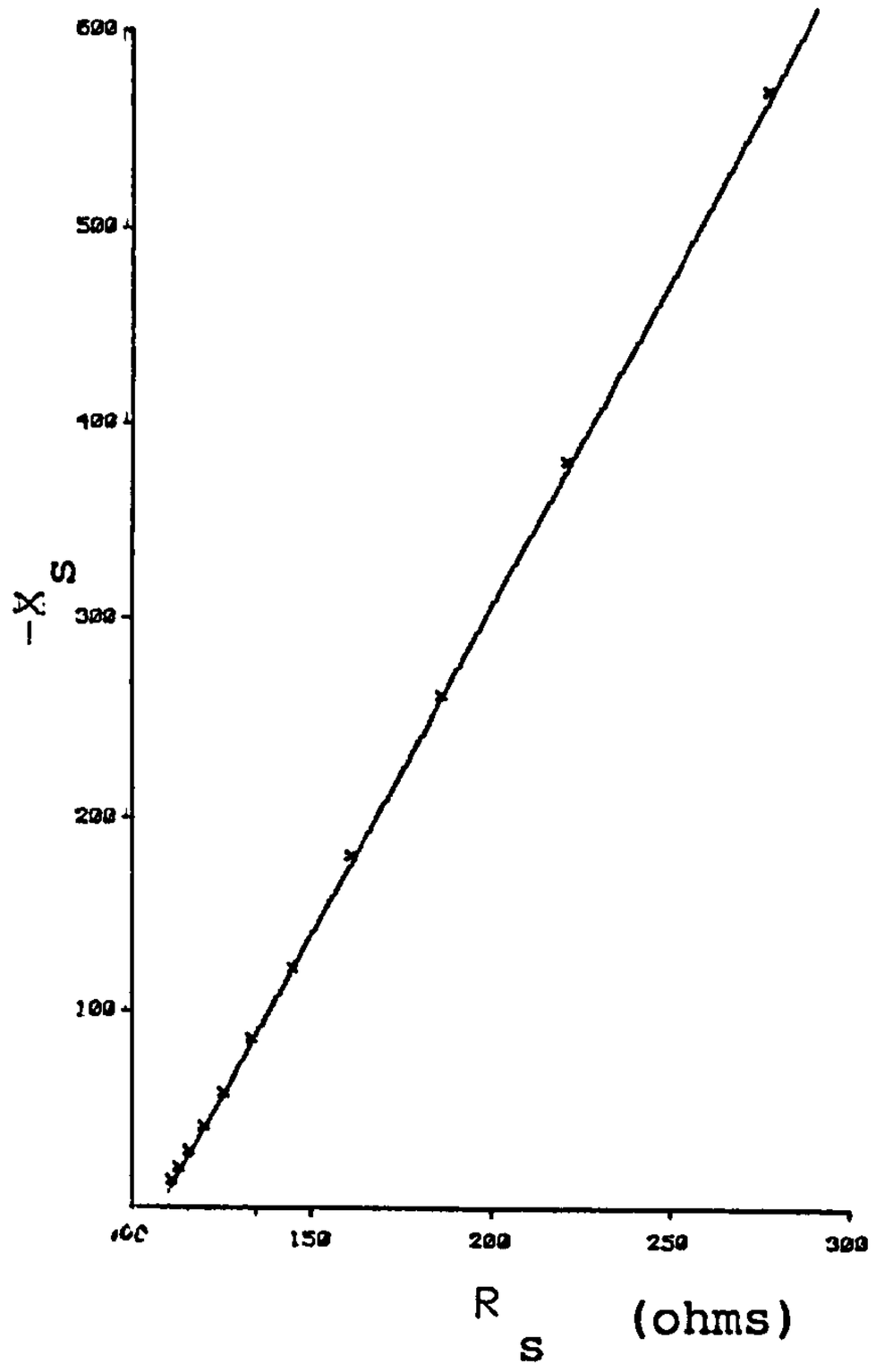

Figure 1.34

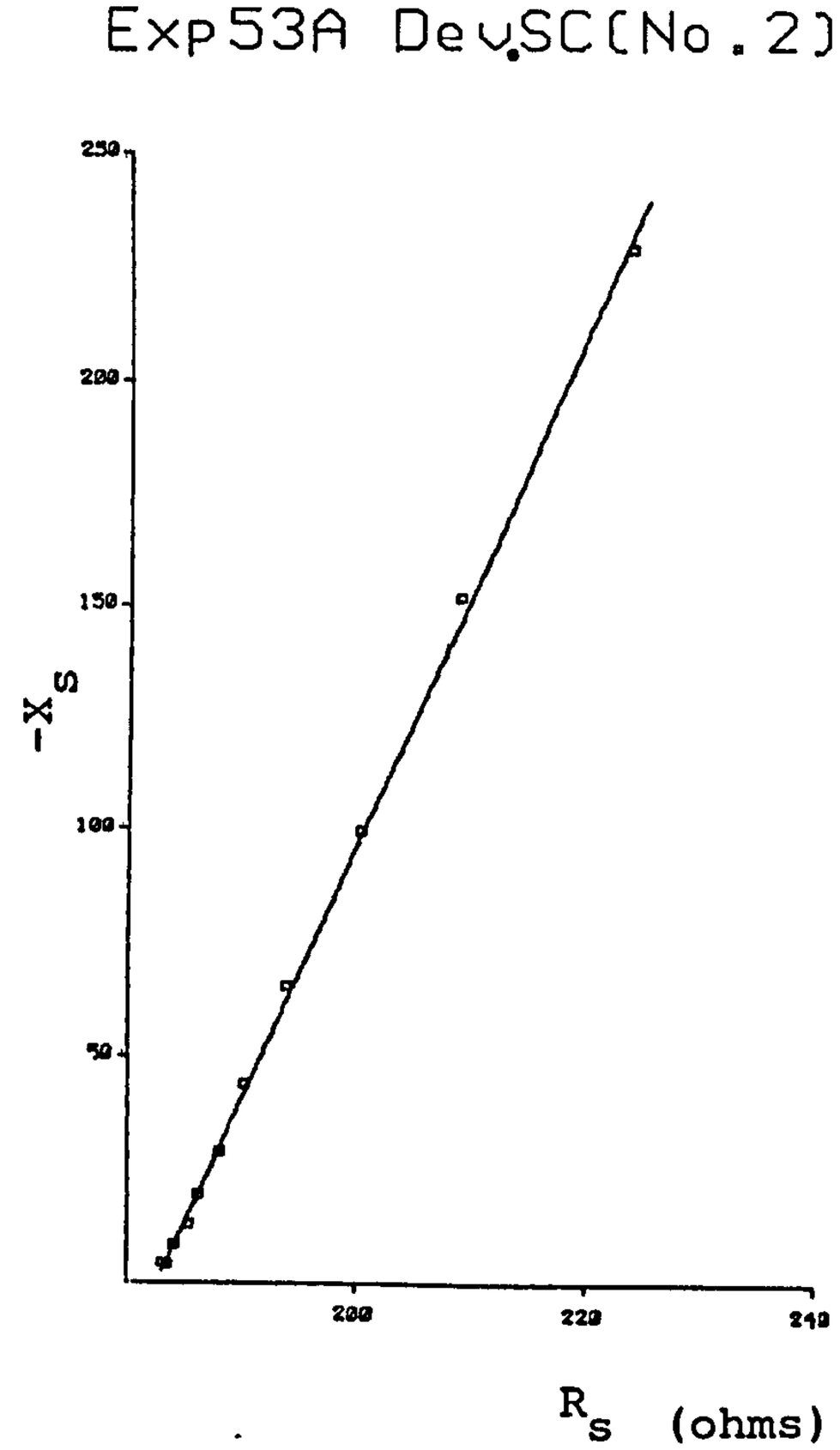

Figure 1.35

- Devices SC ($21mm^2$)

The results of the experiments carried out on the electrodes are listed on table 1.4 . The results for the electrode no.2 are ploted on figure 1.35.

Electrode No	Exp No	$R_T(\Omega)$	ϕ	$K(k\Omega s^{-\beta})$	β	$R_L(\Omega)$	$R_S(\Omega)$
1	53b	178	77	52	.83	132	46
2	53a	183	80	87	.92	139	44
3 (short lead)	80	131	81	93	.91	95	36

$R_T = R_{TOT}$ $R_L = R_{LEAD}$ $R_S = R_{SALINE}$

TABLE 1.4

The value of the measured impedance of electrode No.2 using the Solartron 1250 differs from that found previously using the Wien Kerr bridge. The value of K has increased from 73 k $\Omega s^{-\beta}$ to 87 k Ω $s^{-\beta}$ whereas R_{TOT} and β are approximately the same. This change with time and electrode history seems likely to be due to the gradual adsorption of impurities onto the electrode surface and will be investigated later.

- Telectronic 224 ($10mm^2$) Platinum electrode

This was the only pure platinum electrode tested. As it is an endocardial electrode, mechanical strength is not so important as in the intramural case. For electrode No.2 (Exp. 50, see Figure 1.36) the values of the R_{TOT} - Z_{CPA} equivalent circuit model were found to be:

a) $\phi = 79^{o}$ ($\beta = 0.88$) $R_{TOT} = 164\Omega$

b) $K = 122\ k\Omega\ s^{-\beta}$ $\beta = .84$ ($\phi = 76^{o}$)

As $R_{LEAD} = 87\Omega$, $R_{SALINE} = 77\Omega$

The impedance plot (Figure 1.36) is slightly concave indicating the presence of C_{LF}, however not sufficiently so to enable calculation of its magnitude.

- Time Effects

The effect of time on the impedance of the Telectronic 224 No.3 electrode was investigated.

Time (hrs)	Argand Plot		log-log plot		
	$R_{TOT}(\Omega)$	ϕ	$K(K\Omega S^{-\beta})$	β	ϕ
2	153	76°	142	.84	76°
5	149	75°	144	.84	76°

TABLE 1.5

Exp50 Tet.224(No.2)

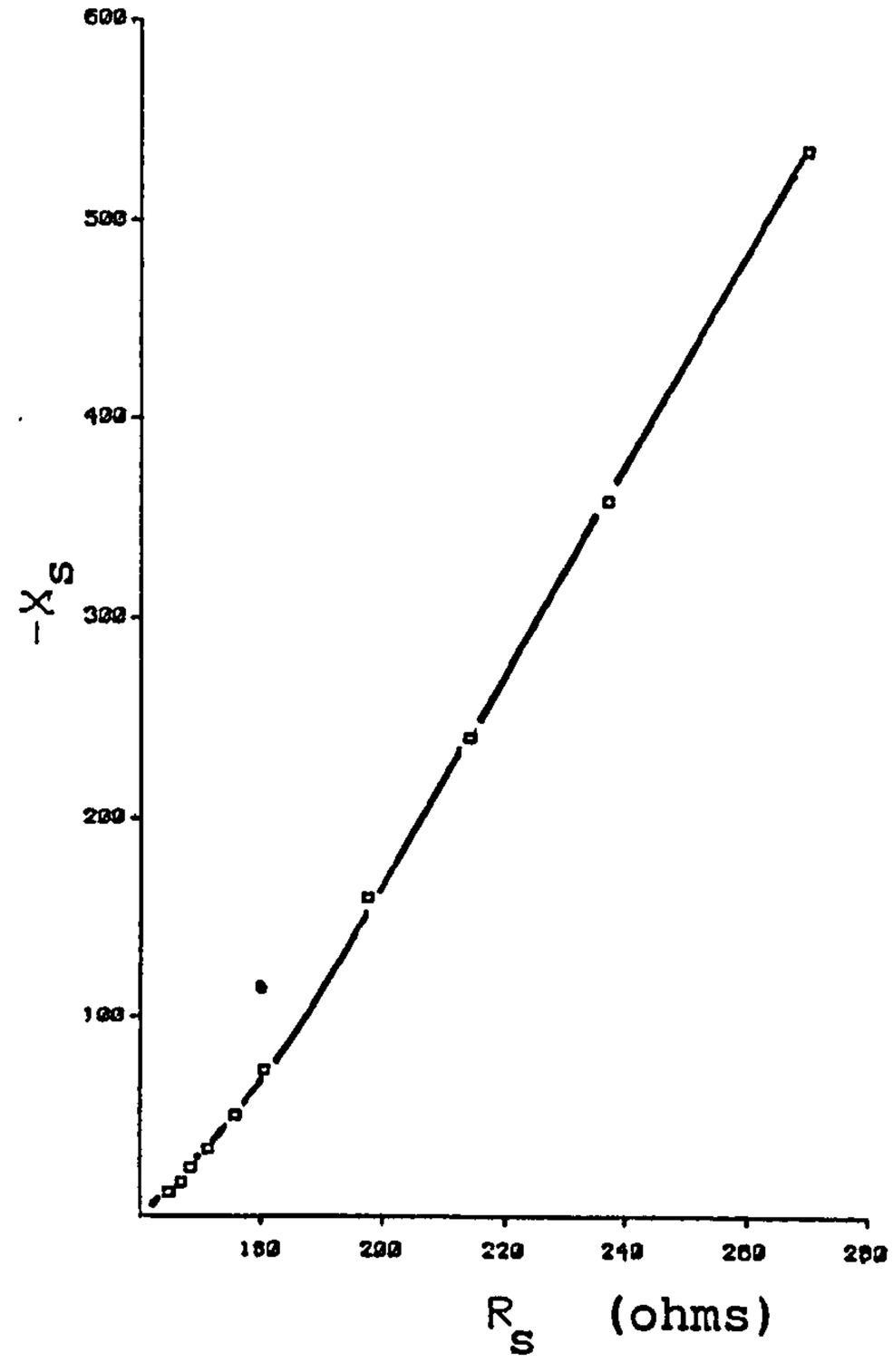

Figure 1.36

Exp60 Vitatron Helifix

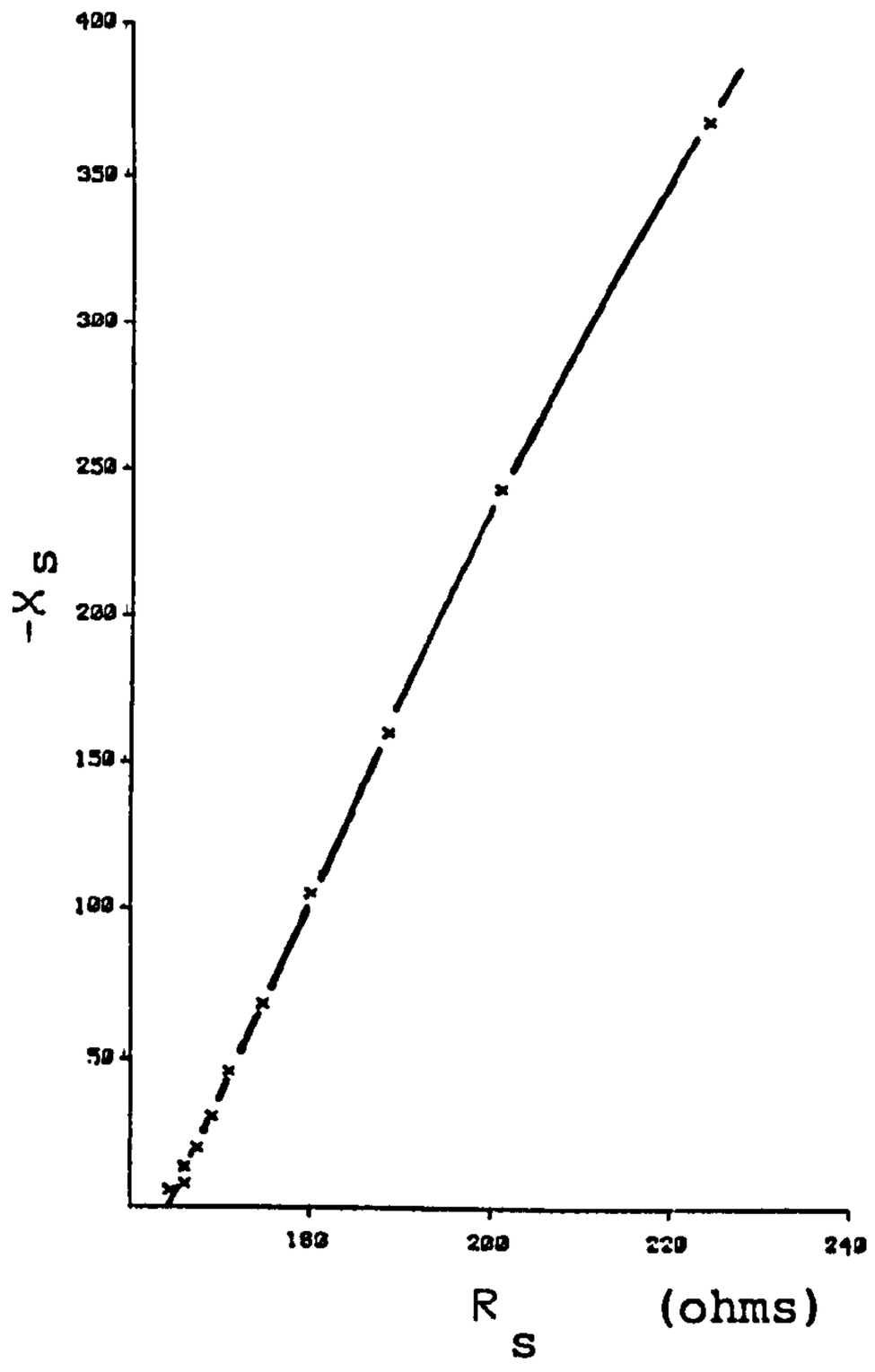

Figure 1.37

As with the Devices S.C. No.2 electrode the value of K is observed to increase gradually with time indicating a gradual decrease in interfacial capacitance

De Rosa and Beard (1977) noted that the series capacitance, C_s, measured at 600 Hz, decreased with time when a platinum wire electrode was placed in various electrolytes. As C_s is inversely proportional to K ($C_s = (1/K)\omega^{(\beta-1)}$ Cosec ($\beta\pi/2$), equation 1.4) a decrease in C_s is equivalent to an increase in K, as observed. Gray and Svaetichin (1951) noted an increase in X_s (proportional to K, eqn. 1.4) with the passage of time.

A decrease in capacitance ($C = A\varepsilon/d$) can indicate one or all of the following:

1) a decrease in the surface coverage of the ion or ions responsible
2) an increase in the interplate distance, d, and/or
3) an increase in the dielectric permittivity.

It is very propable, according to the work of De Rosa and Beard (1977), that the decrease in capacitance is due to the decrease in surface coverage of the oxygen layer as chloride ions and impurities gradually adsorb onto the surface.

- Vitatron Helifix Electrode ($23mm^2$)

Stable fixation of an electrode has been a significant problem in endocardial pacing and has spurred the development of many new lead designs using separate anchoring devices such as barbs, fins or helical coils (Wilson et al, 1983).

The Vitatron electrode is a unipolar endocardial lead with just such a fixation mechanism. The helical electrode can be screwed between the trabeculae without trauma and firmly anchored in good contact with the myocardium.

The impedance of the electrode is plotted on Figure 1.37. A fit using the series R_{TOT} - Z_{CPA} combination gave (Exp. No.60) -

a) $\phi = 81^{o}$ ($\beta = 0.9$) $R_{TOT} = 164\,\Omega$

b) $K = 141\ k\ \Omega\ s^{-\beta}$ $\beta = 0.92$ ($\phi = 83^{o}$)

As $R_{LEAD} = 125\,\Omega$, $R_{SALINE} = 39\,\Omega$

- Medtronic 6917A Myocardial Electrode (6.6mm^2)

This 'corkscrew' electrode can be simply rotated into the myocardium and remains securely in place without sutures.

The R_{TOT} - Z_{CPA} equivalent circuit model had the following parameter values (Exp. 63, Figure 1.38) -

a) $\phi = 78^{o}$ ($\beta = .87$) $R_{TOT} = 64\Omega$

b) $K = 135\ k\ \Omega s^{-\beta}$ $\beta = .85$ ($\phi = 76.5^{o}$)

As $R_{LEAD} = 9\ \Omega$, $R_{SALINE} = 55\ \Omega$

At low frequencies there is a slight bending over towards the real axis. This phenomenon will be investigated in Chapter Two.

-Observations on "Smooth" surfaced electrodes.

Over the applied frequency range the interfacial impedances of the electrodes are well modelled by a Z_{CPA} impedance in series with R_{TOTAL}. Deviation from this model was noticed at higher frequencies for the Telectronic, Vitation and Medtronic electrodes. With these electrodes the phase angle was observed to decrease, sometimes sharply, towards 45^{o}.

Exp63 Med.691/A

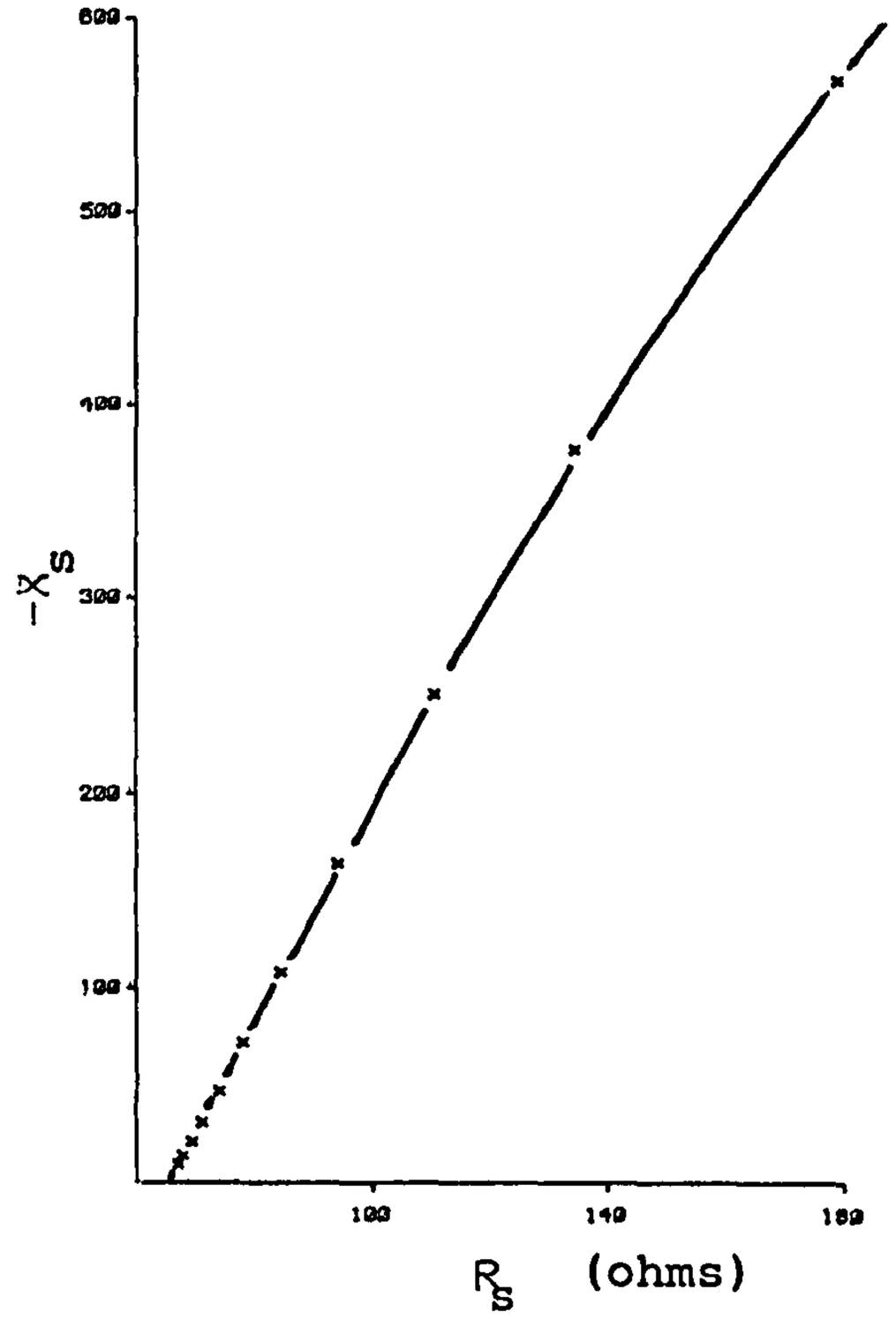

Figure 1.38

Effect of surface roughness

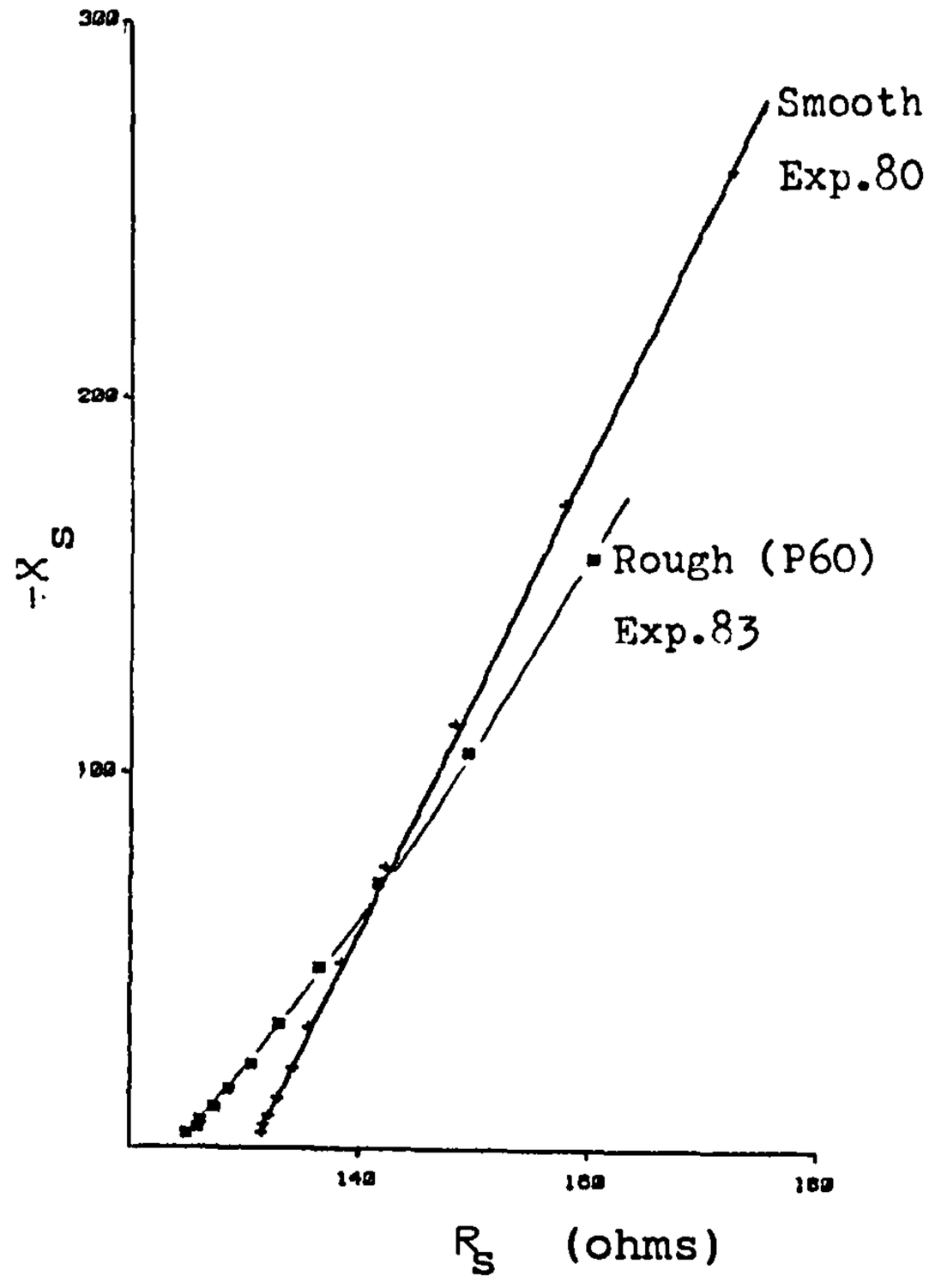

Figure 1.39

In general the resistance of the electrolyte, R_{SALINE} , decreased with the electrode area as expected. The only exception was the Medtronic 6917a cork skew electrode which had a surprisingly small value of the electrolyte resistance (55 Ω) for such a small area (6.6mm²).

In general the magnitude ,K, of the interfacial impedances of these smooth electrodes decreased with the surface area as expected. The only exception was the Vitatron Helifix electrode which had the largest value of K in spite of having the largest area. It is proable that the shape of the electrode is also an important factor. Values of β were found to lie between 0.8 and 0.92.

1.2.3.2.2 Rough Surfaced Electrodes

- Roughened Devices S.C. ($21mm^2$) No.3

It was noticed with several of the 'smooth' electrodes (especially coiled and helifix electrodes) in the last section that at very high frequencies there was some evidence of surface roughness effects - ie a phase angle of approximately 45^{o}. This unfortunately does not show up clearly on the graphs due to chosen scales . It was decided to investigate further these effects by monitoring an electrode's impedance with progressive roughening of the surface.

The impedance of a 'smooth' Devices S.C. (No.3) electrode was initially measured (Exp. 80). The electrode surface was then roughened with P320 emery paper (Exp. 81) and the impedance measured. Finally the surface was further roughened with P60 emery paper and again the impedance measured (Exp. 83).

The impedances of Exp. 80 and Exp. 83 are plotted on Figure 1.39.

The impedance locus of the 'smooth' electrode was a straight line and was hence modelled by the R_{TOT} - Z_{CPA} series combination where -

a) $\phi = 81^{o}$ ($\beta = 0.9$) $R_{TOT} = 131\Omega$

b) $K = 93\ k\Omega s^{-\beta}$ $\beta = .91$ ($\phi = 82^{o}$)

As $R_{LEAD} = 95\ \Omega$, $R_{SALINE} = 36\ \Omega$

The two roughened surfaces had concave impedance loci and were therefore modelled by a R_{TOT}-$Z_{CPA(HF)}$-C_{LF} series combination. The results are listed on table 1.6.

$R_{TOT}(\Omega)$		$K_{HF}(k\Omega S^{-\beta})$	β	C_{LF}(X10-5F)	$R_{SALINE}(\Omega)$
P320	126	2.3	0.54	1.01	31
P60	120.5	1.3	0.5	1.32	25.5

TABLE 1.6

The roughened surfaces have high frequency phase angles of approximately 45°. As the frequency decreases the phase angle increases towards the original 'smooth' value of 81° and not the predicted 90° due to C_{LF}.

It is concluded that roughening the electrode surface -

1) decreases the value of K
2) decreases the value of β
3) increases the value of C_{LF}
4) decreases R_{SALINE} and hence R_{TOT}.

These results agree with Delevie's (1964) theory except that at low frequencies the phase angle is not 90° (i.e. $\beta \neq 1$), as predicited. Such frequency dispersion is possibly due to specific adsorption effects and any residual surface effects. Lower frequency measurements are required to establish whether or not ϕ reaches 90° in the absence of surface effects.

- 'Coil' Electrodes

While testing 'smooth' electrodes it was noticed that coiled wire electrodes have impedances characteristic of surface roughness effects. It was therefore decided to investigate this phenomenon.

Jaron et al (1968) measured the impedances of 0.25mm diameter Pt-Ir, Elgiloy and stainless steel wires. These were first shaped into helical coils having approximately four turns per mm. The diameter of each helix was about 1.1mm. The leads were coated with an

insulating sleeve of silicone rubber tubing with the last few turns of the helix left bare. The bare portion of the coil constituted the electrode and its area was uncertain. The electrodes were immersed in saline (0.9% NaCl) and the impedances measured over the frequency range 75Hz to 10kHz.

Jaron et al obtained very concave impedance loci and fitted their results to Cole-Cole's model, ie to equation 1.36 .

Their equivalent circuit model was the R_{TOT}-Z_{CPA}-C_{LF} series combination as they neglected C_{HF}.
For platinum-iridium, Jaron et al calculated:

$K_{HF} = 9,723\ \Omega s^{-\beta}$ $\beta = 0.6$ ($\phi = 54^{o}$)

$C_{LF} = 16.3\ \mu F$

The low phase angle (54^{o}) observed at high frequencies points to severe surface roughness effects. Comparing the above results with those of the roughened (P320) Devices S.C. electrode (Exp. 81) they are found to be very similar.

Grahame (1952) pointed out that "frequency dispersion" is greater on wires than on spheres. This, he believed, was due to the difficulty of manufacturing smooth wires and hence a wire electrode's surface is generally quite rough.

This may well be correct, however it seems also pos-

sible that the gaps between the turns in the above coiled electrodes behave somewhat like Delevie's surface pores, giving rise to extreme surface roughness effects.

To test this theory the following experiment was carried out. Using a Devices stainless steel myocardial electrode lead (25/52), 6mm of the lead coil was exposed and its impedance in saline measured. The exposed section was then stretched to a length of 40mm and again the impedance was measured. The stretching of the coil will remove the pore-like gaps and the impedance locus should approach that of a smooth surface. The impedances are plotted on Figure 1.40 and were fitted to the R_{TOT} - $Z_{CPA(HF)}$ - C_{LF} model. The results are listed on table 1.7.

Exposed length	Exp. No	$R_T(\Omega)$	$K_{HF}(k\Omega S^{-\beta})$	β	$C_{LF}(x10\mu F)$	$R_S(\Omega)$
6mm	57	57	21	0.48	1.72	49
40mm	59	31	10.3	0.6	6.89	23

$R_T = R_{TOT}$ $R_S = R_{SALINE}$

TABLE 1.7

Effect of Exposed Surface Area (Exp57&59)

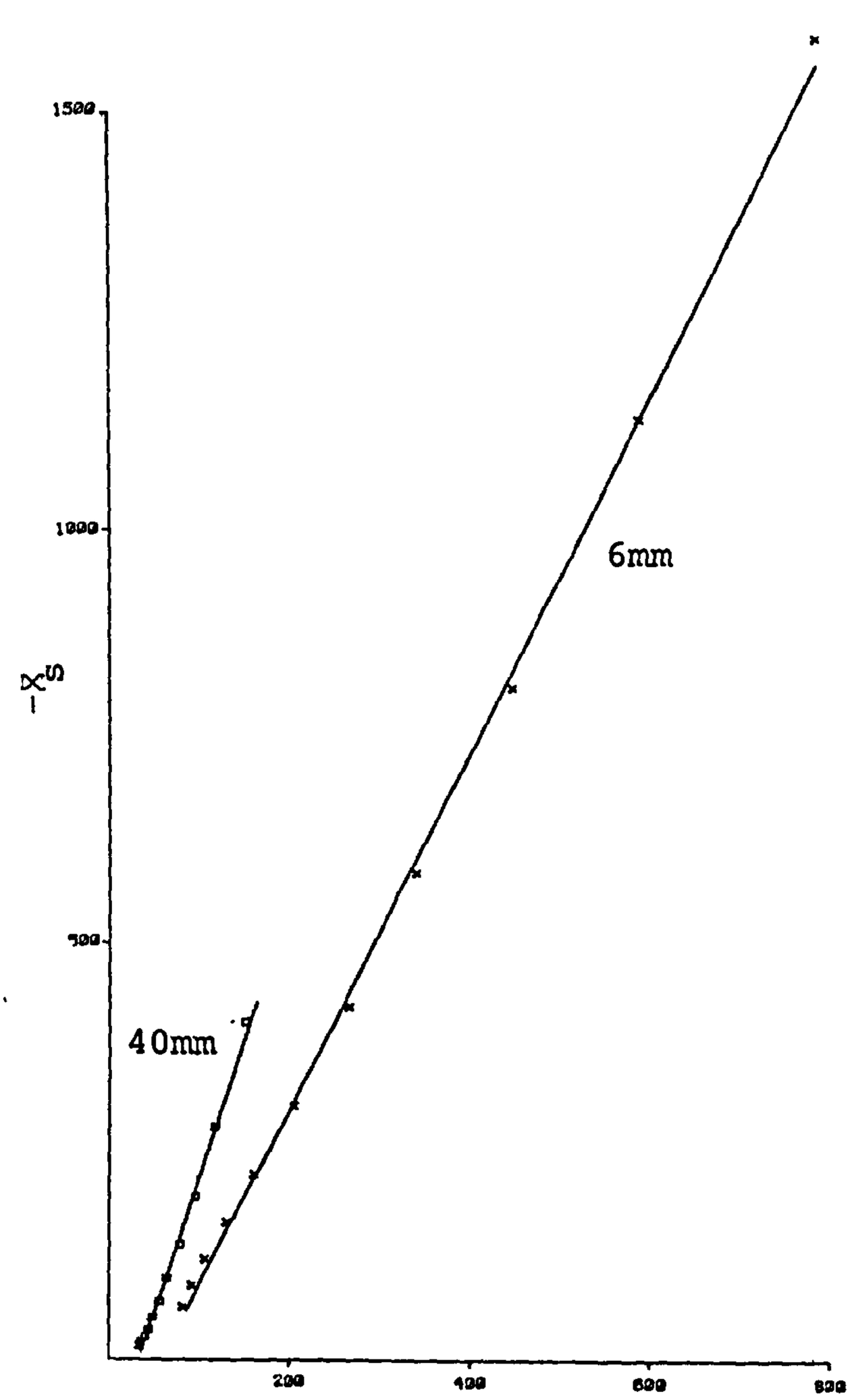

Figure 1.40

It is concluded that extending the coil -

1) decreases the values of R_{TOT} and R_{SALINE} due to an increase in effective area (2 fold)

2) decreases the value of K_{HF}, again due to the increase in effective area and by a factor of two,

3) increases the value of β due to the "smoothing" of the electrode surface, and

4) increases the value of the low frequency capacitance, C_{LF}, due to the increase in effective surface area.

Jaron et al calculated the following parameter values for their stainless steel coil electrode -

$$K_{HF} = 13{,}500\ \Omega\ s^{-\beta} \qquad \beta = 0.74\ (\ \phi = 67^{o}\ )$$

$$C_{LF} = 1.8\ \mu F$$

Comparing our own results for stainless steel coil electrodes (EXP 57), the measured values of K_{HF} and C_{LF} compare very favourably. However Jaron et al's calculated value of β (0.74) is much larger than that found by the author (0.48). A possible explanation is that Jaron et al sometimes used coils which were slightly drawn out, and this, as has been shown, increases the value of β.

- Sorin S80 Electrode

The impedance of the Sorin S80 electrode (No. 3) was measured at different times after placement in saline, and the impedance, as expected, was found to be time dependent. The calculated equivalent circuit parameter values for a R_{TOT} - $Z_{CPA(HF)}$ - C_{LF} series model are listed on table 1.8

TABLE 1.8

Time (hrs)	Exp No	R_{TOT} (Ω)	K_{HF} ($k\Omega s^{-\beta}$)	β	C_{LF} ($10^{-5}F$)	R_{LEAD} (Ω)	R_{SALINE} (Ω)
2	70	131	1.59	.56	1.4	52	79
6	79	131	1.58	.56	1.2	52	79

The results obtained after a settling period of two hours are plotted on figure 1.41.

It is noted that the impedance of the S80 electrode is very similar to that of the roughened Devices SC (No. 3) electrode - in fact the latter has a smaller impedance. The value of C_{LF} was noted to decrease with time whereas the other parameters appeared to remain constant. The overall impedance tends to increase with time as noted before.

The experimental results obtained using a Wien Kerr Bridge for the Sorin S80 (No.1) electrode gave

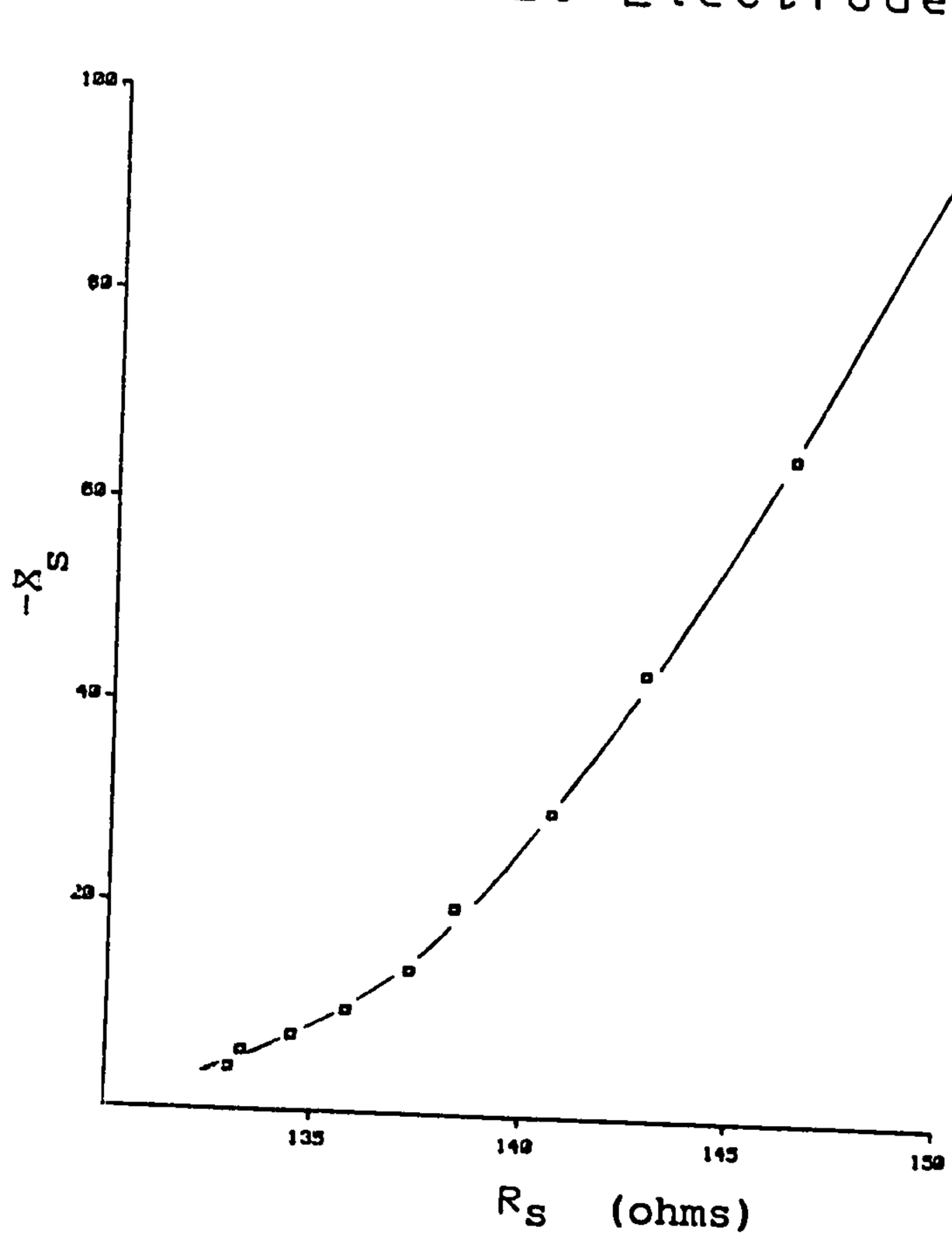
EXP71 Porous Electrode
100
80
60
40
20
$\frac{1}{R_s}$ Ω
135
140
145
150
R_s (ohms)

Figure 1.41

$R_{TOT} = 139\Omega \quad \phi = 61^{o}$

$K = 20\ k\Omega s^{-\beta} \qquad \beta = 0.61$

If a Z_{CPA} impedance is fitted to the Solartron's experimental results over the same limited frequency range used for the Wien Kerr measurements, the following values are obtained

$R_{TOT} = 134\Omega \qquad \phi = 77^{o}$

$K = 22.2k\,\Omega\,s^{-\beta} \qquad \beta = .8$

The values of R_{TOT} and K compare favourably and indicate that the major cause of any apparent difference between the two sets of results is due to the limited frequency range used for the Wien Kerr measurements. The increase in β could be due to electrode contaminating which could have occurred during intervening experiments made on the electrode. Adsorbant tends to decrease the non-uniformity of the surface thus decreasing frequency dispersion (Ramaley and Enke, 1965).

- Observations on rough surfaced electrodes

Roughening the surface of an electrode has been found to decrease the values of K, β and R_{SALINE} - the decrease in K being the most spectacular.

Coil electrodes behave as very rough surfaced electrodes with characteristic low phase angles and impedance magnitudes. This is due to the difficulty in making smooth wires and in the pore-like behaviour of the gaps between turns in the coil.

The rough surfaced Sorin S80 electrode has a very low value of interfacial impedance, several times smaller than that of an equivalent smooth surfaced electrode. The measured value of β is also considerably smaller and there is a slight decrease in the value of R_{SALINE} compared to those found for 'smooth' electrodes.

1.2.3.2.3 Activated Vitreous Carbon Electrode

- Wien Kerr Bridge measurements

It was found in section 1.2.3.1 using the Wien Kerr Bridge that over the frequency range 0.5kHz to 5kHz the impedance of the AVC electrode (No. 1) could be modelled by a series R_{TOT} - Z_{CPA} combination where

$$R_{TOT} = 207\,\Omega\,, \quad \phi = 56.7^{o}, \; K = 12\ k\Omega s^{-\beta}\,, \quad \beta = 0.61$$

$$R_{LEAD} = 135\Omega\,, \quad R_{SALINE} = 72\Omega$$

The value of K was at least 10 times smaller than that of the Devices LC electrode of the same surface area ($12mm^2$). β also was much smaller than for any of the other electrodes.

R_{SALINE}'s value of 72 Ω was much as expected for an electrode of this area (12mm^2) and compared with that of the S80 electrode (area 8mm^2, R_{SALINE} = 79 Ω) and that of the Devices LC electrode (area 12mm^2, R_{SALINE} = 69 Ω)

- Solartron 1170 measurements

Using the Solartron 1170 with a rather large ac signal (300 mv) it was found that the A.V.C. electrode (No. 1) had a phase angle of approximately 51° over the frequency range 50Hz to 1Hz (see figure 1.42). At higher frequencies the phase angle decreased even further to below 45°. This indicates not only extreme surface roughness but also that the low frequency "smooth" surface impedance must have a phase angle less than 90° i.e. it is not purely capacitative.

At frequencies below 1Hz the impedance locus is in this case observed to bend over towards the real axis thus forming an arc. This behaviour is due to the large ac signal amplitude used and will be discussed further in chapters two and four. It is concluded that the impedance can only be modelled by a Z_{CPA} over a limited frequency range.

Both Shigemitsu et al (1979) and Kingma (1977) noted Z_{CPA} behaviour for "glassy" (vitreous) carbon electrodes over the frequency ranges of 1Hz to 1kHz and

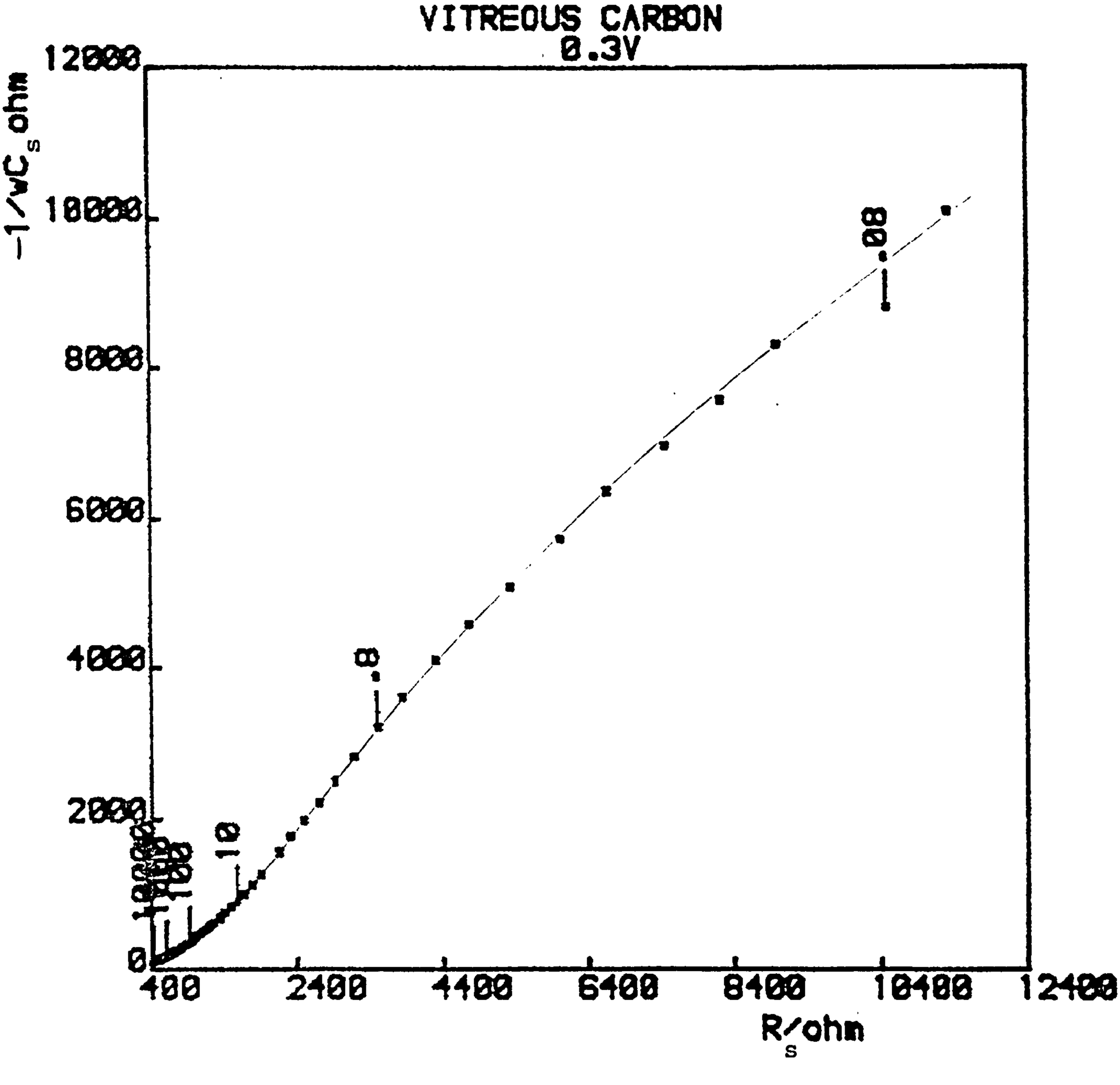
VITREOUS CARBON
0.3V
12000
10000
8000
6000
4000
2000
0
$-1/\omega C_s$ ohm
.08
.8
10
400
2400
4400
6400
8400
10400
12400
R/ohm

Figure 1.42

5Hz to 10kHz respectively. Both groups observed phase angles in the region of 55° to 65°. Kingma (1977) also showed that roughening the vitreous carbon surface decreased the impedance and phase angle as expected.

- Solartron 1250 measurements

Using the Solartron 1250 over the wide frequency range 100 Hz to 10 kHZ for activated vitreous carbon electrode No. 2, the impedance locus shown on figure 1.43 (Exp 85) was obtained. As with the Solartron 1170 results, there was a very low phase angle (less than 45°) in the high frequency region. As the frequency decreases the phase angle increases. The experimental results were therefore fitted to a series model comprising, R_{TOT}, $Z_{CPA(HF)}$ and C_{LF}. The calculated parameter values were

$R_{TOT} = 170\,\Omega \quad C_{LF} = 1.52 \times 10^{-4} F \quad K = 511\,\Omega s^{-\beta}$

$\beta_{HF} = .36 \; (\phi = 32^{o})$

As $R_{LEAD} = 120\,\Omega$ $\quad R_{SALINE} = 50\,\Omega$

At very high frequencies the impedance is dominated by a $Z_{CPA(HF)}$ whose magnitude and phase angle are very small - much smaller than was found for electrode No. 1 using the Wien Kerr Bridge. This apparent conflict of results is due partly to the limited frequency range of the latter. For example, calculating the phase angle

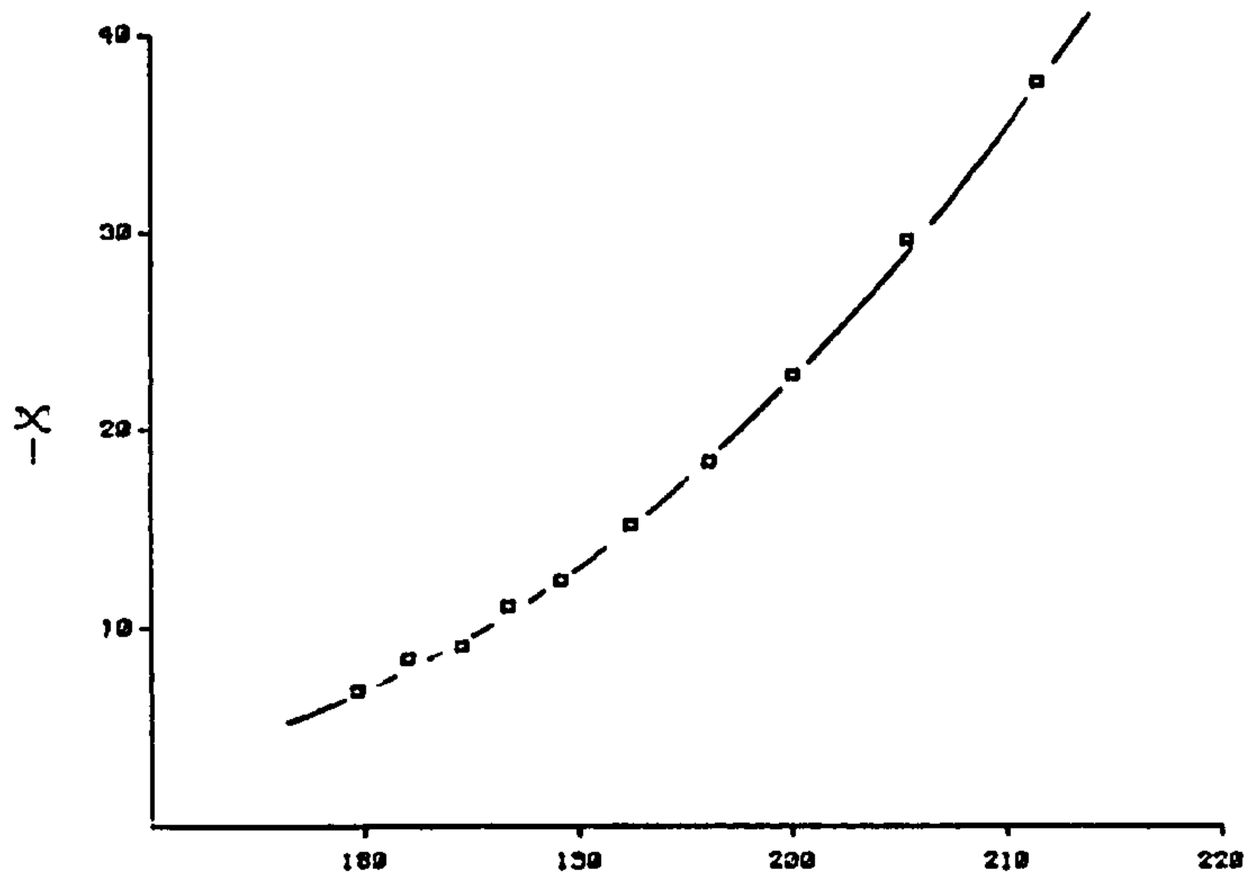

Figure 1.43

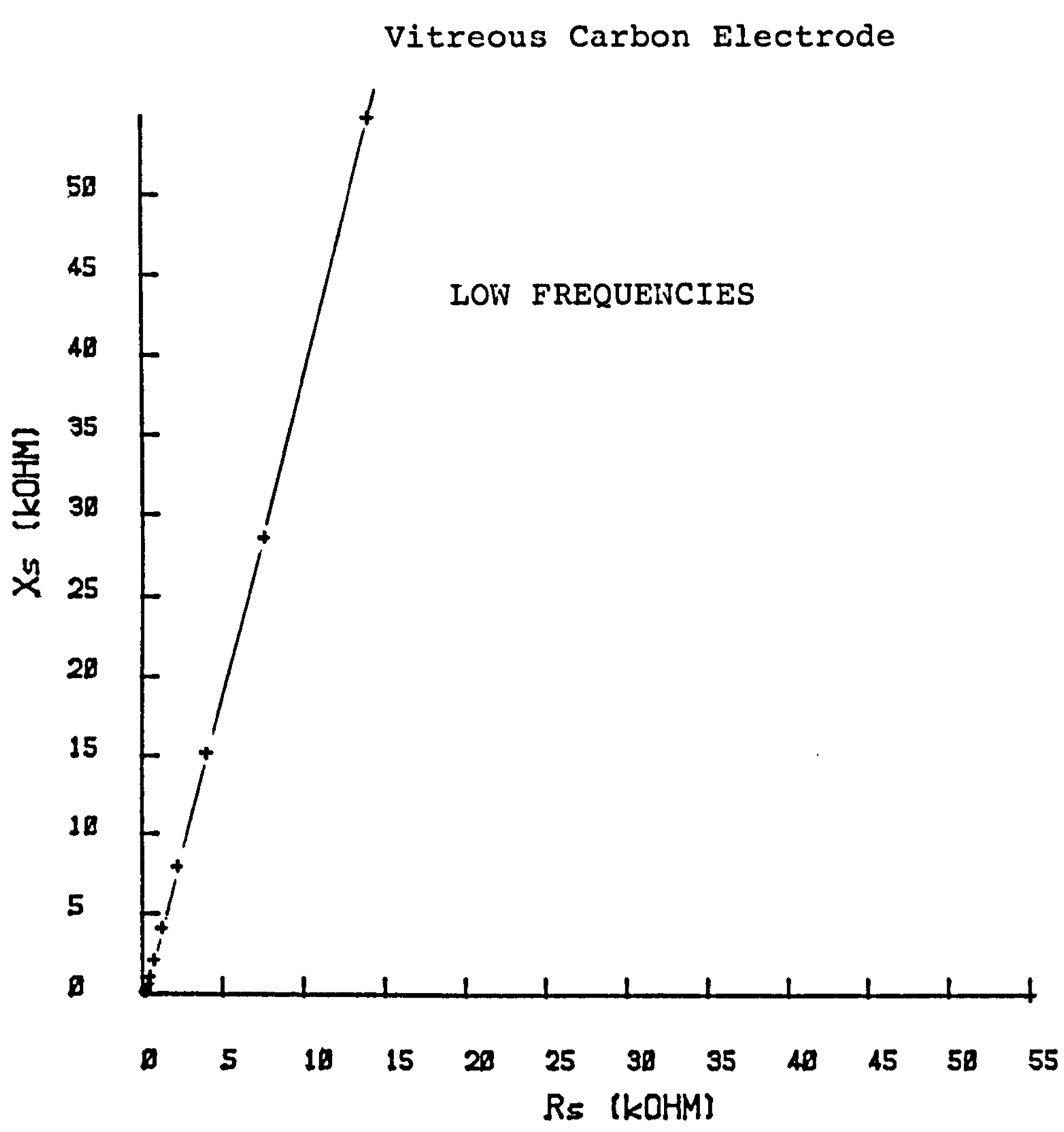

Figure 1.44

of the Z_{CPA} over the same limited frequency range as used by the Wien Kerr gives a value of 55.6° for electrode No. 2 compared to the 56.7° found for electrode No. 1. Intervening experiments will also have caused changes in the interfacial impedance. However the problem appears to be mainly due to observing and modelling the electrode impedance over a limited frequency range. Observing the impedance over a wide range reveals that the phase angle gradually changes with frequency whereas when using a relatively small frequency range the phase angle appears constant. The magnitude of the measured phase angle and impedance will depend on the position of the frequency window.

-Low frequency impedance locus

Edeling et al (1983) observed an impedance locus similar to figure 1.43 for activated vitreous carbon electrodes in 1M H_2 SO_4 over the frequency range 0.1 Hz to above 100 Hz. They found, at very low frequencies ($f < 1Hz$), that the phase angle was constant and was close to, but not quite, 90°.

Our own low frequency results (figure 1.44, see also chapter 2) show that at low frequencies (10 Hz to 10mHz) the impedance tends to that of a Z_{CPA} and not a pure capacitance i.e. $\phi \neq 90°$. Modelling the low frequency impedance by $Z_{CPA(LF)}$ the following values were obtained

(i) from the argand diagram

$$\phi_{LF} = 76^{o} \quad (\beta_{LF} = 0.84)$$

(ii) from the log Z - log f plot

$$K_{LF} = 5{,}500 \ \Omega \ s^{-\beta}$$

$$\beta_{LF} = 0.84$$

The fact that both calculated values of β_{LF} are the same indicates that the low frequency is well modelled by $Z_{CPA(LF)}$.

If one now inserts $Z_{CPA(LF)}$ as the expression for Z_i (the impedance of a 'smooth' surfaced electrode) in to Delevie's equation (see equation 1.39), the high frequency impedance should be given by

$$K_{HF} = \sqrt{R_e K_{LF}} = 560 \ \Omega \ s^{-\beta}$$

[As R_e = 57 Ω/cm for 0.9% saline (Geddes and Baker 1967)]

and $\phi_{HF} = \phi_{LF/2} = 38^{o} \quad (\beta = 0.42)$

The measured values of 514 $\Omega \ s^{-\beta}$ and 32.4^{o} are in fairly good agreement with the above predicted values. Hence the impedance of a rough surfaced electrode can be approximated by the series combination, $Z_{CPA(HF)}$ - $Z_{CPA(LF)}$.

Edeling et al (1983) also fitted their results to Delevie's equation with $Z_i = Z_{CPA(LF)}$. Their model gave a very good match with their results but they were not completely satisfied with the fit at high

frequencies. They therefore proposed that instead of assuming that the electrode surface was homogeneous, one should take into account the inhomogeneity of the surface. They therefore derived a new model based on the arbitrary assumption that the number of pores perpendicular to the electrode surface decreases exponentially towards the centre of the electrode. This altered model was found to give a very good fit with the experimental data both for high and low frequencies.

-Apparent discrepancies in the work of Mund et al.

Mund et al (1976 and 1979) also carried out impedance measurements on, what they term, "non-polarizable" activated vitreous carbon electrodes in 0.15 M NaCl over the wide frequency range 10^{-4} Hz to 10 kHz. Unfortunately Mund et al (1979) decided to only model the measured impedance for frequencies below 10^{-2}Hz as they considered the impedance of the electrode for higher frequencies to be determined only by the, in this case, large series resistor, R_{TOT}. It is easy to make this mistake when viewing the interface impedance on a log/Z/ - log f plot as the large value of R_{TOT} does indeed mask the interface impedance at high frequencies. However simple subtraction would have solved this problem and the high frequency impedance with its low phase angle would then have become discernable. In fact Mund et al (1979) carried out this subtraction for their Pt-Ir electrodes, so it seems remarkable that they did not also investigate the activated vitreous carbon electrode's impedance over the

whole of the measurement frequency range. What is also remarkable is their comparison of the high frequency impedances (1Hz to 10kHz) of other popular electrode materials with the very low frequency impedance (10^{-2}-10^{-4}Hz) of their activated vitreous carbon electrode. Such a comparison is misleading and unfair as the important frequency range for pacing is, according to Mund et al (1979), above 1Hz (the pulse repetition frequency). The author believes this misleading comparison was prompted by Mund et al's (1979) belief that for low energy consumption a pacing electrode's interfacial impedance should have as low a value of K as possible and β should approach the ideal value of 1. As their activated vitreous carbon electrode only approaches the 'desired' capacitative behaviour at ultra low frequencies, it is difficult to avoid the conclusion that this was the reason for the misleading comparison. The activated vitreous carbon electrode, having a very rough surface, will not only have a very small value of K but also a small phase angle for frequencies above 1Hz. Another "high frequency problem" for Mund et al is the relatively large value of lead resistance for the activated vitreous carbon electrode which will cause energy wastage. Mund et al's work will further be discussed in chapter four where it will be shown that the lead resistance becomes a very important parameter as the interfacial impedance is relatively insignificant under the large signal amplitude conditions encountered in pacing.

Mund et al (1976, 1979) modelled the low frequency impedance of their electrode by a Z_{CPA} of the form

$$/ Z_{CPA(LF)} / = K'_{LF} f^{-\beta}$$

where $K'_{LF} = K_{LF} (2\pi)^{-\beta}$

They found that even at these low frequencies the magnitude of the interfacial impedance was still very small

$K^1 = 15.4\ \Omega\ cm^2\ s^{-\beta}$ (Mund et al 1976)

$K^1 = 1.9\ \Omega\ cm^2\ s^{-\beta}$ (Mund et al 1979)

and the phase angle was, not surprisingly, very high

$\beta = 0.94$ (Mund et al 1976)

$\beta = 0.91$ (Mund et al 1979)

This Z_{CPA} behaviour at low frequencies agrees with our own observations and those of Edeling et al (1983). According to Mund et al "K" lies in the region of 10 to 87 $\Omega\ cm^2\ s^{-\beta}$. As the Siemen's activated vitreous carbon electrode tested in this study has an area of $12mm^2$, K should therefore have a value somewhere in the region of $84\ \Omega\ s^{-\beta}$ to $722\Omega s^{-\beta}$ with ϕ above 80^{o}. We however obtained, at not quite so low frequencies, a relatively large value of K ($5{,}500\ \Omega\ s^{\beta}$) and a relatively small phase angle ($\phi = 76^{o}$).

The discrepancy in phase angles could be due to the different frequency ranges used, those of the present study being higher (10Hz to 10mHz) than those of Mund et al (10^{-2} to 10^{-4} Hz), as at low frequencies the phase angle will be larger than at higher frequencies. An interesting observation however is that Mund et al's published values of β for the activated vitreous carbon electrode (measured at ultra low frequencies) makes it appear smoother than their unactivated vitreous carbon electrode (where β = 0.9 and 0.87 measured over the frequency range 1Hz to 10kHz)!

Mund et al's reported very low magnitudes of interfacial impedance for the AVC electrode are rather surprising - assuming they also were calculated at ultra low frequencies. Their results only match those obtained in this study at high frequencies (above 10 Hz) where it was found that $K_{HF} = 514\ \Omega\ s^{-\beta}$. At low frequencies the impedance of a rough electrode will increase in magnitude and approach that of a smooth surface. As Mund et al report values of β above 0.9 (ϕ above 80^{o}) their impedances should be close to those of their 'smooth' surfaced electrodes (as pointed out their reported β values are in fact larger than those found for their 'smooth' surfaced electrodes). The 'smooth' vitreous carbon electrodes had values of

$K' = 10,400$ and $5,300\ \ \Omega cm^2\ s^{-\beta}$

or $K = 218\ k\ \Omega s^{-\beta}$ and $453k\ \Omega s^{-\beta}$

It would appear therefore that Mund et al's activated electrode impedances do not approach those of the smooth electrodes even at ultra low frequencies.
It seems possible that Mund et al calculated the magnitude of their AVC electrode's impedance at high frequencies and its value of β at ultra low frequencies, thus making it appear, according to their criteria, a very good electrode.

- Observations on the Activated Vitreous Carbon Electrode

The very rough surface of the AVC electrode gives it the smallest interfacial impedance of all the electrodes tested. Its impedance locus is one characteristic of surface roughness effects. At high frequencies the phase angle is very small, below 45°! At lower frequencies the phase angle increases but does not appear to ever reach 90° as expected by Delevie (1964). Instead the electrode's impedance locus tends towards Z_{CPA} behaviour at low frequencies with β approximately equal to 0.9.
Over the frequencies of interest to pacing (above 1Hz) the AVC electrode will have very low values of K and β and hence makes a very good pacing electrode. The series resistance, R_{TOT}, is however relatively large and could prove a drawback.

1.2.3.3. Conclusions on the linear, high frequency ac impedance of pacing electrodes

The major cause of the observed frequency dispersion at solid pacing electrodes is surface roughness effects. Specific adsorption and the double layer capacitance presumably determine the magnitude and form of the low frequency "smooth surface" impedance which is observed to be almost purely capacitative i.e. β is almost equal to unity. The lack of significant frequency dispersion on smooth electrodes and the fact that values of capacitance measured are in general agreement with electrochemically determined values of the double layer capacitance (Dymond, 1976) would indicate that adsorption effects at these equilibrium potentials are relatively minor and that the double layer capacitance still makes a significant contribution. It can be deduced therefore that the electrodes are operating within the double layer region (see sections 1.1.2.1 and 1.1.2.3).

Surface roughness affects the interfacial impedance much as Delevie (1964) predicted. Alterations to his model such as using a $Z_{CPA(LF)}$ instead of a capacitance for the expression of the low frequency, smooth surface, interface impedance, Z_i, and the use of an exponential pore distribution (Edeling et al, 1983) lead to better fits with experimental data at the expense of simplicity.

Rough surfaced pacing electrodes are an improvement as they encourage tissue ingrowth thus ensuring stable fixation, minimal fibrous tissue growth, low stimulation thresholds and small interfacial impedances.

Of the electrodes tested the activated vitreous carbon electrode has the smallest interfacial impedance and hence, from this point of view, would appear to be the best electrode of those tested. However the interfacial impedance is known to be very nonlinear and as pacing involves large amplitude pulses, the impedances of the electrodes under pacing conditions will not be the same as under linear small signal conditions. Firm conclusions can not therefore be drawn from linear impedance measurement. This aspect of the interfacial impedance will be studied in Chapters 4 and 5.

- A note on the reproducibility of results.

It has been shown that the inter-electrode impedance varies with time after immersion in electrolyte. As the interface impedance is sensitive to the condition of the electrode surface (i.e. to the amount of adsorbed material and to the presence of oxides etc.), the inter-electrode impedance also varies with electrode history, preparation and storage. Until a technique is found which can repeatedly restore electrode surfaces to some, yet to be defined, standard condition, impedance measurements will not be reproducable to an acceptable level. In this thesis results were therefore chosen which were found typical of an electrode system.

Chapter 2

Modelling the interfacial impedance under low frequency, small signal a c conditions

2.1 Theoretical Section

Introduction

While investigating the impedances of the electrodes over the frequency range 100 Hz to 10kHz it was observed, for some of the electrodes at the lower frequencies, that the impedance locus showed signs of bending over towards the real axis and thus deviated from the expected low frequency "capacitative" behaviour. This observation led to a further review of the literature available to establish if other researchers had noticed a similar effect. Any physical and/or equivalent circuit models proposed to explain/represent this behaviour were also of interest.

Unfortunately most researchers in the past have used only limited frequency ranges to obtain their impedance measurements and it is only in very recent papers that researchers, using advanced equipment similar to our own (Solatron 1250), have noticed this low frequency effect.

2.1.1. Form of the low frequency impedance

If the "Fricke" (1932) relationship, $Z_{CPA} = K(j\omega)^{-\beta}$, remained valid at very low frequencies, the interfacial impedance would become infinite at $\omega = 0$ and no dc current would be able to flow across the electrode - electrolyte interface. This observation also applies to Delevie's model which approaches a pure capacitance at low frequencies.

It is well known, however, that direct current can be passed through an electrode - electrolyte interface (Geddes et al, 1971) and for this reason the simple Z_{CPA} and / or C_{LF} equivalent circuit elements cannot be considered wholly representative of the interfacial impedance.

Nowotny et al (1980) found for their electrodes that "above 1Hz the slope of log /Z/ and the value of ϕ (plotted against log frequency) are constant. This indicates that the data can be analysed according to $/Z/ = K\omega^{-\beta}$. Below 1Hz the behaviour of the electrode does not follow this theory". It is obvious that in order to enable the flow of dc current the impedance locus on an Argand diagram must deviate from the high frequency, Z_{CPA} behaviour and "bend over" to reach a purely resistive value, R_{dc}, at $\omega = 0$. It is this "bending away" from Z_{CPA} behaviour which was noticed in the last chapter and by Nowotny et al (1980).

On plots of phase angle, ϕ, and log /Z/ versus log frequency one should note a decrease towards zero in the phase angle and /Z/ should reach a limiting value equal to R_{dc} at low frequencies. The above deviations have indeed been observed in the past by, for example, Pollak (1974), Mund et al (1979) and Nowotny et al (1980).

Having established that the impedance locus bends over to the real axis at low frequencies it now remains to determine the form of the locus as it bends over, to derive an equivalent circuit model and to suggest a

physical explanation of the observed phenomenon.

- Equivalent circuit model

Recently Onaral and Schwan (1982) measured the impedance of platinum electrodes in 0.9% NaCl down to 10 mHz. They observed that the impedance locus formed a fairly smooth arc at low frequencies similar to that schematically shown on figure 2.1 . This arc, they pointed out, could be approximated by a semi circle whose centre was below the real axis. The equation of such an arc, derived by the simple mathematical operation of tilting a semi circle through $(1-\beta)\pi/2$ radians, is

$$Z = R_{\infty} + \frac{R_o - R_{\infty}}{1 + (j\omega\tau)^{\beta}} \qquad 2.1$$

Where R_{∞} is the resistance the arc tends to at high frequencies, R_o is the resistance the arc tends to for $\omega = 0$, and $\omega_o = 1/\tau$ is the frequency at which $-X_s$ has its maximum value.

Equation 2.1, describing the low frequency arc, characterises the impedence of several different equivalent circuit models which include frequencey dependant $Z_{CPA's}$. Below, two such circuits are reviewed which could possibly be used to physically represent the electrode system. Note that the circuits are completely equivalent and should both provide a good fit with the experimental data.

Circuit No.1 (Figure 2.2) is derived by considering the admittance of the arc shown on figure 2.1, i.e.

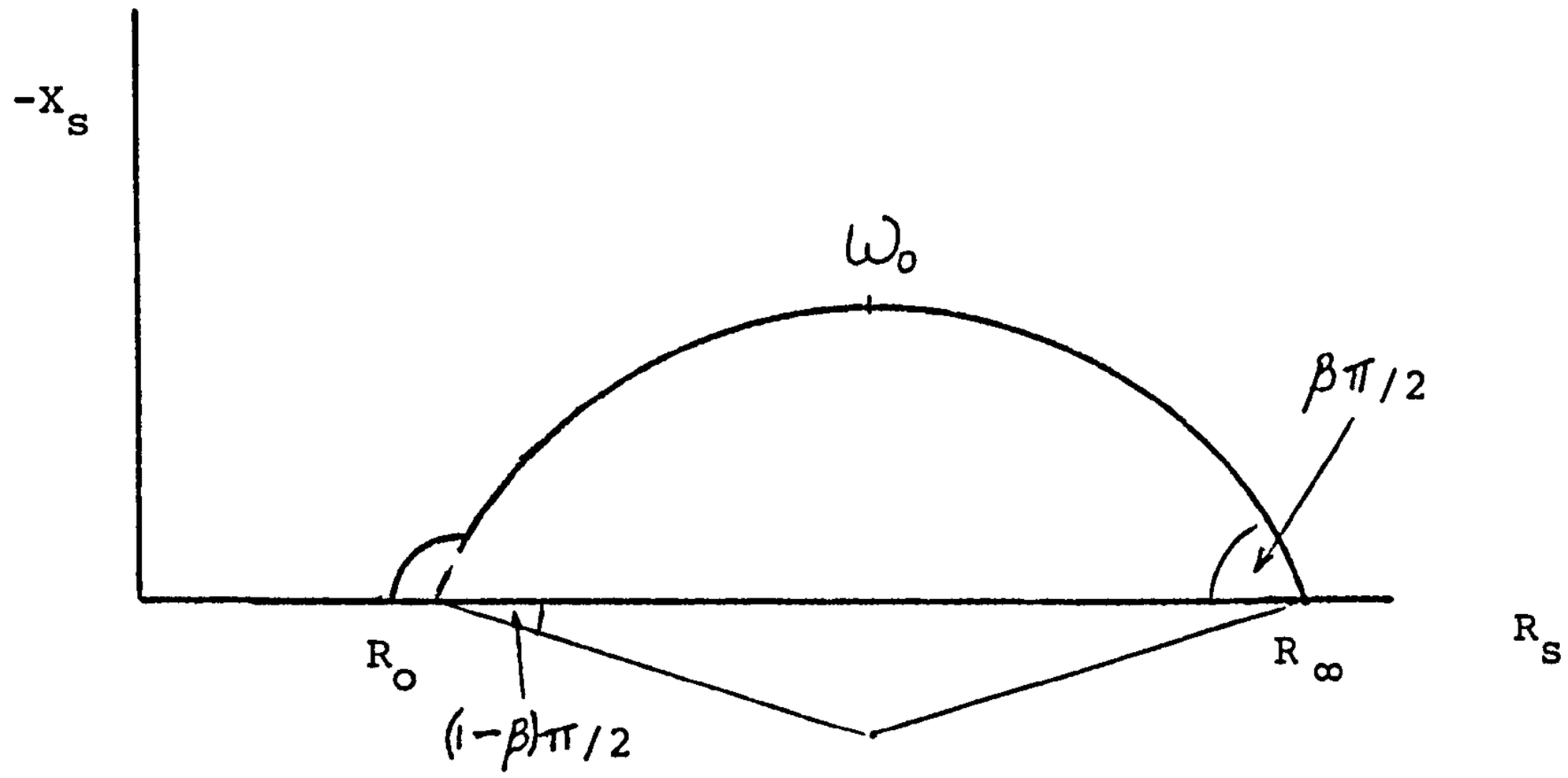

SCHEMATIC PLOT OF ONARAL AND SCHWAN'S RESULTS FOR PLATINUM ELECTRODES IN SALINE (65mv.,0.0855cm^2)

Figure 2.1

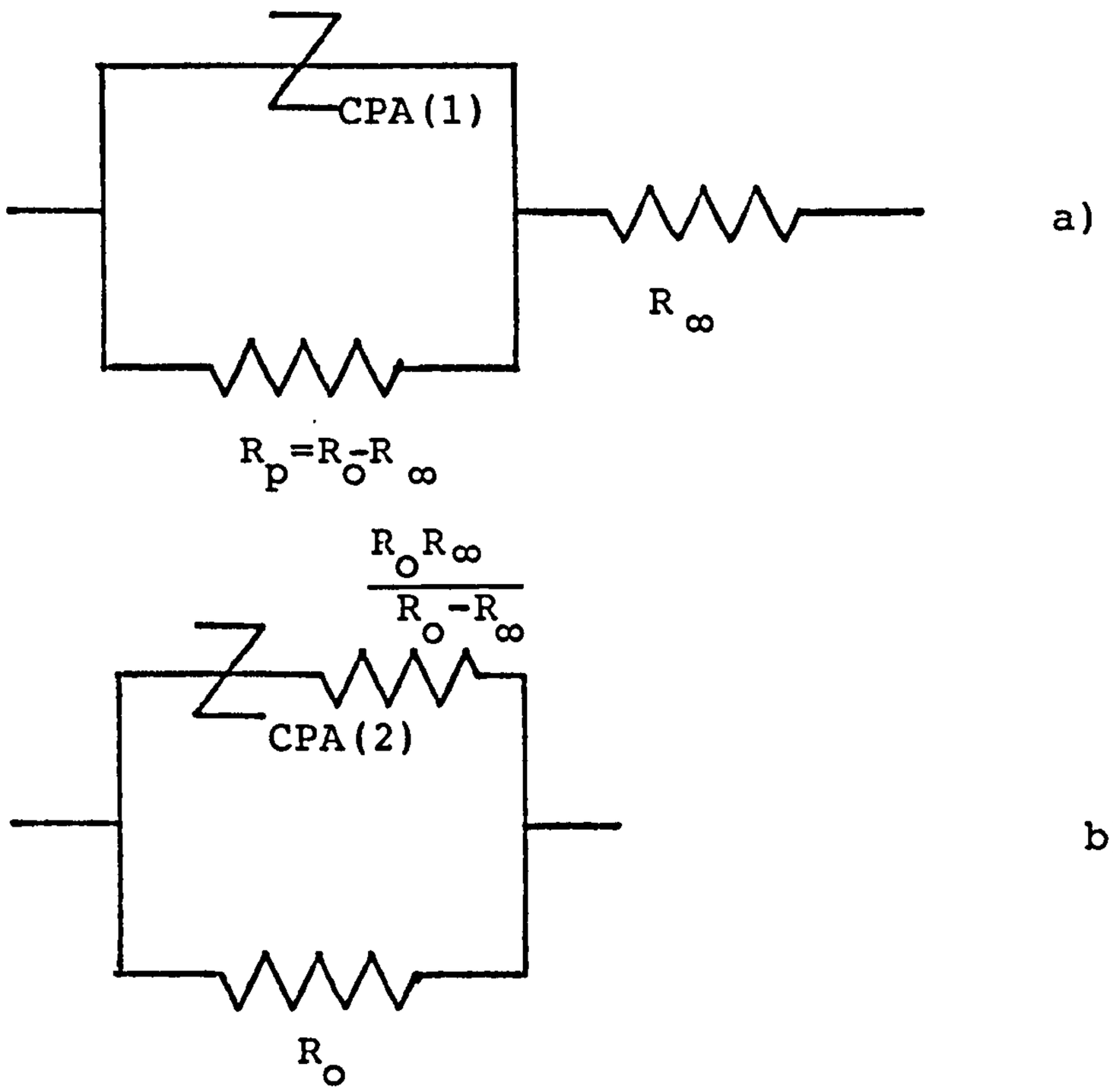

EQUIVALENT CIRCUIT MODELS OF THE ADOVE IMPEDANCE LOCUS

Figure 2.2

$$Y = \frac{1}{R_o - R_\infty} + \frac{(j\omega\tau)^\beta}{R_o - R_\infty}$$

The above expression represents the admittance of a resistance, R_p equal to $R_o - R_\infty$, in parallel with a constant phase angle impedance, Z_{CPA}, where

$$Z_{CPA} = \frac{R_o - R_\infty}{\tau^\beta} \frac{1}{((j\omega)^\beta)} = K_1 (j\omega)^{-\beta} \qquad 2.2$$

$$\text{with } K_1 = \frac{R_o - R_\infty}{\tau^\beta}$$

(Onaral and Schwan, 1982).

In Circuit No.2 (figure 2.2) the parallel resistance is made equal to R_o and there is an additional resistance, equal to $\frac{R_o R_\infty}{R_o - R_\infty}$, in series with another constant phase angle impedance $Z_{CPA(2)}$ described by the equation

$$Z_{CPA(2)} = \frac{R_o^2}{R_o - R_\infty} (j\omega)^{-\beta} = K_2 (j\omega)^{-\beta}$$

Circuit No.1 would seem to best represent physically the electrical properties of the electrode-electrolyte interface. The high frequency series resistance, R_∞, represents the sum of all the series resistances present in the electrode system - circuit No.2 fails in this respect. Z_{CPA} is the low frequency, constant phase angle impedance due to any residual

surface roughness effects or those of specific adsorption. The shunting resistance, which causes the deviation from Z_{CPA} behaviour at low frequencies, remains to be accounted for. Although Onaral and Schwan (1982) pointed out its presence they did not, unfortunately, suggest a physical interpretation.

It is interesting to note, that medium and high frequency points (above 0.4Hz) do not lie on the low frequency arc described by equation 2.1. From the high frequency end the locus rises with a constant phase angle, bends over forming part of an arc (R_p=25kΩ), and then rises again to form the beginning of the low frequency arc (R_p=200kΩ). Onaral and Schwan observed that there was a break down in Z_{CPA} behaviour ($\phi=\beta\pi/2$) over the "flattened out" section (0.4Hz to 10Hz). It would therefore appear that this region is one of transition from a high frequency Z_{CPA} behaviour to that of a low frequency Z_{CPA} (in parallel with R_p).

In the next sections an attempt will be made to attribute physical meaning to the parallel resistance R_p and explain the observed 'kink' in the impedance locus at medium to high frequencies.

2.1.2 Physical interpretation of R_p

As the interface allows the passage of dc, or faradaic current, a faradaic process must be present.

In chapter one only the "nonfaradaic" processes of adsorption and double layer capacitance, coupled with surface roughness effects, were considered. One must now consider, therefore, the additional contributions

made to the over all interfacial impedance by the faradaic processes of charge transfer and diffusion coupled with any surface effects. In section 1.1.2.2 it was shown that the faradaic branch comprises, in series, a charge transfer resistance, R_{CT}, and a diffusion impedance Z_W. This faradaic branch, as shown on figure 1.3, is in parallel with those of the double layer capacitance and the adsorption pseudo capacitance.

From Onaral and Schwan's work (1982) it is known that the low frequency arc can be well represented by a $Z_{CPA(LF)}$ in parallel with a resistance, R_p, which enables the flow of dc, or faradaic, current. This faradaic resistance must therefore be that due to a finite rate of charge transfer, i.e. $R_p \equiv R_{CT}$.

The contribution of Z_W over this frequency is apparently negligable. Hence the parallel resistance, R_{CT}, is equal to $\frac{RT}{nFi_o}$

and is a measure of the polarisability of an electrode system (section 1.1.2.2). It is incorrect therefore to talk of "a shunting resistance across the polarisation impedance" (Onaral and Schwan,1982). To put it more correctly, there is a "polarisation" resistance, R_{CT} in parallel with the constant phase angle impedance, Z_{CPA}, as Z_{CPA} is independent of "polarisation" in the electrochemical sense.

Edeling et al (1983) also concluded that the parallel resistance is attributable to charge transfer. 'Good' electrodes will have small values of R_{CT} and

will therefore be characterised by small diameter impedance arcs.

At low frequencies the constant phase angle impedance, $Z_{CPA(LF)}$ in parallel with R_{CT}, is that due to a "smooth" electrode surface as surface roughness effects no longer dominate at these frequencies. There is relatively little frequency dispersion in this region (β is almost unity) and what dispersion there is can probably be attributed to specific adsorption and some residual surface effects. There remains the problem of attributing a physical cause for the observed kink at the high frequency end of the above arc. This is possibly due to surface effects on an electrode system where a shunting, charge transfer resistance is present. This situation was not studied in chapter one and is therefore considered in the next section.

2.1.3 Impedance of a rough surfaced electrode interface across which charge is being transfered.

In section 1.1.2.5, when investigating surface roughness effects, it was assumed that the interfacial impedance of the equivalent smooth surface was due solely to either a non-faradaic double layer capacitance or a $Z_{CPA(LF)}$. As dc current can flow through the system a faradaic process, charge transfer, must also be present in parallel with the above. Therefore taking into account the presence of R_{CT} in parallel with, for example, the double layer

capacitance, a surface pore can be modelled by the ladder network show on figure 2.3.

The impedance of this network is

$$Z_o = (Z_i\ R_e)^{1/2}\ \text{Cotanh (p l)} \qquad \text{(eqn 1.38)}$$

where this time

$$Z_i = \frac{R_{CT}}{1+j\omega C_{dl}R_{CT}} \qquad 2.3$$

At high frequencies current will flow mainly through the parallel capacitors and the impedance approximates to

$$Z_o = (1-j)\left(\frac{R_e}{2\omega C_{dl}}\right)^{1/2}$$

as before, and has a phase angle of 45° (or $\frac{\beta\pi}{4}$ if a Z_{CPA} is used instead of C_{dl}).

At low frequencies most of the current flows through R_{CT} and the impedance will approach the limit (Franklin 1975)

$$Z_o = (R_{CT}\ R_e)^{1/2} \qquad 2.4$$

and the impedance locus forms a lemniscate (Fatt and Falk, 1963; Delevie 1964, 1967) with a maximum imaginary component when

$$\omega = \frac{1}{R_{CT}C_{dl}}$$

The above, however, is only valid for frequencies high enough that the 'cotanh' term approximates to unity i.e. at frequencies were surface roughness effects dominate. This condition has apparently not been generally appreciated.

At low frequencies, where surface roughness

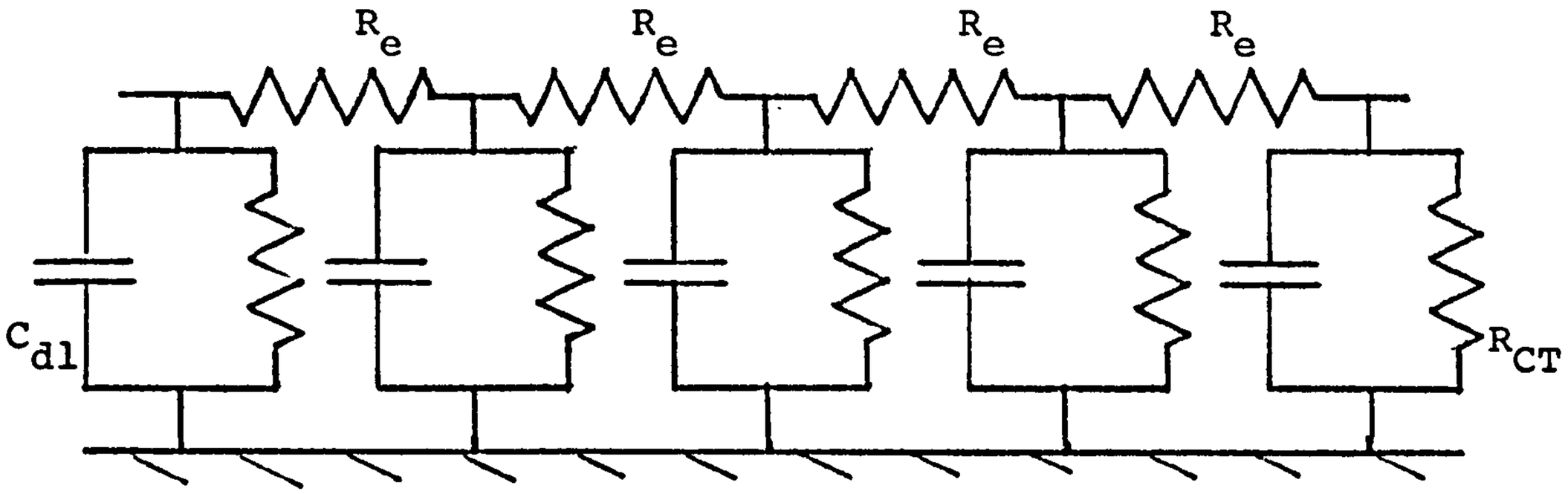

DELEVIE'S TRANSMISSION LINE MODEL
WITH CHARGE TRANSFER

Figure 2.3

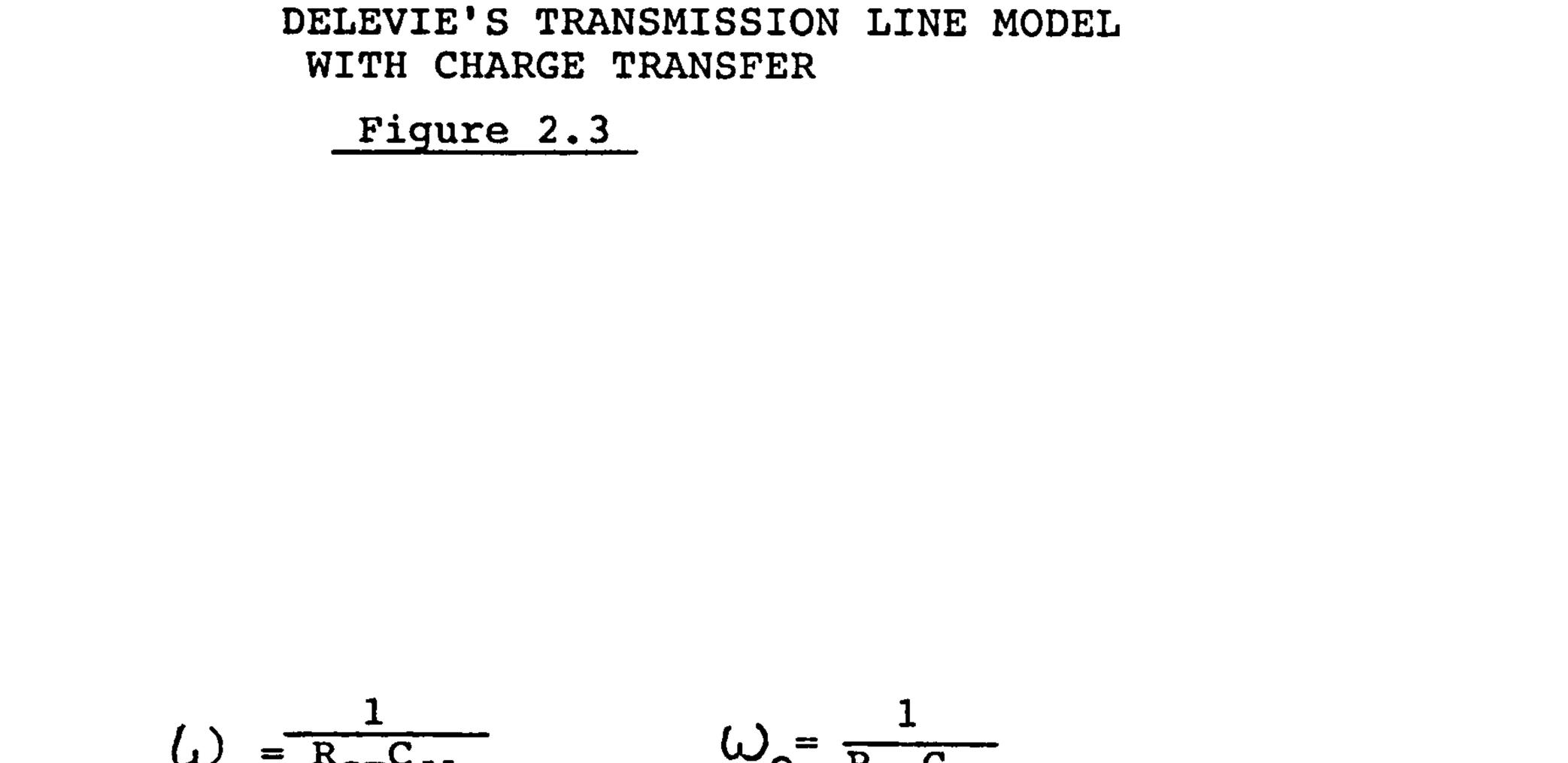

SCHEMATIC PLOTS OF THE EFFECT OF SURFACE ROUGHNESS
ON THE IMPEDANCE LOCUS

Figure 2.4

effects no longer dominate, the impedance locus will deviate from the observed lemniscate and approach the locus of a smooth surfaced electrode, i.e. a semi circle or arc due to C_{dl} or $Z_{CPA(LF)}$ in parallel with R_{CT} (figure 2.4). Hence the low frequency impedance will now tend towards $R_{dc}=R_{CT}$ and not $(R_{CT}R_e)^{1/2}$ as assumed above. This can be shown from Delevie's expression (equation 1.38). At low frequencies the "cotanh(x)" term becomes very large, approximating to 1 +1/x, and the overall impedance tends to

$$Z_o = (Z_i R_e)^{1/2} + Z_i/l \quad \text{(equation 1.39)}$$

where Z_i is expressed by either equation 2.3 or equation 2.1.

For Z_i given by equation 2.3, equation 1.39 becomes

$$Z_o = \left(\frac{R_{CT}}{1+j\omega C_{dl}R_{CT}}\right)^{1/2} + \left(\frac{R_{CT}/l}{1+j\omega C_{dl}R_{CT}}\right) \qquad 2.5$$

At low frequencies the second term on the right hand side of equation 2.5 dominates the interfacial impedance. The impedance locus approximates to a semi circle (or arc if equation 2.1 is used for Z_{CPA}) in this low frequency region which is 'free' of surface effects.

The above approximation applies when the penetration depth exceeds the pore depth i.e. when

$$\left(\frac{Z_i}{R_e}\right) \gg l^2$$

or when $$\omega \ll \frac{1}{R_{CT}C_{dl}}\left(\frac{R_{CT}}{l^2 R_e} - 1\right)$$

which approximates to

$$\omega \ll \frac{1}{l^2 R_e C_{dl}} \qquad 2.6$$

(or $\omega^{\beta} \ll \left(\frac{K}{l^2 R_e}\right)$ if a Z_{CPA} impedance is used instead of C_{dl})

When ω equals zero, equation 1.38 becomes (using equation 2.3 for Z_i),

$$Z_{o(\omega=o)} = (R_{CT}R_e)^{1/2}\text{Cotanh}\left[\left(\frac{R_e}{R_{CT}}\right)^{1/2} 1\right] \qquad 2.7$$

which approximates to

$$Z_{o(\omega=o)} = (R_{CT}R_e)^{1/2} + R_{CT/1} \simeq R_{CT/1} \qquad 2.8$$

i.e. the dc resistance is that due to the transfer of charge across the electrode interface.

It is concluded therefore that the total impedance locus is made up of two overlapping arcs. At higher frequencies the locus may, in cases of extreme surface roughness, have the form of a lemniscate as predicted by Delevie (1964). At lower frequencies the locus forms the characteristic semi circle or arc due to the impedance of the interface in the absence of surface effects. This low frequency arc is due to the double layer capacitance (if β equals 1) and/or the adsorption pseudo capacitance (if β <1) in parallel with the charge transfer resistance.

How clearly the lemniscate will appear at the

higher frequencies depends on the relative magnitudes of R_e, R_{CT}, C_{dl} (or $Z_{CPA(LF)}$) and the degree of surface roughness.

R_{CT} will dominate the interfacial impedance when

$$\omega < \omega_o = \frac{1}{R_{CT}C_{dl}}$$

(or $\omega^\beta < \omega_o^\beta = \left(\frac{K}{R_{CT}}\right)$,if there is Z_{CPA} behaviour)

and surface roughness effects will be less dominant for

$$\omega << \frac{1}{l^2 R_e C_{dl}} \quad [\text{or } \omega^\beta << K/l^2 R_e]$$

Generally R_{CT} is so large, that surface effects on the impedance locus will have "worn off" before the presence of R_{CT} influences the form of the locus. In this general case, a concave, high frequency locus will be observed, which will rejoin the "smooth surface" arc at lower frequencies (before ω_o, figure 2.4 curve b).

For rougher electrodes, especially when there is a small charge transfer resistance and a large electrolyte resistance, the surface roughness effects may still be appreciable at the low frequencies where R_{CT} influences the form of the locus. In such a case a substantial portion of the lemniscate may be observed, causing the locus to have a 'bump' at medium frequencies (curve c). For an example see Onaral and Schwan (1982, figure 3).

In more extreme cases most of the lemniscate will appear and the locus will eventually rejoin that for a smooth surface at frequencies below ω_o (eg Mund et al, 1977).

The above model is of course a very simple one and in practice it may be found necessary to include other circuit elements, e.g. C_{LF}, in the expression for Z_i (equation 1.38). Falk and Fatt (1964) have reviewed the impedance loci due to various forms of the impedance, Z_i, and this work may prove very useful to those studying the electrical properties of rough surfaced electrodes in electrolytes.

2.1.4 Review of other theories proposed to explain the low frequency arc.

Low frequency arcs have often been observed by electrochemists for a variety of electrode systems. Several physical and equivalent circuit models have been proposed to explain the observed behaviour. Although the author believes them to be inappropriate, at least for the electrode systems in this study, they will be briefly reviewed in the next few pages as they have been referred to in the past by Biomedical Engineers as possible explanations of the observed electrical behaviour.

2.1.4.1. Diffusion

It may at first appear surprising that the diffusion impedance, Z_W, should be suggested as the cause of the observed deviation from Z_{CPA} behaviour at low frequencies and the eventual, purely resistive behaviour at $\omega = 0$. After all, Z_W is a constant phase angle impedance with a particular value of β (i.e. 0.5). Such an impedance should continue to increase towards infinity as the frequency is decreased towards zero.

However the expression for Z_W (equation 1.23) was derived assuming the system was semi-infinite i.e. that there was an infinite distance between the electrodes. It will be shown that rectifing this and other assumptions made changes the behaviour of Z_W to the extent that it enables the passage of dc current.

- Convection limited diffusion

It was perhaps Schuhmann (1966) who first pointed out that at low frequencies the diffusion impedance must become equal to the observed dc resistance and cannot continue towards infinity as predicted by Warburg's theory.

It was shown in section 1.1.2.2 that when a potential step, E, is applied to an electrode system, the concentrations of the oxidised and reduced species at the surface quickly adjust to values governed by the Nernst equation (equation 1.10). There is then a sharp

difference in the above concentrations between the surface of the electrode and the bulk of the electrolyte. This difference in concentrations is assumed to take place over a very small distance termed the Nernst diffusion layer, which gradually increases with time (figure 1.11). The resultant time dependent concentration gradient gives rise to the frequency dependence of the diffusion impedance (equation 1.23).

It was assumed in section 1.1.2.2 that the Nernst diffusion layer continued to grow indefinitely with time, thus infering that the diffusion impedance, Z_W, increases indefinitely as frequency tends to zero.

However, convection, either forced or natural, has been found to disturb the growth of the diffusion layers. Schuhmann simplified this problem by assuming that outside a certain layer of thickness, δ_o , convective transport maintains the concentration uniform at the bulk concentration, C_b. Therefore diffusion layers can only increase up to a maximum value of δ_o beyond which the concentration gradient is zero and Z_W behaviour ends.

Taking into account this new boundary condition Schuhmann derived the following expression for the convection limited diffusion impedance, Z_{CLD}.

$$Z_{CLD} = \sigma \omega^{-1/2} \quad (1-j) \tan\left[\frac{\delta_o (j\omega)^{1/2}}{D}\right] \qquad 2.9$$

Where σ = Warburg Coefficient

δ_o = Maximum thickness of the diffusion layer

D = Diffusion Coefficient

For high frequencies the 'tan' term approximates to unity and the impedance is that of Z_W, i.e.

$$Z_{CLD} = (1-j)\sigma\omega^{1/2}$$

At low frequencies the ac diffusion layer becomes comparable with the maximum thickness possible, δ_o. The impedance will then begin to deviate from Z_W behaviour and will eventually reach a purely resistive value at $\omega = 0$ given by

$$Z_{CLD(\omega = o)} = R_{dc} = \sigma\delta_o(2/D)^{1/2} \qquad 2.10$$

The form of this locus is as shown on figure 2.5. Buck (1968) pointed out that the maximum for Z''/R_{dc} is equal to 0.417 and this can be used to determine if convection limited diffusion is indeed present.

Such a locus, coupled with a high frequency semi circle/arc due to the double layer capacitance in parallel with R_{CT}, is somewhat similar to that shown on figure 2.4.C. However the low frequency arc generally does not have a phase angle of 45^o nor does its maximum height equal R_{dc} x 0.417 as would be expected if convection limited diffusion was the cause of the observed low frequency behaviour.

It is concluded that the above physical model is not relevant to the electrode systems under study.

- Separation Limited Diffusion

This, as the title suggests, is a physical model very similar to the last one and, as will be shown, suffers from the same draw backs.

Generally, as mentioned, the electrode problem has been treated as a semi-infinite, one dimensional

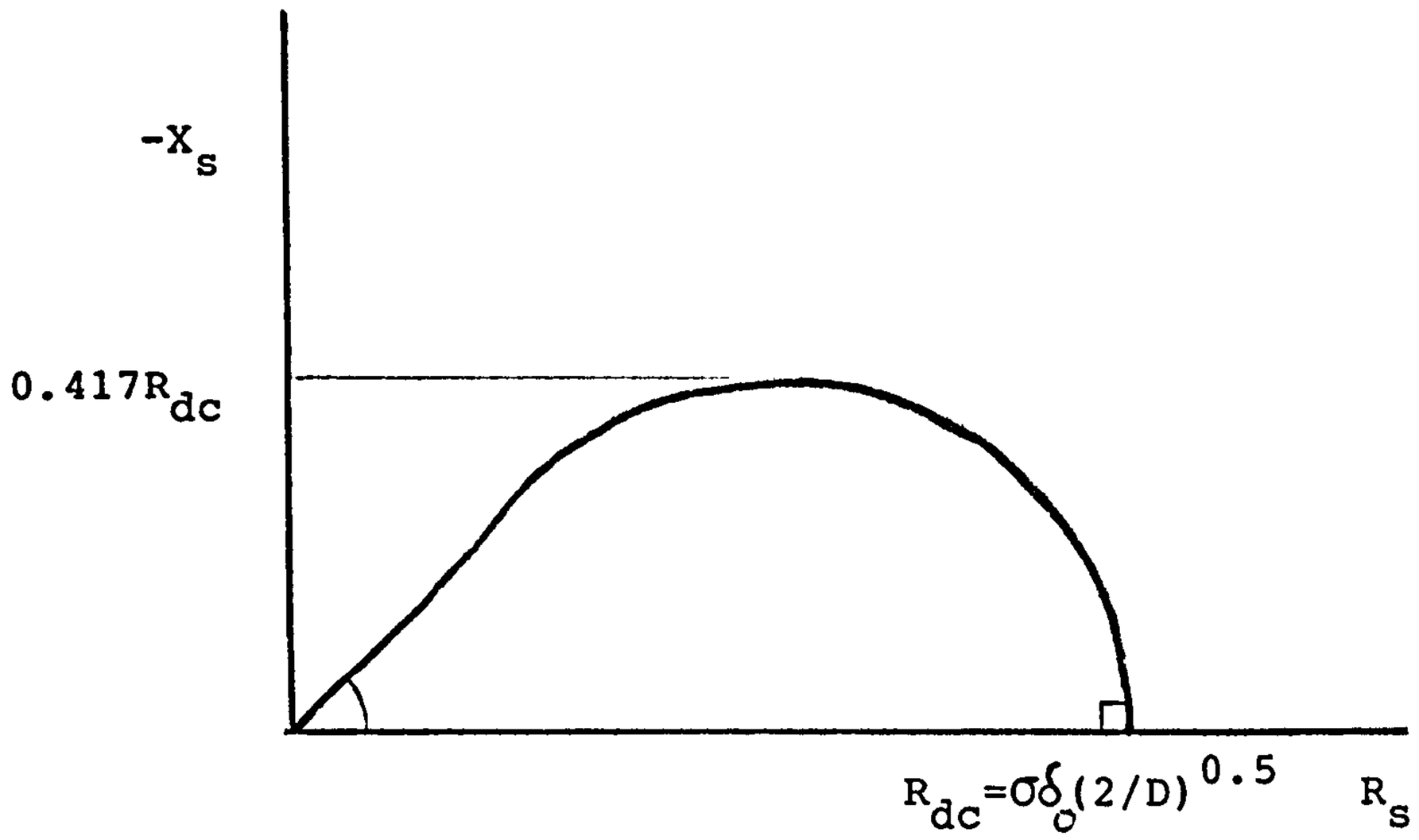

CONVECTION LIMITED DIFFUSION

Figure 2.5

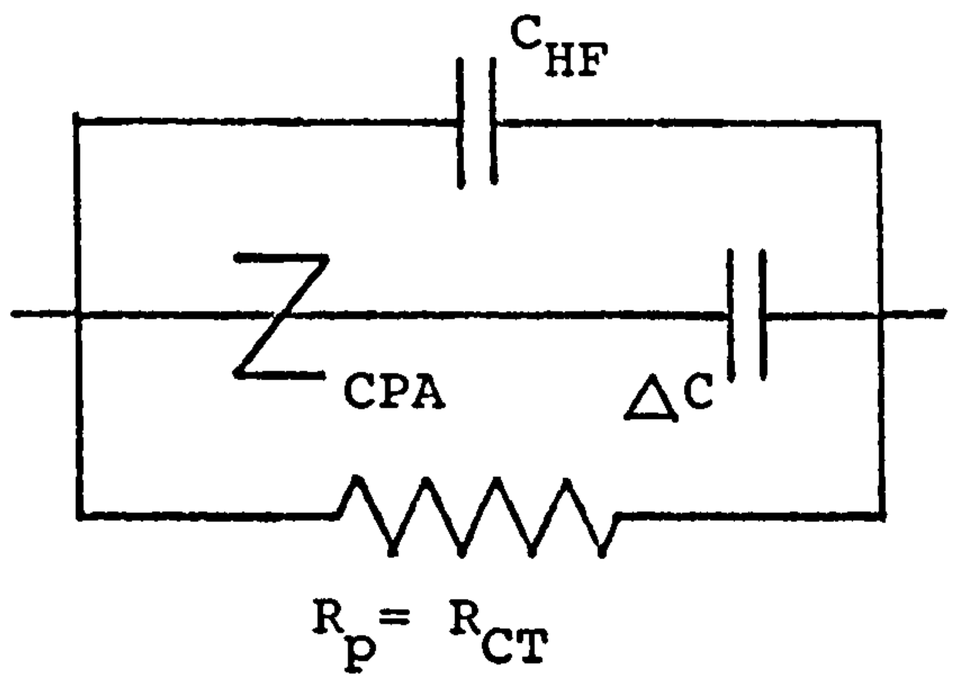

A "DISTRIBUTION OF RELAXATION TIMES" WITH A PARALLEL CHARGE TRANSFER RESISTANCE

Figure 2.6

system. However at very low frequencies the ac diffusion layer will be of the same order of magnitude as the distance between the electrodes.

The problem is treated in the same way as convection limited diffusion with δ_o equalling d/2, i.e. one half of the distance between the electrodes (assuming the electrodes are of the same size; Schuhmann, 1977). As the diffusion layers of both electrodes meet in the middle, both electrodes will have their boundary at this point and the concentration of this point will be held at the bulk, or initial concentration, C_b.

The resultant impedance locus has the same form as that for convection limited diffusion and hence the same criticisms apply.

2.1.4.2 A Distribution of dielectric relaxation times shunted by a charge transfer resistance.

Equation 2.1 is very similar to that proposed by Cole-Cole (1941) for a "distribution of dielectric relaxation times" (see equation 1.36). This similarity has lead some researchers to adopt the concept and apply it to the interface problem. It may be useful to point out that an arc on the complex dielectric plot is not equivalent to an arc on the impedance plot.

In section 1.1.2.4 the work of Bockris et al (1958, 1966) was reviewed. Bockris et al suggested that relaxation in the reorientation of solvent dipoles adjacent to the electrode surface accounted for the

observed high frequency dispersion at the electrode-solution interface. It was also noted that Jaron et al (1968) fitted their electrode impedances to Cole-Cole's mathematical and equivalent circuit models (see figure 1.28a). Cole-Cole (1941) considered the cell membranes they were studying as non conductors (i.e. they ignored the parallel resistance, R_p, due to the bulk conductivity) and modelled only the capacitative branch representing the dielectric properties.

According to certain researchers (Wapenaar and Schoonman, 1981; Hyde, 1971) a more general equivalent circuit would include the parallel resistance (figure 2.6). Hyde (1971) suggested that this model was not only applicable to bulk but also to interfacial impedances although he did not attribute specific significance to the parameters of the equivalent circuit.

Such an equivalent circuit would have an impedance similar to that shown on figure 2.2a,especially if the contributions of C_{HF} and ΔC could be ignored.

For example, Epelboin and Keddam (1970) noted that it was impossible to model adequately their electrode's impedance by the parallel combination of a double layer capacitance and a charge transfer resistance. They deduced that the "double layer impedance" was the source of the observed deviation and concluded that it could not be described simply as a constant capacitance. Instead they represented it by a distribution of capacitive time constants about a characteristic value Υ (borrowing from Cole and Cole's

work, 1941), whose impedance is given by $\frac{R_{CT}}{(j\omega\tau)^{\beta}}$

Their model therefore comprised a Z_{CPA} in parallel with a resistance, R_{CT}, similar to that shown on figure 2.2a.

However the same criticisms made for "the distribution of dielectric relaxation times" mentioned in section 1.1.2.4. apply to this slightly altered version of the model and hence the above theory is unacceptable in spite of the equivalent circuit model being very promising.

The suggestions that the parallel resistance is the faradaic charge transfer resistance, R_{CT}, and that the parallel capacitance was the source of the observed frequency dispersion are important ones and will be enlarged upon in following sections.

2.1.4.3. A Distribution of Relaxation times.

This approach also follows closely the work of Cole-Cole who observed an arc with a depressed centre in the complex dielectric plane. This they suggested could be expressed in terms of a distribution of dielectric relaxation times.

A somewhat similar explanation has been suggested for arcs observed on complex impedance plots. The general explanation offered is in terms of heterogeneity of the relevant properties of the interface and a statistical distribution of the corresponding relaxation frequencies. Thus if an

impedance cannot be characterised by a single time constant it may be thought of as being composed of a series of time constants. In such a case the complex impedance will be expressed as

$$Z = R_{oo} + (R_o - R_{oo}) \int \frac{F(\tau)}{1+j\omega} d\tau \qquad 2.11$$

Where $F(\tau)$ is the distribution function of the time constants.

The most general function which characterises an arc whose centre is below the real axis is of the form (Schwan, 1957)

$$Z = R_{oo} + \frac{R_o - R_{oo}}{1+(j)^{\beta} F(\omega\tau)} , \qquad 2.12$$

Where $\beta\pi/2$ is the angle of depression and $F(\omega\tau)$ is some function of frequency. As j and ω always appear in combination for linear systems, the expression for the impedance must be (as observed by Onaral and Schwan, 1982)

$$Z = R_{oo} + \frac{R_o - R_{oo}}{1 + (j\omega\tau)^{\beta}} \qquad \text{(Eqn 2.1)}$$

Where τ is the average time constant and β is a measure of both the depression of the arc and the distribution of the time constants.

Stibitz and McCann (1974), for example, used a statistical model for both membrane and interface impedances. They concluded that the observed depressed arc did not necessarily imply the presence of special

frequency dependent impedance elements (Z_{CPA}'s) but could simply be accounted for by statistical variation of electrical parameters from point to point over the system.

However Cole and Cole pointed out that in order to generate the observed values of β (approximately 0.8) an exceedly large distribution of relaxation times is required. Great difficulty is encountered in accounting for such broad distributions.

Cole and Cole concluded that "in the absence of any satisfactory explanation of these features, the distribution function is nothing more than a means of expressing the experimental results which is equivalent to the circular arc locus."

Hence although the distribution function has been shown to model well the observed results for biomedical electrode systems (Onaral and Schwan, 1982) the physical significance of this equation is still to be attributed.

2.1.5 Conclusions

It has been found that at low frequencies the impedance locus deviates from the Z_{CPA} behaviour observed at high frequencies. This is due to the presence of a charge transfer resistance in parallel with Z_{CPA}. If the electrode surface is very rough a kink or lemniscate may also be observed at the high frequency end of this arc. Such behaviour, qualitatively at any rate, may be explained by Delevie's "transmission line" model when the low frequency, smooth surface impedance is that due to a Z_{CPA} in parallel with R_{CT}.

This is believed to be the first time such behaviour has been physically explained. Such a model fits the high, medium and low frequency experimental data,both in the linear and nonlinear (as will be shown in chapters 4 and 5) regions.

2.2 EXPERIMENTAL SECTION

2.2.1 Experimental Set up

Two pieces of equipment were used for recording the impedance of pacing electrodes at low frequencies. Initially a Solartron 1170 frequency response analyser was used, on loan from the Department of Physics, Leeds University. Later the more advanced Solartron 1250 was made available and most of the experiments were carried out using this instrument. It is regretted that this advanced equipment was only used for the last few months of my stay at Leeds General Infimary, as much more in depth research could have been carried out. As it was, the earlier, high frequency work done using the Wein Kerr bridge was repeated, experiments were then carried out over a much wider frequency range, the effect of electrode failure on the system's overall impedance was investigated as was the nonlinearity of the electrode system for a variety of input waveforms - all in the matter of three or four months. It will become obvious to the reader that in many instances, the relatively few experiments carried out revealed intriguing aspects of the electrode-electrolyte interface impedance which time, unfortunately, did not allow to be further investigated . It is hoped that this will be rectified in the future.

- Results obtained using the Solartron 1170

While using the Solartron 1170 the set up was as shown on figure 2.7. The electrode system was connected in series with a resistance, R, which enabled the calculation of the current, $I_E = V_x/R$, flowing through the electrodes. In order to keep the voltage dropped across the electrode system, V_E, constant, it was necessary to ensure that it remained equal to the voltage dropped across R, ie $V_E = V_X = V_Y/2$. As the impedance of the electrode system increases as the frequency is lowered, the resistance R had also to be increased to ensure the above condition.

Figure 2.8 shows the impedance locus of a Telectronic 224 (Exp 3) obtained using the above set up with V_Y = 10 mV. Frequencies at which the resistance R had been altered are indicated on the plot. It can be seen that, unless R is corrected for each of the lower frequencies, errors will be introduced by the resultant variation in V_E.

It is interesting to note that figure 2.8 is very similar to that published by Onaral and Schwan (1982 figure 3) for platinum electrodes in 0.9% saline. The low frequency impedance is well represented by equation 2.1 with the following parameter values

$$K = 215k\Omega s^{-\beta} \quad \beta = .81$$

$$R_{CT} = 0.92M\Omega$$

The above electrode had been much used and this has resulted in a relatively large value of K and a small value of R_{CT} relative to those of a fresh electrode (see later sections on the effects of electrode

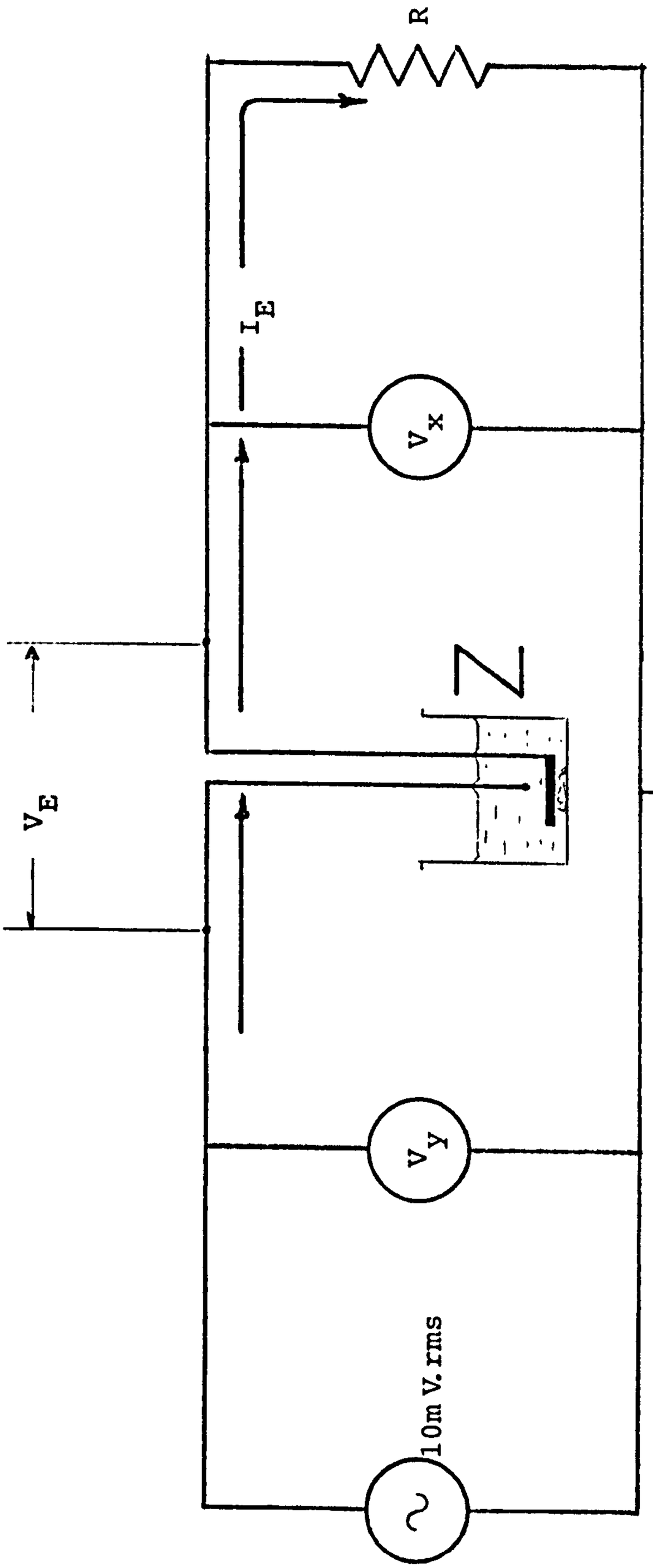

INITIAL IMPEDANCE MEASUREMENT SYSTEM

Figure 2.7

Voltage across Electrodes, $V_E = V_y - V_x$

Current through Electrodes, $I_E = V_x/R = V_y/(Z+R)$

Impedance of Electrode System, $Z = \frac{(V_y - V_x)R}{V_x}$

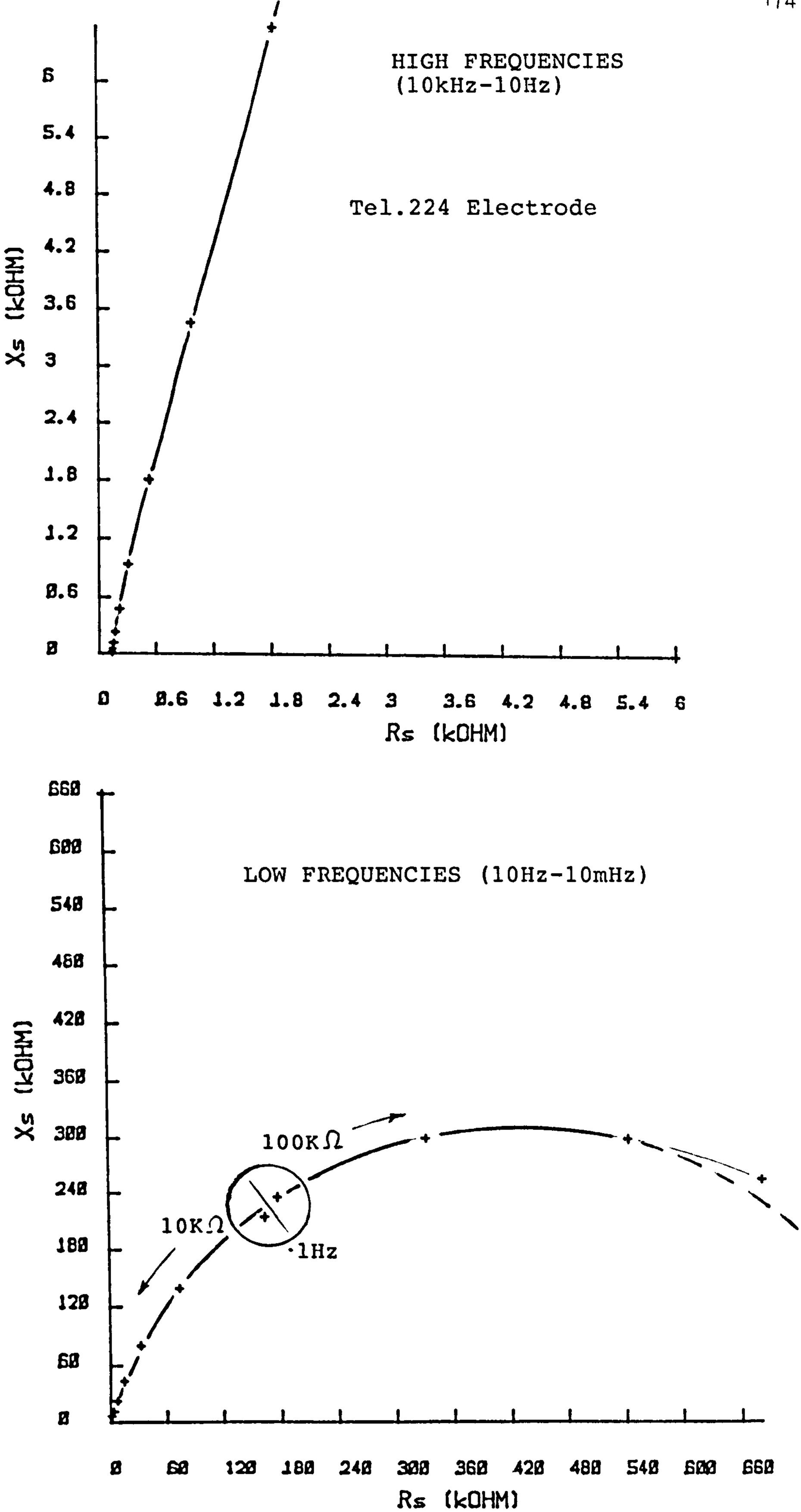
HIGH FREQUENCIES
(10kHz-10Hz)
Tel.224 Electrode
Xs (kOHM)
6
5.4
4.8
4.2
3.6
3
2.4
1.8
1.2
0.6
0
0 0.6 1.2 1.8 2.4 3 3.6 4.2 4.8 5.4 6
Rs (kOHM)
LOW FREQUENCIES (10Hz-10mHz)
Xs (kOHM)
660
600
540
480
420
360
300
240
180
120
60
0
100KΩ
10KΩ
·1Hz
0 60 120 180 240 300 360 420 480 540 600 660
Rs (kOHM)

Figure 2.8

history

There appears to be a deviation from the arc for frequencies above 2.15Hz similar to that observed by Onaral and Schwan (1982) and discussed in section 2.1.3.

- Results obtained using the Solartron 1250

In order to investigate the low frequency impedance of the electrodes a frequency range of 100Hz down to 10mHz was chosen, with three logarithmic steps per decade. The applied signal amplitude was 10mV as before.

The delay between the application of a stimulus and a measurement, following a change of frequency, was arbitrarily set at one cycle. The measurements were averaged over three complete cycles.

In this low frequency range the resistance used to measure the current flowing through the electrode system would have needed to be varied for each frequency reading as the system's impedance can change quite markedly from one frequency to the next. This obviously would be impractical and hence an operational amplifier was used to keep the voltage across the electrode constant (figure 2.9). Channel 2 of the Solartron 1250 was connected to the signal generator as shown. As the voltage on the indifferent electrode is held at zero by the use of the operational amplifier, the voltage across the electrode system is that applied by the signal generator (10 mV) and monitored by Channel 2 (V_2). The current flowing

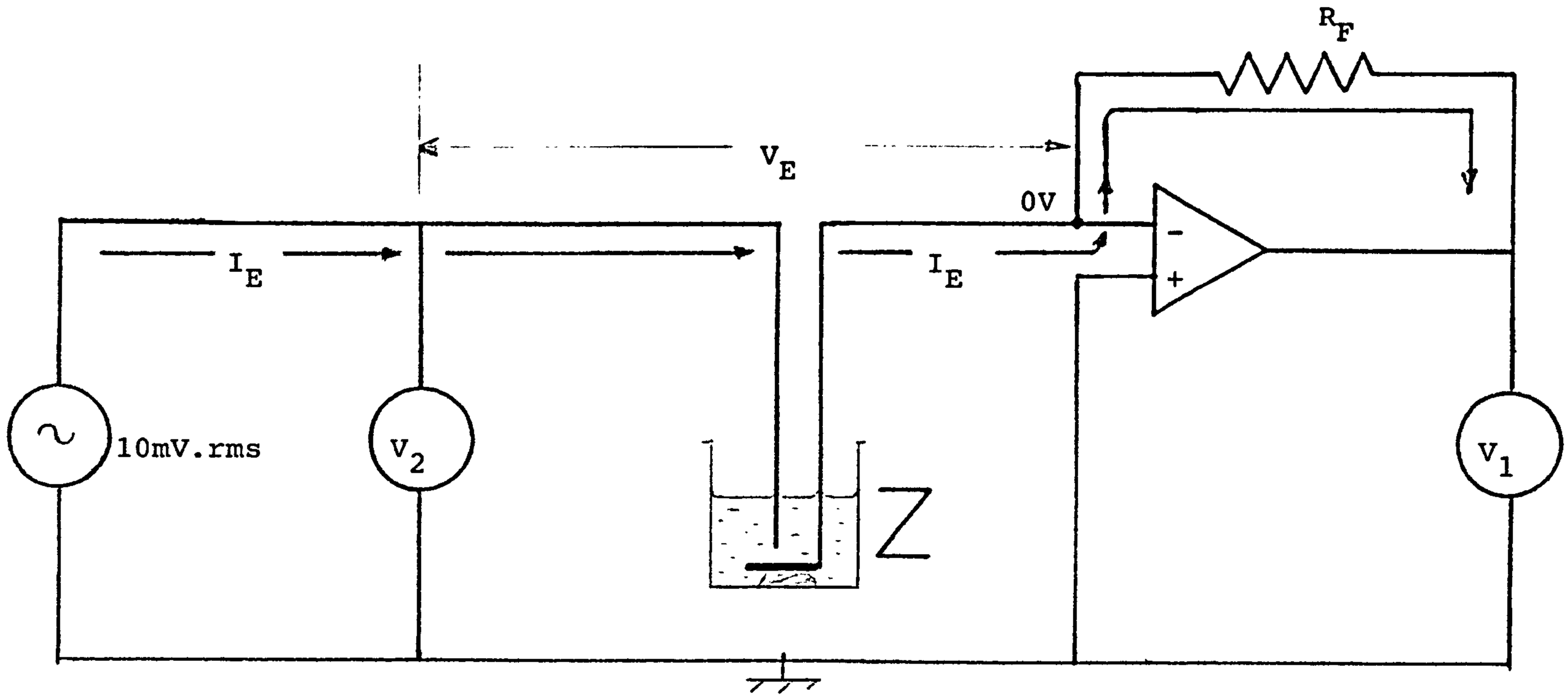

Voltage across Electrode System, $V_E = V_2 - 0 = V_2$
Current flowing through Electrode System, $I_E = V_1/R_F$
Impedance of Electrode System, $Z = R_F V_2/V_1$

IMPEDANCE MEASUREMENT SYSTEM

Figure 2.9

through the electrode system flows through the feed back resistance, R_F, and hence can be calculated by dividing the voltage dropped across R_F (V_1) by R_F.

As the impedance of the electrode system equals the voltage dropped across it (V_2) divided by the current flowing through it (V_1/R_F) the impedance is given by

$$Z = R_F \; V_2/V_1$$

i.e. the ratio of the voltages measured by Channels 2 and 1 had to be multiplied by R_F to obtain the electrode system's impedance.

2.2.2 Experimental Results

2.2.2.1 Smooth Platinum Iridium electrodes

- Devices SC ($21mm^2$)

The impedance of electrode number 3 (Exp 80) is plotted on figure 2.10. The results were fitted by computer to the parallel combination of a Z_{CPA} and a charge transfer resistance, R_{CT}. It was calculated that

$$K = 62\ k\Omega s^{-\beta} \qquad \beta = 0.85 \quad (\emptyset = 76.5^{o})$$

$$R_{CT} = 4.4\ M\Omega$$

Only the first quarter or so of the arc is visible. In order to see just one half of the arc the frequency range would need to go down to

$$\omega_o = \left(\frac{1}{T}\right)^{1/\beta} = \frac{K}{R_{CT}} = 14 \times 10^{-3} \text{ radians}$$

or $f_o = 2$ mHz i.e. below the present frequency range with its lower limit of 10mHz. To go

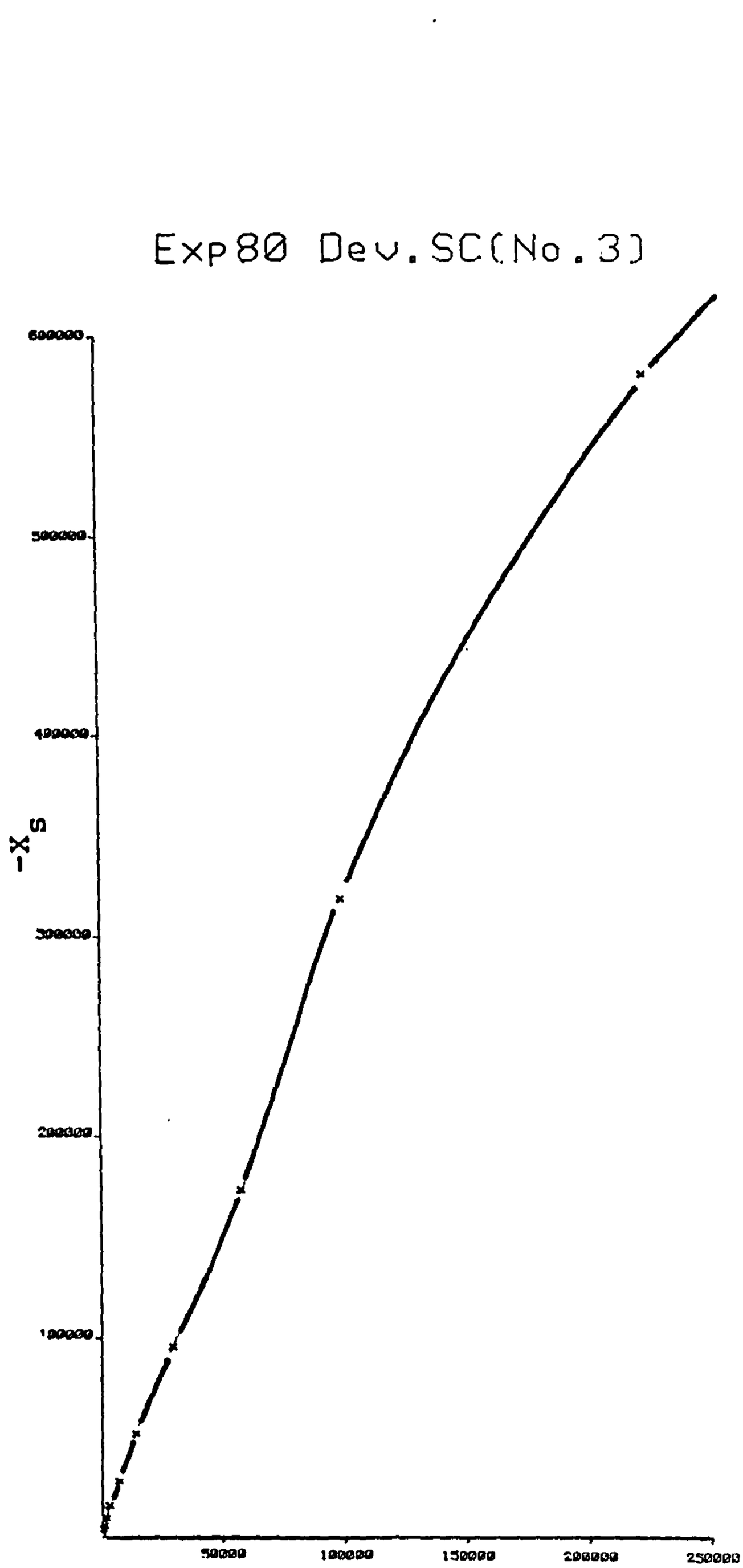
Exp80 Dev.SC(No.3)
600000
500000
400000
300000
200000
100000
-Xs
50000
100000
150000
200000
250000
Rs (ohms)

Figure 2.10

down to such very low frequencies is not practical. Each measurement involves at least 4 cycles at the desired frequency. To measure the frequency of the electrode system at 1mHz would take over an hour - just for one point ! Within such a time period it is very probable that the low frequency impedance would have changed sufficiently to render the accurate calculation of the point, averaged over 3 cycles, impossible.

The measured points form part of an arc describable by equation 2.1 as expected. There appears, however, to be a slight kink for frequencies above 0.1Hz similar to that observed by Onaral and Schwan (1982) between 10 Hz and 0.4 Hz. This is probably due to surface effects (section 2.1.3.) and will be investigated later.

The large value of R_{CT} indicates that there is very little charge transfer occuring across the interface and hence the electrode is very 'polarisable'.

- Telectronic 224 ($10mm^2$)

The impedance of a fresh electrode (no 3) is plotted on fig 2.11 and the following values of equivalent circuit parameters were calculated (Exp 74)

$$K = 101k\Omega s^{-\beta} \qquad \beta = 0.79$$

$$R_{CT} = 3.4\ M\Omega$$

In the high frequency range this electrode had parameter values of

$$K = 142k\Omega s^{-\beta} \quad \text{and } \beta = .84$$

Again K and β are observed to have decreased in the low frequency range.

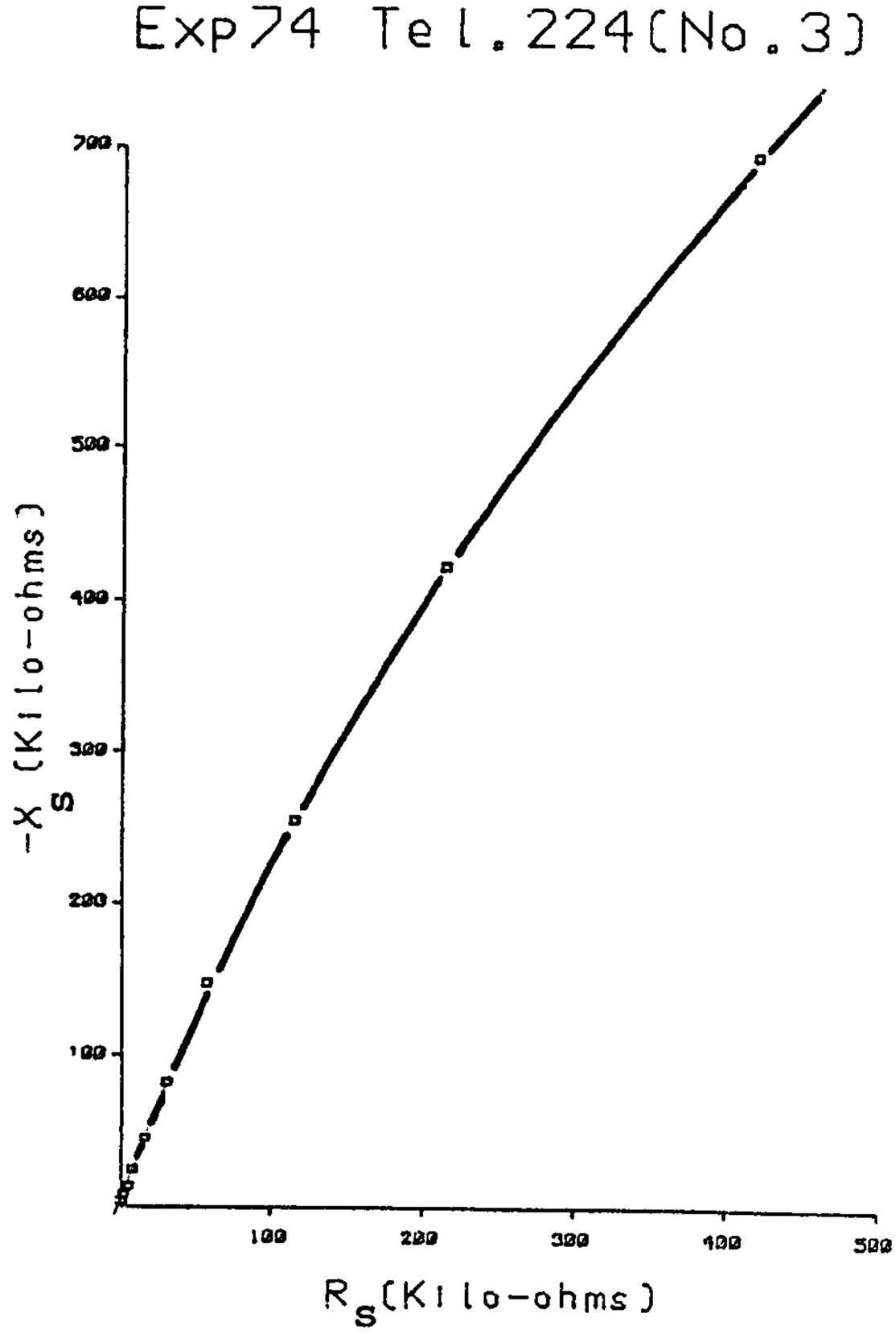
Exp74 Tel.224(No.3)
700
600
500
400
300
200
100
-X (Kilo-ohms)
S
100
200
300
400
500
R_S(Kilo-ohms)

Figure 2.11

- Time effects

The effect of time after immersion in saline on the above electrode's impedance was investigated.

The results are listed on Table 2.1

TABLE 2.1

Time	Exp no	($k\Omega s^{-\beta}$)	β	$R_{CT}(M\Omega)$
2 hours	74	101	.795	3.4
5 hours	76	101.2	.77	2.25

K apparently remains unchanged or increases relatively slowly. If the latter is the case (as was observed in chapter 1) the increase could be due to a gradual decrease in surface coverage of the adsorbed oxygen, presumably being replaced by chloride ions or impurities.

The value of R_{CT} decreases markedly indicating that the transfer of charge is facilitated by the increasing coverage of the chloride ions being adsorbed onto the surface.

2.2.2.2 Rough Surfaced electrodes

- Roughened Devices SC electrode

As in chapter one, the effect of roughening the surface of a Devices SC ($21mm^2$, No 3) electrode was investigated. As previously described, the initially 'smooth' surface was progressively roughened while its

impedance was monitored. The resultant impedance loci are plotted on figure 2.12.

The calculated equivalent circuit parameter values are listed on Table 2.2 and plotted of figure 2.13.

TABLE 2.2

	Exp No	$K(k\Omega s^{-\beta})$	β	$R_{CT}(M\Omega)$
'Smooth' surface	80	62	0.85	4.4
Roughened with P320 emery paper	82	40	0.845	1.05
Roughened with P60 emery paper	83	26	0.83	0.5

In the high frequency range it was noted that the impedance locus became concave as the surface was roughened. At the highest frequencies the measured values of K and β decreased towards the limits $(R_e K_{LF})^{1/2}$ and $\beta_{LF}/2$. As the frequency decreased the locus tended towards that of the smooth surface. i.e. K and β increase.

This trend appears to continue for the medium frequencies where the slope of the loci of the rough surfaces approach that of the 'smooth' surface (figure 2.12). However as the frequency is further lowered the loci of the rough surfaces deviate from that of the "smooth" surface. In this region the loci have a slight kink. At the higher frequencies the loci appear to follow a relatively small diameter arc - due presumably to surface roughness effects (see figure 2.4 curve b). The loci then rise sharply from this arc to

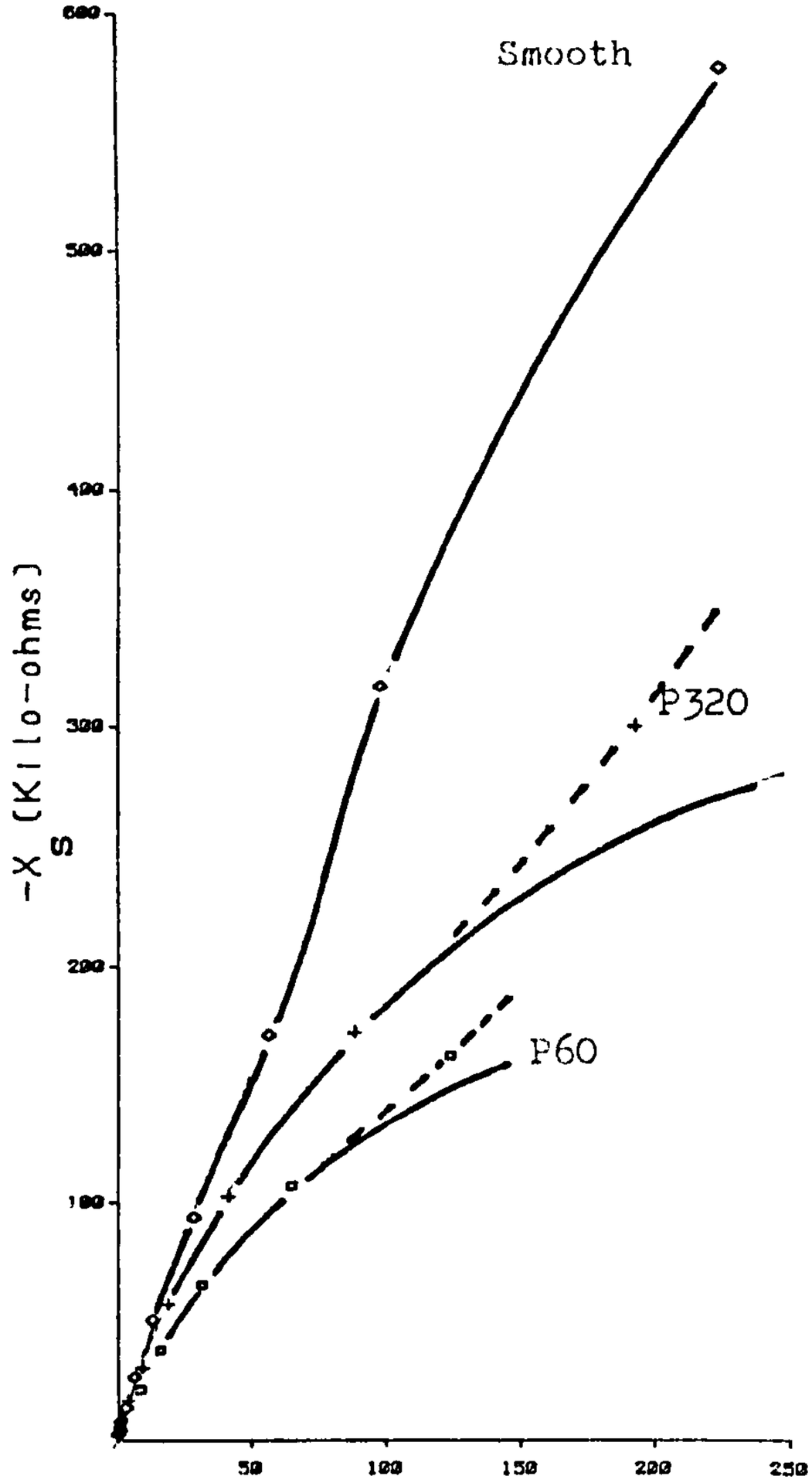

Figure 2.12

Effect of Surface Roughness

on circuit parameters

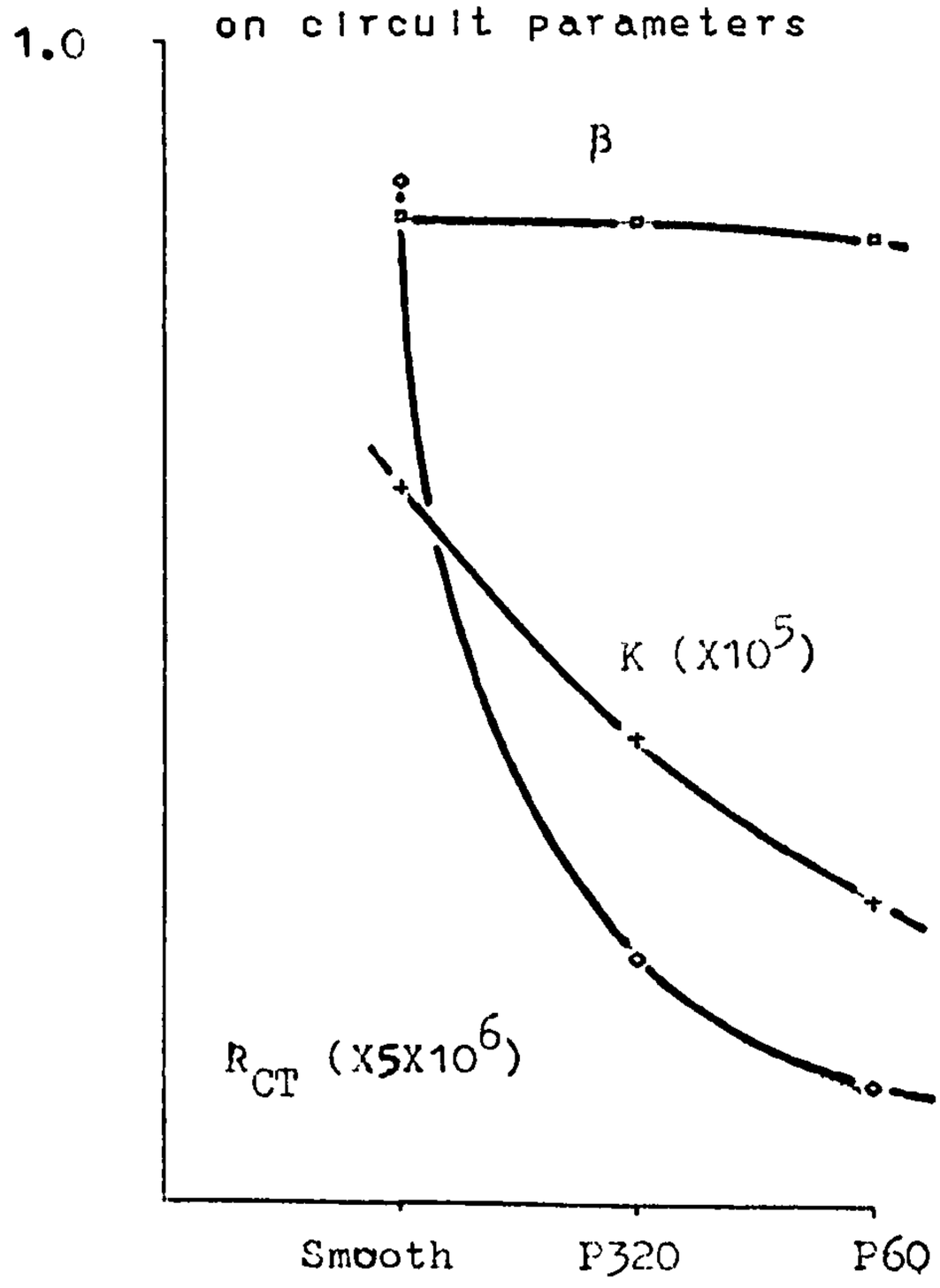

Figure 2.13

join a larger diameter, low frequency arc due to the impedance of the smooth surface. The 'kink' is more pronounced for the rougher surfaces whose loci form smaller diameter arcs at high frequencies (the diameter depending on the degree of roughness).

The loci were fitted to the Z_{CPA} - R_{CT} parallel model inspite of the kinks and low frequency rise in order to give some means of comparing the impedances. The calculated values will reflect mainly the impedance of the higher frequency, small diameter arc due to surface effects.

From the above table (2.2) in can be seen that roughening the surface decreases K and β as found in the high frequency range (Chapter 1). The decreases are not however as marked in this, the low frequency range as the effect of surface roughness is not as dominant in this region as at the higher frequencies. The decrease in 'R_{CT}' is very dramatic with the measured value of 'R_{CT}' tending towards $(R_{CT}R_e)^{1/2}$ for extremely rough surfaces.

- Sorin S80 Pt-Ir electrode ($8mm^2$)

The low frequency impedance of a fresh porous electrode (no 3) is plotted on figure 2.14 (exp 71). The calculated values for the equivalent circuit elements were

$$K = 44k\Omega s^{-\beta} \qquad \beta = 0.94$$

$$R_{CT} = 1.75M\Omega$$

The S80 electrode showed signs of severe surface roughness in the high frequency range (figure 1.41)

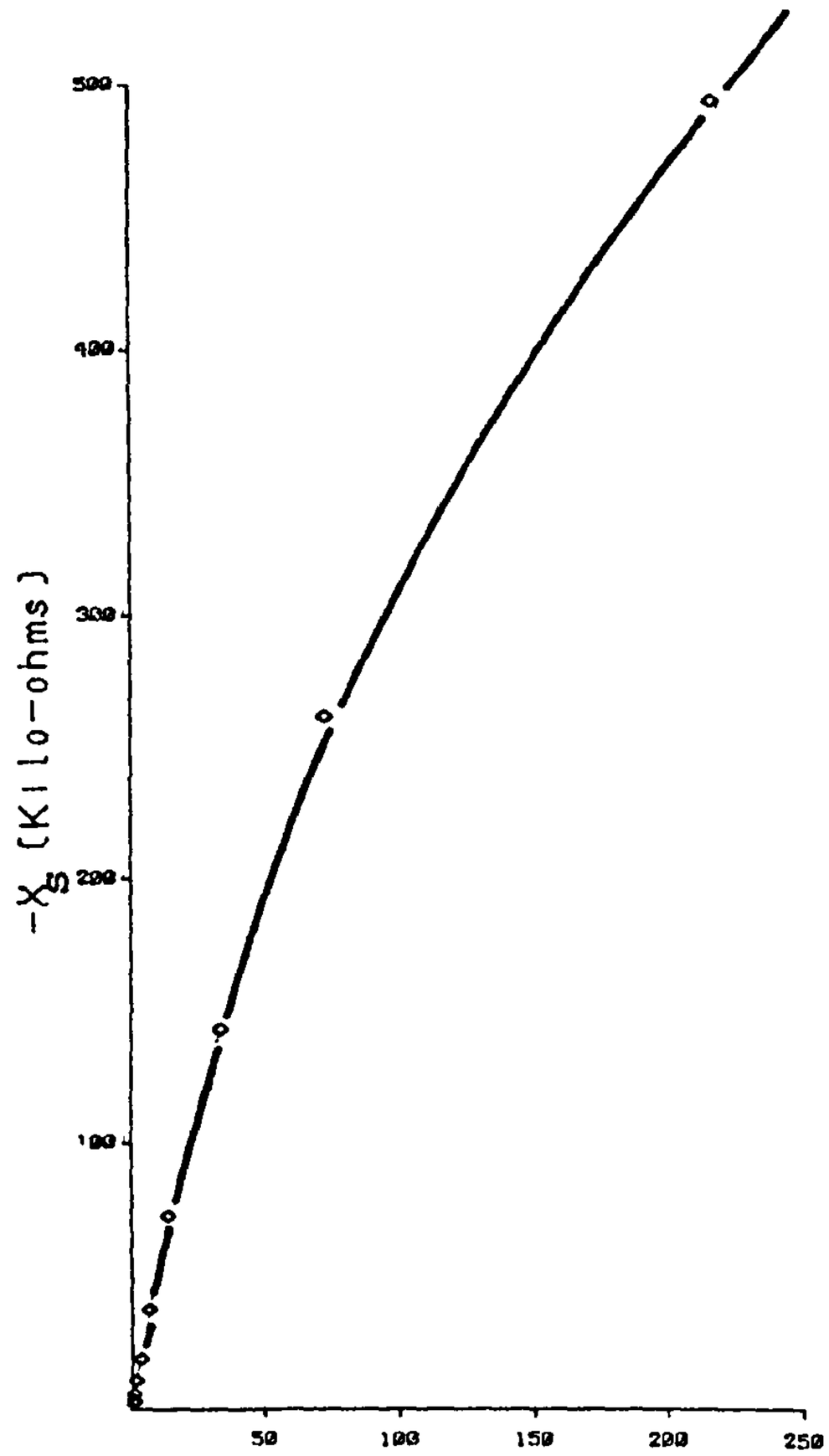
Exp 71 Sorin S80
500
400
300
200
100
$-X_S$ (Kilo-ohms)
50
100
150
200
250
R_S (Kilo-ohms)

Figure 2.14

with very low values of magnitude and phase angle (K_{HF} = 1,590Ω $s^{-\beta}$ β_{HF} = 0.56)

In the low frequency range (10Hz - 10mHz) the observed locus approaches a semi circle (β_{LF} = .94), indicating that the rough surface 'transmission line' effects are no longer dominant in this frequency range. The relatively small values of K and R_{CT} indicate a large effective surface area in spite of the small nominal area of 8 mm^2 .

- Time and history effects

The effect of time on the low frequency impedance of the above S80 (no 3) electrode was investigated. After a total of four hours immersed in saline the impedance had become (Exp 72)

$$K = 49\ k\Omega\ s^{-\beta} \qquad \beta = 0.94 \qquad R_{CT} = 1.66\ M\Omega$$

and after six hours (Exp 73)

$$K = 49.3\ k\Omega\ s^{-\beta} \qquad \beta = 0.92 \qquad R_{CT} = 1.57\ M\Omega$$

As with the 'smooth' Telectronic electrode, K increases slightly and R_{CT} decreases with time. It is interesting to note that for both electrodes β decreases with time indicating possibly an increase in adsorption and / or surface effects.

2.2.2.3 Very rough surfaced electrode

- Activated vitreous carbon electrode (12mm^2)

The low frequency impedance of a fresh electrode (no 2) is plotted on figure 2.15 (Exp 84). The form of the impedance locus is surprising as it does not bend over as expected but remains a straight line, indicative of simple Z_{CPA} behaviour. The parameter values of the series R_{TOT} - Z_{CPA} circuit were calculated as

(i) from Argand diagram

$R_{TOT} = 196\Omega$ $\quad \phi = 76^{o}$ $\quad (\beta = 0.84)$

(ii) from log Z - log f plot

$K = 5,500\Omega s^{-\beta}$ $\quad \beta = .84.$

Although the above calculated value of β is larger than that calculated at very high frequencies (β_{HF} = .36, figure 1.43) the very small value of K indicates that surface effects still influence the impedance of this very rough electrode at these low frequencies. Compare, for example, Mund et al's (1976, 1979) calculated values of K and β , $218k\Omega s^{-\beta}$ - $453k\Omega s^{-\beta}$ and 0.87 - 0.9, for 'smooth' vitreous carbon electrodes.

The impedance of a much used A.V. carbon electrode (no 1) differed significantly from that of the above fresh electrode (no 2). The results (Exp 23a) for the old electrode are plotted on figure 2.16.

Instead of being characterised by Z_{CPA} behaviour over the entire frequency range, the old electrode's impedance locus forms part of an arc at medium

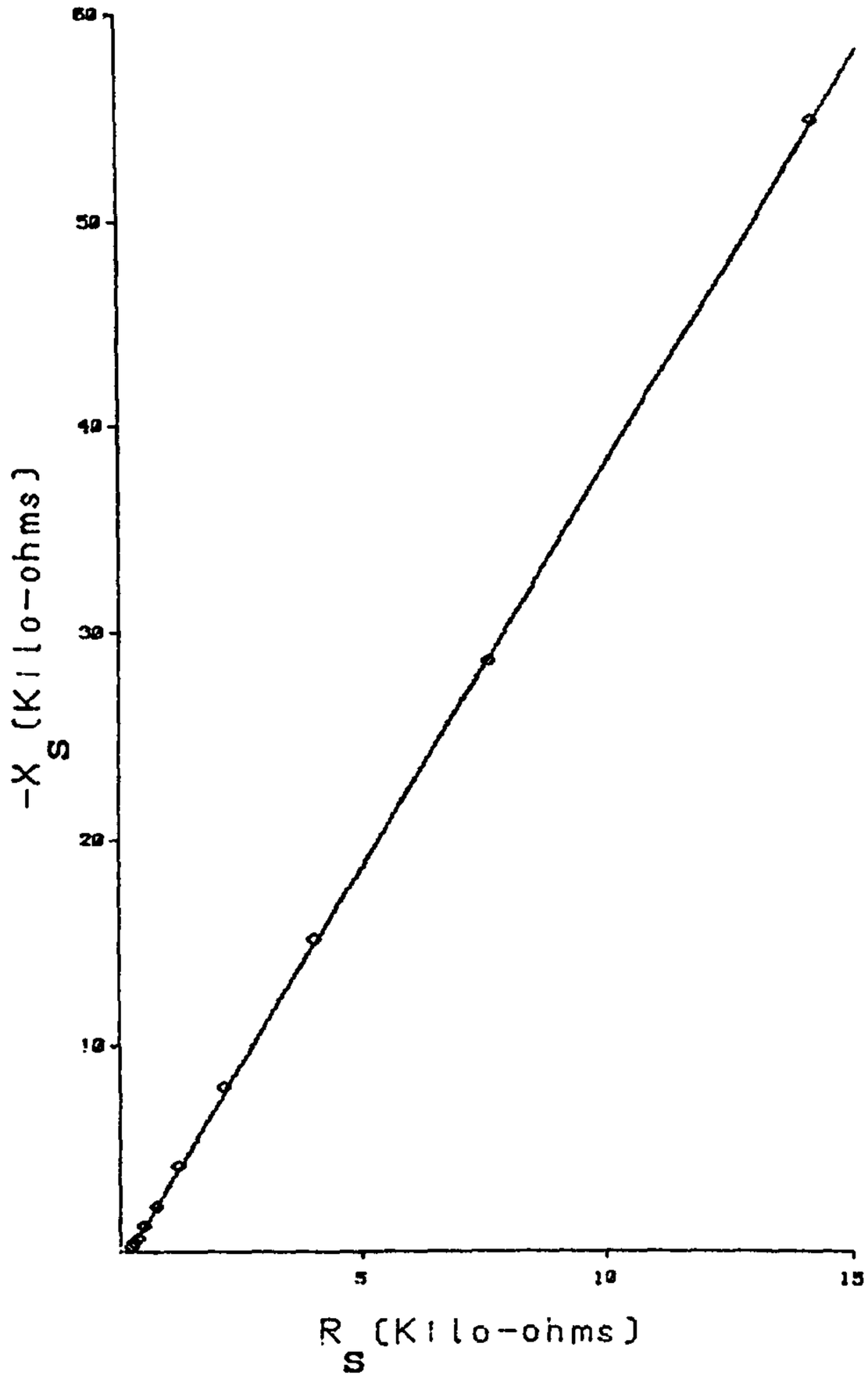

Figure 2.15

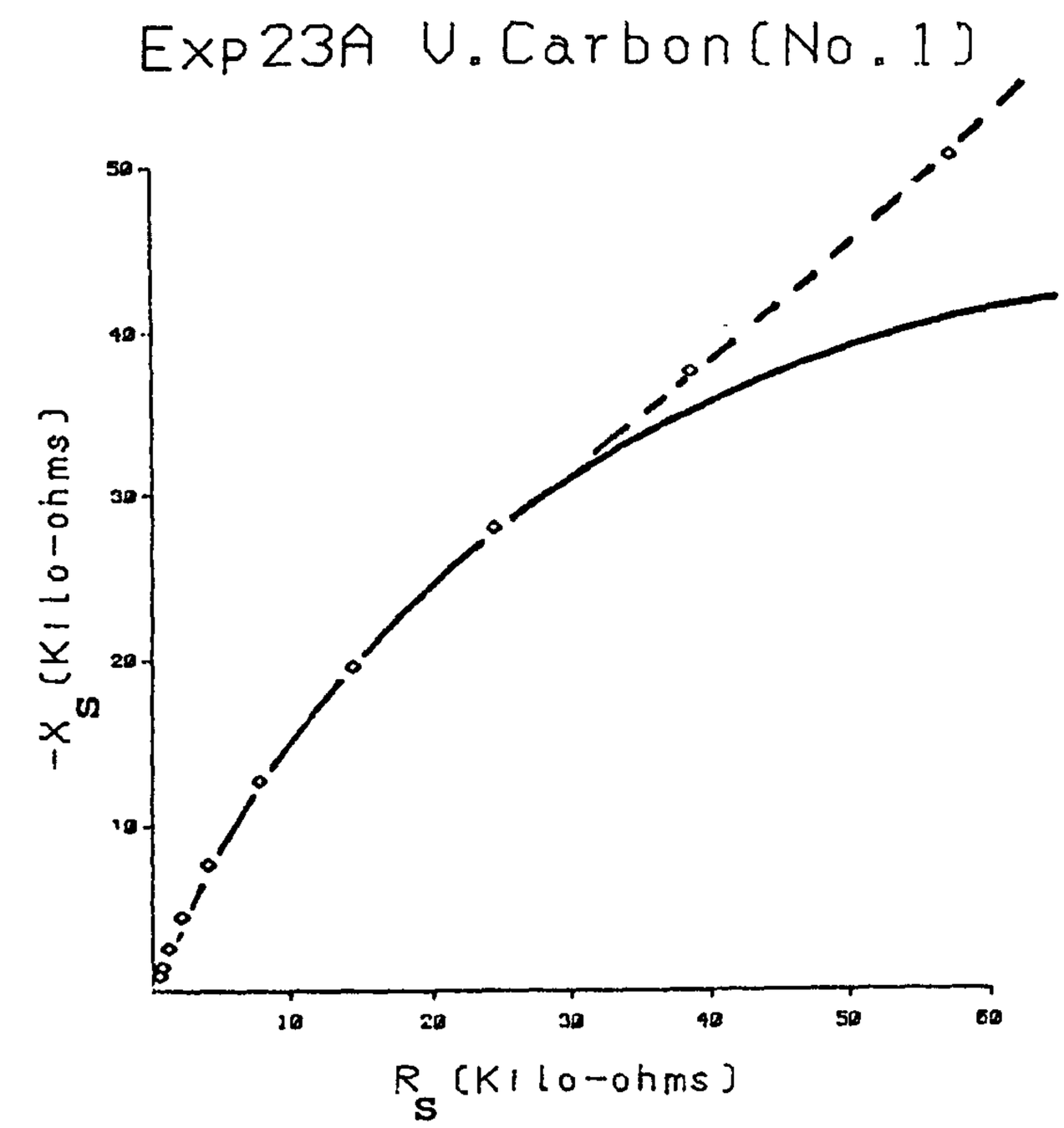

Figure 2.16

frequencies and then rises at low frequencies towards smooth surface Z_{CPA} behaviour. The above locus is very similar to those of the Devices electrode when roughened with emery paper (figure 2.12). The impedance parameters for the 'high' frequency arc were calculated as

$K = 17k\Omega\, s^{-\beta}$ $\qquad$ $\beta = 0.64$

$R_{CT} = 221k\Omega$ $\qquad$ (f_o = 12 mHz)

The very low value of β indicates that surface effects dominate the form of the locus. Not surprisingly K and R_{CT} have very small values - smaller than those for the Devices SC electrode roughened with P60 emery paper.

At lower frequencies the locus deviates from the 'high' frequency arc or lemniscate, and tends towards that due to low frequency, 'smooth' surface behaviour. Edeling et al (1983) found that impedance locus of a smooth glassy (vitreous) carbon electrode formed an arc describable by equation 2.1. They calculated the value of charge transfer resistance as $2.5 \times 10^5 \Omega\, cm^2$ (for an area of $12mm^2$, $R_{CT} = 2M\Omega$).

2.2.3. Conclusions on the low frequency ac impedance of pacing electrodes.

Although surface effects are less dominant in this low frequency range they are still significant.

The low frequency loci of 'smooth' surfaced pacing electrodes tested indicated the presence of a faradaic resistance in parallel with Z_{CPA}. This parallel

resistance has been equated with the charge transfer resistance, R_{CT}. Measured values of R_{CT} are very large, generally several megaohms, indicating that the pacing electrodes are quite polarisable and will deviate greatly from their reversible potentials upon the passage of faradaic (or dc) current.

The calculated equivalent circuit parameter values are reproduced on Table 2.3 to enable comparison and their loci are plotted on figure 2.17.

TABLE 2.3

Electrode	$K(k\Omega\ s^{-\beta})$	β	$R_{CT}(M\Omega)$
Devices Sc	62	.85	4.4
Tel. 224	101	.79	3.4
Sorin S80	44	.94	1.75
AV Carbon No2	5.5	.84	-
AV Carbon No1	17	.64	.22

The loci of rough surfaced electrodes show signs of a 'high' frequency arc or lemniscate due to the 'transmission line' effect of surface pores. Generally only a small portion of this arc is observed forming a kink at the high frequency end of the low frequency 'smooth' surface arc (eg Onaral and Schwan, 1982, figure 3). The rougher the electrode surface, the more of the high frequency arc visible, (figure 2.4) and the smaller it's diameter which approaches, according to Delevie, a value of $(R_e R_{CT})^{1/2}$ (where R_{CT} is the diameter of the smooth surface, low frequency arc; see figure 2.12). Values of K and β calculated from this high frequency arc are also found to decrease as the

Comparison of Electrode Impedances

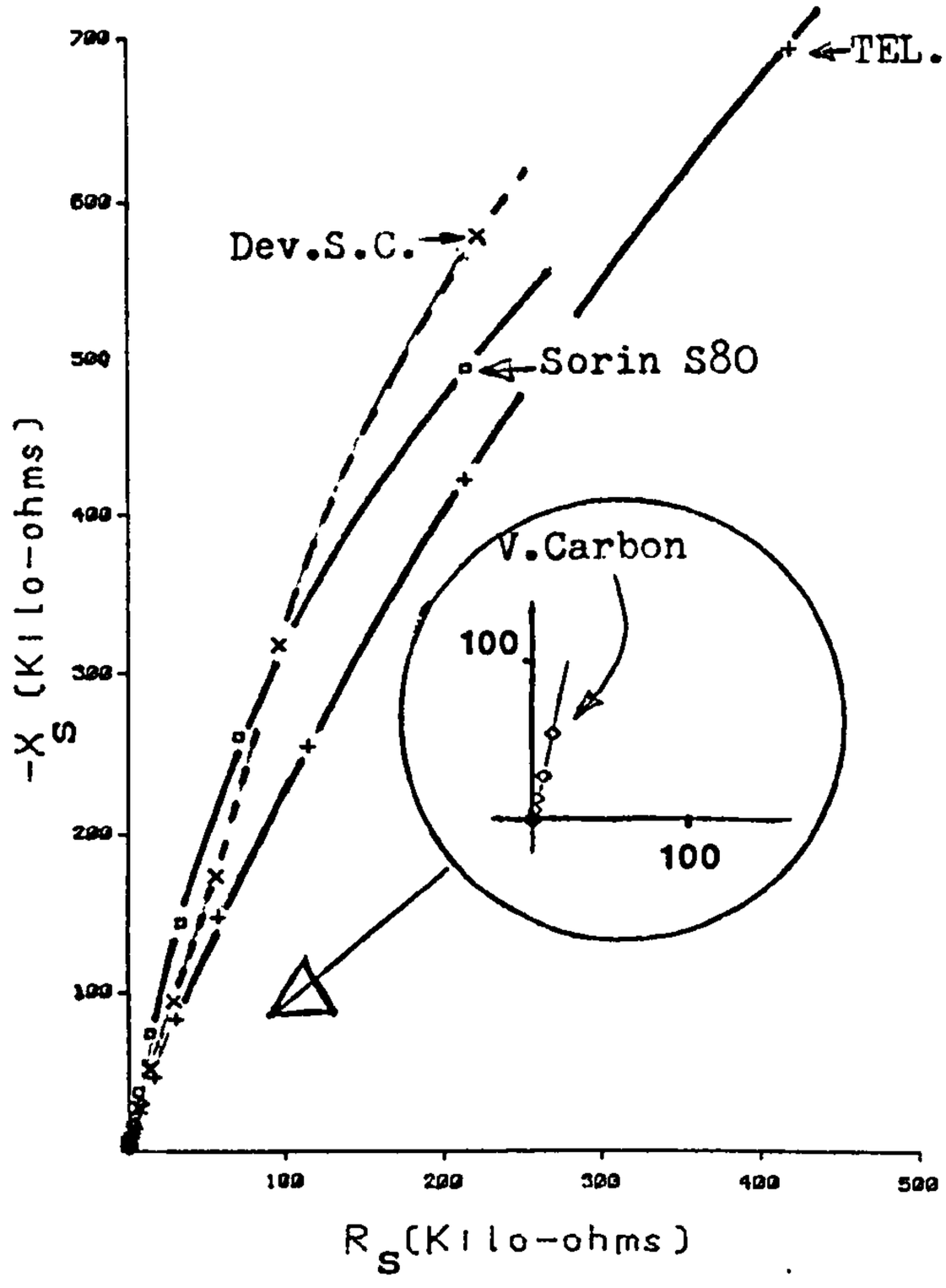

Figure 2.17

surface of the electrode is roughened. In extreme cases this arc should be describable by the equation

$$Z = (Z_i \; R_e)^{1/2}$$

Where Z_i is the interfacial impedance in the absence of surface effects (equations 2.1 or 2.3).

It was noted that generally the low frequency 'smooth' surface arc is not a semi circle, i.e. β is less than 1. Such frequency dispersion, in the absence of surface effects, is probably attributable to the voltage and frequency dependent, adsorption pseudo capacitance which shunts and generally dominates the frequency independent double layer capacitance, C_{dl}. Morkrid et al (1980) and Edeling et al (1983), however, came to a rather different conclusion. They divided the Z_{CPA} equivalent circuit element into two parallel components. Starting with the expression for its admittance

$$Z_{CPA}^{-1} = \left(\frac{1}{R_o - R_\infty}\right)\left[\;(\omega T)^{\beta}\cos(\pi\beta/2) + j(\omega T)^{\beta}\sin(\pi\beta/2)\right] \qquad 2.13$$

they concluded that it represents the parallel coupling of a 'resistive' element.

$$R_p' = \frac{R_p}{(\omega T)^{\beta}\cos(\pi\beta/2)} = \frac{K}{\omega^{\beta}\cos(\pi\beta/2)} \qquad 2.14$$

(where $R_p = R_o - R_\infty$) and a 'capacitive' element

$$C_p' = \frac{T^{\beta}\omega^{\beta-1}\sin(\pi\beta/2)}{R_p} = \left(\frac{\omega^{\beta-1}}{K}\right)\sin(\pi\beta/2) \qquad 2.15$$

Morkrid et al (1980) and Edeling et al (1983) equated

this latter 'capacitance' with the double layer capacitance

$$\text{i.e.} \qquad C_{dl} = \frac{\text{Sin } (\pi\beta/2)}{2\pi K f^{1-\beta}} \qquad 2.16$$

The above is however very improbable as the double layer capacitance is a frequency independent capacitance. There would also be the problem of attributing physical significance to the parallel 'resistance', R_p', a problem which was ignored by the above researchers. There is no physical reason why such a separate resistance, due to what ever cause, should be related to a shunting capacitance by the expression $R_p' = (1/\omega C_p') \tan (\pi\beta/2)$.

One must conclude that the Z_{CPA} impedance cannot be subdivided and that it represents one physical process. It is suggested that such an impedance element represents fairly well the effects of specific adsorption of ions onto the electrode surface. The model is of course only approximate and is valid only over limited frequency ranges (β is known to change gradually with frequency).

The measured value of K was observed to increase and those of β and R_{CT} to decrease with time after a clean electrode was placed in saline. These are probably attributable to the gradual adsorption of chloride and other ions present which leads to a decrease in the double layer capacitance (Breiter 1963) and deviation from pure capacitive behaviour.

Of the pacing electrodes tested, it was found that

the activated vitreous carbon electrode had by far the smallest interfacial impedance (figure 2.17). Contrary to Mund et al's claim (1979) the AVC electrode is not 'non-polarizable' as it has a finite value of charge transfer resistance (above 0.2MΩ). It is however the least polarizable of the electrodes tested and it's superior proporties are largely due to it's very rough surface.

Chapter 3

Small Signal, time domain analysis of the electrode-electrolyte interface.

3.1 Introduction

This chapter is concerned with the analysis of the electrode-electrolyte interface impedance using transient techniques.

Two approaches have been implemented in the past by biomedical engineers in order to study the impedance of electrode systems. So far only the ac technique has been considered, however some researchers have used the time domain to explore the electrical properties of electrode systems. In pacing, where large voltage or current pulses are applied to electrodes, the applied waveforms have also been used to investigate the inter-electrode impedances. Unfortunately the signals applied are generally so large as to drive the system under the study into nonlinear behaviour. In this chapter only work carried out in the linear (small signal) region will be reviewed and published results compared with those obtained using the ac technique. If an electrode system is linear, the equivalent circuit models derived using each technique should be the same.

-Advantages in using the transient technique

A possible drawback of the ac impedance method is that a complete set of measurements over a range of frequencies can take a considerable time. During this time the system's impedance may change, even after stabilisation. The resulting impedance plot may hence be distorted (see figure 1.33).

With the transient technique a voltage or current step or pulse is applied to the electrode system and

the resultant current or voltage waveform recorded, photographically or otherwise. By close analysis of the response waveforms the system's impedance can be derived. The advantage of the transient technique is that only a relatively short time is needed to record the system's response. Deriving an equivalent circuit model from the response is however more difficult than in the ac impedance method.

- Disadvantages in using the transient technique

In linear transient analysis a small current or voltage step (or pulse) is applied to the system under study and the resultant voltage or current response observed. To derive an equivalent circuit model the response of the system is generally compared, either visually or by computer, with those of several very simple equivalent circuits and the circuit whose response is closest to that of the electrode system is chosen. This approach is often of rather limited accuracy as complicated circuits are generally not tried. The difficulty in using this method is further increased by the close visual similarity in the transient responses of different equivalent circuits. For example, the response of a circuit which includes a constant phase angle impedance, Z_{CPA}, does not differ markedly from that of one without (Poon and Choy 1978). Hence, unless the researcher is aware of the possibility of the presence of a Z_{CPA}, the response would, apparently quite well, be fitted to a simple equivalent circuit comprising one or two resistors and

capacitors. Many researchers have therefore missed the subtle indications of the presence of a Z_{CPA} in the transient response of their electrode systems. With the ac technique, on the other hand, the presence of a Z_{CPA} is generally relatively easy to identify - although this fact has not hindered researchers from modelling the observed ac impedance with equivalent circuits containing no such frequency dependent elements.

The above short comings can of course be overcome by use of the Fourier Transform which transforms the transient data from the time domain into the frequency domain where analysis is much easier (see Chapter 5).

3.2 Form of an electrode system's response to a step input

3.2.1 "3 component" model

Over the years the "3 component" model has been most commonly proposed to represent the electrode system as the response of the system is observed to vary with time in a roughly exponential manner (e.g. Weinmann and Mahler, 1964, Block, 1968). The proposed equivalent circuit is shown on figure 3.1a.

The parallel capacitance and resistance have been associated with the double layer capacitance, and the 'leakage' or charge transfer resistance. This theoretical model is very similar to the one suggested in the last chapter by the author. However the effects

"3 COMPONENT" MODELS OF THE INTER-ELECTRODE IMPEDANCE

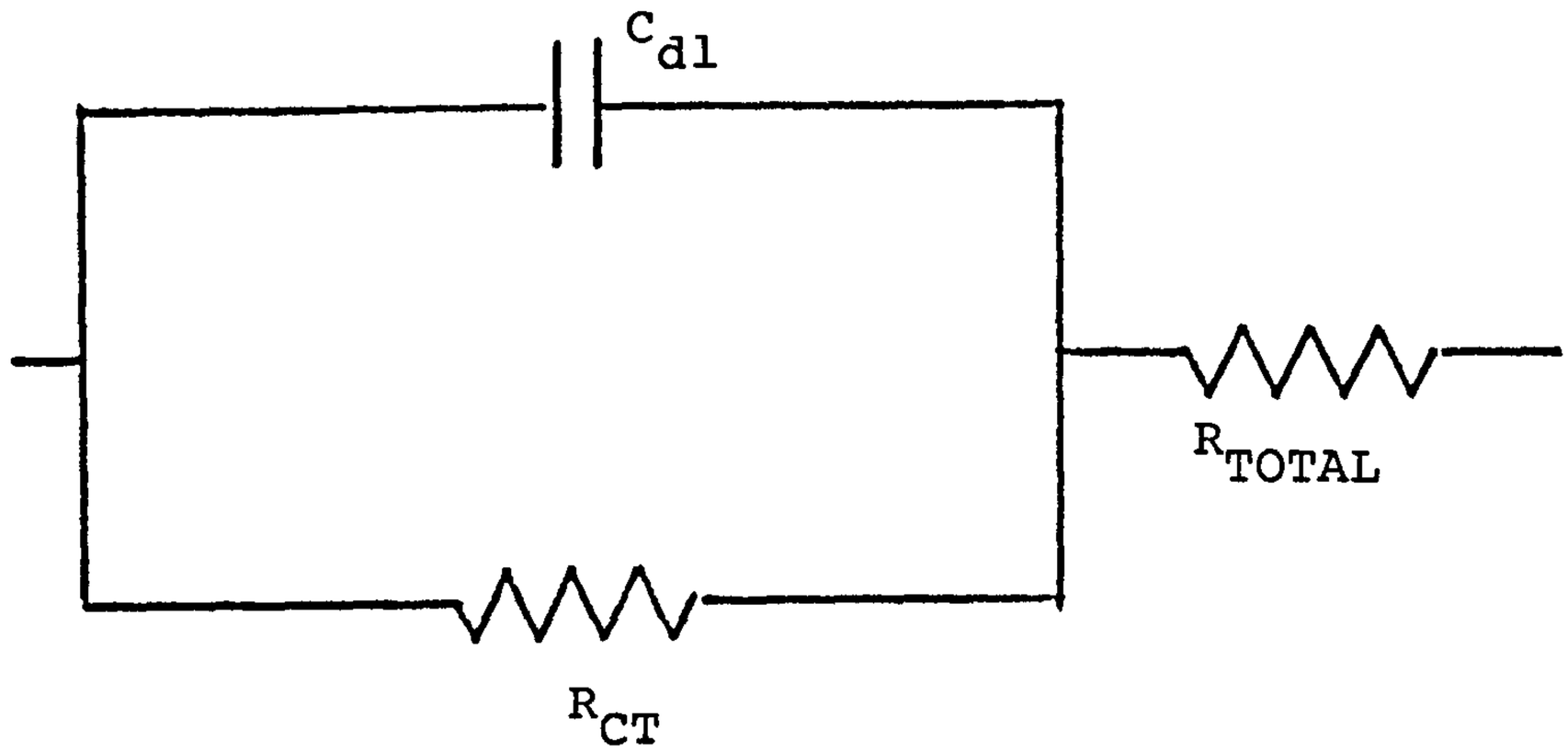

Figures 3.1 a and b

of surface roughness and adsorption on the non-faradaic capacitance have not been taken into account and hence the above model fails to represent and explain the observed frequency dependence of the non-faradaic impedance.

Another circuit, completely equivalent to the first, has been suggested by Chardack et al (1964) and Fischler (1979) and is shown on figure 3.1b.

Turney (1967) however showed, by plotting log i(t) against time, t, for an applied voltage step, that the time constant of the current response changed with time. The response of an electrode system could not therefore be represented by a circuit containing only one time constant. Since then various equivalent circuits comprising several time constants have been suggested in an effort to better reproduce the electrode system's observed response. In such circuits however the individual elements have generally no physical meaning and the circuits, although complicated, fail to adequately reproduce the observed response.

3.2.2 "$R_{TOT} - Z_{CPA}$" model

In the frequency domain the interfacial impedance is found to be well modelled over a wide range of frequencies by a Z_{CPA} impedance i.e.

$$Z_i = K(j\omega)^{-\beta} + R_{TOT}$$

-Current response

In order to derive the current response, i(t), for

example, of the above impedance to a voltage step, V_{dc}, one must resort to the use of Laplace transforms. The Laplace transform, I(s), of the current response, i(t) is calculated as follows

$$I(s) = \frac{V(s)}{Z_i(s)} \qquad 3.1$$

$$\text{where } F(s) = \mathcal{L}[f(t)] = \frac{1}{2\pi}\int_0^{\infty} e^{-st} f(t)dt \qquad 3.2$$

and $s = a + j\omega$.

Hence

$$I(s) = \frac{V_{dc}}{s}\left(\frac{1}{R_{TOT} + K/s^{\beta}}\right) \qquad 3.3$$

The current response in the time domain, i(t), is given by the inverse Laplace transform of equation 3.3, where the inverse transform,

$\mathcal{L}^{-1}\{F(s)\}$ is given by

$$f(t) = \int_{-\infty}^{\infty} e^{st} F(s)ds, \; t>o \qquad 3.4$$

In order to derive the inverse transform of equation 3.3 one must rewrite it as follows

$$I(s) = \frac{V_{dc}}{R_{TOT}} \quad \frac{1}{s} \quad \left(1 + \left(\frac{K}{R_{TOT}}\right) s^{-\beta}\right)^{-1}$$

which can be written

$$I(s) = \frac{V_{dc}}{R_{TOT}} \left(\frac{R_{TOT}}{K}\right)^{1/\beta} \frac{1}{Ts} \left(1+(Ts)^{-\beta}\right)^{-1} \qquad 3.5$$

where $T = \left(\frac{R_{TOT}}{K}\right)^{1/\beta}$ 3.6

Hence I(s) is a function of Ts such that,

$$I(s) = \frac{V_{dc}}{R_{TOT}} \left(\frac{R_{TOT}}{K}\right)^{1/\beta} F(Ts) \qquad 3.7$$

$$\text{Where } F(s) = \frac{1}{s\,(1+s^{-\beta})} = \int [\, f(t)] \qquad 3.8$$

By the scaling rule for Laplace transforms (Fitzhugh and Cole, 1973)

$$F(Ts) = \int \left(\frac{f(t/T)}{T}\right) = \frac{1}{T} \int f(\bar{t}) \qquad 3.9$$

The inverse transform of equation 3.7 is therefore

$$i(t) = \int^{-1} I(s) = \left(\frac{V_{dc}}{R_{TOT}}\right) f(\bar{t}) \qquad 3.10$$

$$\text{Where} \quad \bar{t} = t/T = t(K/R_{TOT})^{1/\beta} \qquad 3.11$$

$\bar{t}$ is dimensionless as it is measured in units of T

In order to derive the expression for i(t), one must first take the inverse transform of equation 3.8, and thus obtain an expression for f(t). This is rather difficult but can be achieved by first expanding equation 3.8 such that

$$F(s) = \left[s(1+s^{-\beta})\right]^{-1} = 1/s \sum_{n=0}^{\infty} (-1)^n s^{-\beta n}$$

$$F(s) = \sum_{n=0}^{\infty} (-1)^n s^{-(1+\beta n)} \qquad 3.12$$

The series is convergent for /s/>1.

$$\text{As} \int^{-1} [s^{-(1+\beta n)}] = \frac{t^{\beta n}}{\Gamma(1+n\beta)}$$

(Where $\Gamma(\ )$ is the gama function defined by

$$\Gamma(1+n\beta) = \int_0^\infty e^{-t} t^{n\beta} dt \quad) \qquad 3.13$$

equation 3.12 can be transformed term by term to give

$$f(t) = \sum_{n=o}^{\infty} \frac{(-1)^n}{\Gamma(1+n\beta)} t^{\beta n} \qquad 3.14$$

(Fitzhugh and Cole, 1973)

One can now derive an expression for the current response, i(t) using 3.10, 3.11 and 3.14

$$i(t) = \frac{V_{dc}}{R_{TOT}} \sum_{n=o}^{\infty} (-1)^n \left(\frac{K}{R_{TOT}}\right)^n \frac{t^{\beta n}}{\Gamma(1+n\beta)} \qquad 3.15$$

(de Boer and Van Oosterom, 1978)

For very short periods of time (using equation 3.14)

$$f(t)_{t\to 0} = 1 - \frac{t^{\beta}}{\Gamma(1+\beta)} \qquad 3.16$$

and

$$i(t) = \frac{V_{dc}}{R_{TOT}} \left[1 - \frac{K \quad t^{\beta}}{R_{TOT} \ \Gamma(1+\beta)} \right] \qquad 3.17$$

Equation 3.15 converges for all t>o and therefore could in principle be used to calculate i(t) to the required accuracy for any value of t. In practice, however, for "large" values of t, such that $\frac{Kt^{\beta}}{R_{TOT}} >> 1$, the number of terms needed for the calculation becomes prohibitive (Fitzhugh and Cole, 1973). As K is

generally many times larger than R_{TOTAL}, the above constraint will even apply at relatively short time durations. Equations 3.16 and 3.17 cannot therefore be used in practice for the calculation of the current response for values of t of the order of 1 millisecond (deBoer and Van Oosterom, 1978).

Expressions for f(t) and i(t) valid for longer times can be derived by rewriting equation 3.8 as

$$F(s) = \frac{1}{s}\left(1 - \frac{1}{1 + s^{\beta}}\right)$$

$$= \sum_{n=1}^{\infty} (-1)^{n+1} S^{\beta n-1} \qquad 3.18$$

This series (3.18) may also be transformed term by term to yield the following asymptotic expansion for f(t)

[using $s^{\beta n-1} = s^{-(1-\beta n)}$

and $\int^{-1} \left(s^{-(1-\beta n)}\right) = \frac{t^{-\beta n}}{\Gamma(1-\beta n)}$]

$$f(t) = \sum_{n=1}^{\infty} (-1)^{n+1} \frac{t^{-\beta n}}{\Gamma(1-\beta n)} \qquad 3.19$$

As t tends to infinity the first term of the series is most important and one has the approximation

$$i(t) \cong V_{dc} \frac{t^{-\beta}}{K\,\Gamma(1-\beta)} \qquad 3.20$$

(Gesteland, 1959, Onaral and Schwan 1983).

Hence the current response of an electrode system

to a voltage step, V_{dc}, for "large" values of t is proportional to $t^{-\beta}$. At large times (low frequencies) the magnitude of the Z_{CPA} impedance is very large relative to R_{TOTAL}, and it therefore, along with its fractional power, β, dominates the form of the current response.

Using a small amptitude voltage step de Boer et al (1978) found good correlation between the above formulae and their experimental results (Pt electrodes in 0.9% NaCl for times up to 1.8m sec (f > 88 Hz).

- Voltage response

The deviation of the voltage response V(t) of the system to a step in current is a much simpler problem.

$$V(s) = I(s) \quad Z_i(s)$$

$$V(s) = \frac{I_{dc}}{s} \left(R_{TOT} + \frac{K}{s^{\beta}}\right)$$

$$= I_{dc}\left[\frac{R_{TOT}}{s} + \frac{K}{s^{\beta+1}}\right] \qquad 3.21$$

Taking inverse transforms

$$V(t) = I_{dc}\left(R_{TOT} + \frac{K\, t^{\beta}}{\Gamma(1+\beta)}\right) \qquad 3.22$$

(Cole 1934, de Boer et al, 1978)

The voltage response to a current step is therefore characterised by t^{β} behaviour. Plotting log[V(t)] against log(t) one should obtain a straight line (over the range were the interfacial impedance is well modelled by Z_{CPA}) with a gradient equal to β.

Weinman and Mahler (1959) observed t^{β} behaviour for the voltage response of stainless steel electrodes in saline. De Boer and Van Oosterom (1978) fitted equation 3.22 to the voltage response of their platinum electrodes for durations up to 1.8 ms. Very good fits with experimental data were obtained. Onaral and Schwan (1983) found the range of validity of the above model (R_{TOT} and Z_{CPA}) extended to approximately 100 msec (10 Hz).

3.2.3 "R_{TOT} - Z_W" model

The diffusion or Warburg impedance, Z_W, is a special case of Z_{CPA} behaviour with $\beta = 0.5$.

In this case (Fitzhugh and Cole, 1973)

$$F(s) = \frac{1}{s+s^{0.5}} \qquad 3.23$$

$$\text{and} \quad f(t) = \exp(t)\ \text{erfc}\ (t^{0.5}) \qquad 3.24$$

where erfc is the complimentary error function,

$$\text{erfc}\ (y) = \frac{\exp(-y^2)}{\pi^{1/2}\, y}\left[1 - \frac{1}{2y^2} + \frac{1.3}{(2y^2)^2} + \ldots\right]$$

The current response, i(t), of such an impedance to a voltage step, V_{dc}, is (Bard and Faulkner, 1980)

$$i(t) = \frac{V_{dc}}{R_{TOT}} \exp(a^2 t)\ \text{erfc}\ (a\, t^{0.5}) \qquad 3.25$$

where $a = \sigma / R_{TOT}$

and $$\sigma = \frac{RT}{n^2 F^2 \sqrt{2}} \left[\frac{1}{C^{o}_{b} D^{1/2}_{o}} + \frac{1}{C^{R}_{b} D^{1/2}_{R}}\right]$$

For large times such that $a t^{0.5} > 5$

$$i(t) = \frac{V_{dc}}{\pi^{0.5} a t^{0.5} R_{TOT}} \qquad 3.26$$

For such long time durations diffusion is the dominating process and its impedance dominates that of the electrode-electrolyte interface. The current response in such a case is characterised by $t^{0.5}$ behaviour.

Not surprisingly, it has mainly been electrochemists who have used this model to represent the electrode system under both a.c. and transient conditions (eg Thirsk and Harrison, 1972). Although, in certain cases, Z_W gives a reasonable representation of experimental results, the model is unacceptable for the majority of biomedical electrode systems where β is not equal to 0.5.

3.2.4 - "$Z_{CPA} - C_{LF}$" model

In 1942 Cole and Cole derived the transient response of their earlier "distribution of relaxation times" model (figure 1.28). The current response of their equivalent circuit to a small voltage step, V_{dc}, is

$$i(t) = V_{dc} \frac{\Delta C}{T} (1-\beta) \left(\frac{t}{T}\right)^{-\beta} \sum_{n=1}^{\infty} \frac{(-1)^n n}{\Gamma[1+n(1-\beta)]} \left(\frac{t}{T}\right)^{(n-1)(1-\beta)} \qquad 3.27$$

$$\text{Where} \quad T = \left(\frac{K}{\Delta C}\right)^{1/(1-\beta)}$$

For $t/T \ll 1$

$$i(t) = V_{dc}\left(\frac{\Delta C}{T}\right)\frac{1}{\Gamma(1-\beta)}\left(\frac{t}{T}\right)^{-\beta} \qquad 3.28$$

and for $t/T \gg 1$

$$i(t) = V_{dc}\left(\frac{\Delta C}{T}\right)\frac{(1-\beta)}{\Gamma(\beta)}\left(\frac{t}{T}\right)^{-(2-\beta)} \qquad 3.29$$

Cole - Cole's derived current response for values of t much smaller than T is proportional to $t^{-\beta}$ as observed experimentally. For longer times the presence of ΔC becomes noticable and the response deviates from that of $t^{-\beta}$.

Jaron et al (1968) simplified the equivalent circuit of Cole and Cole (1941) by ignoring the contribution of the parallel high frequency capacitance. The model reduces to a Z_{CPA} in series with a low frequency capacitance C_{LF}.

The voltage response to a small current step of this circuit is derived as follows

$$V(s) = I(s)\,Z(s)$$

$$V(s) = \frac{I_{dc}}{s}\left[\frac{1}{C_{LF}s} + \frac{K}{s^{\beta}}\right]$$

$$= I_{dc}\left[\frac{1}{C_{LF}s^2} + \frac{K}{s^{\beta+1}}\right]$$

Taking inverse transforms

$$V(t) = I_{dc}\left[\frac{t}{C_{LF}} + \frac{K\,t^{\beta}}{\Gamma(1+\beta)}\right] \qquad 3.30$$

(Jaron et al, 1968 ; Onaral and Schwan, 1983)

The voltage response, V(t), rises, first proportionally to t^{β} for short periods of time and then becomes a linear function of t for larger times due to the presence of the series low frequency capacitance, C_{LF}.

Jaron et al found this model acceptable for times up to 1 msec (or in terms of frequency, down to 1kHz). Onaral and Schwan (1983) took the step duration up to 10 msec (f = 100 Hz) and still found good agreement with experimental results. However beyond this range they found the model unsatisfactory in representing the electrode system.

It is concluded that a model comprising a Z_{CPA} in series with a capacitance, C_{LF}, gives good representation of the electrode system for short times or high frequencies. At lower frequencies or longer times a better fit would probably be achieved if C_{LF} was replaced by a low frequency, constant phase angle impedance, $Z_{CPA(LF)}$, as pointed out in Chapter 1. For very long times the effect of the shunting charge transfer resistance will also affect the form of response.

3.2.5 - Z_{CPA} in parallel with R_{CT}

The transient response of a circuit comprising a Z_{CPA} shunted by a resistance to a voltage or current step was perhaps first investigated by Cole in 1934 while studying membrane impedances. More detailed treatments of the problem have since been carried out

by Fitzhugh and Cole (1973), Poon and Choy (1978) and Chabli et al (1982).

The main difficulty in deriving the transient response of the above circuit is that the form of the interfacial impedance (equation 2.1) is not related to any known time function as provided by conventional Laplace transform tables (Poon and Choy, 1978). Fitzhugh and Cole (1973) applied a series approximation to the interfacial impedance followed by a term-by-term inverse transformation, as previously illustrated in section 3.2.2. The results are given by two infinite series (eqns 3.14 and 3.19) corresponding to large and small values of time. For intermediate values of time a rational approximation has to be made which imposes limitations on the accuracy.

The approach of Fitzhugh and Cole has however been chosen in order to derive transients for the above equivalent circuit as it is relatively simple and accurate enough for our needs.

- Voltage response

For a step in current, I_{dc}, the voltage response of the above impedance is calculated as follows

$$V(s) = I(s)\ Z(s)$$

$$= \frac{I_{dc}}{s}\left[R_{TOT} + \frac{R_{CT}}{1 + (R_{CT}/K)\ s^{\beta}} \right]$$

$$= \frac{I_{dc}}{s}\left[R_{TOT}+R_{CT} - \frac{R_{CT}}{(K/R_{CT})\ s^{-\beta} + 1} \right]$$

$$V(s) = I_{dc}\left[\frac{R_{TOT} + R_{CT}}{s} - \frac{R_{CT}}{s\left[\frac{K\ \bar{s}^{\beta}}{R_{CT}} + 1\right]}\right]$$

$$= I_{dc}\left[\frac{R_{TOT} + R_{CT}}{s} - \frac{R_{CT}\ T}{(Ts)\ [(Ts)^{\bar{\beta}} + 1]}\right]$$

where $T = (R_{CT}/K)^{1/\beta}$. 3.31

It follows that

$$V(s) = I_{dc}\left[\frac{R_{TOT} + R_{CT}}{s} - R_{CT}\ T\ F(Ts)\right] \quad 3.32$$

where F(s) and F(Ts) are defined by equations 3.8 and 3.9.

The inverse transform of equation 3.32 is

$$V(t) = I_{dc}\ [R_{TOT}+R_{CT}\ \{\ 1-\ f(\bar{t})\}] \quad 3.33$$

where $\bar{t} = t/T = t\ (K/R_{CT})^{1/\beta}$ 3.34

and f (t) is given by equation 3.14 and approximated by equations 3.16 and 3.19.

Plots of $\log[1-f(\bar{t})]$ against $\log(\bar{t})$ for various values of β are shown on figure 3.2a. The log-log plot is linear with a slope equal to β for normalised times, $\bar{t}$, smaller than $\bar{t} = 0.7$.

For times larger than $t = 0.7$, $[1-f(\bar{t})]$ approaches a limiting value of 1.

As V(t) is proportional to $[1-f(\bar{t})]$ (see equation 3.33) a log V(t) - log (t) plot will have the same form as figure 3.2a.

(i) For small time durations such that

$$t < 0.7\ T = 0.7/\omega_o$$

equation 3.14 approximates to equation 3.16

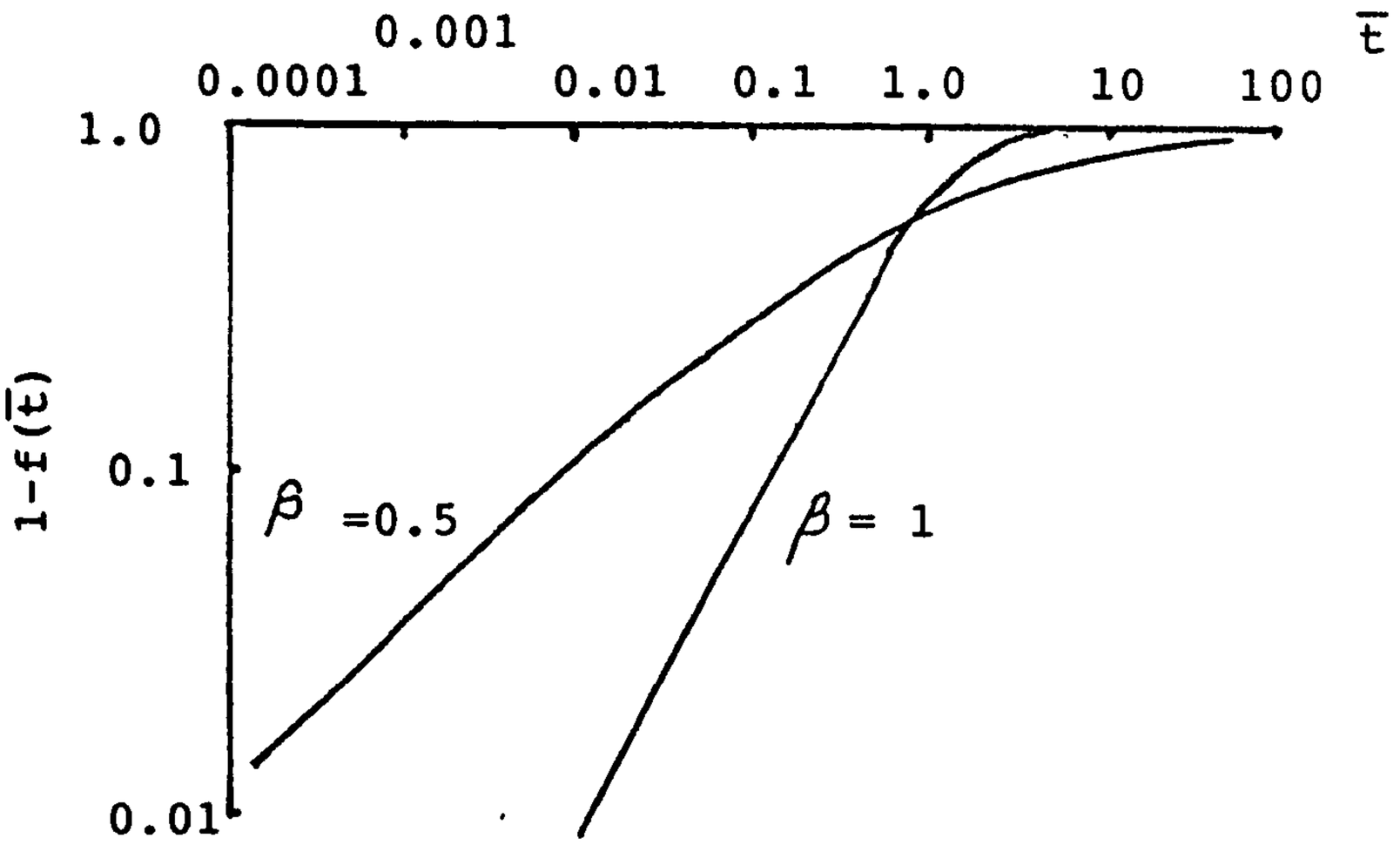

Log(1-f($\bar{t}$)) vs. Log($\bar{t}$)

Figure 3.2a

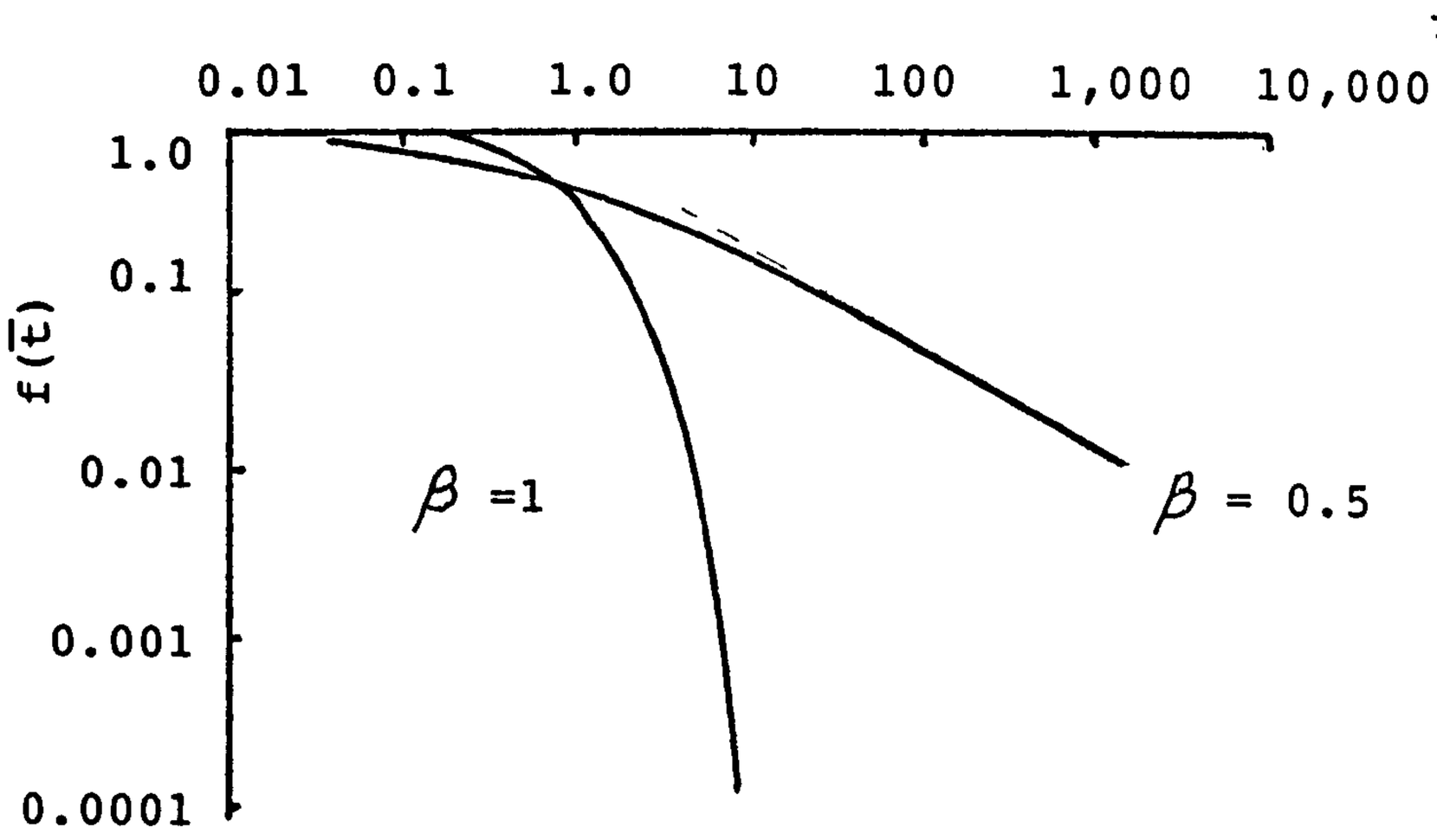

Log(f($\bar{t}$)) vs. Log($\bar{t}$)

Figure 3.2b

$$\text{i.e.} \qquad f(t) = 1 - \frac{t^{\beta}}{\Gamma(1+\beta)}.$$

Using equations 3.9, 3.16 and 3.31 equation 3.33 becomes

$$V(t) = I_{dc}\left[R_{TOT} + \frac{Kt^{\beta}}{\Gamma(1+\beta)} \right] \qquad 3.35$$

The interfacial impedance and its voltage response are dominated by the constant phase angle impedance, Z_{CPA}. A plot of log V(t) will be a straight line of slope, β, as expected.

(ii) For long durations such that

$$t > 0.7\ T = 0.7/\omega_o,$$

f(t) (see figure 3.2b) becomes very small and equation 3.33 tends to the limiting value

$$V(t)_{max} = I_{dc}\,(R_{TOT} + R_{CT}),$$

i.e. the interfacial impedance and its voltage response are dominated by the presence of R_{CT} in parallel with Z_{CPA}.

- Current response

The current response to a voltage step, V_{dc} can be derived as follows

$$I(s) = V(s)/Z(s)$$

$$= \frac{V_{dc}}{s}\left[R_{TOT} + \frac{R_{CT}}{1 + (R_{CT}/K)s^{\beta}} \right]^{-1}$$

$$= \frac{V_{dc}}{s}\left[\frac{K\,s^{-\beta}}{R_{TOT}R_{CT}} + \frac{1}{R_{TOT}} \right] \qquad 3.36$$

$$\frac{(Ts)^{\beta} + 1}{}$$

where $$T = \left(\frac{R_{CT}R_{TOT}}{R_{TOT}+R_{CT}}\right)^{1/\beta} \left(\frac{1}{K}\right)^{1/\beta}$$

Hence
$$I(s) = \frac{V_{dc}}{s}\left[\frac{1}{R_{TOT}+R_{CT}} + \frac{\frac{R_{CT}}{R_{TOT}(R_{TOT}+R_{CT})}}{1 + T\,s^{-\beta}}\right]$$

which can be rewritten as

$$I(s) = V_{dc}\left[\frac{1}{s(R_{TOT}+R_{CT})} + \frac{R_{CT}\;T\;F(Ts)}{R_{TOT}(R_{TOT}+R_{CT})}\right] \qquad 3.37$$

where F (s) and F(Ts) are defined in equations 3.8 and 3.9.

The inverse transform of equation 3.37 is

$$i(t) = V_{dc}\left[\frac{1}{R_{TOT}+R_{CT}} + \frac{R_{CT}}{R_{TOT}(R_{TOT}+R_{CT})}\;f(\bar{t})\right] \qquad 3.38$$

where $\bar{t} = t/T = t\,(k)^{1/\beta}\left(\frac{R_{CT}+R_{TOT}}{R_{CT}\;R_{TOT}}\right)^{1/\beta}$ 3.39

Plots of log $f(\bar{t})$ against log $\bar{t}$ are shown on figure 3.2b for a range of β.

(i) For very short times the function f(t) is approximated by equation 3.16.

and
$$i\,(t) = \frac{V_{dc}}{R_{TOT}}\left[1 - \frac{K\;t^{\beta}}{R_{TOT}\;\Gamma(1+\beta)}\right]$$
(equation 3.17)

The current response initially rises to its maximum value of V_{dc}/R_{TOT} and then decreases

(ii) For medium time periods the function f(t) is approximated by the first term of equation 3.19 and the current response, i(t), is approximated by

$$i(t) = V_{dc}\left[\frac{1}{R_{TOT}} + \frac{t^{-\beta}}{K\;\Gamma(1-\beta)}\right] \qquad 3.40$$

(iii) For long times f(t) tends to zero and the

current response, i(t), approaches the limiting value

$$i(t)_{min} = \frac{V_{dc}}{R_{TOT}+R_{CT}}$$

Onaral and Schwan (1983) have plotted, for durations up to 10 seconds, the voltage response of platinum electrodes in 0.9% saline to very small amptitude current steps (12μA). Plotting log $[V(t)/I_{dc}]$ against log(t) they found that the gradient of the log-log plot, β (see equation 3.35), changes from approximately 0.5 to approximately unity as time is increased from 0.1ms to 1ms (i.e. down to 1kHz). This indicated the validity of Jaron et al's (1968) model for short pulse durations (equation 3.30). For durations above 10ms (f<100Hz) β was observed to decrease again coinciding with the range of frequencies were the 'kink' was observed in the corresponding frequency domain measurements (Onaral and Schwan, 1982, figures 2 and 3).

In chapter two the 'kink' in the frequency domain plot was attributed to the presence of a shunting resistance. The combination of the shunting resistance and the effects of surface roughness cause the impedance locus to bend over and form part of a high frequency arc whose diameter approaches $(R_e\ R_{CT})^{0.5}$ As surface effects decrease with the lowering of the frequency, the locus returns to that of a smooth surface, forming the lower end of a low frequency arc whose diameter is equal to R_{CT} (figure 2.4).

Onaral and Schwan (1982, 1983) attributed the 'kinks' on their impedance and transient plots to the

onset of nonlinearity as, in this region, the value of m (where m = 1-β) calculated from the slope of their log C_s - log f plot (eqn 1.4) no longer equalled the value calculated from the phase angle (ϕ =(1-m)π/2) as required for linear Z_{CPA} behaviour. Onaral and Schwan's conclusion is partially correct. The observed deviation from Z_{CPA} behaviour does not necessarily infer nonlinearily. It was shown in chapter 2 that the deviation is due to the presence of the shunting charge transfer resistance, R_{CT}. However, as shall be seen in Chapter 4, R_{CT} is a very nonlinear "resistance" (equation 1.22 only applies for very small signals when V is less than 5mV) and hence domination of the interfacial impedance by R_{CT} is generally synonymous with nonlinear behaviour.

As the kinks, the author believes, are due to the combined effects of the presence of R_{CT} and surface roughness, nonlinear behaviour should indeed be observed over this frequency / time region. However for longer durations (t> 0.4 sec) or lower frequencies (f<0.4 Hz) the effect of surface finish "wears off" and there is a return to linear, smooth surface Z_{CPA} behaviour. In this region Onaral and Schwan (1983) observed that the two calculated values of m (as described above) agree and the impedance locus is once again a straight line.

On the log $[V(t)/I_{dc}]$ - log (t) plot a straight line is also observed and there is equivalence with the frequence domain results (Onaral and Schwan, 1983).

Although not measured by Onaral and Schwan, the

transient plot should however level off for very long durations (t > 100 sec, f < 0.01 Hz) and tend to a constant value,

$$\log \left[\frac{V(t)_{max}}{I_{dc}} \right] = \log (R_{CT})$$

3.3 Conclusions

As in the frequency domain the interfacial impedance is found to be well represented by a constant phase angle impedance, Z_{CPA}, over a wide range of times. For longer time durations an additional low frequency capacitance, C_{LF}, or constant phase angle impedance Z_{LF} is required to model the observed gradual increase in β with time.

A kink was observed which has been attributed to the combined effects of surface roughness and the parallel charge transfer resistance.

At longer time durations Z_{CPA} behaviour will once again become evident, eventually giving way to purely resistive behaviour, due to R_{CT}, as t becomes relatively very large (ie over one minute).

In chapter 5 the transient technique will be used to investigate the nonlinearity of the interfacial impedance.